CF-54-8-237

REACTORS—POWER

UNITED STATES ATOMIC ENERGY COMMISSION

A TEN MEGAWATT BOILING HETEROGENEOUS PACKAGE POWER REACTOR

Reactor Design and Feasibility Problem

By
M. A. Rosen
D. B. Coburn
T. A. Flynn
E. H. Hemmerle
C. E. Klotz
J. MacPhee
T. W. McIntosh
G. K. Rhode
J. R. Struyk

August 1954

Oak Ridge School of Reactor Technology
Oak Ridge, Tennessee

Technical Information Service Extension, Oak Ridge, Tenn.

DISCLAIMER

Date Declassified: November 1957.

Printed in USA. Price $3.50. Available from the Office of Technical Services, Department of Commerce, Washington 25, D. C.

AEC Technical Information Service Extension
Oak Ridge, Tennessee

CF-54-8-237

OAK RIDGE SCHOOL OF REACTOR TECHNOLOGY

F. C. VonderLage, Director

Reactor Design and Feasibility Problem

"A TEN MEGAWATT BOILING HETEROGENEOUS PACKAGE POWER REACTOR"

Prepared by:

M. A. Rosen, Group Chairman
D. B. Coburn
T. A. Flynn
E. H. Hemmerle
C. E. Klotz
J. MacPhee
T. W. McIntosh
G. K. Rhode
J. R. Struyk

OAK RIDGE NATIONAL LABORATORY
Operated by
Union Carbide Nuclear Company
Oak Ridge, Tennessee

August 1954

THIS PAGE

WAS INTENTIONALLY

LEFT BLANK

PREFACE

In September, 1953, a group of men representing various scientific and engineering fields embarked on the twelve months of study which culminated in this report. For nine of these months, formal classroom and student laboratory work occupied their time. At the end of that period, these nine students were presented with a problem in reactor design.

This is a summary report of the study, the research, the problems and the solutions which developed during the final ten-weeks period of the school term. It must be realized that, in so short a time, a study of this scope can not be guaranteed complete or free of error. This "thesis" is not offered as a polished engineering report but rather a record of the work done by the group under the leadership of the group leader. It is reproduced for use by those persons competent to assess the uncertainties inherent in the results obtained in terms of the preciseness of the technical data and analytical methods employed in the study. In the opinion of the students and faculty of ORSORT, the problem has served the pedagogical purpose for which it was intended.

As a matter of historical fact and pride we point out that similar investigations by student groups of previous ORSORT classes have led to sufficiently encouraging results to warrant more exhaustive studies; in at least one instance, a reactor first investigated by a student group is soon to become a physical reality. There is also recorded an instance in which calculations contained in a similar report were uncritically abstracted and applied to a study for which they were never intended. It is to avoid the recurrence of the latter experience that we have taken some pains to acquaint the reader with the character of this report.

The faculty wishes to join the authors in an expression of appreciation for the assistance which various members of the Oak Ridge National Laboratory have so generously contributed. In particular, the guidance of the group consultant, R. S. Livingston, is gratefully acknowledged.

F. C. VonderLage

for

The Faculty of ORSORT

This investigation of a design for a nuclear reactor package power plant suitable for use in remote locations was undertaken by nine students in the 1954 class of the Oak Ridge School of Reactor Technology. As background material the group was referred to the report "A Conceptual Design of a Pressurized-Water Package Power Reactor," ORNL 1613, and to numerous studies of boiling reactors at the Argonne National Laboratory. Dr. Untermeyer and Dr. Draley, of that Laboratory, provided valuable preliminary information which enabled the group to evaluate their major problems at an early date.

The studies by the Operations Research Office, John Hopkins University, of the economics of nuclear electrical generation stations for the Arctic showed that the extent of usefulness of nuclear power is very sensitive to the capital costs of the reactor system. It was our belief at the inception of this study that the boiling heterogeneous system, and its attendant reductions in ancillary equipment, offered the best possibility of reducing the costs, as compared with the design developed from the pressurized-water reactor. The results of the present study have corroborated this belief.

The group attempted to investigate the critical points of design thoroughly; many non-controversial or non-critical items were treated casually in order to permit thorough investigations of the more definitive problems. The group is to be complimented for its sensitive appreciation of the problems involved and for its mature and well-planned approach to them.

Robert S. Livingston
Director
Electronuclear Research Division

ACKNOWLEDGEMENTS

The preparation of this report was facilitated by the assistance and advice of many individuals. A. L. Boch, A. M. Perry and G. F. Leichsenring of the ORNL Package Reactor Group and W. R. Gall (ORNL), contributed much to all aspects of our work.

Talks on boiling reactor systems by S. Untermeyer (ANL) and R. G. Mallon (Bendix Aviation Corporation) helped start the project off in the right direction. J. E. Draley (ANL), L. Schreib (American Machine and Foundry Company), and J. E. Cunningham (ORNL) aided in metallurgical problems and fuel element design. Advice on nuclear calculations was received from R. L. Murray (North Carolina State College) and M. C. Edlund (ORNL). Help in heat transfer problems was given by A. S. Jameson (ANL), P. C. Zmola (ORNL), and L. G. Alexander (ORNL). Shielding calculations were eased by the help of W. R. Pearce (Bendix Aviation Corporation) and E. P. Blizard (ORNL). R. C. Robertson, (University of Tennessee) and W. P. Walker (ORNL) aided in the steam system design and instrumentation, respectively. Advice on the reactor simulator study was given by E. R. Mann (ORNL) and P. R. Kasten (ORNL). F. T. Howard (ORNL) assisted with the editorial work.

A final word of thanks to our group advisor, R. S. Livingston, who gave us the problem, and provided us with much sound advice and guidance.

ABSTRACT

This design study describes a reactor and associated power plant designed to produce 1050 kw of net electric power and 3535 kw of steam for heating purposes. The total thermal output of the reactor is 10,000 kw. The fuel plates consist of highly enriched UO_2 imbedded in a matrix of stainless steel and clad on all sides with stainless steel. The core is cooled and moderated by naturally circulated, boiling, light water. At full power the core has an average void fraction of 20% by volume in the coolant. The saturated steam, at 415 psia and 448.2°F, is used to drive a turbogenerator. This steam is also used to generate non-radioactive steam for space heating.

The reactor is loaded with 18.1 kg of U 235 and will supply 15 megawatt-years of energy before refueling is required. This corresponds to 2.5 years of operation at an average load factor of 60%. Burnout poison in the form of B_4C is incorporated to reduce the reactivity excursion and thus facilitate control.

The major objective has been to design a reactor which will require a minimum of development effort and yet be reliable and inexpensive. The estimated capital investment is $1,258,400. The estimated cost per kilowatt-hour for net electric and steam power at the bus, based on a 60% load demand is 4.43 cents and 1.08 cents, respectively.

TABLE OF CONTENTS

1.0 GENERAL CONSIDERATIONS

1.1 Statement of the Problem

Problem: To design a 10-Mw boiling, heterogeneous, enriched-uranium reactor to produce 3535 kw of barracks space heating and at least 1000 kw of electricity for a remote, arctic, military installation.

Design philosophy: The design of the reactor and its associated steam system will be governed by the following:

a. The system must be reliable.

b. The system must be simple both in design and operation.

c. Design will be based on a minimum development effort; equipment items will be chosen from catalogues and "off the shelf" insofar as possible.

d. The overall plant cost must be as low as possible.

e. The power cost should be competitive with conventional fuel power costs in the same location.

1.2 Site Conditions

Location is a major factor which influences the design of a package reactor power plant. The chief usefulness of the package reactor is its portability. It can be located in remote places where transportation is difficult and even impossible for extended periods of time.

A typical application for which a package nuclear powered plant would be ideally suited is an Aircraft Control and Warning (AC & W)

station. These installations are in remote locations and are generally difficult to supply. Depending on the station location, logistic support is by one of the following*:

1. Ocean shipping (Liberty ship)

   a. Permissible weight - 30 tons
   b. No limit on cubage
   c. Equipment size limited by largest liberty ship hatch - 35 x 20 ft. Larger equipment could be deck loaded.

2. Air lift (C-119 aircraft)

   a. Permissible weight - 15 tons
   b. Cargo space - 36 x 9 x 8 ft
   c. Equipment size limited by size of cargo door - 9 x 8 ft.

3. Overland tractor-train

   a. Permissible weight - 10 tons
   b. Equipment size limited by size of sled - 24 x 8 ft.

If the reactor is to be used at these stations, such physical characteristics of the site as the weather conditions and the terrain must be investigated insofar as they will directly affect the design. The following site conditions are assumed or found to be applicable** to the design of the nuclear powered plant:

1. Water supply is limited to amounts that can be hauled by trucks.
2. All structures must be constructed above grade, due to existence of permafrost.
3. The ambient air temperature range is from -50 F°to +75° F.

---

* Study of the Possible Military Application of Nuclear Energy at Remote AC & W Stations, Mil. Plans Div., O.C.E., ORNL-CF-53-7-135, July 23, 1953.

** Arctic Construction, Dept. of the Army, TM5-560, June 1952.

4. The maximum wind velocity is 50 mph.

5. All materials for construction and operation must be transportable by air. Aggregates for concrete are available at the site.

6. Supplies for a 13-month period must be shipped in during the summer months and stored at the site.

1.3 Load Analysis

A typical Type-II AC & W Station* is generally located at the base of a mountain with the radar towers and operating buildings at the top of the mountain. In a few cases the entire installation is located on the mountain top. To minimize the costs of electric, heating, and water distribution systems , the camps at Type-II stations are designed in two units. Each unit has a separate electric plant and heating plant rated at 500 kw electric generating capacity and 200 boiler horse power heating capacity. Low-pour diesel oil is the fuel for both systems.

The following data concerning electric and heat systems is for a typical Type-II AC & W Station:

ELECTRICAL SYSTEM

Connected load, kw	1000
Average demand load, kw	600
Stand-by provided, kw	400
Peak demand load, kw	1000
Generators, diesel driven, 3-phase, 60-cps	10
Rated capacity, each, kw	100
Voltage, volts	120/208
Transmission line, volts	4160
Station lighting, volts	120
Radar and associated equipment, volts	120/208

* Study of the Possible Military Application of Nuclear Energy at Remote AC & W Station, Mil. Plans Div., O.C.E., ORNL CF-53-7-135, July 23, 1953.

HEATING SYSTEM

Design temperature range, °F	-40 to +70
Design heating load, Btu/hr	11.2×10^6 (46,700 EDR* or 3800 kw, including transmission losses)
Steam generators, Cyclotherm, number	2
Capacity, each, boiler hp	200
Boilers, maximum working pressure, psi	150
Rated heating surface, sq ft	648
Rating, boiler hp	176
Steam lb/hr	6900
Steam distribution pressure, psig	45 to 50

Graphical heating load data for Thule, Greenland, indicate average values as follows:

For any one month:

Maximum heating load, kw	2650 (37,700 EDR)
Minimum heating load, kw	550 (7,820 EDR)

For any one day:

Maximum heating load, kw	3800 (54,060 EDR)
Minimum heating load, kw	0.00

The average annual mean heating load is indicated as 1,800 kw (25,600 EDR)

On the basis of the above data, the following design values were used for the reactor:

Electrical

Installed capacity of generator, kw	1,250
Peak demand, kw	1,000
Peak demand of plant auxiliaries, kw	250
Average demand, kw	600
Average demand of auxiliaries, kw	225
Total average generator load, kw	825

* EDR = Equivalent Direct Radiation, 1 EDR = 239.8 Btu/hr.

Heating

Peak heating load	*
Average heating load, kw	1,800 (25,600 EDR)
Minimum heating load, kw	0

1.4 Selection of Design Parameters

1.4.1 Selection of Reactor Core Type. The following reactor core types were initially considered:

a. Borax type core** in which the fuel is in the form of solid fuel plates and water acts as both moderator and coolant.

b. Bendix type core*** in which the fuel is in the form of fuel tubes. The reactor is moderated by heavy density graphite and cooled by boiling water in the tubes.

c. KAPL type core**** in which the fuel is in the form of slugs. The reactor is moderated both by graphite and pre-heat water and cooled by boiling water in process tubes concentric with fuel slugs.

---

* Since it was difficult to arrive at a value for the maximum heating load based on available data for arctic bases, this load was not fixed for design purposes. The reactor was designed for 10 Mw at full power output, the electrical system designed for 1300 kw gross generation, and the remaining heat available for the peak heating system load computed to be approximately 3535 kw (12,070,000 Btu/hr, 60,300 EDR, 362 Bhp). This value appears to be capable of supplying the heating requirements.

** Transient and Steady-State Characteristics of a Boiling Reactor, Borax Experiments, 1953, ANL-5211, Feb. 1953.

*** Coneybear, J. F., et al, A 1000 Kw Reactor Power Plant, BAC/RL-610, June 15, 1953.

**** Weil, J. W., et al, Study of a Boiling Reactor Steam Plant for Central Station Power, KAPL-1136, May 17, 1954.

Both the Bendix and KAPL cores incorporate a non-variable density moderator (graphite) for stability. In this way they are able to produce large fractions of steam per pass of water. The Borax type core, on the other hand, depends on the water for all its moderation as well as for cooling. This core produces a small fraction of steam per pass in order to maintain stability. Obviously, the Borax core is the more simple as far as fabrication and construction are concerned. It also promises to have a lower core cost. For these reasons, the Borax core was selected for this reactor.

1.4.2 Selection of Core Construction Material. The following materials were considered for fuel cladding and core structure:

a. Aluminum
b. Zirconium
c. Stainless steel

All three of the materials have found favorable use in reactor designs in the past. Aluminum has been used mainly in low temperature systems while zirconium and stainless steel have found application at higher temperatures. A thorough investigation of the high temperature corrosion properties of aluminum indicated that this material would not be suitable for a boiling system where long core life and reasonably high temperatures were expected (see Appendix 12.1). Although zirconium has excellent high temperature properties and a low thermal neutron absorption cross section, it was ruled out because of the high cost of fabrication. As a result, stainless steel was selected as the core structural material. A thorough discussion of a stainless steel fuel element similar to the one selected for this reactor has been reported elsewhere* and will not be treated further here.

*A. L. Boch, W. R. Gall, G. F. Leichsenring, and R. S. Livingston, "A Conceptual Design of a Pressurized-Water Package Power Reactor". ORNL Report 1613, July 1954 (Hereafter referred to as ORNL-1613).

1.4.3 Selection of Operating Temperature and Pressure. Because of the excellent high temperature properties of stainless steel, a wide range of temperatures and pressures is available. The following points were used to select the operating conditions of this reactor:

a. Quality of steam at the exit of turbine

b. Volume flow rate of steam

In order to keep this system simple, it was decided not to use super heat or reheat in the cycle. Therefore, the exit quality at the turbine became a direct function of the steam pressure at the turbine inlet. It was decided to keep this exit quality below 15% moisture in order to avoid erosion of the last row of blades in the turbine. At the same time it was desirable to keep the volume flow rate of steam in the system at a reasonably low figure. A study of turbine-exit-steam quality vs inlet pressure (see Fig. 1) and volume flow rate vs pressure (see Fig. 24) indicated a saturated steam pressure of 415 psia as a reasonable operating pressure. The saturated temperature corresponding to this pressure is 448.2 °F.

1.4.4. Core Design. The following items were considered in arriving at the core design:

a. Since stainless steel was chosen as the core structural material, it was decided to use the same type of fuel element as the pressurized-water package reactor (see ORNL-1613). This element consists of the following:

1. Fuel matrix consisting of stainless steel, UO_2 with the uranium enriched to 93.5% U 235, and B_4C as the burnup poison.

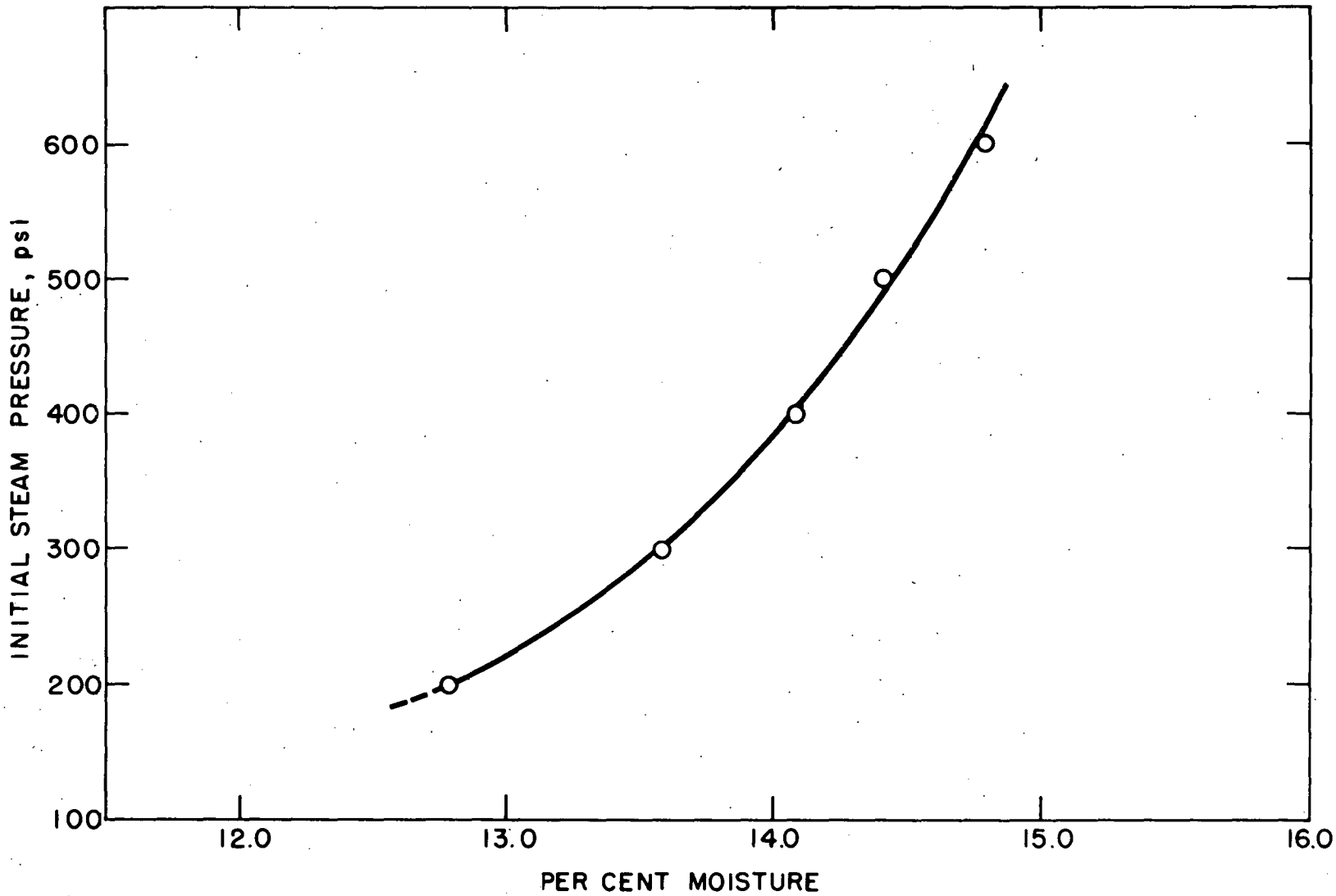

INITIAL STEAM PRESSURE VS. PER CENT MOISTURE
FOR A 1500 KW. TURBINE

Figure 1

2. The matrix is clad with 5 mils of stainless steel.

3. The plates are held together by two side plates 80 mils thick*.

b. For simplicity in thermal and nuclear calculations, a core shaped in the form of a cube was decided upon. This was to be accomplished by a 7 x 7 loading of fuel assemblies.

c. Since the critical mass was an uncertainty it was decided to allow for up to 35 kg of U 235 in the matrix.

d. Metallurgical considerations require that the UO_2 content of the fuel matrix be kept below 50% by volume.

e. Boiling heat transfer considerations indicated that a small heat transfer area and a plate spacing of about one-half inch were desirable.

f. A bare reactor calculation based on a one-velocity model, with a fast leakage correction term and reflector savings, showed that the critical mass increased with increasing metal-to-water ratio in the core, as was expected.

When all these considerations were combined, the calculations yielded a metal-to-water ratio of 0.132. By using the same nuclear model as described in (f) above with this metal-to-water ratio, a plot was made of buckling vs critical mass (see Fig. 2). The minimum point on this curve gave a core size of 23.2 in. on a side. This value, coupled with the metal-to-water ratio and the required 7 x 7 loading, yielded the final fuel plate and fuel assembly design.

* Recent developments indicate that side plate thickness can be reduced considerably. See Chapter 11, this report.

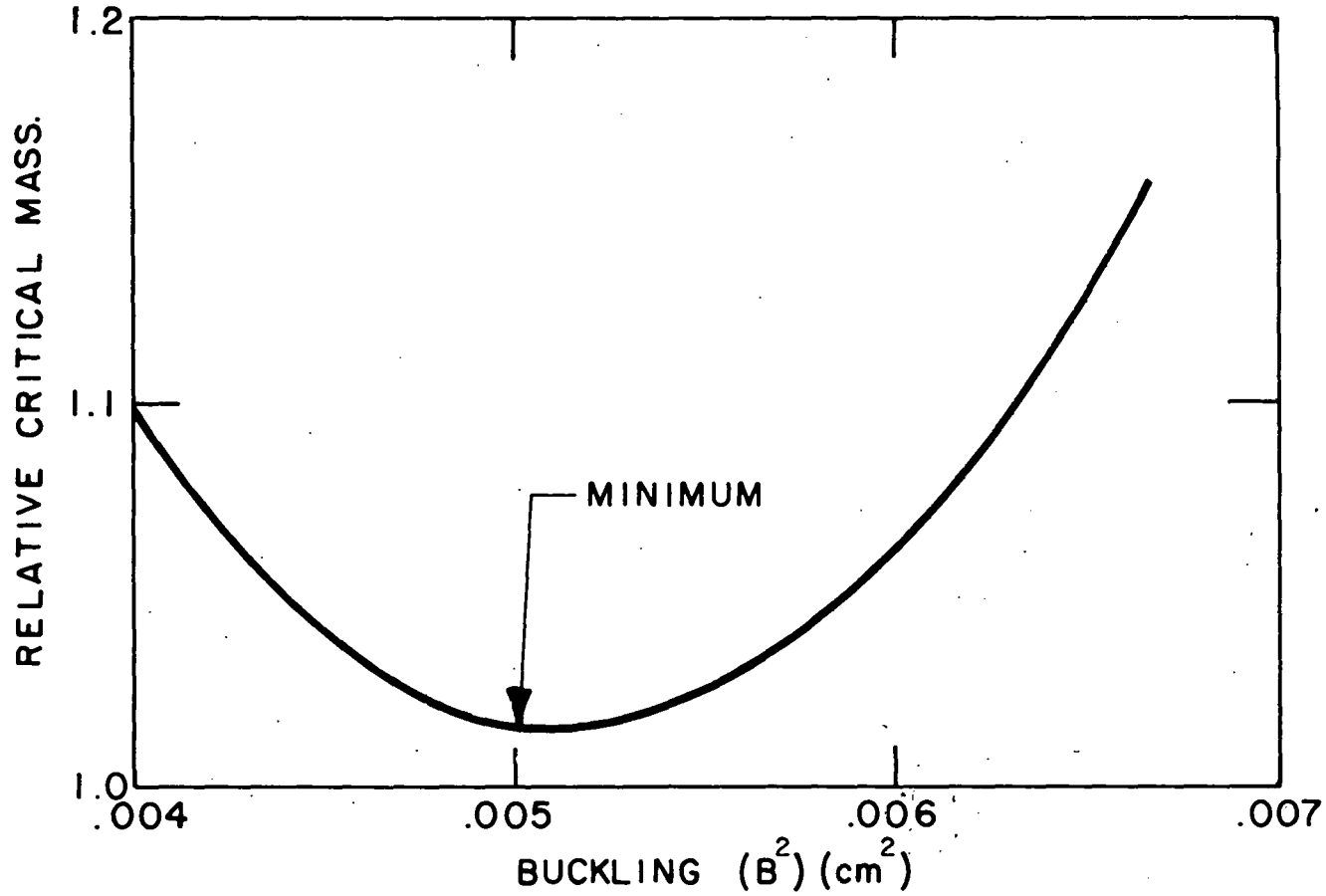

RELATIVE CRITICAL MASS. VS. B^2

Figure 2

1.4.5 Selection of Steam Void Fraction. The average steam void fraction in the core was selected by comparing the effect of the steam void fraction on both recirculation ratio and critical mass. These effects are opposing; i.e., with increasing void fraction the recirculation ratio goes down (see Fig. 3) and the critical mass goes up (see Fig. 4). An average void fraction of 20% was chosen since it gave a reasonably low recirculation ratio without prejudicing, too much, the critical mass.

1.5 Plant System

The main essentials of the plant are the reactor, barracks heat exchanger, turbine-generator, turbine condenser, deaerating heater and associated pumps. (see Fig. 5).

Steam is generated in the reactor core and removed by natural circulation. The vapor is separated from the entrained moisture by several baffles and a toroidal dry pipe in the top of the reactor vessel. Steam conditions leaving the reactor are 415 psia, 448.2 °F, with a quality of approximately 99.8%. The steam flows directly from the reactor vessel to the barracks heat exchanger and turbine-generator which are connected in parallel.

The barracks heat exchanger utilizes reactor steam to heat condensate, from the barracks heating system, to saturated steam. This exchanger consists of a preheater in which the condensate is heated from 100 °F to 252 °F prior to entering the evaporator, where the condensate is evaporated to steam at 60 psia. Reactor steam on the other hand is condensed in the evaporator and subcooled to 328 °F in the preheater and then drained to the deaerator.

ORNL-LR-Dwg. 6060

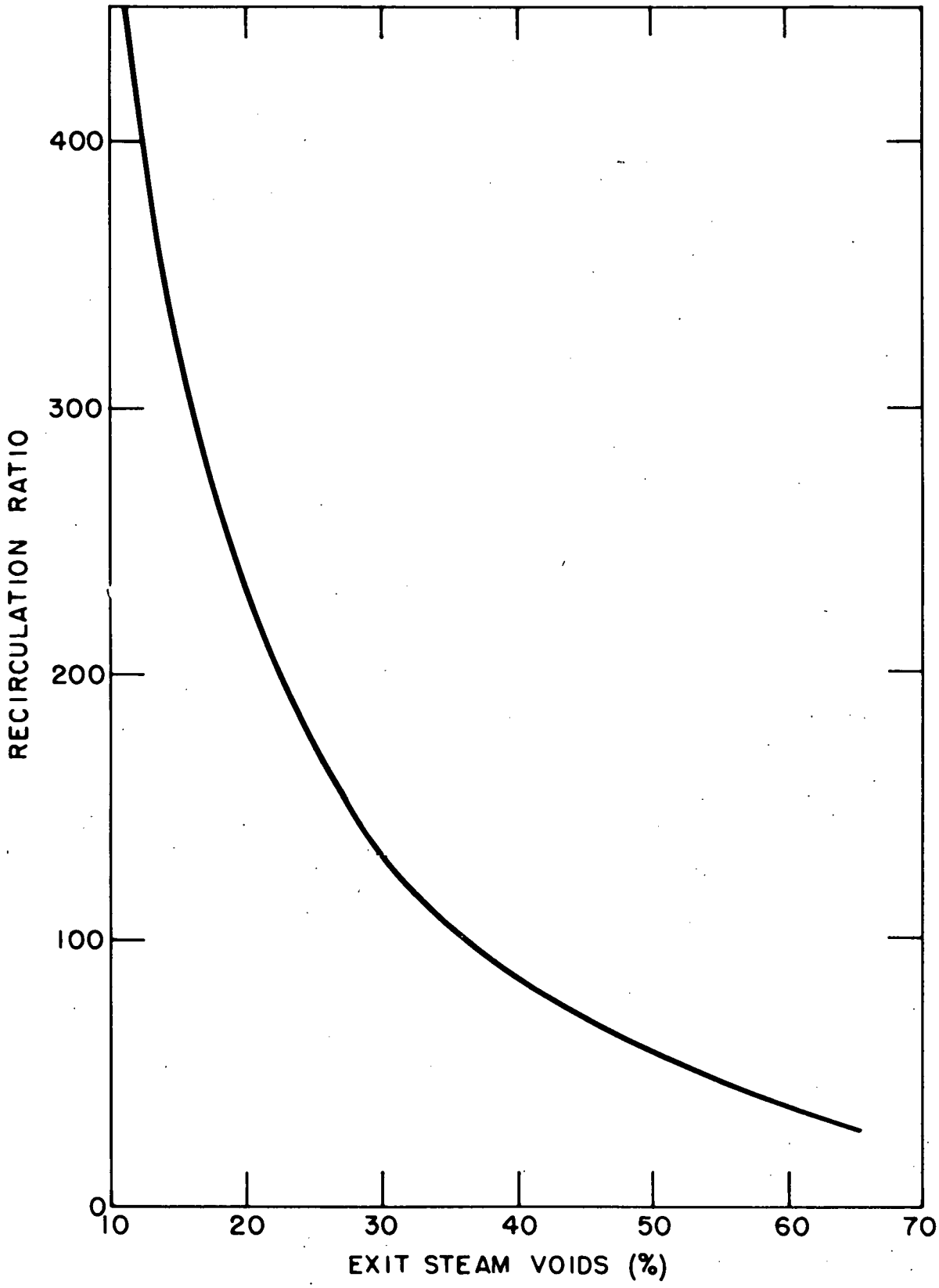

RECIRCULATION RATIO VS. EXIT STEAM VOIDS
FOR 415 psia SATURATED STEAM
AT 33710 POUNDS PER HOUR

Figure 3

ORNL-LR-Dwg. 6061

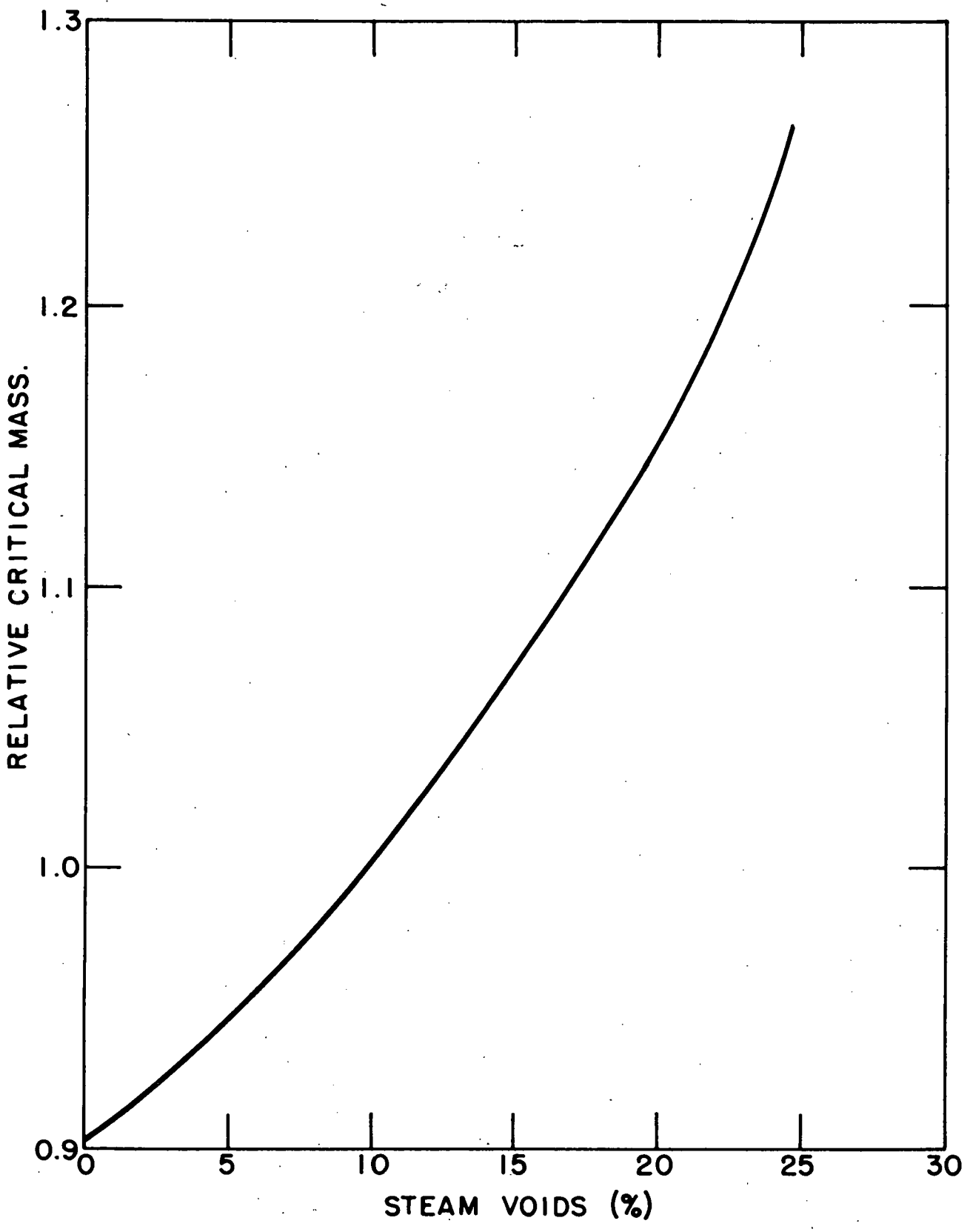

EFFECT OF STEAM VOIDS ON CRITICAL MASS.

Figure 4

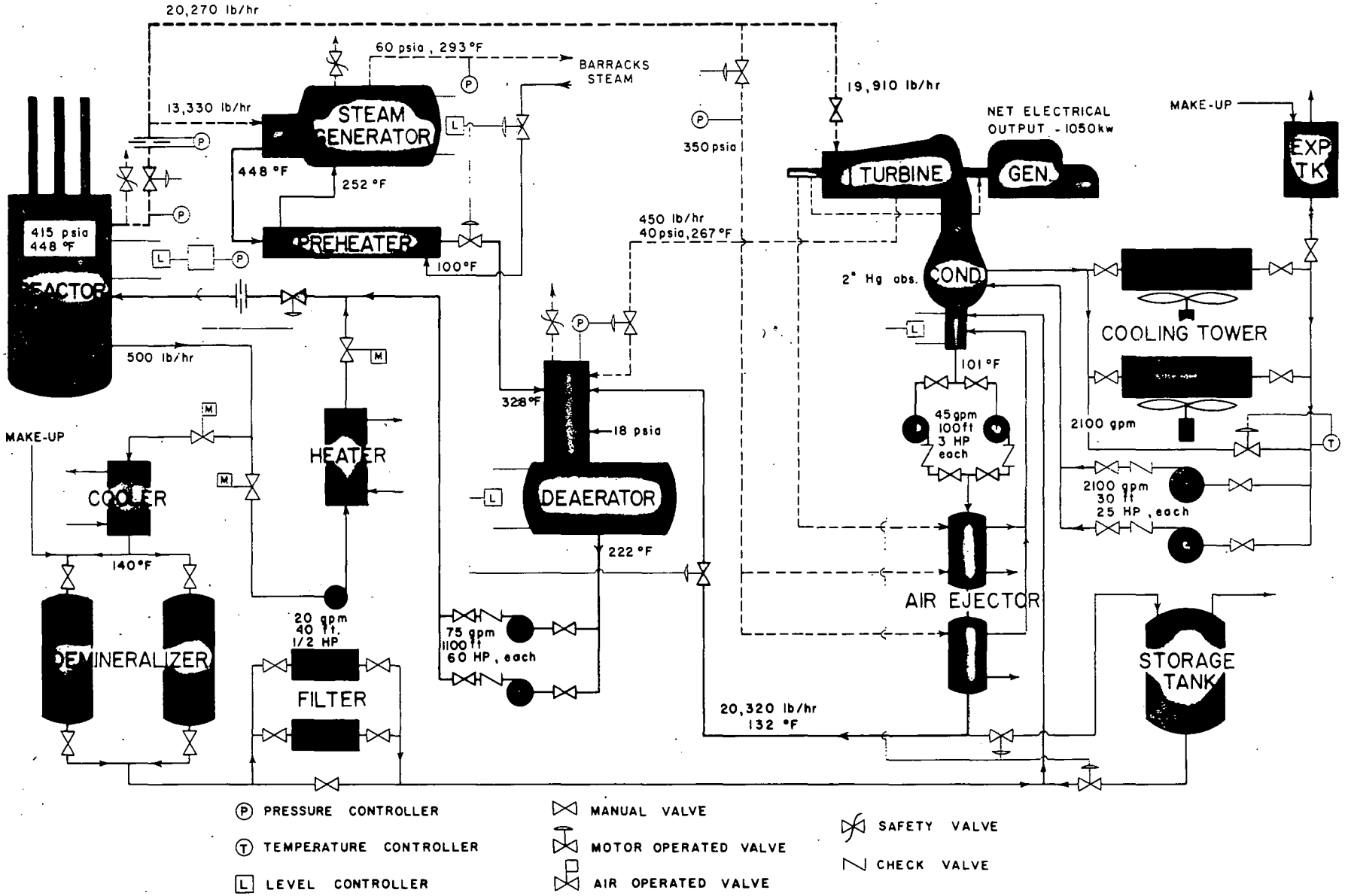

FLOW DIAGRAM

Figure 5

Reactor steam is also utilized to generate the required electrical energy with the turbine-generator. Part way through the turbine some steam is bled off to the deaerator where it is used to heat the condensate from both the hotwell and the barracks heat exchanger to saturated water at 18 psia. The main flow is, however, through the turbine to the turbine condenser where the steam is condensed and the condensate pumped from the condenser hotwell to the deaerator.

A small amount of reactor steam is used as motive steam for the steam jet air ejector and the gland steam air ejector. This steam is condensed by condensate going to the deaerator and returned to the systeam by way of the condenser. The steam jet air ejector removes non-condensable gases from the turbine condenser while the gland steam air ejector removes a steam-air mixture from the outboard leak-off point on the turbine shaft which results in the elimination of reactor steam leakage into the turbine room.

The deaerator removes gases from the condensate and drains, heats the feedwater to saturation temperature and serves as a surge tank for the reactor feed pumps during load swings.

Apart from the main system just described, there are several other systems which are essential to the operation of the plant. These are the condenser cooling system, the water purification system and the start-up system.

The condenser cooling water removes the heat given up in the turbine condenser by the condensation of the exhaust steam and dissipates this heat in the air-cooled heat exchanger.

The high water purity of the system is maintained by bleeding off a quantity of feedwater from the reactor, cooling it down to 100 °F and passing it through a demineralizer and a micrometallic filter to remove the impurities. Make-up to the system is added to the bleed off after the cooler. The purified water is returned to the system through the turbine condenser.

During start-up, the feedwater in the reactor is circulated through a small heat exchanger by a pump. Site steam is used to heat the water up to operating temperature and pressure. In a similar manner, the feedwater in the reactor can be cooled after shutdown by circulating the feedwater through the start-up heat exchanger. In this case, condenser cooling water is used to cool the feedwater.

1.6 Design Data

The following is a summary of design data on the boiling heterogeneous package reactor. More complete descriptions of the individual components listed here may be found in subsequent sections of the report, along with some of the design considerations involved.

1.6.1 Overall Plant Performance.

Thermal power developed in reactor	kw Btu/hr	10,000 3.41×10^7
Electric power generated	kw	1300
Net electric power delivered	kw	1050
Power required for auxiliaries	kw	250
Steam heat load delivered	kw	3535
Overall thermal efficiency	%	45.9

Thermal efficiency of net electric power generation	%	16.2
Power density of reactor core	kw/liter	48.3
Core life before refueling	mw-yr	15

1.6.2. Reactor Data

Core:

Height	in.	23.25
Width	in.	23.315
Breadth	in.	23.315
Volume of core	cu. in. liters	12,638 207.1
Uranium content of new core 93.5% U 235 U 235	 kg kg	 19.4 18.1
Critical mass after 15 Mw-yr	kg U 235	10.6
Stainless steel content	kg	171.2
Poison content, natural boron	kg	0.220
B_4C content	kg	0.281
UO_2 content	kg	22.0
Water content	liters	183.0
at 448.2 °F, 20% voids at 68°F, 0% voids	kg kg	121.4 183.0
Metal-to-water volume ratio		0.132
Steam voids at full power average	%	20
Reactivity in 20% steam voids	%	3
Excess reactivity, new, cold, clean core	%	13
Maximum reactivity during operating period, hot, 20% steam voids cold, 0% steam voids	% %	7 19

Neutron flux, average, thermal, at end of 15 Mw-yr cycle	n/cm^2-sec	1.9×10^{13}
Reflector thickness (water) (across flats)	in.	8

Fuel Plates (Regular):

Type of plates:
Rectangular, flat, UO_2-SS-B_4C core, clad in 304L stainless steel

Geometry of plates		Fuel Core	Overall
Thickness	in.	0.025	0.035
Width	in.	2.925	3.205
Length	in.	23.25	24.25
Stainless steel cladding			
Thickness	in.		0.005
Spacing between plates	in.		0.440
Composition of fuel section of plates			
UO_2	wt %		27.29
SS	wt %		72.36
B_4C	wt %		0.35
Geometry of stainless side plates			
Thickness	in.		0.080
Width	in.		3.285
Length	in.		27.25
Atom ratios in reactor core			
U 235		atoms	1
H_2O		molecules	87.52
Fe, Ni, Cr		atoms	40.55
B		atoms	0.264

Fuel Plates (control-rod active assembly):

Type of plates: previously described

		Fuel	Overall
Geometry of plates:			
Thickness	in.	0.0452	0.0552
Width	in.	2.265	2.545
Length	in.	23.25	24.25
Stainless steel cladding			
Thickness	in.		0.005
Spacing between plates	in.		0.376
Composition of fuel section of plates:		previously described	
Geometry of stainless steel side plates			
Thickness	in.		0.080
Width	in.		2.315
Length	in.		27.25
Fuel plates per fuel assembly		7	
Number of fuel assemblies		44	
Fuel plates per control rod assembly		5	
Number of control rod assemblies		5	
total number of fuel plates		333	
Dimensions of fuel assembly (Overall)			
Thickness	in.	3.285	
Width	in.	3.285	
Length	in.	31.25	
Tolerances			
Particle size of UO_2, max.	μ	86	
min.	μ	44	
Thickness of fuel plates	in.	±0.001	

Control Rods:

Type: Upper section absorber material, cylindrical.
Lower section fuel assembly, rectangular.
Both to fit fuel space in lattice.

Composition:

Upper Section: 16.3% B_4C by weight in Cu, 1/8 in. thick; clad with 304L ss, 1/32 in. thick; formed into cylinder
Lower Section: Previously described

Geometry:

Upper Section: 2.565 in. O.D. cylinder x 30 in.
Lower Section: 2.625 x 2.315 x 38.5 in.

Number:

Shim rods	4
Regulating rod	1

Travel:

Shim rods	in.	23.25
Regulating rod	in.	23.25
Acceleration of rods after release	ft/sec^2	32.2
Maximum distance for rods to drop	in.	23.25

Thermal Data of Reactor at Full Power (10,000 kw):

Operating pressure in reactor	psia	415
Feedwater inlet temperature	°F	222.4
Steam outlet temperature	°F	448.2
Properties of coolant		
Density at inlet of core	lb/ft^3	51.5
Density at outlet of core	lb/ft^3	31.1
Average density in core	lb/ft^3	41.5
Quality at core outlet	%	1.155
Coolant flow through core	lb/hr	2.87×10^6
Number of flow passes through reactor		1
Flow area in core	ft^2	3.336
Recirculation ratio		85.0

Core inlet velocity	ft/sec	4.65
Design heat output	Btu/hr	3.41×10^7
Heat transfer area	ft^2	324.0
Average heat flux	Btu/hr-ft^2	105,300
Peak-to-average heat flux ratio (assumed for design purposes)		4:1
Maximum surface temperature	°F	~480
Maximum fuel temperature	°F	~522

Pressure Vessel (SA 212B clad with 304 ss):

Inside diameter	in.	48
Wall thickness (excluding cladding)	in.	1
Thickness of cladding	in.	0.109
Design stress	psi	17,000
Overall length of vessel	in.	184
Thickness of head	in.	5
Diameter of head	in.	50
Diameter of opening at top of vessel	in.	38
Inside diameter of thermal shield	in.	40
Thickness of thermal shield	in.	1
Length of thermal shield	in.	29
Insulation (Foamglas) thickness	in.	4

1.6.3. Control-Rod Drive Mechanism:

(See ORNL-1613, page 25)

1.6.4. Water Purification System:

Capacity	gpm	2.3
Effluent purity	megohms/cm	10

Concentration of solids in reactor	ppm	2
Operating temperature	°F	100
Maximum water temperature	°F	140

Design for Oak Ridge make-up water:

Make-up water	gpm	1.0
Recirculating water	gpm	1.3
Total feed	gpm	2.3
Hardness of feed water		
Anion concentration	grains/gal	3.78
Cation concentration	grains/gal	3.78
Dimensions of demineralizer vessel	18 in. dia x 6 ft long	
Resin volume		
Amberlite IR 120	ft^3	2
Amberlite IRA 400	ft^3	4
Cycle time	days	5
Regenerant required		
NaOH	lbs/cycle	40
H_2SO_4	lbs/cycle	40
Regenerant concentration		
NaOH	%	4
H_2SO_4	%	10

Design for Pure Make-up Water:

Make-up water	gpm	1.0
Recirculating water	gpm	1.3
Total feed	gpm	2.3
Hardness of feed water		
Anion concentration	grains/gal	0.21
Cation concentration	grains/gal	0.21

Dimensions of demineralizer vessel	14 in dia x 7 ft long	
Resin volume		
Amberlite IR 120	ft^3	1.5
Amberlite IRA 400	ft^3	3
Cycle time	days	120
Regenerant required		
NaOH	lbs/cycle	30
H_2SO_4	lbs/cycle	30
Regenerant concentration		
NaOh	%	4
H_2SO_4	%	10

1.6.5 Shield, ordinary concrete:

Density	gm/cc	2.33
Tolerance dose for 56-hr week	mrep/hr	5.36
Thickness of concrete required around reactor vessel operating at 10 Mw:		
for 1/10 of tolerance dose rate	ft	11.4
for tolerance dose rate	ft	10.2
for ten times tolerance dose rate	ft	9.0
Thickness of concrete required above reactor vessel operating at 10 Mw:		
For 1/10 tolerance	ft	9.2
For tolerance	ft	7.9
For ten times tolerance	ft	6.6
Total volume of concrete in shield	cu yd	700
Weight of shield	tons	1340
Design tolerances in multiples of 5.36 mr/hr		
Top of shield		1
Side away from control room		10
Side toward control room		0.1
End toward serivce area		1
End away from service area		10

Shield Ventilation

Maximum heat to be removed	$Btu/hr\text{-}ft^3$	9,200
Air temperature entering shield	°F	50
Air temperature leaving shield	°F	150
Air flow required	cfm	11,000
Pumping head required in.	H_2O	3
Number of holes required in shield (~11 ft thick shield)		415

1.6.6. Steam System.

Turbogenerator, straight, condensing direct drive		1
Steam to throttle, saturated	psia	415
Exhaust pressure, absolute in.	Hg	2
Rating, at 0.8 power factor	kw	1250
Voltage	volts	4160
Frequency	cps	60
Exciter-direct-connected		
Generator-open-air cooled		
Extraction nozzle, at 450 lb/hr	psia	40
Steam to throttle, full load	lb/hr	19,910
Turbine efficiency, full load	%	65
Generator efficiency, full load	%	96
Automatic controls: frequency and voltage		
Safety devices: overspeed, low vacuum, vacuum breaker		
Exhaust quality, full load	%	86

Condenser, horizontal, shell and tube, two pass		1
Heat transfer rate	Btu/hr	21×10^6
Steam flow, max	lb/hr	22,100
Coolant temperature in, max	°F	95
Effective surface	ft^2	1200
Velocity in tubes	ft/sec	6.6
Tubes: 18 gage, 3/4 in. dia. O.D.		
Coolant, summer: water winter: ethylene glycol solution		
Coolant circulation		
Water	gpm	2100
Ethylene glycol solution	gpm	2100
Ethylene glycol		
Specific gravity		1.08
Specific heat	Btu/lb-°F	0.70
Composition, ethylene glycol	wt %	60
water	wt %	40
Viscosity	millipoises	45
Air removal equipment		
Two element, two-stage steam-jet air ejector with inter-and after-condensers		
Liquid Coolers, horizontal, air-cooled		2
Heat transfer rate	Btu/hr	21×10^6
Liquid circulation rate		
Water	gpm	2100
Ethylene glycol	gpm	2100
Face area, each	ft^2	360
Air flow, each	cfm	240,000
Fan power, each	hp	40

Temperature, liquid in	°F	125
Mean daily maxiumum air temperature	°F	70
Dimensions each	ft	23 x 19 x 13
Deaerating Feed-water Heater, tray type		
Storage tank		
Capacity	gal	500
Supply at full load	min	7
Outflow rate, max	lb/hr	34,000
Operating pressure	psia	18
Outflow temperature	°F	222
Performance, O2/liter	cc	0.005
Controls: float, overflow, low water pressure, relief, pressure		
Boiler Feed Pump, 3-stage centrifugal		2
Number running at full load		1
Speed	rpm	3600
Capacity, each	gpm	75
Head	ft	1100
Water temperature	°F	222
Estimated efficiency	%	35
Rated power, each	hp	60
Hotwell Pump, single stage centrifugal		2
Number running at full load		1
Speed	rpm	3600
Capacity, each	gpm	45
Head	ft	100

Water temperature	°F	100
Estimated efficiency	%	38
Rated power, each	hp	3
Coolant Circulating Pump, single-stage, double entry		2
Number running at full load		1
Fluid: water or 60% ethylene glycol		
Speed	rpm	1800
Capacity, each	gpm	2100
Head	ft	30
Fluid temperature	°F	95
Estimated efficiency	%	60
Drive motor size, each	hp	25
Condensate Return Pump, single-stage centrifugal with float-control and alternator		2
Number running at full load, 1/3 of time		1
Receiver capacity	gal	100
Pump capacity, each	gpm	75
Water temperature	°F	100
Head	ft	75
Estimated efficiency	%	35
Drive motor size, each	hp	2
Barracks Heat Exchanger		
Heat transfer rate	Btu/hr	10.2×10^6
Steam flow from reactor	lb/hr	13,330
Inlet pressure (tube side)	psia	415

Outlet temperature	°F	448
Barracks steam flow	lb/hr	10,870
Entering condensate temperature	°F	252
Outlet steam pressure (shell side)	psia	60

Barracks Heat Exchanger Pre-heater

Heat transfer rate	Btu/hr	1.7×10^6
Flow from the heat exchanger	lb/hr	13,330
Drain temperature	°F	328
Barracks condensate flow	lb/hr	10,870
Entering condensate temperature	°F	100

2.0 REACTOR COMPONENTS

2.1 Core Assembly

Some details of the reactor core were given in preceeding sections but a complete description requires some clarification. There are 49 lattice positions, 44 of which are filled with fuel assemblies; the other 5 positions each contain a control rod. The elements are arranged in a 7 x 7 square which gives an approximate cubical shape to the core. There is one central control rod and the other four are on a concentric circle 2 lattice positions from the center and equally spaced on the circle. Maximum obtainable reactivity occurs when all the control rods are in their upper-most position. This removes all poison rods and inserts all of the fuel possible.

The core assembly is shown in Fig. 6. To aid in visualizing the assembly a typical shutdown and fuel loading will be described. The control rods are driven down until the poison sections are in the core. Withdrawal of the water in the vessel through the demineralizer cooler, the pump, and then back into the vessel is begun. This is continued until the water is cooled below 212°F and the pressure in the reactor vessel is at one atmosphere. The control rods are then driven to their bottom-most position which unlatches the drive rods from the control rods proper. The pit above the reactor is flooded with water to a depth of about 2 feet and the water level in the reactor is brought up to the top. After the shield plugs are removed, an impact wrench is used to remove the 22 bolts holding the top cover to the pressure vessel. The overhead crane is then used to lift the cover (after electrical connections are broken) and remove it to a shielded section of the building.

ORNL-LR-Dwg. 6063

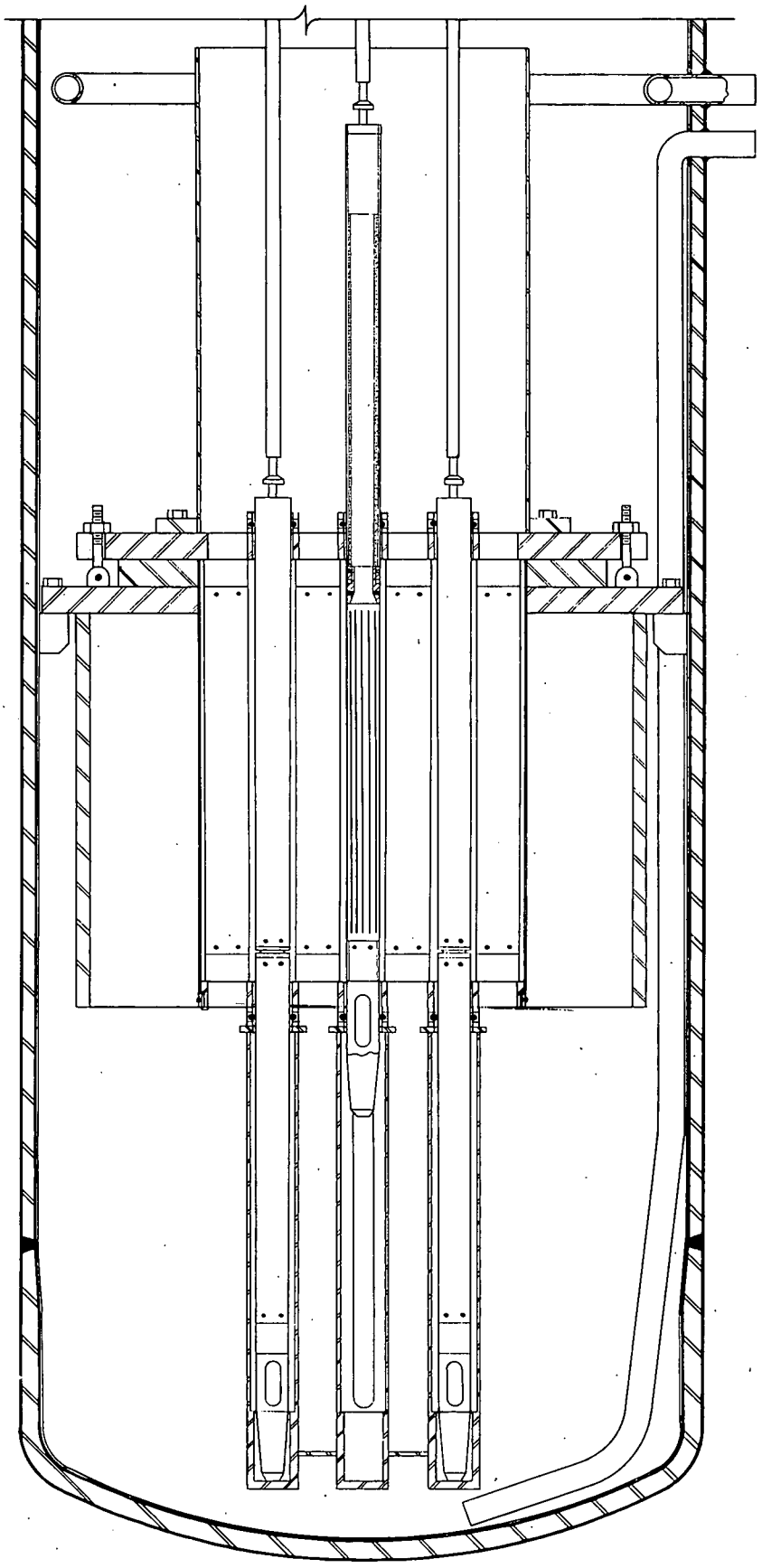

CORE ASSEMBLY

Figure 6

It will be necessary to place the cover on a stand so that there will be no damage to the drive rods projecting below the cover. Next the swing-away bolts securing the baffle plate are loosened and the baffle plate removed. The bolts securing the riser are then loosened and the riser lifted out of the vessel. It is anticipated that there will be sufficient space inside the reactor's pit to store the baffle, riser, and upper grid. The upper grid is removed after loosening of the bolts and the fuel elements are then accessible. By means of a special long-handled tool that attaches to grooves in the end box, the fuel elements will either be removed to the water storage tank placed along the outside of the pressure vessel or turned over and reinserted into the lower grid. After reloading, the upper grid will be replaced and then the reverse of the procedure described before will be followed. On startup, the reactor water will be circulated through the by-pass heater and brought up to 448° F before any attempt is made to allow the reactor to go critical. Following this the startup procedure, described in Section 2.4, will be used.

2.1.1 Fuel Assemblies

The fuel assemblies for this reactor are similar to those designed for the APPR and described in ORNL-1613. Referring to Figs. 7 and 8 it can be seen that the active (fuel bearing) section of the elements consists of 7 fuel plates brazed to stainless steel side plates. The two outside fuel plates and the two side plates extend 1 1/2 in. in each direction beyond the end of the fuel plates. These extended sections are plug welded to square end boxes, made of cast stainless steel. The end boxes serve as fastening pieces to hold the fuel in the lattice

ORNL-LR-Dwg. 6064

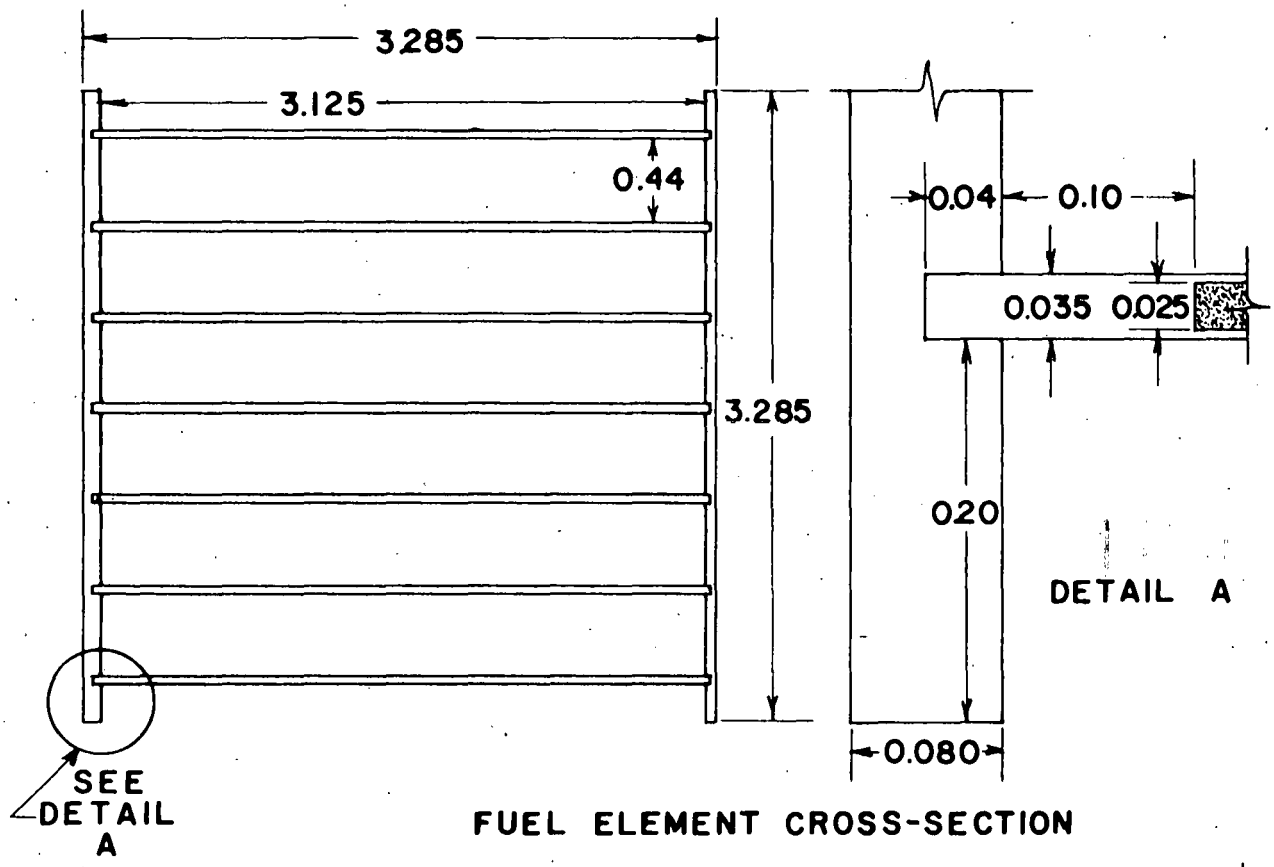

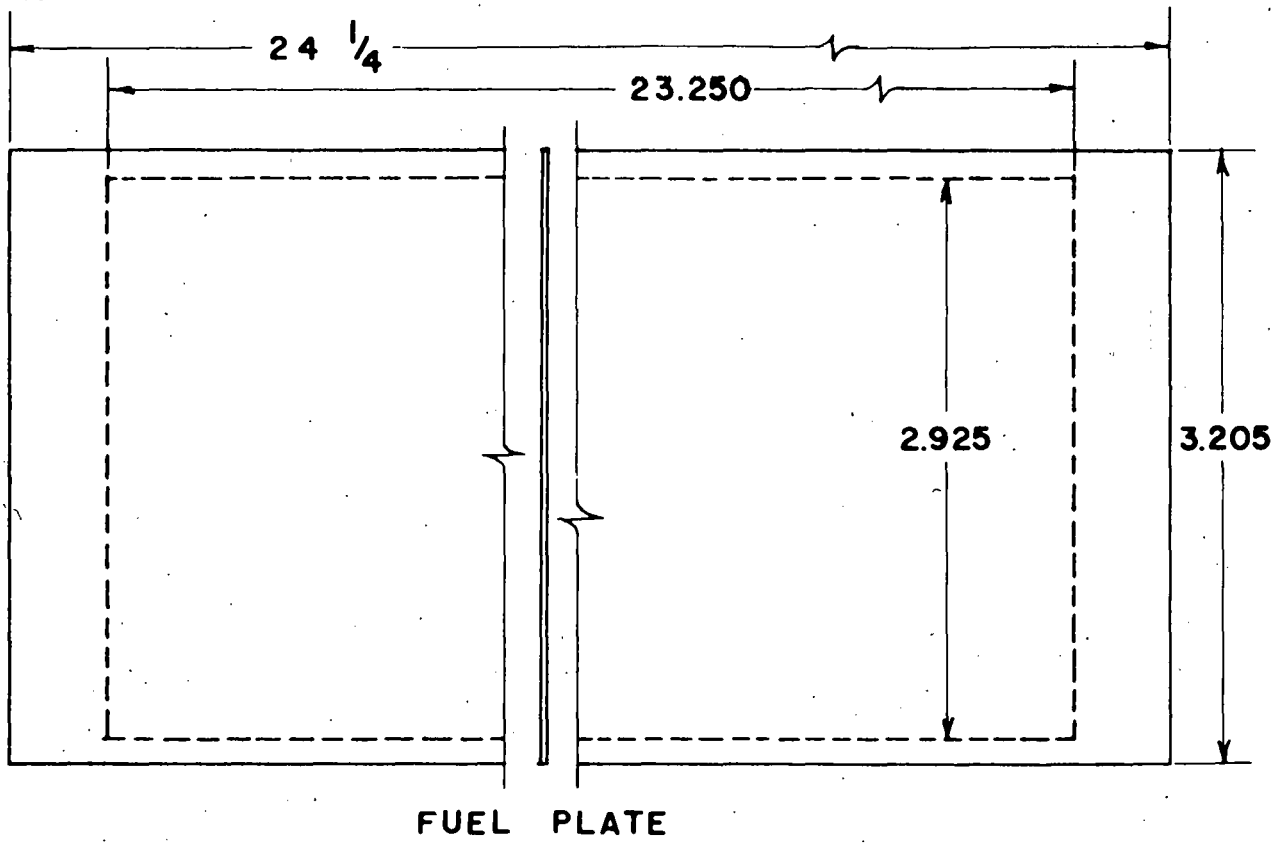

Figure 7

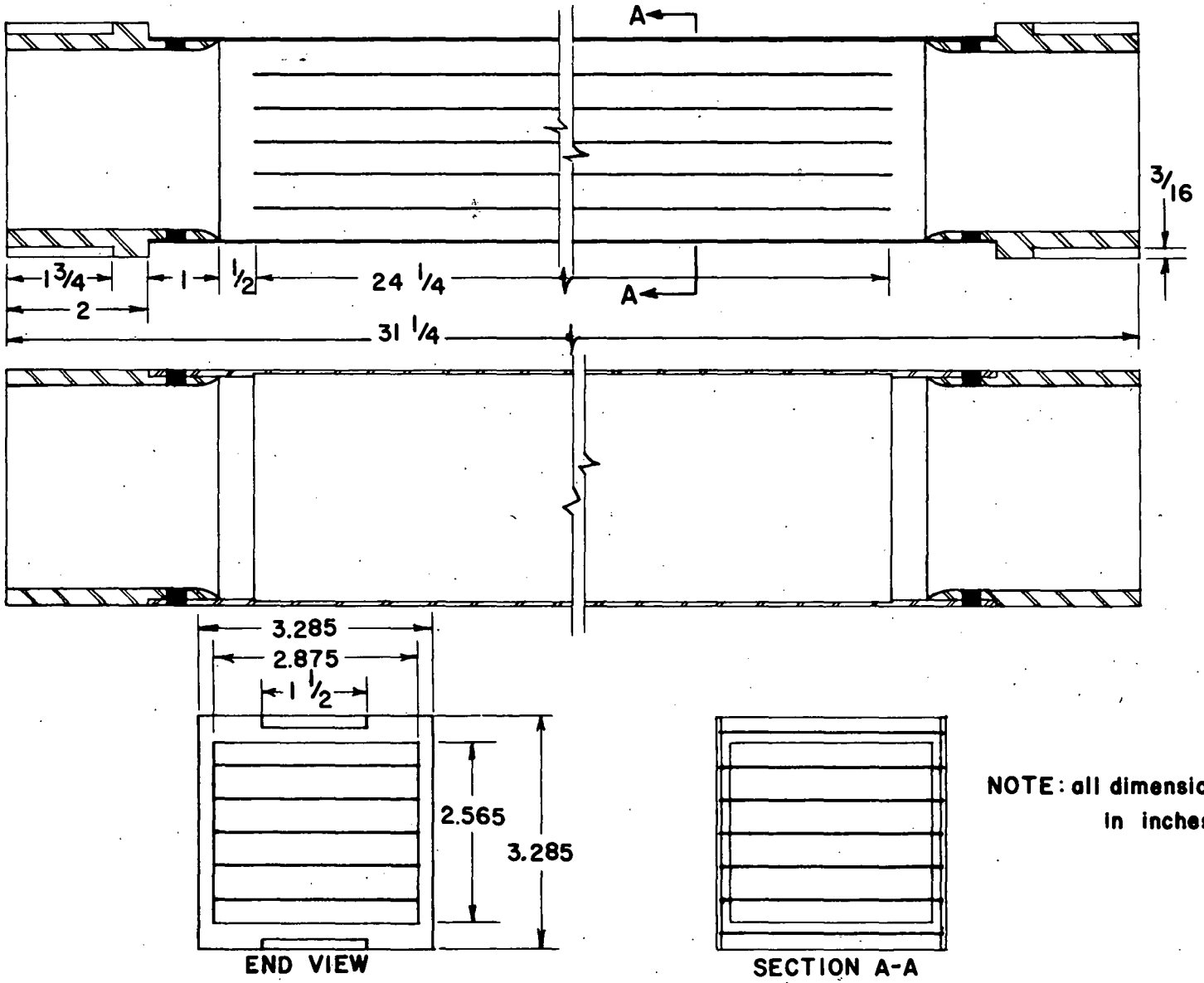

FUEL ASSEMBLY

Figure 8

configuration. They are identical so that in the event of non-uniform burn-up of the fuel (as is expected because of poisoning by the control rods) the fuel elements may be removed at some time during their life cycle, inverted, and reinserted into the core. The alteration of the shape from round to square was made to give greater flow area and thus smaller pressure drop from the same flow volume. This was necessary to insure natural circulation of the coolant water.

The individual fuel plates, show in Fig. 7, are made by the picture-frame, sandwich technique. In this method, a fuel mixture of graded uranium dioxide and 304 ss powder, with a suitable binder, is compacted into a small block about 3/4 x 3/4 x 1/8 in. This block is sintered to drive off the binder and give a reasonable strength. This piece is then coined to exact size and is placed in a 304 ss frame, covered on both sides with stainless steel plate and the edges welded. The whole sandwich is rolled to the desired thickness, x-rayed to determine fuel location, and then trimmed to size. The plates are jig assembled into the grooved side plates with brazing powder, dried, and brazed in a hydrogen atmosphere. The jig used for assembly is also used for brazing and is made from alumina-coated graphite. Very close tolerances are held with this technique.

There are virtually no limitations on the plate specifications other than a maximum of 50 vol % UO_2 in the stainless steel and a finished "meat" thickness of 0.125 in. The UO_2 content is limited by the decreased uniform dispersion UO_2 in stainless steel at high concentrations and poorer green strength of the compact. The thickness is

limited by the equipment available at ORNL for fabrication.

This type element shows no dimensional instability in a radiation field. A burnup of 3.5 atom % is permissable.

2.1.2 Control Rods. Again in the case of the control rod it was found possible to use the same general design and construction features as incorporated into the APPR. The control element proper is a unit 74 in. long consisting of two parts. The lower section is an active, fuel-bearing, plate-type assembly similar to a typical fuel assembly but containing only 5 plates and entirely enclosed by 80-mil thick stainless steel plates. This is done to provide good bearing surfaces on the rods. Although the plates are narrower (space limitations) and fewer in number, a control rod contains the same amount of fuel as normal fuel element. This is accomplished by making the "meat" section of the element thicker; this device does not give thermal stresses in excess of the allowable. It seemed more advisable to thicken the element and maintain the same fuel alloy composition so that only one type fuel mix would be required.

To the lower end of the active section is attached a transition piece (square to round) and the shock absorber piston. Deceleration of the rod on scram is accomplished with a dash-pot like device. The piston is tapered with the narrow end at the bottom. The lower end of the shock absorber housing contains a cup. As the piston enters the cup further and further, less flow area is available around the piston for escape of the fluid trapped in the cup thus effecting an ever-increasing retarding force. This device has proven quite satisfactory in tests and should provide continually reliable operation.

To the upper end of the active section and the lower end of the top piece, which is the poison section, is attached a coupling mechanism which allows separation of the upper and lower pieces. This is desirable from a transportation standpoint in that, after use, the rods will be very radioactive and, since they can be disassembled, they are easier to handle and can fit into the same shipping coffins as are used for the standard fuel elements. The connector is a breach-lock-type device that can be disengaged by pushing down on the top of the assembly, twisting the upper section about 30° , and then lifting it out of the core.

As mentioned previously, the upper section of the control rod contains neutron absorbing material. It is a boron carbide-copper alloy clad on both sides and ends with stainless steel sheet and rolled into a cylinder. This in turn is fastened inside a stainless steel housing which has the connector piece at one end and part of the latching mechanism at the other end. The entire rod assembly is designed so that there is a water passage up the center of the rod for moderating and cooling purposes.

The poison section was made round for two reasons. First, it was more convenient in view of space limitations and second, it seemed to have certain operational advantages over the APPR control rod. A certain amount of clearance is required in the connector for easy operation and this would increase the possibibility of misalignment of the two halves due to twisting of the rod in the guides. By making the upper section round and by using the guides shown in Fig. 9, this problem should be reduced, if not eliminated. Since the fail-proof operation

ORNL-LR-Dwg. 6066

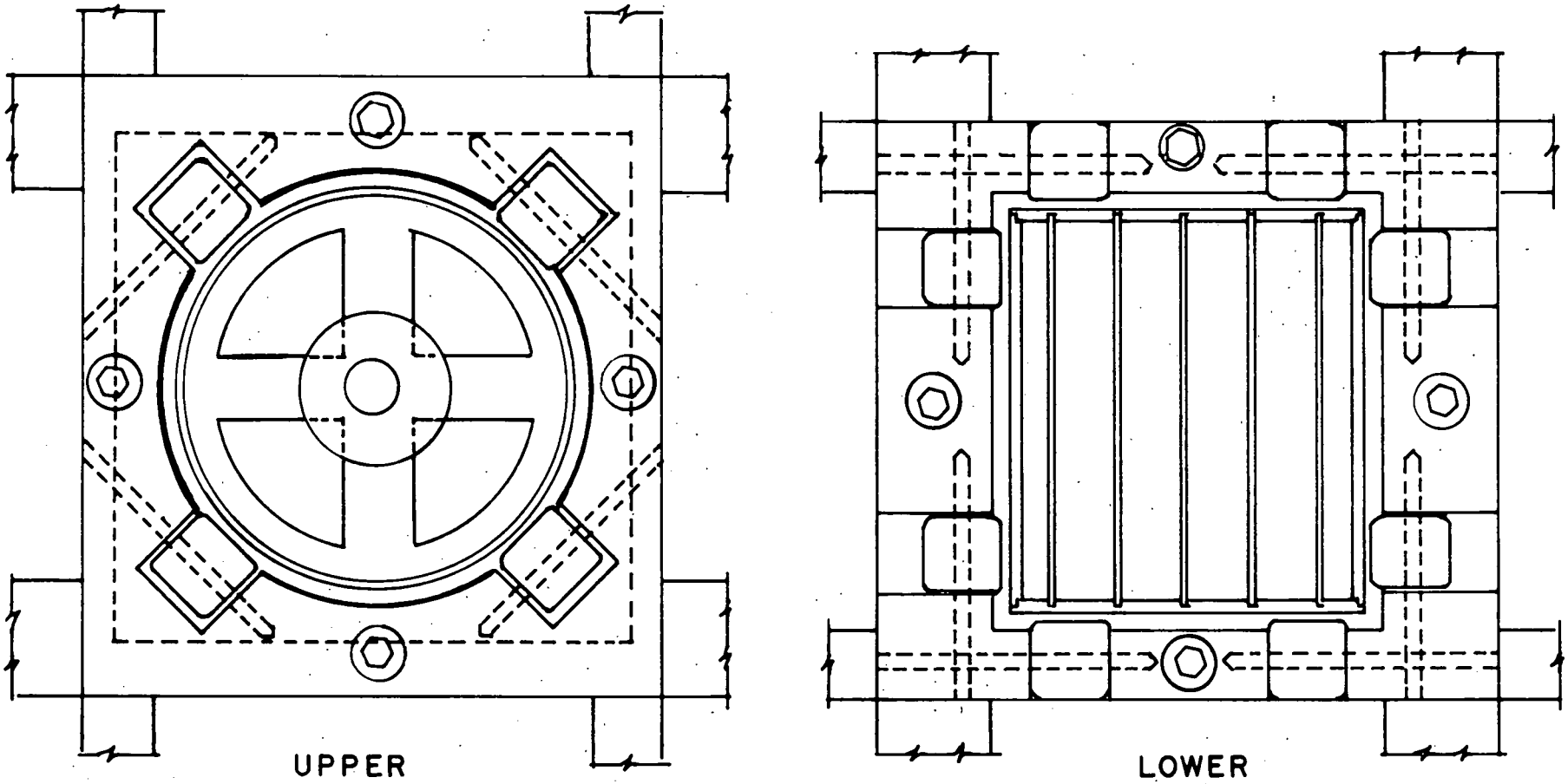

CONTROL ROD GUIDE MECHANISIM

Figure 9

of the control rods is necessary, this was thought to be a worthwhile modification of the already designed mechanism. The rack-latch mechanism and drive assembly chosen is identical with that on the APPR. A minimum of steam leakage is expected round the packing gland because of lower pressure operation. The water seal will not be used; any leakage that does occur will be collected and sent to the contaminated drain.

2.1.3 Grids and Supports. The grids and support structure are shown in Figs. 6, 10, and 11. The lower grid structure is a square plate 2 in. thick with 49 square holes in it and hangs from the lower support plate by a square 1/16 in. thick can. The 56 lugs projecting rigidly from the grid slide into the grooves cut on two sides of the end box of each element and hold the element, thus preventing any transverse motion. The end of the element is accurately machined and sits squarely on top of the grid. Also attached to the lower grid are the control-rod shock absorber housings and the control-rod roller guide assemblies. These two items are bolted to the bottom of the grid. The guides are shown in Fig. 9.

The upper grid is slightly differenct in that the holes for the control rod are round and the lug arrangement is different. In this case, the lugs are movable, see Fig. 11. Spring loading these lugs insures a tight fit of the grid and elements and still allows for differences in the finished lenghts of the elements. The springs are expected to be strong enought to hold the elements during any vibrations caused by flow and boiling. The springs are affixed in such a manner that remote removal

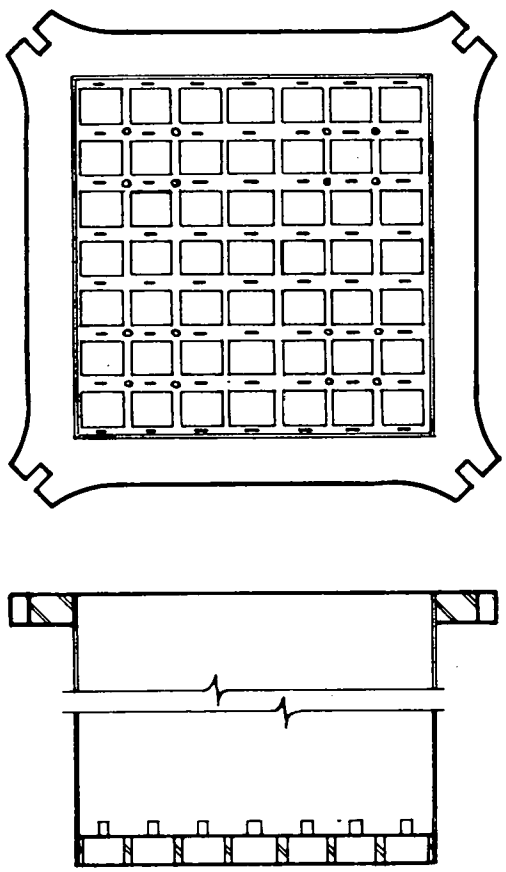

LOWER GRID
AND SUPPORT

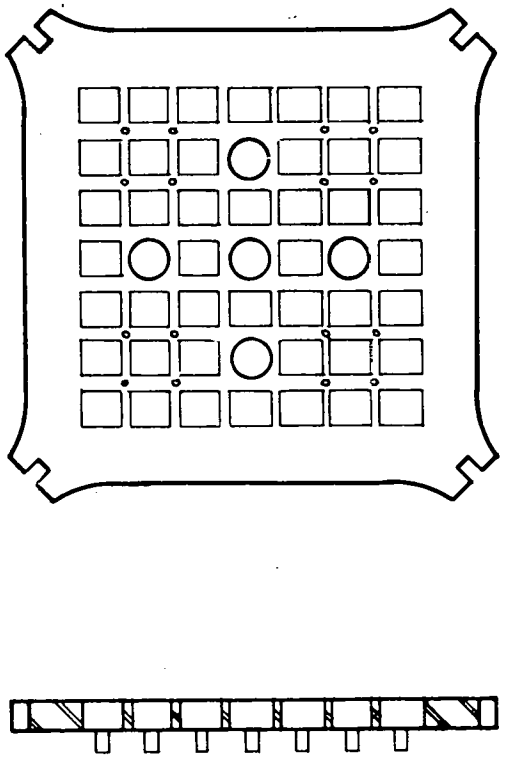

UPPER GRID

GRID DETAILS

Figure 10

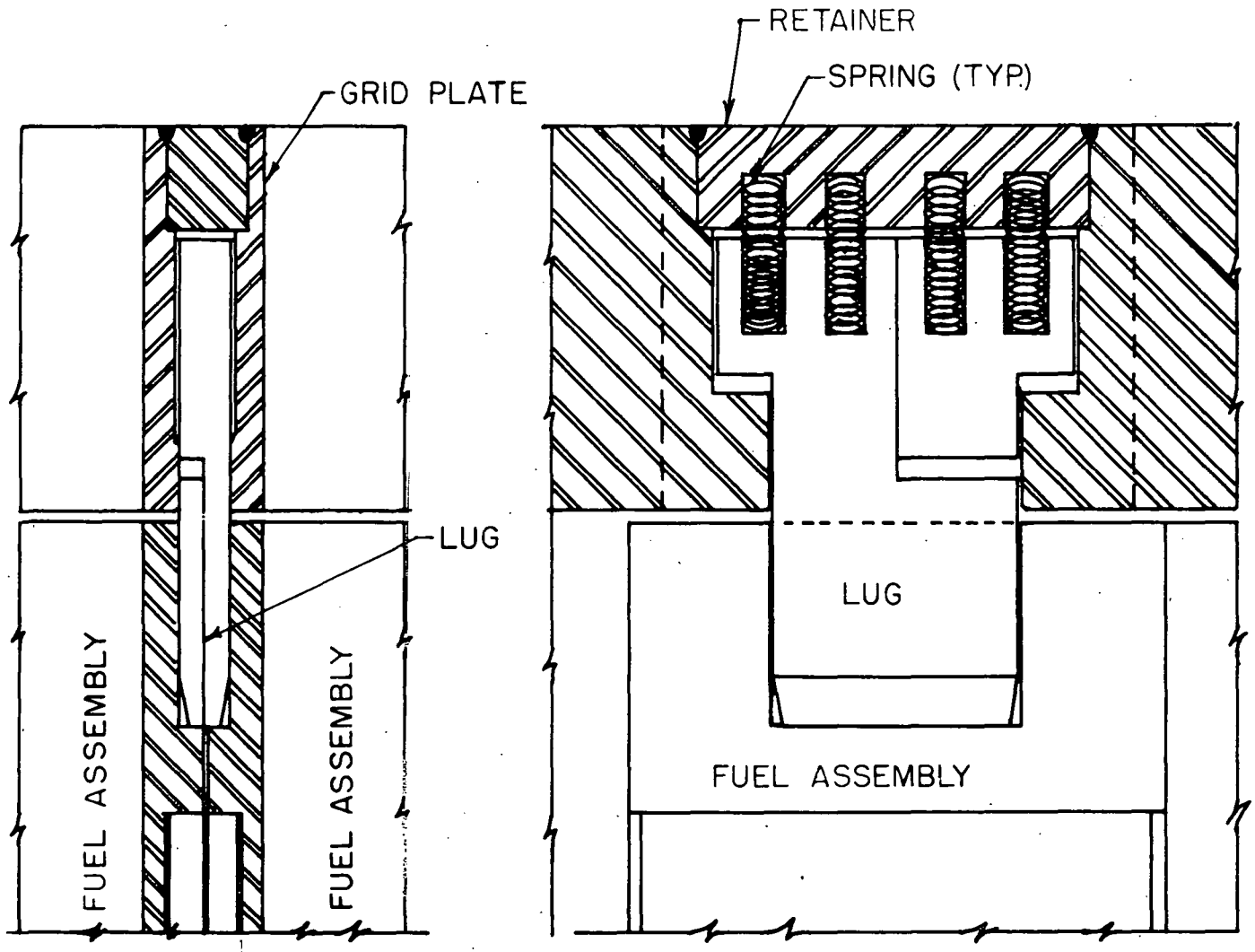

UPPER GRID LUG DETAIL

Figure 11

and replacement of broken and damaged parts should be reasonably easy. Also, it is arranged so that a broken spring, which is probably the only anticipated difficulty, will not fall into the pressure vessel.

The upper grid and lower grid, are held to the lower support plate by 4 swing-away bolts attached to the support plate. The riser bolts separately to the upper grid. The entire assembly of lower grid, upper grid, fuel elements, and riser can be removed as a unit if necessary.

The upper grid also has 5 control-rod roller guide assemblies bolted to the top of it. The guide assemblies are lubricated only by the reactor water and are similar to the arrangement used by the APPR. A sample control rod unit has been on test at the American Machine and Foundry Company and has shown quite satisfactory performance. Details and test results are given in ORNL-1613.

2.2 Pressure Vessel Design

The design of a pressure vessel for a nuclear reactor presents certain unique problems, not encountered in the design of a pressure vessel for normal service. Among other important things that must be considered are (1) generation of heat in the walls of the vessel, (2) radiation damage by high energy neutrons and gamma radiation, (3) degree and type of corrosion by liquids encountered in the reactor, and (4) possible temperature and pressure surges caused by sudden excursions in reactivity.

The design of this reactor vessel has been, where possible, consistent with rules laid down in the Unfired Pressure Vessel Section of

the ASME Boiler Code. It was necessary to deviate from these standards in calculating vessel wall thickness because of the combined thermal and pressure stresses in the metal. Since pressure stress is important for thin vessels, and thermal stress becomes important in thick vessels, it was necessary to design about the minimum in the stress vs thickness curve. For this reactor the minimum occured at 1 3/8 in. (Fig. 12); code dictated a thickness of about 1 1/8 in. from pressure considerations only. However, by using a 1-in. thermal shield, the thermal stress contribution was reduced and it was felt that substantial savings in vessel cost could be effected by using a wall thickness of 1 in. The resulting tangential stress on the inner surface of the vessel was calculated to be slightly less than 17,000 psi with a design pressure of 600 psi (working pressure -- 400 psi); the methods outlined in Theory of Elasticity by Timoshenko and Goodier were used. The allowable working stress for SA 212B Firebox grade steel is 17,500 psi. After fabrication, the entire vessel is to be stress relieved and radiographed. Surges in pressure above 600 psi will be accomodated by a pressure relief valve on the outlet steam line. This safety valve will be spring loaded with a water seal (overflow to the contaminated drain system) and the outlet will lead to the stack used for radioactive gases and vapors.

The vessel has five openings, as shown in Fig. 13. The four 2-inch openings do not require reinforcing but the 4-inch steam outlet will be adequately reinforced by a 1-inch thick saddle ring with 9 inches outside diameter welded to the vessel and outlet pipe.

ORNL-LR-Dwg. 6069

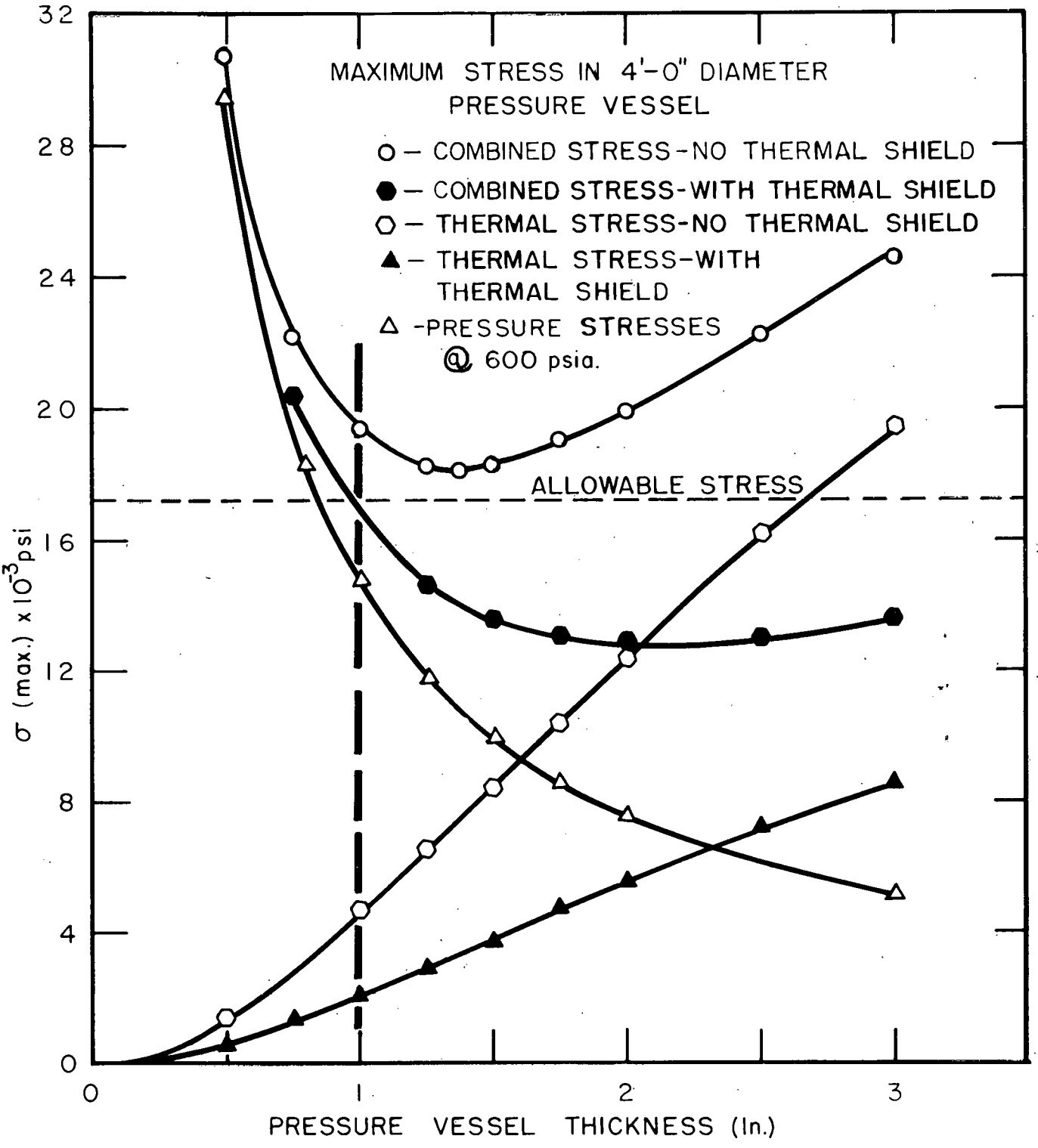

Figure 12

ORNL-LR-Dwg. 6070

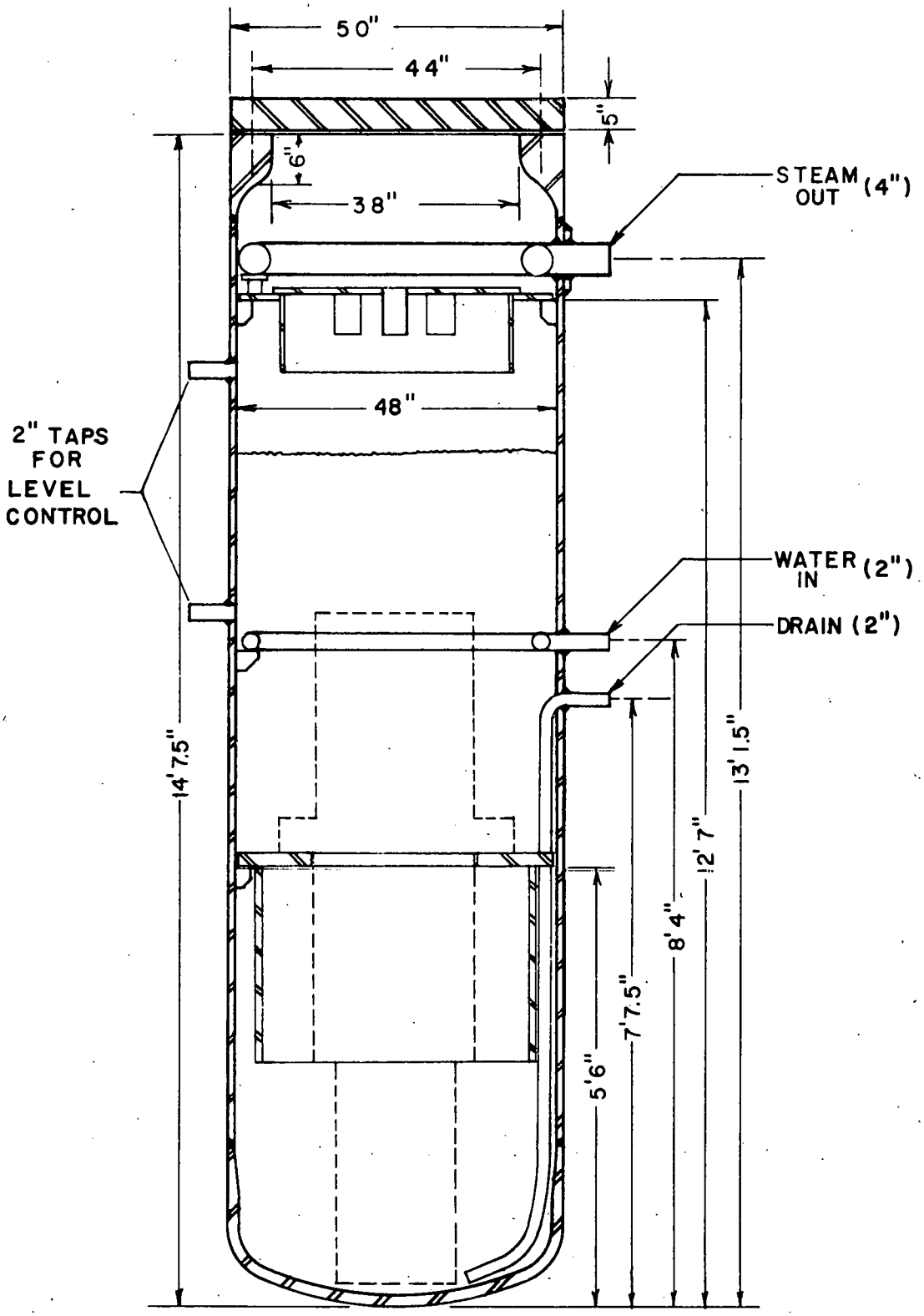

PRESSURE VESSEL

Figure 13

The vessel is designed and the internals sized so that a maximum number of pieces can be replaced easily in the event of damage. Necessarily there are certain items that must be built into the vessel when it is fabricated. Referring to Figs. 13 and 14 it will be noted that the steam outlet line, upper support plate, water inlet line, drain line and lower support plate are built into the vessel. It was thought desirable to have all other components removable, especially the lower grid structure and shock absorber assembly. It is of course necessary to remove the baffle, riser, and upper grid to change fuel elements.

Briefly, the vessel will function as follows: Water will enter the vessel through the toroid near the center of the vessel. There are slots in the toroid, sized so that there will be an even distribution of feed water around the periphery of the vessel. Being cooler than the water already in the reactor vessel, the feed water will promote natural circulation down between the wall of the vessel and the core and then up through the core and riser. The thermal shield attached to the lower support plate reduces stresses in the vessel walls. A drain line is provided which penetrates the vessel at its mid-point and then runs along the wall to a low point in the vessel. The normal function of this line is to remove a by-pass stream of about 1.3 gpm to a demineralizer. This allows the solids content in the circulating water to be held down to about 2 ppm, or less. It was felt desirable to have the line enter the vessel at this point rather than have a tap at the bottom of the vessel so as to reduce the possibility of draining

ORNL-LR-Dwg. 6071

Figure 14

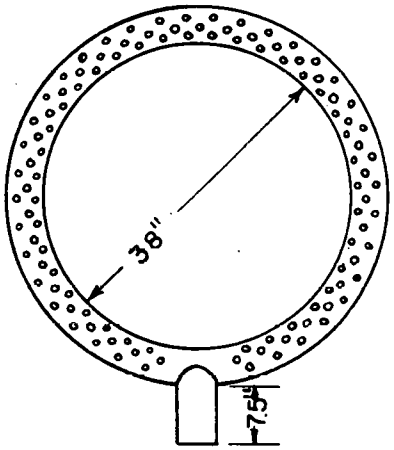

STEAM OUTLET LINE

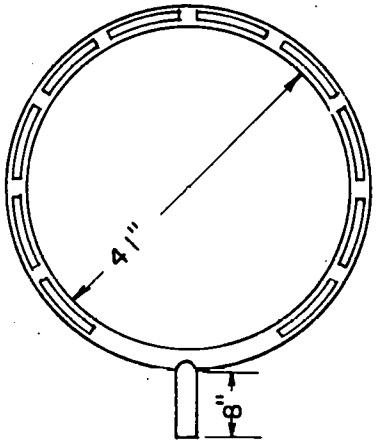

WATER INLET LINE

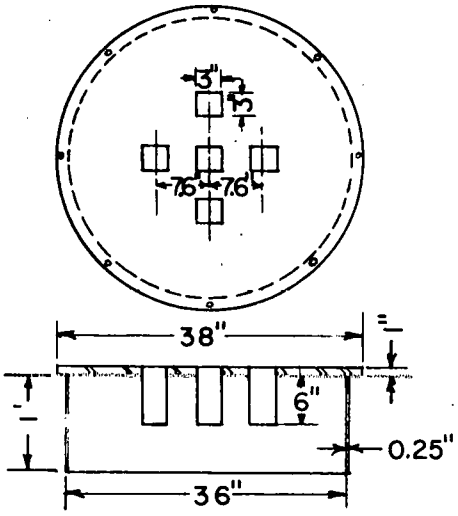

BAFFLE

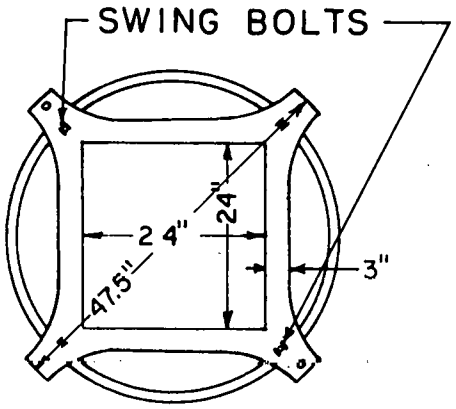

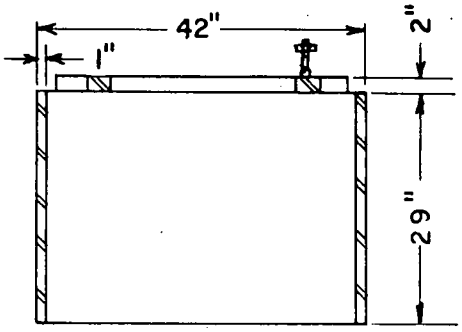

LOWER SUPPORT PLATE

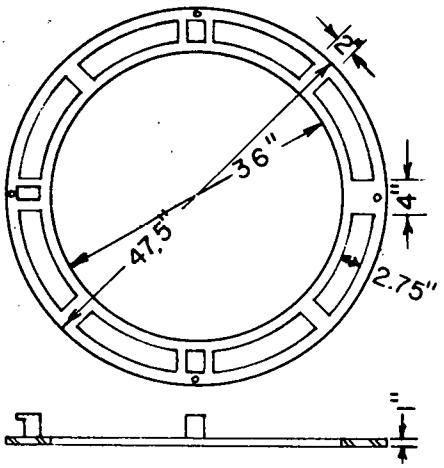

UPPER SUPPORT PLATE

INTERNAL DETAILS OF PRESSURE VESSEL

the reactor vessel completely in the event of a weld or line failure. Also having the drain close to the bottom tends to promote the removal of any sedimentation from the vessel.

As the water passes through the core, some of it is vaporized to steam and the velocity increases from 4.65 fps to 7.69 fps. As the steam bubbles leave the surface of the water some water will be entrained and the steam-water mixture will impinge on the baffle plate, separating most of the water from the steam. The steam will flow down and around the skirt on the baffle and then up through holes in the upper support. From there, the steam flows around the upper toroid, through the holes in the top of the toroid, and out of the vessel to the turbine and barracks steam generator.

The vessel is 48 in. inside diameter and 15 ft high with a 1 in. wall thickness, 5 in. thick cover and is made of SA 212B steel. The inside of the vessel and cover are clad with 0.109 in. thick 304 ss for corrosion resistance. All internals are 304 ss, which results in carbon steel to stainless steel welds on all the taps to the pressure vessel. However, no difficulties are expected in this regard as there are many such successful welds in service. The inside diameter of vessel opening is 38 in. The seal is accomplished by using 22 equally spaced 2 in. stud bolts and nuts holding the cover to the vessel; the gasket is spiral wound stainless steel asbestos. The vessel is supported by a bottom ring 50 in. O.D. and tie rods attached to the vessel about 1/3 down from the vessel top and connected to the concrete shield structure.

2.3 Control Rod Drive Mechanism

The drive mechanism for the control rods is identical to that as described and illustrated in ORNL 1613 and will not be elaborated on here.

2.4 Reactor Control

2.4.1 The Problem. The control problem can be divided into two parts: (1) The effect of bubble formation time on nuclear stability and (2) the effect of changes in load on the stability of the system.

2.4.2 Nuclear Stability. Experiments* to date indicate that for reasonable changes in reactivity, bubble formation time does not prejudice nuclear stability. Henceforth, it will be assumed that bubble formation time can be neglected and that for constant load, the reactor will be self-regulating.

2.4.3 Response of the System to Changes in Load. Although the reactor is self-regulating, the pressure excursions which occur when the load is changed, can be tremendous. Fig. 16 is a plot of average core fluid density vs saturation temperature. Curves of constant power extracted from the core (P_X) and constant vapor fraction curves (f_v) are shown. The design conditions are $P_X \simeq 100\%$ and $f_v \simeq 0.20$.

Fig. 16 shows that at the design point an increase in pressure results in an increase in reactor power. This is due to the following: (1) The density coefficient of reactivity is such that an increase in average fluid density results in an increase in reactivity, (2) the

* Transient and Steady-State Characteristics of a Boiling Reactor, ANL-5211.

DWG. TD-D-2457

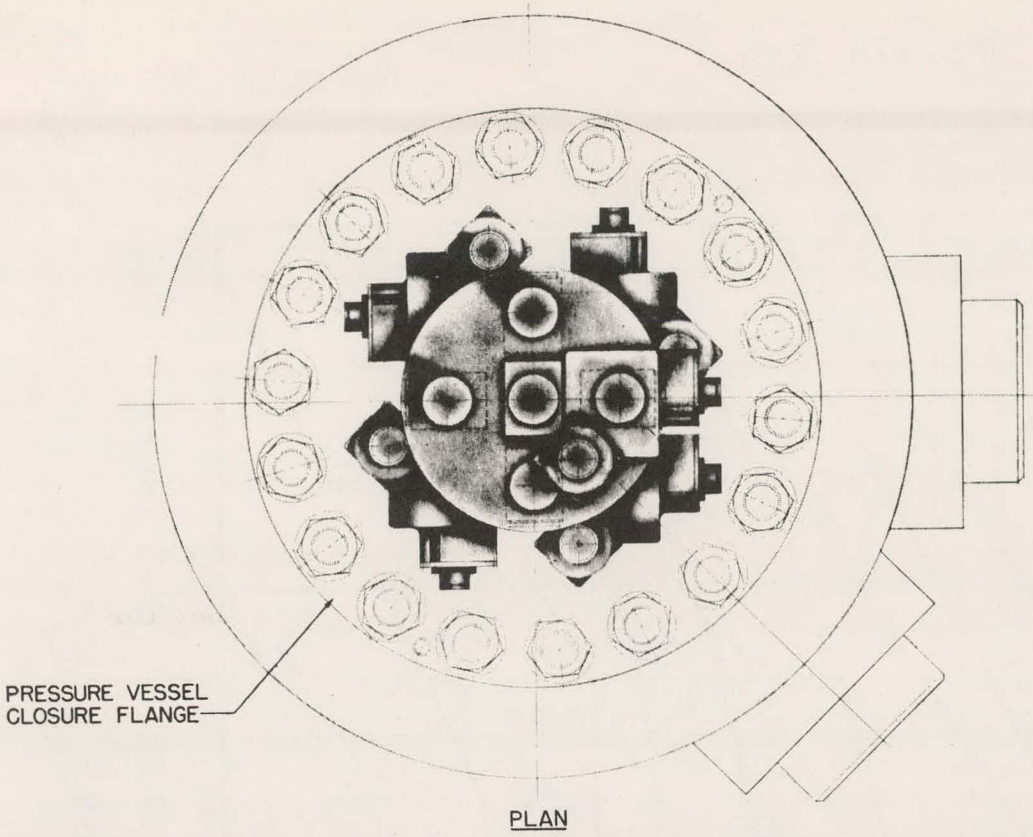

PLAN

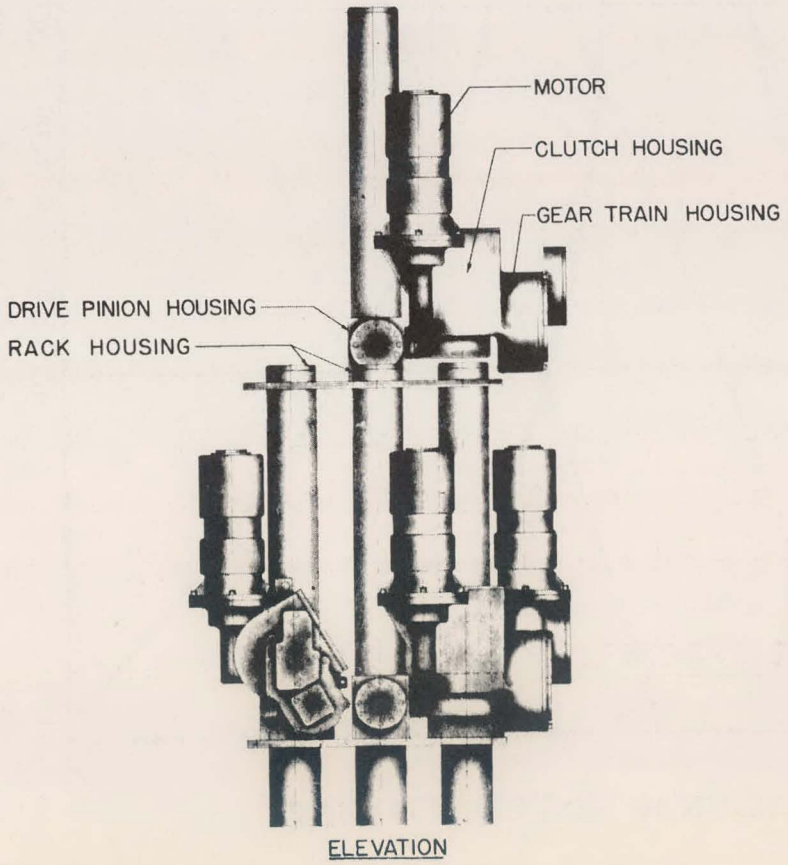

ELEVATION

Figure 15 Control Rod Drive, Plan and Elevation.

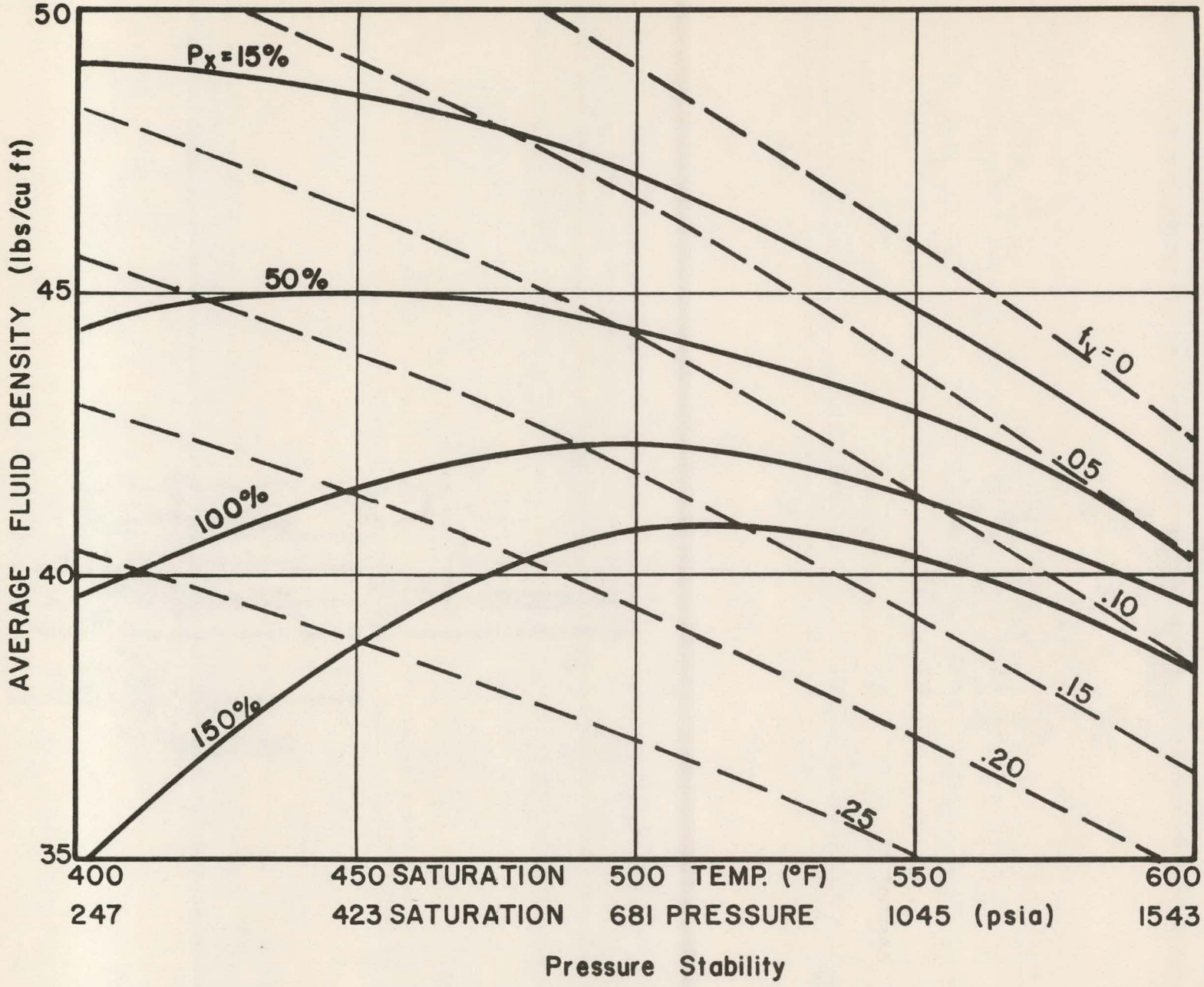

Figure 16

ORNL-LR-Dwg. 6072

temperature coefficient, while negative, is very small in comparison with the void coefficient of reactivity. Since a decrease in load causes the pressure to rise, the reactor will be regenerative (power wise) up to the temperature corresponding to the maximum of the 100% power curve. Eventually, the system will adjust itself so that power demand and reactor power are equal.

If the reactor were operating at design conditions, a 50% change in load would result in a final steady-state temperature of about 580° F. This can be demonstrated with Fig. 16. Since the reactor is assumed to respond in a manner to maintain constant fluid density, the steady-state temperature following the above change in load will be that temperture where the 50% power curve intersects the constant density (41 lb/ft^3) line. This temperature (580° F) corresponds to a saturation pressure of 1325 psia.

For the design point chosen two facts are readily apparent: (1) The design point represents a region of instability, i.e., perturbations in pressure will be regenerative and (2) changes in load cannot be acacomplished without experiencing large pressure excursions.

These facts could lead to a difficult control problem. However, if the response of the system is fairly slow, control should not be difficult. If future study shows that the system is very fast, then the system should be operated in a region where perturbations in pressure are self-stablizing. For the same power such a point would be at the maximum of the 100% power curve (490° F). Operation at 50% power at design temperature (448° F) would also be a stable region. Operation

at either of these two points would require some control since changes in load would still result in pressure excursions.

2.4.4 Response Time of System. It has been shown that the equilibrium condition resulting from a power demand change can be determined very quickly. However, the equations describing the transient behavior of the system are very difficult to solve. Moreover, the solutions to these transient equations are a prerequisite in determining the detailed specifications (i.e., speed of response) of the reactor control system.

An attractive method for solving these equations is with an electronic analog computer. Toward this end, the differential equations describing the system were derived, Appendix 12.2. A schematic of the analog computer together with a description is given in Appendix 12.3. The computer was not set up because sufficient equipment was not available at this Laboratory. Appendices 12.2 and 12.3 represent the major portion of the work required to simulate the system on an analog computer. If, at some future date, it is desired to simulate the system, the computer can be setup quite rapidly.

As a poor substitute for simulating the system, it is possible to make an approximate calculation of the initial time rate of temperature rise for the worst condition (step change in load from rated to zero power). Eq. (1) is an energy balance on the entire reactor.

From this equation

$$C_r \frac{dT_c}{dt} = P - P_o$$

where C_r = heat capacity of coolant in pressure vessel, steel in pressure vessel and steam chest, and steam in steam chest $\approx 8{,}000$ Btu/°F

T_c = coolant (liquid) temperature

P = reactor power ≈ 9480 Btu/sec at full power

P_o = power extracted (demand)

the calculated initial time rate of temperature change is slightly greater than 1° F/sec. While this calculation is by no means adequate to predict the reactor transient behavior, it at least gives an indication of what can be expected.

Because of the complexity of the equations describing the system, it is not felt that any further predictions of response can be made, without running a great risk of arriving at the wrong answer. If further information is required, it is strongly recommended that the system be simulated, or else that an actual model be constructed, as intended by Argonne National Laboratory*.

2.4.5 Power Range Reactor Control System. For reasons outlined in the previous section, it is not possible at this time to determine the detailed specifications of the control system. The most important of these specifications is the speed of response of the system. The cost of the system will decrease and its reliability will be improved as the required response is decreased. However, indications are that this will not be a prohibitive factor in the design of this plant.

* Quarterly Report on Reactor Development, Boiling Reactor Simulator, ANL-5272, Apr. 30, 1954.

The system proposed is shown in Fig. 17, minus auxiliary circuits for such functions as calorimetric calibration of neutron detectors. The load is represented by a turbine whereas in actuality it consists of a turbine and barracks heating. The main purpose of the control system is to regulate the reactor power so that it equals the power demanded by the load at all times. A change in power demand manifests itself as a change in steam pressure and steam flow. Since it is intended to maintain constant pressure over the operating range, steam flow will give a direct measure of power demand.

The control system consists of two loops. One loop adjusts the reactor power so as to maintain constant pressure. In Fig. 17 this is shown to consist of a pressure comparator, a servo-amplifier, and the control rods and their drive mechanisms. An increase in system pressure (p) over the design pressure (p_o) produces an error signal. This error signal is amplified by the servo-amplifier. The output of the servo-amplifier is such as to move the control rods in a manner which reduces reactor power, thereby reducing steam pressure. In a similar manner, a reduction in steam pressure results in an increase in reactor power. The function of this control loop is to compensate for small variations in steam pressure, i.e., acts as a trimmer on reactor power.

The second control loop operates in the same manner as the pressure control loop except that power demand (steam flow) is compared with reactor power (neutron flux). The function of this loop is to compensate for large sudden changes in power demand or reactor power. The design is such that this loop overrides the pressure control loop when

ORNL-LR-Dwg. 6073

Figure 17

REACTOR CONTROL SYSTEM (POWER RANGE)

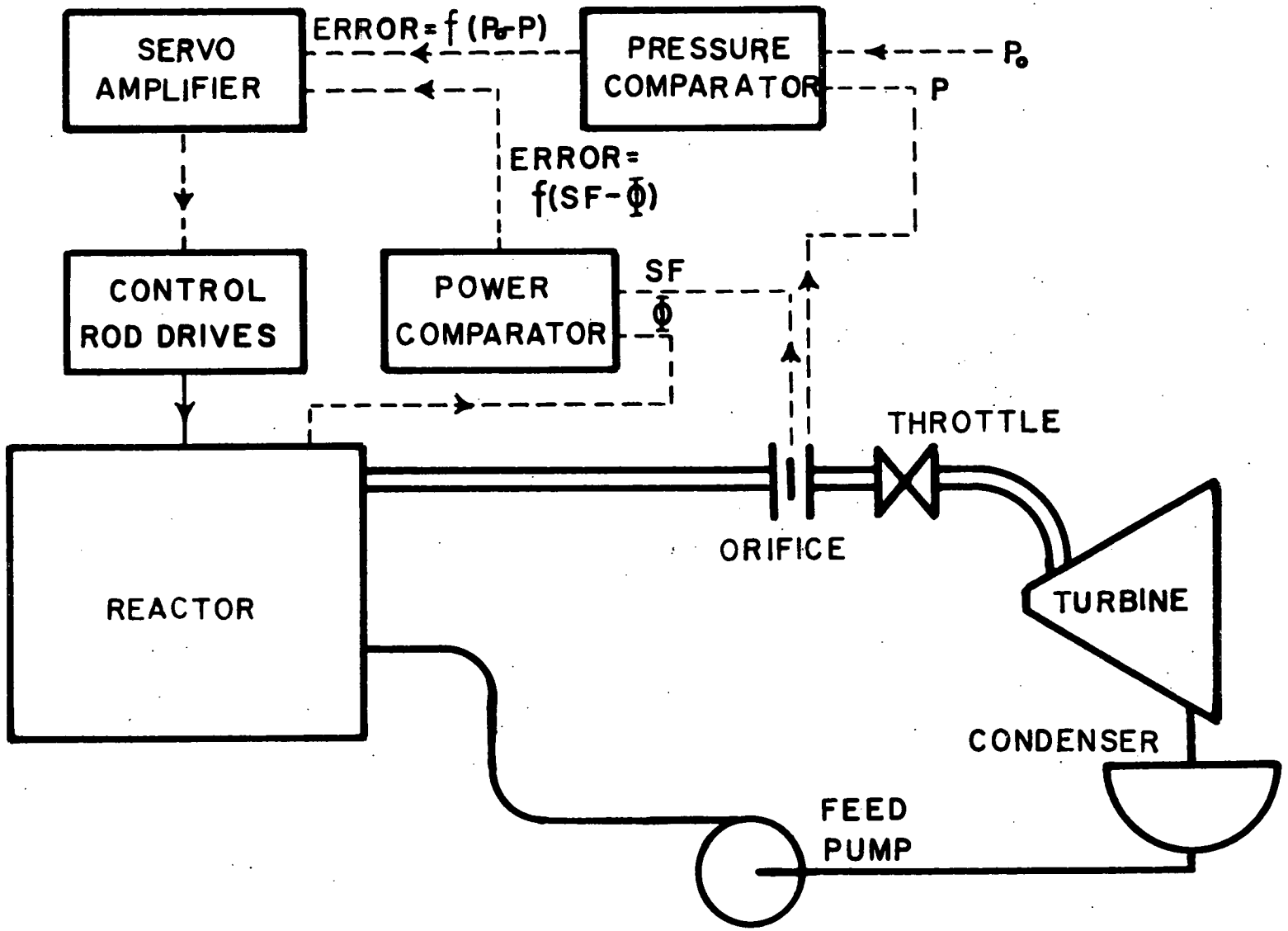

the error signal, f (S.F. - I), exceeds a certain prescribed value. Therefore, for small variations, this loop is essentially disconnected.

The reasons behind this design are: 1) it is mandatory that system pressure be maintained at 415 psia, 2) large sudden changes in power demand are manifested first in changes in steam flow, in other words, the change in pressure is anticipated by the change in steam flow, and 3) the pressure control loop should provide smoother control for small variations.

The system will respond to a change in power demand in the following manner. Assume the reactor has been delivering rated power to the load, and that suddenly the throttle is closed halfway. The steam flow is the first parameter which changes, and in this case it decreases. The steam pressure begins to increase but at a much slower rate. Since the difference between reactor power, Ⓟ, and power demand, S.F., is now negative, an error signal is produced which causes the control rods to be inserted, so as to decrease reactor power. When the reactor power approaches the value of power demanded, the pressure control loop takes over and and trims reactor power, so as to adjust the steam pressure until it again equals 415 psia.

2.4.6 Startup Control System. The startup procedure is outlined in Section 9.1. Since the startup problem in this reactor is not unique, startup instrumentation similar to that proposed for the pressurized water package reactor (see ORNL-1613) should be sufficient.

2.4.7 Scram System. The following conditions should initiate a scram:

a. Water in reactor below certain prescribed level.
b. Excessive period (during startup).
c. Reactor power greater than 125%.
d. Power failure.

The scram system is intended as a safety device which protects the plant against the consequences of failures or maloperation. Since reliability is an important factor in this design, resort to scramming should be avoided as much as possible. A scram should be initiated only when no other means of corrective action is available.

The only two conditions, which in themselves, would endanger the integrity of the plant are excessive fuel temperature and excessive steam pressure. Excessive fuel temperature is dangerous in that it may lead to rupture of the fuel elements thereby releasing fission products. Excessive steam pressure is hazardous due to the possibility of developing abnormal stresses in pressure vessels and piping.

There are many conditions, in themselves not dangerous, which would lead to excessive fuel temperature and/or steam pressure. They are listed as follows:

1. Level of water in reactor below top of fuel plates.
2. Reactor power greater than power removed.
3. Excessive period during startup.

The system contains a pressure relief valve which acts as a safety device to prevent excessive pressures. Unless future analysis of power demand response shows that the maximum possible time rate of pressure change is so high that the reactor pressure can reach unsafe values before the pressure relief valve has time to operate, the scram system need only

prevent excessive fuel temperatures. Since condition (2) listed above also leads to high pressure it need not initiate a scram. In view of this, scrams can be limited to conditions (1) and (3). In addition, it would be advisable to initiate a scram at some high reactor power level - say 125%. The design of the rod drive mechanisms is such that a power failure will result in a scram.

Although imminent rupture of the fuel plates is justification for a scram, it is not felt that the detection of such a rupture by the monitoring system should automatically cause a scram. While excessive radioactivity is undesirable, it is only hazardous in terms of long periods of plant operation. Therefore, the decision to shut down the reactor in the event of such a failure should be left to the discretion of the operator. In other words all possible means should be used to prevent fuel rupture, but once it has occurred, immediate plant shutdown is not mandatory.

3.0 NUCLEAR PHYSICS

3.1 Introduction

The nuclear characteristics of the boiling package reactor were determined by the two-group diffusion theory. Spherical geometry, total homogenization of the core, and fissioning in the thermal group only were postulated. The work was greatly facilitated by close direction from A. M. Perry, who had done intensive work on report ORNL-1613. Due to the nuclear similarity of the two systems, many approximations justified in the latter were applicable to the present problem.

3.2 Critical Equation

Calculations of the critical mass and the effective multiplication of the reactor under various conditions were based on the following assumptions:

(a) $\epsilon \cdot p$ equals one.

(b) Spherical geometry with a volume equal to the actual volume of the reactor.

(c) The core materials and steam voids are homogeneously distributed.

(d) An infinite reflector of water at the reactor temperature.

The critical determinant was expanded in the following form:

$$-\alpha = \frac{\beta \frac{Z_1'}{Z_1}(n_2 S_3 - MF) + n_2 \frac{Z_2'}{Z_2}\left\{ n_1 N \frac{Z_1'}{Z_1}(F - G) + \beta(NG - S_3)\right\}}{\beta N(F - G) + \frac{Z_1'}{Z_1}(MG - n_2 S_3) + n_2 \frac{Z_2'}{Z_2}(S_3 - NF)}$$

where: $\alpha = \mu \operatorname{Ctn} \mu R - \frac{1}{R}$ $\qquad M = \frac{D_{1R}}{\tau_c D_{2C}}$

$\beta = \nu \coth \nu R - \frac{1}{R}$ $\qquad N = \frac{D_{1C}}{\tau_c D_{2C}}$

$\kappa_{2c}^2 = \frac{1}{L_{2C}^2}$ $\qquad F = \frac{1}{\kappa_{2c}^2 - \nu^2}$

$n_1 = \frac{D_{1R}}{D_{1C}}$ $\qquad G = \frac{1}{\kappa_{2c}^2 + \mu^2}$

$n_2 = \frac{D_{2R}}{D_{2C}}$

and other terms retain their original meanings, as defined by Glasstone and Edlund.*

With a given core composition, values of μ and ν related by $\nu^2 - \mu^2 = \kappa_{2c}^2 + 1/\tau_c$ are found to satisfy the above equation and also a critical value of thermal utilization, f, to satisfy the relation

$$\mu^2 = \tfrac{1}{2}\left[-\left(\kappa_{2c}^2 + \frac{1}{\tau_c}\right) + \sqrt{\left(\kappa_{2c}^2 + \frac{1}{\tau_c}\right)^2 + 4\frac{\kappa_{2c}^2}{\tau_c}(nf - 1)}\right]$$

The effective multiplication is then defined as

$$K_{eff} = \frac{f \text{ material}}{f \text{ critical}} \quad ;$$

f material is the actual thermal utilization of the core.

---

* Glasstone and Edlund, The Elements of Nuclear Reactor Theory, p. 246, D. Van Nostrand Company (1952).

3.3 Cross Sections

The cross sections used in computing the group constants were taken chiefly from the compilation of the ORNL Reactor Calculations Group. The average thermal-fission cross section of U 235 was obtained by numerical integration of the cross section curve in report BNL-170B* over a Maxwell distribution at 450°F. The resulting average cross section was normalized to agree with the assumption that $(1 + \alpha)$ is constant and equal to 1.184, below 1 ev. The average absorption cross section is then $1.184\ \bar{\sigma}_f$. A similar average was obtained for the cross section of Xe 135, taken from TAB-84.** All other absorbers were assumed to have 1/v cross sections, taken from AECU-2040.*** The average cross sections over a Maxwell distribution at the reactor temperature were used.

Values of the average cross sections used are shown in the following table:

Temp. (°F)	$\bar{\sigma}_f$ (barns)	$\bar{\sigma}_a$ (U 235) (barns)	$\bar{\sigma}_a$ (Xe 135) (barns)
68	509.0	602.7	2.87×10^6
450	372.3	440.8	2.66×10^6

* Brookhaven National Laboratory report BNL-170B, Neutron Cross Sections, Supplement 2, (1953).

** Greuling and Goertzel, Temperature Dependence of Xenon-135 Cross Section, TAB-84, (1950).

*** Compilation of the AEC Neutron Cross Section Advisory Group, AECU-2040.

3.4 Slowing Down Length

The slowing down length was computed by a method outlined by Tittle* and can be expressed as

$$6\tau = \sum_{o}^{n} 2\lambda_n^2 + 6L_{sa}^2$$

λ_n is obtained from Tittle's work. It results from assuming that all nuclear masses except hydrogen are infinite and every collision with hydrogen produces an increase in neutron lethargy of one unit. Inelastic scattering was neglected. With the base of the lethargy scale set at 10 Mev, n was chosen as three. Below 183 kev ($\mu = 4$), age theory was used to determine L_{sa}^2, i.e.,

$$L_{sa}^2 = \int_{\mu=4}^{\mu^{th}} \left[3 \xi \Sigma_t(\mu) \Sigma_{tr}(\mu)\right]^{-1} d\mu$$

The age of fission neutrons was then assumed to be that of a monoenergetic source of 2 Mev. Age for 450°F and 20% steam voids was also determined using the normalized fission spectrum as a source. The two methods produced identical results. Fig. 18 shows the age in the core as a function of effective water density, which is defined as the total mass of water in the core divided by the core volume. Ages in the reflector, taken from ORNL-1613, are:

Temp. (°F)	τ (cm^2)
68	31.4
450	45.6

* NP-1418.

ORNL-LR-Dwg. 6074

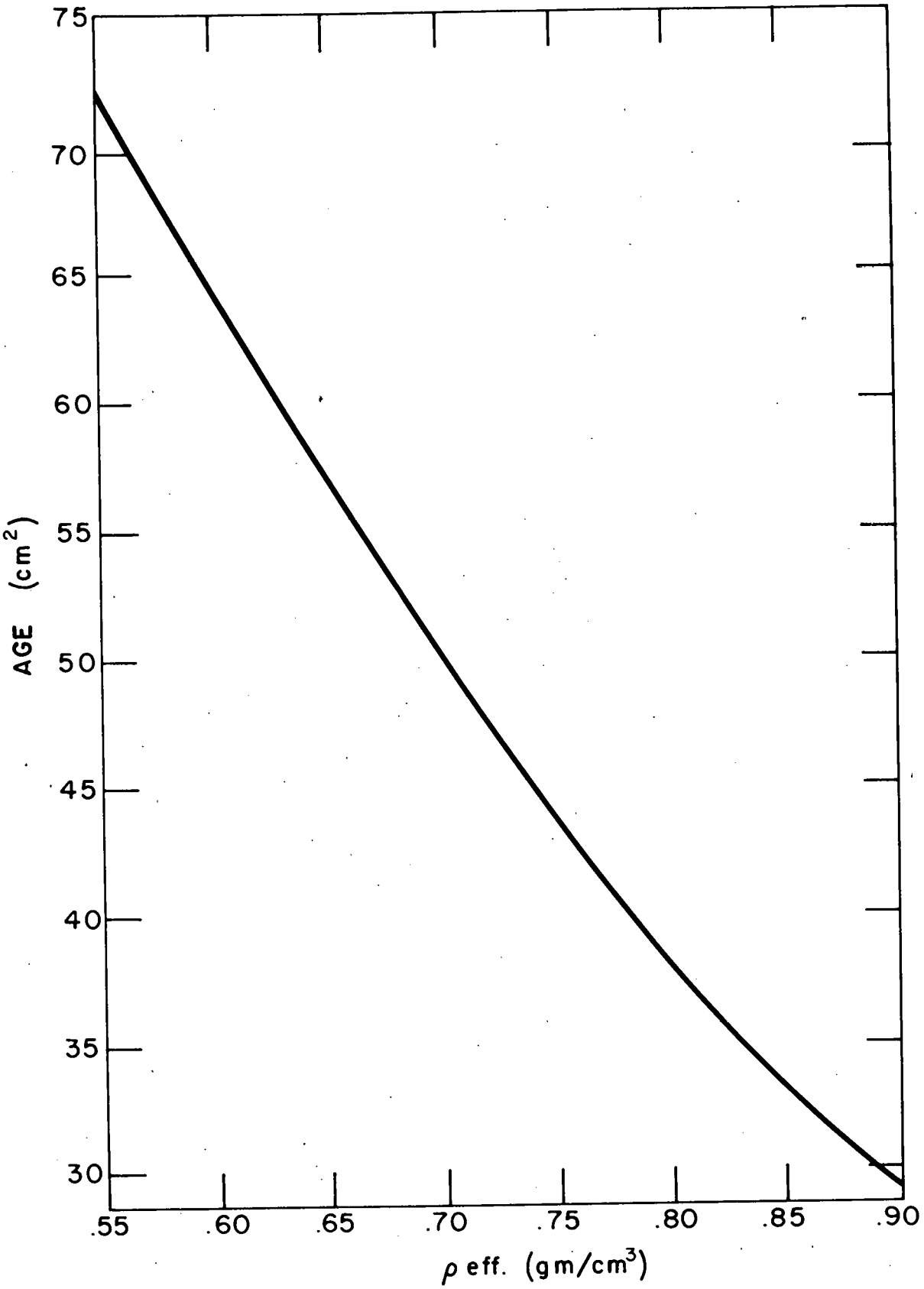

AGE TO THERMAL IN CORE VS. EFFECTIVE WATER DENSITY (450°F)

Figure 18

3.5 Fast Group Diffusion Coefficient

The fast group diffusion coefficient is the flux-weighted average over the fast group, i.e.,

$$D_1 = \frac{\int_0^{\mu^{th}} 1/3\, \lambda_{tr}(\mu)\, \varphi(\mu)\, d\mu}{\int_0^{\mu^{th}} \varphi(\mu)\, d\mu}$$

It was assumed that the fast neutron flux was expressible as $\varphi(r,\mu) = F(r)\,\varphi(\mu)$ and that the nuclei other than hydrogen have infinite mass. The slow down equation becomes

$$\left[\Sigma_a(\mu) + \Sigma_s^H(\mu) + D(\mu)\, B^2(\mu)\right] \varphi(\mu) = f(\mu) + \int_0^{\mu} \Sigma_s^H(\mu')\, \varphi(\mu')\, \ell^{\mu'-\mu}\, d\mu'$$

with the solution

$$\varphi(\mu) = \lambda^{-1}(\mu) \exp\left[-\int_0^{\mu}[1-g(\mu)]\, d\mu\right] \int_0^{\mu} \left[f(\mu') + f'(\mu')\right] \exp\left[\int_0^{\mu'}[1-g(\mu)]\, d\mu\right] d\mu'$$

where: $\Sigma_a(\mu)$ = total macroscopic absorption cross section

$\Sigma_s^H(\mu)$ = macroscopic scattering cross section of hydrogen

$D(\mu) = \left[3\, \Sigma_{tr}(\mu)\right]^{-1}$

$B^2(\mu) = \left[\frac{\pi}{Re + \rho_s + 0.71\, \lambda_{tr}(\mu)}\right]^2$

$f(\mu)$ = normalized fission spectrum

$\lambda(\mu) = \Sigma_a(\mu) + \Sigma_s^H(\mu) + D(\mu)\, B^2(\mu)$

$g(\mu) = \Sigma_s^H(\mu)\, \lambda^{-1}(\mu)$

Re = physical radius of the spherical core

ρ_s = reflector savings

The fast diffusion coefficient of the core as a function of effective water density is shown in Fig. 19.

Values for the reflector taken from ORNL-1613 are:

$$D_{1R}\ (68°F) = 1.54 \text{ cm}$$

$$D_{1R}\ (450°F) = 1.85 \text{ cm}$$

3.6 Thermal Diffusion Coefficient

The thermal diffusion coefficient is given by $D_2 = L^2 \Sigma_a$, where L is the thermal diffusion length and Σ_a the total macroscopic absorption cross section. For a mixture, as in the core,

$$D_{2C} = \left[j\rho \left(L^2 \Sigma_a\right)^{-1}_{H_2O} + (1-j)\, 3\, \Sigma'_{tr}\,(ss) \right]^{-1}$$

where: j = fraction of the volume occupied by water

ρ = density of the steam-water mixture

$(L^2 \Sigma_a)_{H_2O}$ is the appropriate value for the reactor temperature based on a water density of one gram per cm^3.

The diffusion length of thermal neutrons in water was obtained from a curve, computed by A. Radkowsky,* which takes into account the chemical binding energy of the atoms in the water molecule. The variation of D_{2C} with steam voids is shown in Fig. 20.

The thermal diffusion coefficients for the reflector are

$$D_{2R}\ (68°F) = 0.150 \text{ cm}$$

$$D_{2R}\ (450°F) = 0.230 \text{ cm}$$

---

* A. Radkowsky, Temperature Dependence of Thermal Transport Mean Free Path, ANL-4476, Fig. 22, p. 89.

ORNL-LR-Dwg. 6075

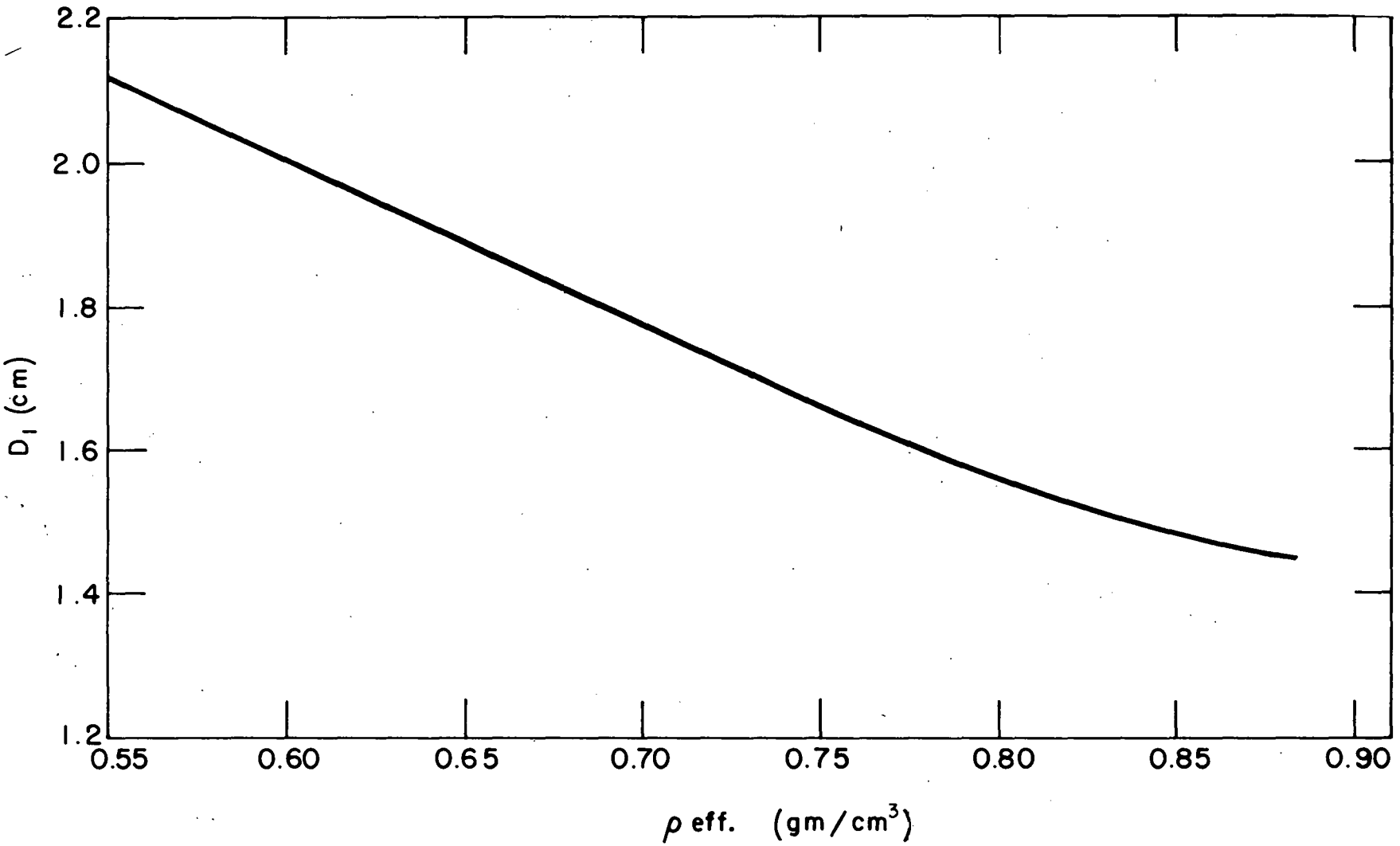

FAST DIFFUSION COEFFICIENT IN THE CORE VS. EFFECTIVE WATER DENSITY (450°F)

Figure 19

ORNL-LR-Dwg. 6076

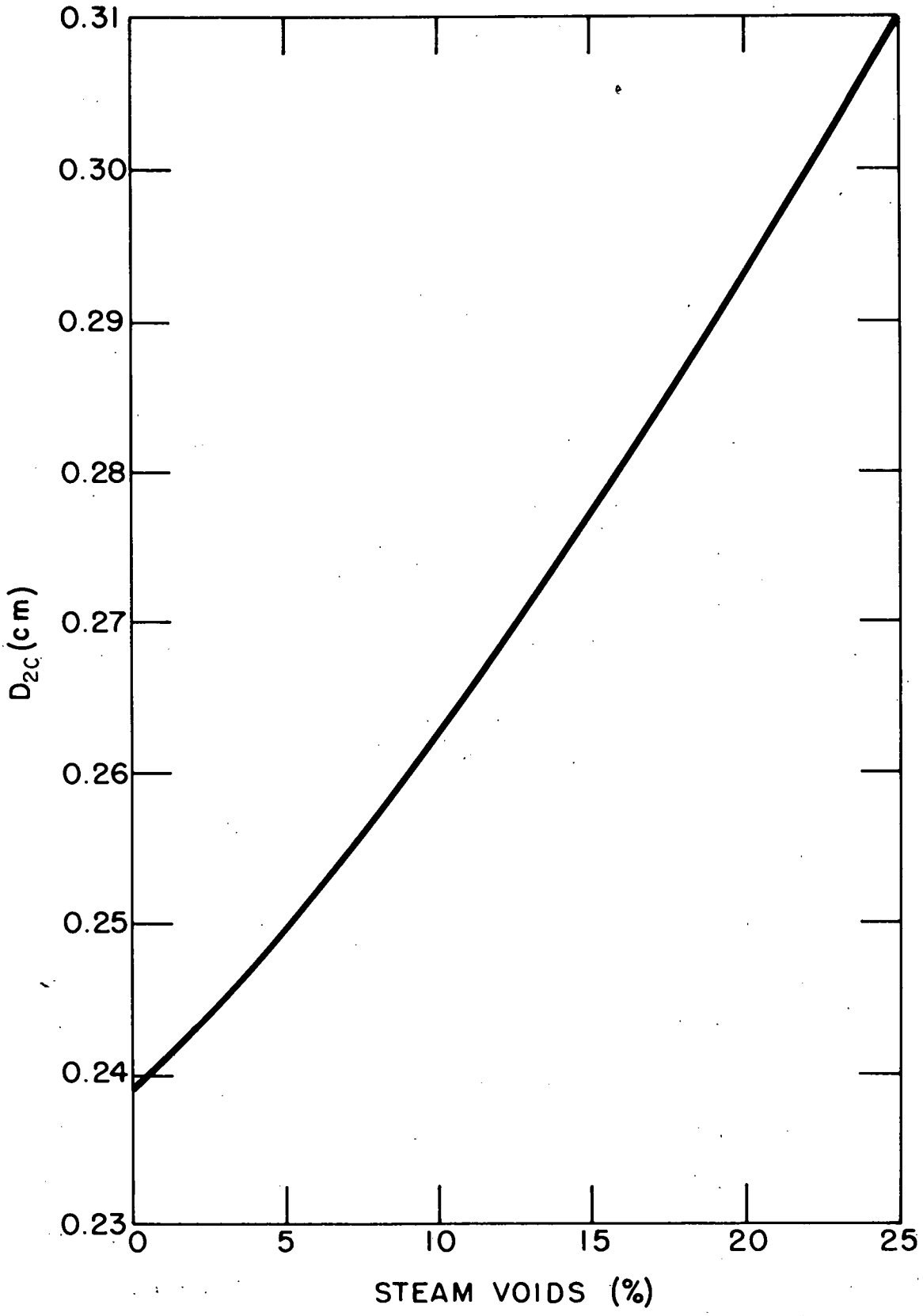

THERMAL DIFFUSION COEFFICIENT IN THE CORE VS. STEAM VOIDS (450°F)

Figure 20

3.7 Reactivity and Steam Voids (Fig. 21)

The dependence of reactivity on steam voids was determined for the critical loading of a clean core. A linear relationship was found between 0% and 25% steam voids equal to 0.154% reactivity per percent steam void.

3.8 Reactivity and Fuel Burnup

In order to reduce the reactivity excursions during the 15 Mw-yr core life, boron burn-out poison was incorporated into the core. A critical mass for the end of 15 Mw-yr operation was found with equilibrium fission product and peak xenon poisoning. Fuel was added to accommodate burnup and enough boron added to reduce the initial reactivity with peak xenon poisoning to zero.

Fuel consumption was 500 g/Mw-yr or 7.5 kg total burnup. Boron burnup follows the relation

$$B(t) = B(0)\left[\frac{U(t)}{U(0)}\right]^{g}$$

For a completely thermal reactor

$$g = \frac{\sigma_a^{th}(B)}{\sigma_a^{th}(U)}$$

If resonance absorptions are considered, g is found to be somewhat smaller than the ratio of thermal cross sections. A value of 5.8, obtained from ORNL-1613 was used in this report.

An extensive study and evaluation was made by A. M. Perry of all fission products that would influence the reactor considered in the above report. A curve of barns of poison per fission as a function of reactor life was obtained on the basis of an initial thermal neutron flux of

ORNL-LR-Dwg. 6077

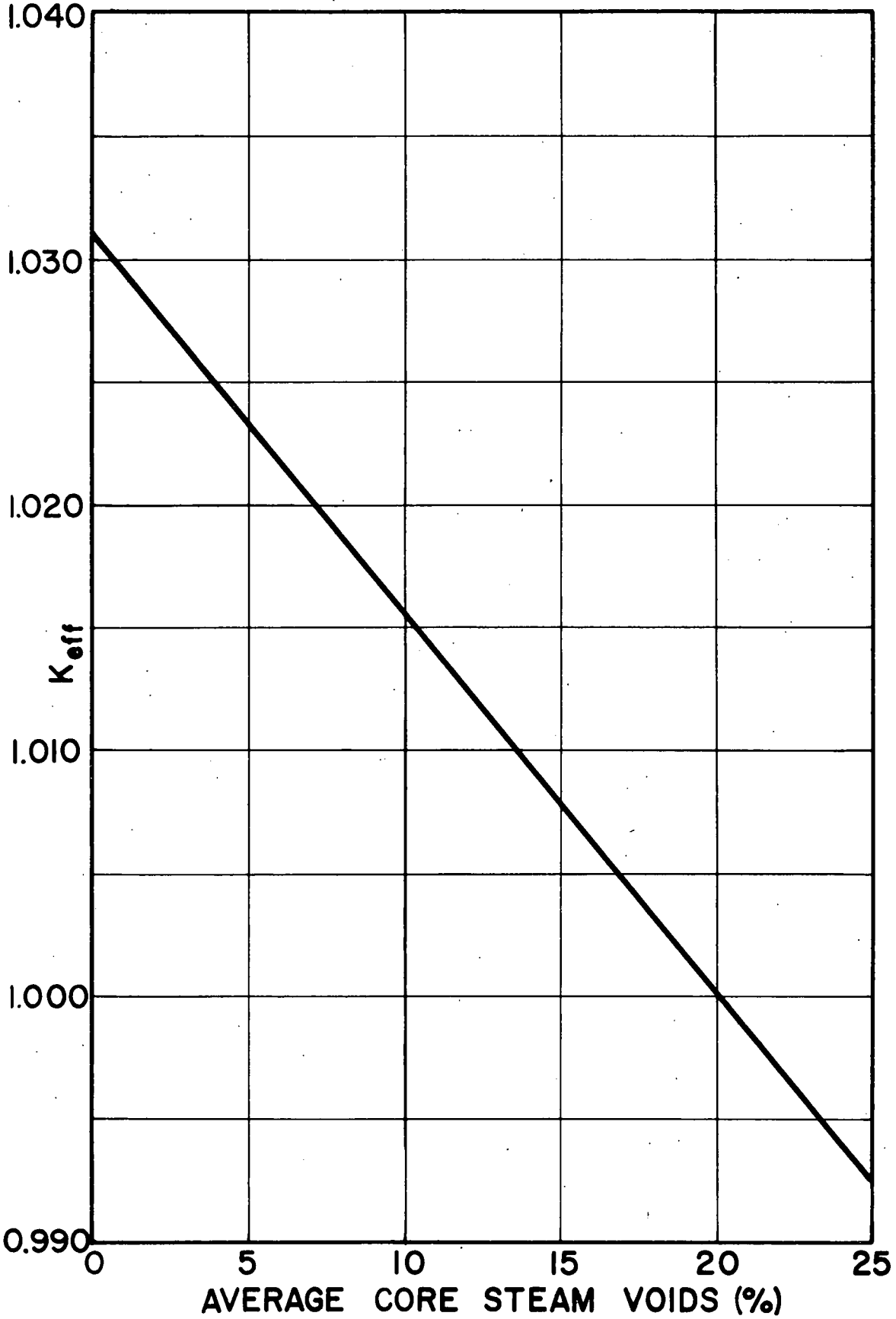

Steam Void Reactivity

Figure 21

1.17×10^{13} neutrons/cm^2-sec. The results of this curve were applied directly to the present problem. Xenon and samarium poisoning were computed from the expression 11.56.1 of Glasstone and Edlund by assuming a constant neutron flux over the reactor. The variation of effective multiplication with reactor life is shown in Fig. 22.

(a) 450°F, 20% steam voids, equilibrium concentration of xenon, samarium, and other fission products.

(b) 68°F, 0% steam voids, no xenon, equilibrium concentration of samarium and other fission products.

3.9 Results of Critical Mass Calculations

Fuel loading - Uranium-235

Clean core (20% steam voids - 450°F)	8.49 kg
Initial loading of poisoned core	18.1 kg
Loading after 15 Mw-yr	10.6 kg

Boron-10 Poison

New core	0.0382 kg
Core after 15 Mw-yr	0.00172 kg
Initial neutron flux	1.12×10^{13} n/cm^2-sec
Final neutron flux (15 Mw-yr)	1.91×10^{13} n/cm^2-sec

3.10 Neutron Fluxes

The fast and thermal neutron fluxes for a spherical model are plotted in Fig. 23. The magnitude of the ordinate arbitrarily resulted by choosing the coefficient of the spherical function of the fast flux equal to unity.

3.11 Control Rods

External control of the reactor is effected by five control rods, one central and four placed on a concentric circle. It was assumed, for ease of calculation, that the control rods were inserted in an equivalent bare square cylinder and that the fuel concentration increased to make the

ORNL-LR-Dwg. 6078

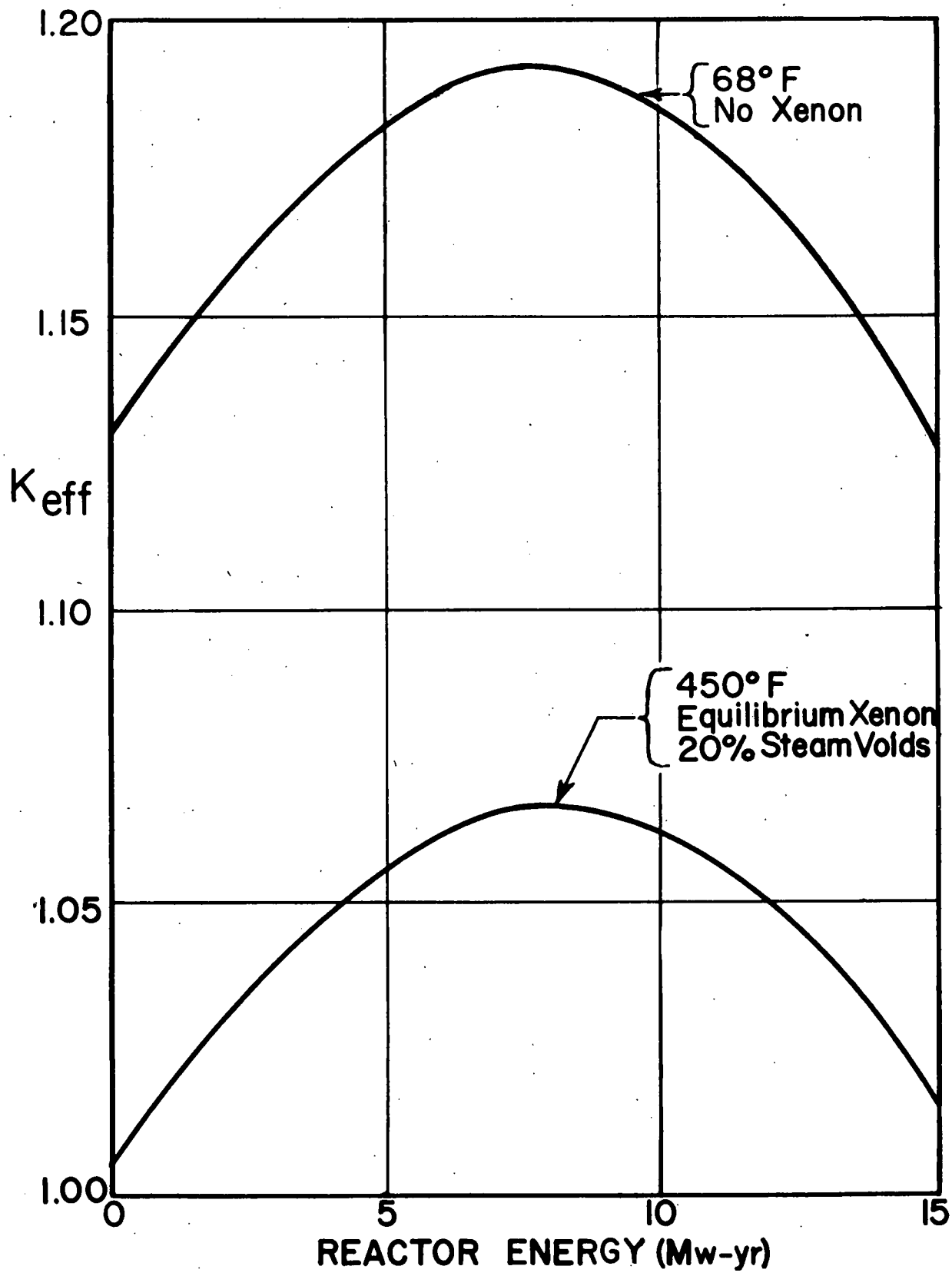

K_{eff} vs. Time

Figure 22

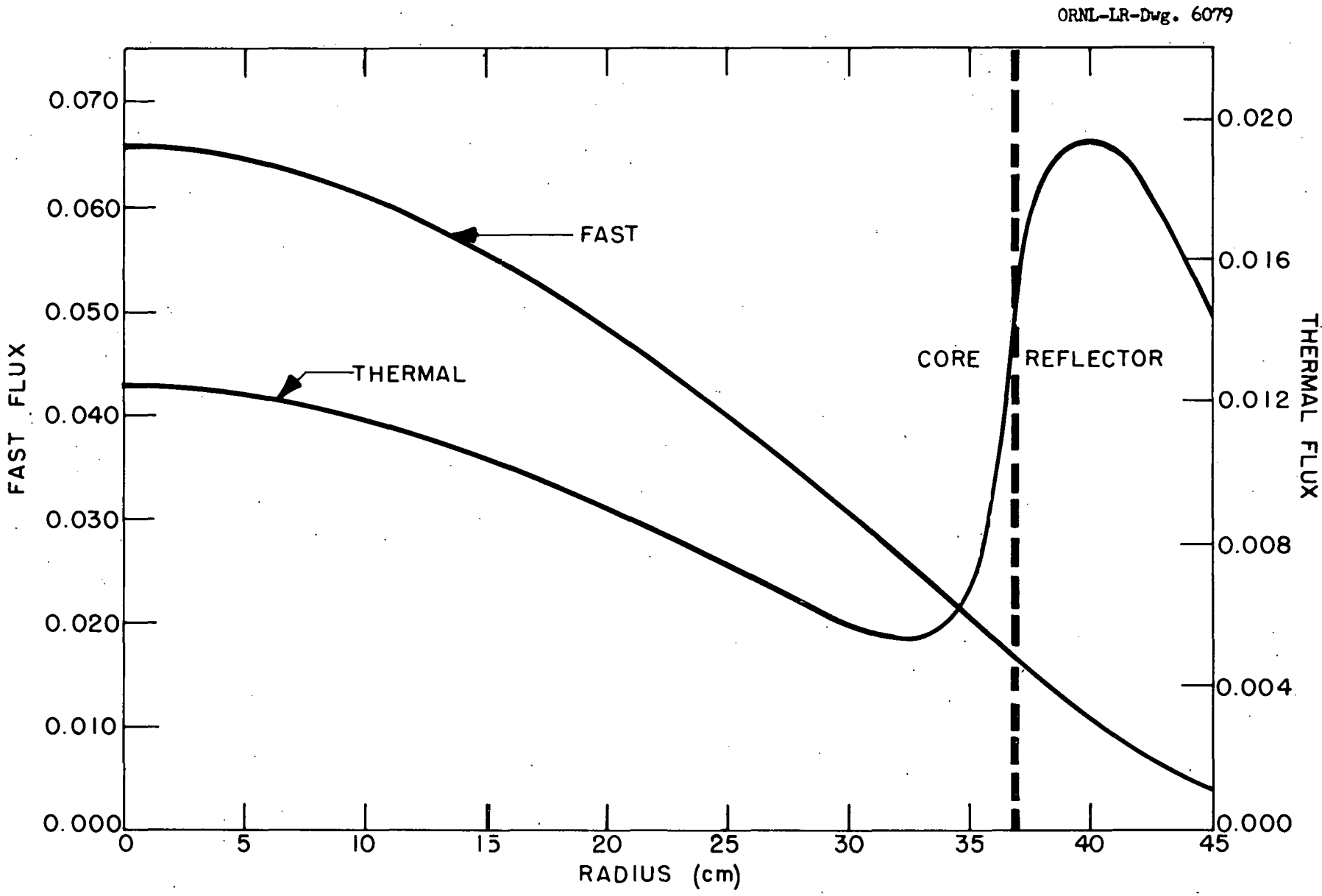

NEUTRON FLUX (450°F, 20% STEAM VOIDS, SPHERICAL MODEL)

Figure 23

reactor critical. The core composition, except for the fuel concentration, was assumed to be the same as the reactor at 68°F after 7.5 Mw-yr life.

The value of the rods was taken as

$$\frac{\text{f with control rods}}{\text{f without control rods}}$$

where f is thermal utilization.

The value of five control rods was computed from the Nordheim-Scallettar approximation as expressed by Garabedian.* Due to the relative value of the elements of this determinant it was approximated by

$$0 = \begin{vmatrix} 1 & Y_o(\mu' a) & Y_o(\mu' b') + \frac{2}{\pi}\frac{S_2}{S_1} K_o(\nu' b') \\ J_o(\mu' a) & \frac{1}{N}\left\{ L_{oo} + Y_o(\mu' b') + \frac{2}{\pi}\frac{S_2}{S_1} K_o(\nu' b') \right\} & Y_o(\mu' a) \\ J_o(\mu' R) & J_o(\mu' a)\, Y_o(\mu' R) & Y_o(\mu' R) \end{vmatrix}$$

where: b' = the extrapolated radius of the control rods, i.e., physical radius less $0.71 \lambda_{tr}$ (core)

a = radius of the ring of rods

R = radius of the equivalent bare reactor

$L_{oo} = \sum_{n=2}^{4} Y_o(\mu' \rho_{1n})$

$\mu' = \left[\mu^2 - \left(\frac{\pi}{H}\right)^2\right]^{1/2}$

$\nu' = \left[\nu^2 + \left(\frac{\pi}{H}\right)^2\right]^{1/2}$

H = extrapolated height of the equivalent cylinder

ρ_{1n} = distance between centers of outer control rods

μ, ν, S_1 and S_2 are the two-group expressions for buckling and coupling coefficients.

---

* H. L. Garabedian, Control Rod Theory for a Cylindrical Reactor, p. 40, WAPD-18.

The value of one central control rod and no off-center rods is given by the critical determinant of Garabedian (p. 44) which can be approximated as

$$J_o(\mu' b)\, Y_o(\mu' R) - J_o(\mu' R) \left[Y_o(\mu' b) + \frac{2}{\pi} \frac{S_2}{S_1} K_o(\nu' b) \right] = 0$$

The reactivity of one central control rod was also computed by the two-region method of R. L. Murray (ORNL-1613, p. 139). The control rod was assumed to be a cylindrical boron shell filled with water (no steam) at the reactor temperature. The fast neutron group was assumed to be moderated in the rod, as in the case of an internal reflector. The boron shell was taken to be transparent to fast neutrons but opaque to thermals. In the critical equation, no approximations relating to the rod size were made. The fast group extrapolation length into the rod was taken as

$$d_1 = \frac{D_{1C}\, I_o(\mathcal{K}_1' b)}{D_{1R}\, \mathcal{K}_1'\, I_1(\mathcal{K}_1' b)}$$

where $(\mathcal{K}_1')$ is the inverse slowing down length in the rod and b the rod radius $\mathcal{K}_1' = \left[\mathcal{K}_1^2 + \left(\frac{\pi}{H} \right)^2 \right]^{1/2}$

The critical determinant can be put into the form

$$\frac{J_o(\mu' R)}{Y_o(\mu' R)} = \frac{\begin{vmatrix} \frac{J_o(\mu' b)}{d_1} + \mu' J_1(\mu' b) & \frac{K_o(\nu' b)}{d_1} + \nu' K_1(\nu' b) \\ S_1 \left[\frac{J_o(\mu' b)}{d_2} + \mu' J_1(\mu' b) \right] & S_2 \left[\frac{K_o(\nu' b)}{d_2} + \nu' K_1(\nu' b) \right] \end{vmatrix}}{\begin{vmatrix} \frac{Y_o(\mu' b)}{d_1} + \mu' Y_1(\mu' b) & \frac{K_o(\nu' b)}{d_1} + \nu' K_1(\nu' b) \\ S_1 \left[\frac{Y_o(\mu' b)}{d_1} + \mu' Y_o(\mu' b) \right] & S_2 \left[\frac{K_o(\nu' b)}{d_2} + \nu' K_1(\nu' b) \right] \end{vmatrix}}$$

where $d_2 = 0.71\,(3D_{2C})$.

This latter value of the central control rod was multiplied by the ratio of the value of five control rods to the value of one, determined by the Nordheim-Scallettar determinant, to obtain a better estimate of the five control rods.

The dimensions of concern in these computations are:

$a = 16.89$ cm
$b = 3.009$ cm
$b' = 2.756$ cm
$R = 39.67$ cm

$\rho_{13} = 33.78$ cm
$\rho_{12} = 23.88$ cm

The results of the calculations were:

Number of Control Rods	Method of Computation	Σk Controlled
1	Nordheim-Scallettar	0.091
5	Nordheim-Scallettar	0.308
1	Two region method	0.074
5	Two region method (Est.)	0.250

It is therefore estimated that the control rods can control the reactor if $K_{eff} < 1.250$.

4.0 HEAT TRANSFER AND HYDRODYNAMICS

4.1 Advantage of a Boiling System

A boiling system, consisting of a steam generator coupled directly to a turbine, is one of the most simple and well known methods of electric power generation. The elimination of intermediate heat exchangers is a reduction in cost of large magnitude, and, since a large number of power plant failures occur in heat exchangers, another possible source of trouble is eliminated. With boiling, much larger heat transfer coefficients are possible than with ordinary forced convection (non-boiling). Since forced convection coefficients must be modified by appropriate safety factors to insure that no boiling takes place in the core, there can be an increase in the design heat transfer coefficient by at least a factor of ten for a boiling system. In effect, this allows low circulation rates of coolant, limited only by permissible vapor fraction in the core. The problem of heating tube burnout is incurred, however, brought about by excessive heat release in the core or loss of coolant flow. The core is therefore designed to operate well below the burnout point. A major result of these high rates of heat transfer is, of course, a substantial reduction in heat transfer area. Where the size of the unit is important, boiling is very desirable.

Formerly, it was feared that a boiling system would be unstable. It was thought that density fluctuations might have a disasterous effect on nuclear stability and that bubble formation might not take place with sufficient speed to make the reactor self-regulating. It has since been

demonstrated by ANL* that boiling reactors, when properly designed, are as stable to moderate changes in reactivity as other aqueous reactors and that bubble delay time is so small that it is almost inconceivable that this could produce disasterous results, the time being on the order of 0.001 second.

4.2 Selection of Operating Pressure

In order to remove 10 megawatts of heat from the core, it is necessary to circulate about 296,000 cubic feet of steam per hour at 50 psia; 37,800 cubic feet per hour at 415 psia; or about 15,200 cubic feet per hour at 1000 psia (see Fig. 24). From this it is apparent that in order to keep equipment size reasonable, a high pressure is desirable. On the other hand, any substantial increase in pressure above about 600 psia will result in decreased steam quality in the final stages of the turbine. This effect is quite detrimental to the life of the turbine blade. In the range 400-600 psia, there is little change in steam quality, and below 400 psia the steam quality increases.

Another factor which tends to limit pressure is the cost of high pressure equipment. The pressure vessel, piping, pumps, etc., will be much more expensive if designed for 1000 psia than for the 415 psia decided upon. The weight of the equipment is also a function of steam pressure and could conceivably reach a point where portability (i.e., pressure vessel) would be a serious problem. After carefully considering these factors, 415 psia was thought to approach the optimum pressure, although time did not permit an elaborate analysis of the factors. Saturation temperature is not an important factor for stainless steel elements, since the allowable temperature for steel is quite high.

*ANL Report Nos. 5211, 4921, 5208, 5272, 5228, 4915, 4916, 4627 (Argonne National Laboratory Quarterly Progress Reports).

ORNL-LR-Dwg. 6080

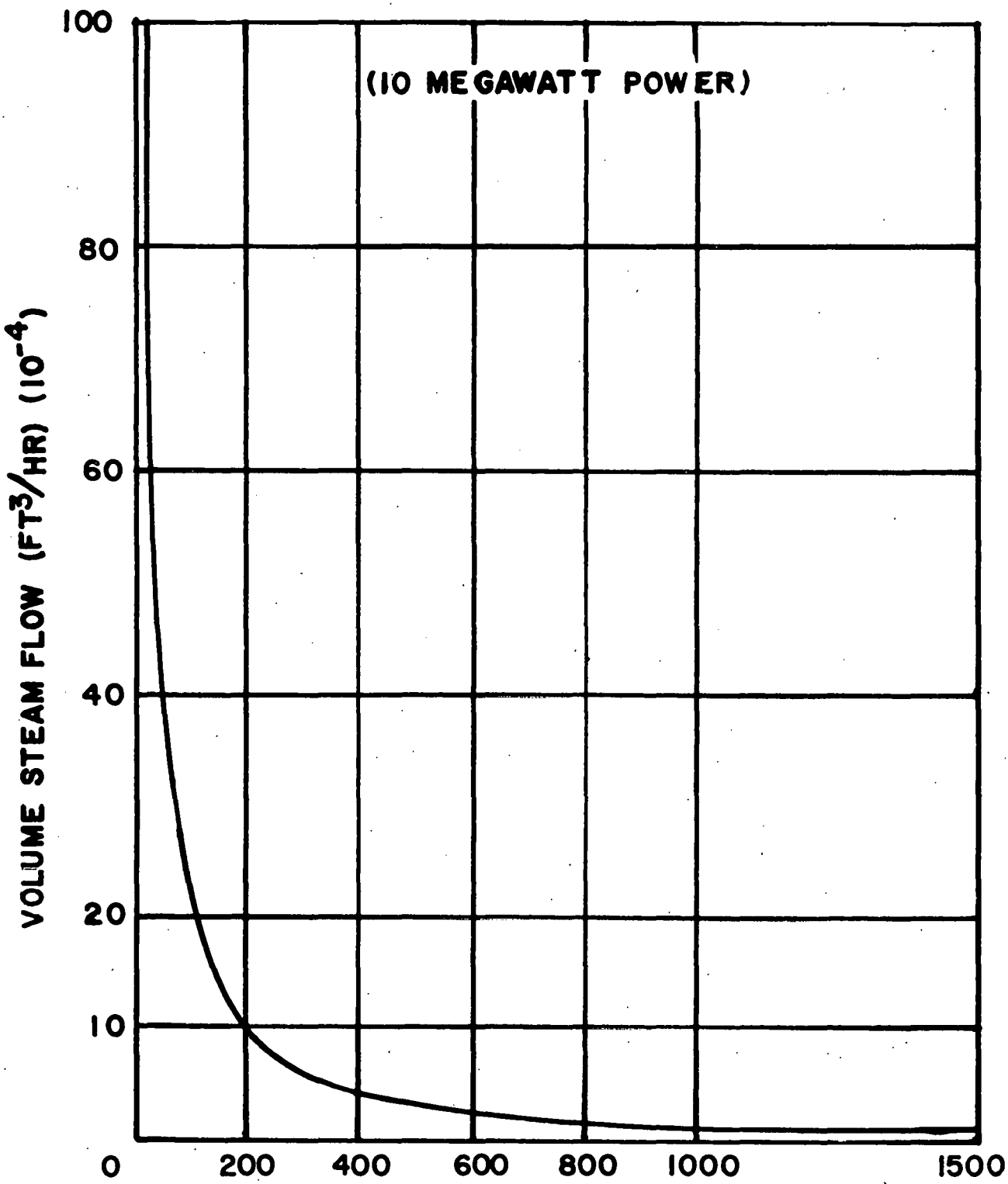

VOLUME STEAM FLOW VS SATURATED STEAM PRESSURE

FIGURE 24

4.3 Advantages of a Natural Circulation System

Both forced and natural circulation systems were studied; it was decided to adopt the latter type. For a given power level, the coolant recirculation ratio (CRR) is a function (see Appendix 12.4) of only the average core density as shown by equation 4.1.

$$CRR = \left[\frac{v_{fg}}{\rho_f \left(\frac{\rho_i - .125\rho_f}{.875} \right) - \frac{1}{\rho_f}} \right] - 1 \qquad \text{Equation 4.1}$$

where ρ_i is the average core density

ρ_f is the fluid density (saturated)

v_{fg} is the specific volume change from liquid to vapor

With boiling in 7/8 of the core and an average steam void of 20%, the recirculation ratio is 85. The pressure drop throughout the core is less than one psi. This indicates that a forced circulation pump of very large capacity and low head is required. To keep velocities and pressure drops low, quite large recirculating pipes would be necessary. It seems almost pointless to recirculate such a large volume of fluid outside the core and incur the expense of such pipes and pumping work if a system can be devised without them. In a natural circulation system, the available head can be varied by adding a riser at the top of the core such that the gain in head will just balance the system losses. Once this riser is installed, the available head is still adjustable by varying the water level in the pressure vessel. These calculations (see Appendix 12.4) show that a riser of 3.7 ft is required,

including a 6-in. end box on each fuel element . This is not considered to be excessive for a package reactor, since the entire pressure vessel can be built not to exceed 15 ft in height. A diameter of about 4 ft is required for the pressure vessel to allow room for the core assembly and still have sufficient area for the downcomer to produce very low velocities in that section. Since steam is being permitted to separate from the liquid phase at a liquid-steam interface, vapor entrainment in the downcomer must be considered. With the area of the downcomer adjusted so that the liquid velocity will be less than the slip velocity between vapor bubbles and liquid, any entrained vapor will rise countercurrent to the downcomer flow and separate at the liquid-vapor interface. Calculations (see Appendix 12.4) show that under operating conditions bubble slip velocity, $(V_g - V_f)$ is defined as:

$$(V_g - V_f) = \frac{1.88\ (e^{4560t} - 1)}{e^{4560t} + 1} \qquad \text{Equation 4.2}$$

where $\underline{t}$ = time in seconds

This indicates that bubble slip velocity will be held to about 1.9 fps, while for a downcomer area of 8.6 ft, the liquid velocity will be held to about 1.8 fps.

It is also important to note that at pressures of 500 psia and less, the burnout point is not effected by coolant velocity. Hence, there is no advantage in using high velocity, forced circulation instead of low velocity, natural circulation.

4.4 Steam Separation at Liquid-Vapor Interface

From elementary boiler theory,* it is known that only limited amounts of steam separation can be obtained from a given surface area, this being a function of only the saturation temperature (see Fig. 25). At 415 psia, about 2200 lbs of steam can be separated per hour per square foot of liquid surface. A four foot pressure vessel, giving approximately 12 ft^2 of liquid surface and operating at 10 Mw, would require a heat release rate of about 2750 lbs of steam per square foot per hour. This is somewhat above the permissable rate and as a result, it is expected there will be a tendency for vapor entrainment in the downcomer. It is expected that vapor entrainment, if any, will be very slight and with such low fluid velocities in the downcomer, counter-current vapor flow should remove almost 100% of any entrainment. Cold feed water will also tend to condense any entrainment.

4.5 Fuel Plate Burnout

Fig 26, Heat Flux vs Temperature Difference, is a rough indication of the heat transfer coefficient at varying heat flux. At very low fluxes, the heat transfer coefficient is low and approximately that calculated by Nusselt's equation for single phase flow. Various experimenters have developed empirical expressions, curves, and methods of arriving at the heat flux necessary for the inception of boiling (the point at which the heat transfer coefficient changes abruptly). For our operating conditions

---

* Modern Power and Engineering, 35, April 1941.

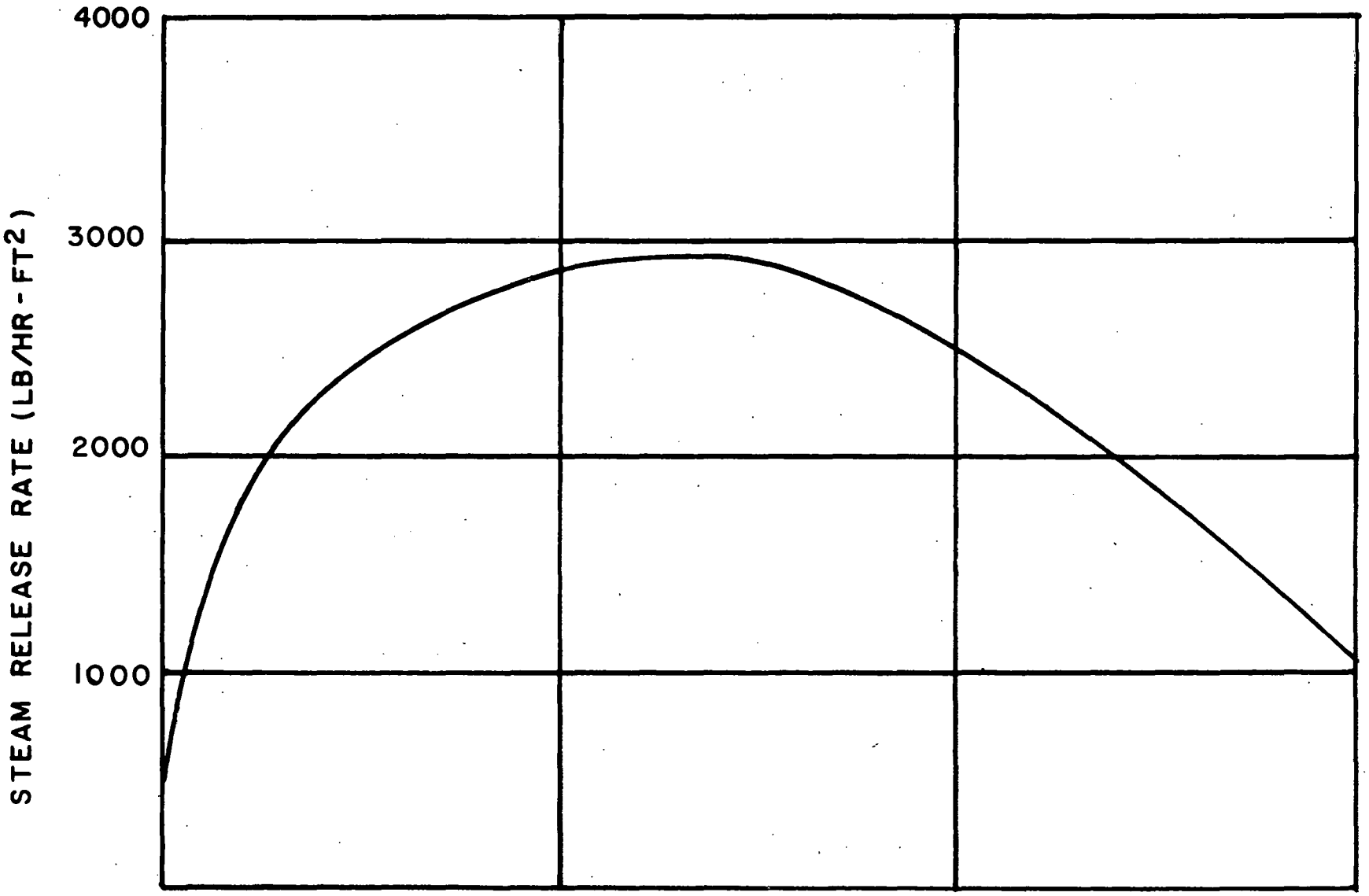

STEAM RELEASE RATE VS SATURATION PRESSURE

FIGURE 25

ORNL-LR-Dwg. 6081

ORNL-LR-Dwg. 6082

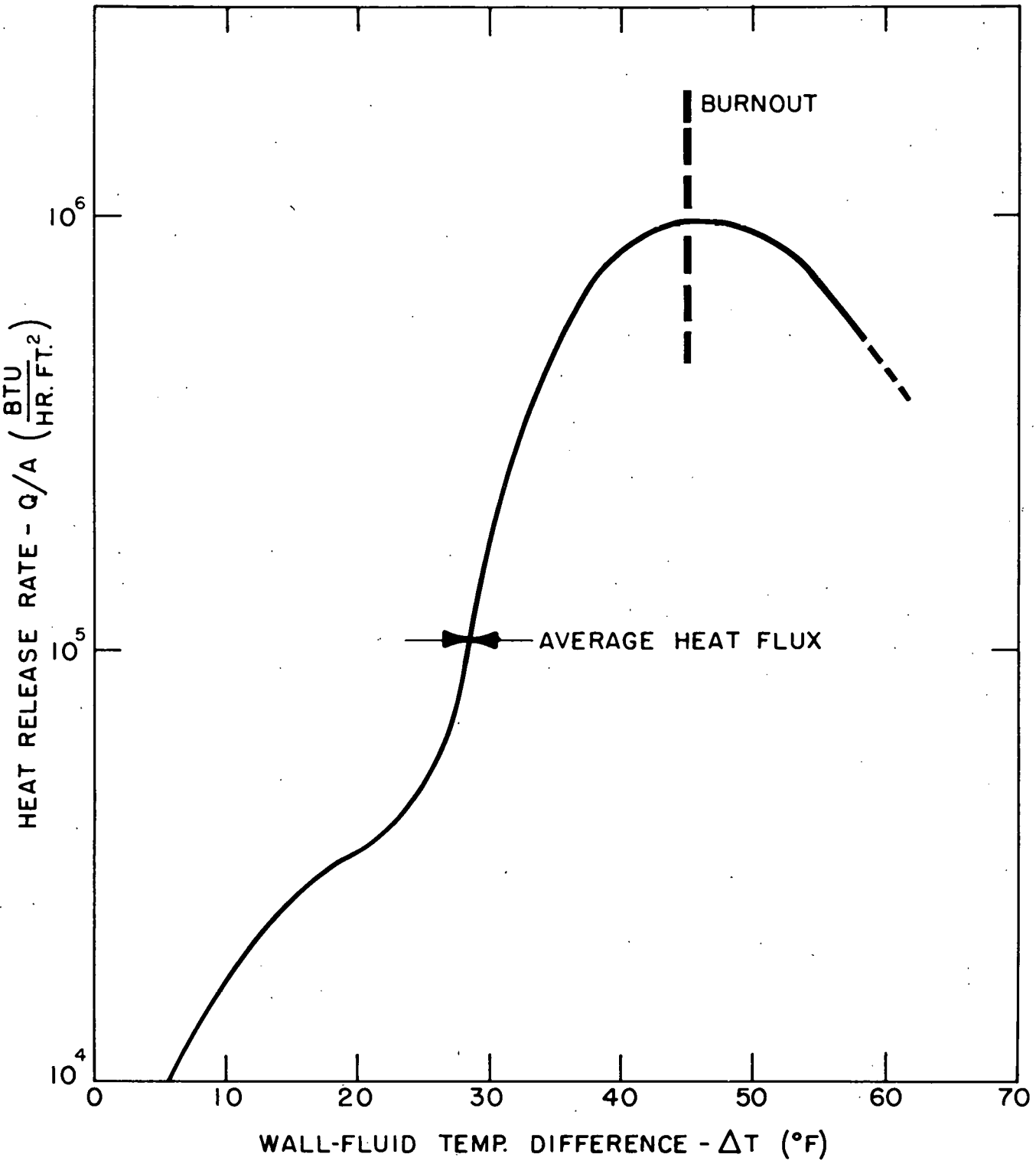

HEAT RELEASE RATE VS. TEMPERATURE DIFFERENCE

Figure 26

the best estimate of this point, based on extrapolation of experimental results,* is at a heat flux of about 40,000 BTU/hr-ft^2. Checking experimental results for the point of maximum heat flux (burnout) is rather discouraging, since results vary widely, depending on many factors. A very conservative figure, however, is about 10^6 BTU/hr-ft^2 at a temperature difference of about 45 °F, which is plotted. Since the average heat flux of this core is about 105,000 BTU/hr-ft^2 and the maximum to average heat flux is not expected to exceed 4/1, this allows a safety factor of about 2 1/2 at the very least. A discussion on individual channel vapor lock and restriction of flow leading to burnout is included in this report under paragraph 4.11.

4.6 Head Losses in System

An accurate calculation of the system head losses is quite important since this is the determining factor for the height of riser required, as shown in Fig. 27. In the analysis of the natural circulation system, it was assumed as a good first approximation, that

$$\Delta P = \frac{K \bar{\rho} U_2^2}{2g}$$

where U_2 is the core exit velocity

$\bar{\rho}$ is the average density for the entire system

and K is a dimensionless head loss coefficient, presumably constant for a given system, being a function only of geometry.

---

* Studies in Boiling Heat Transfer, University of California, COO-24.

ORNL-LR-Dwg. 6083

FIGURE 27

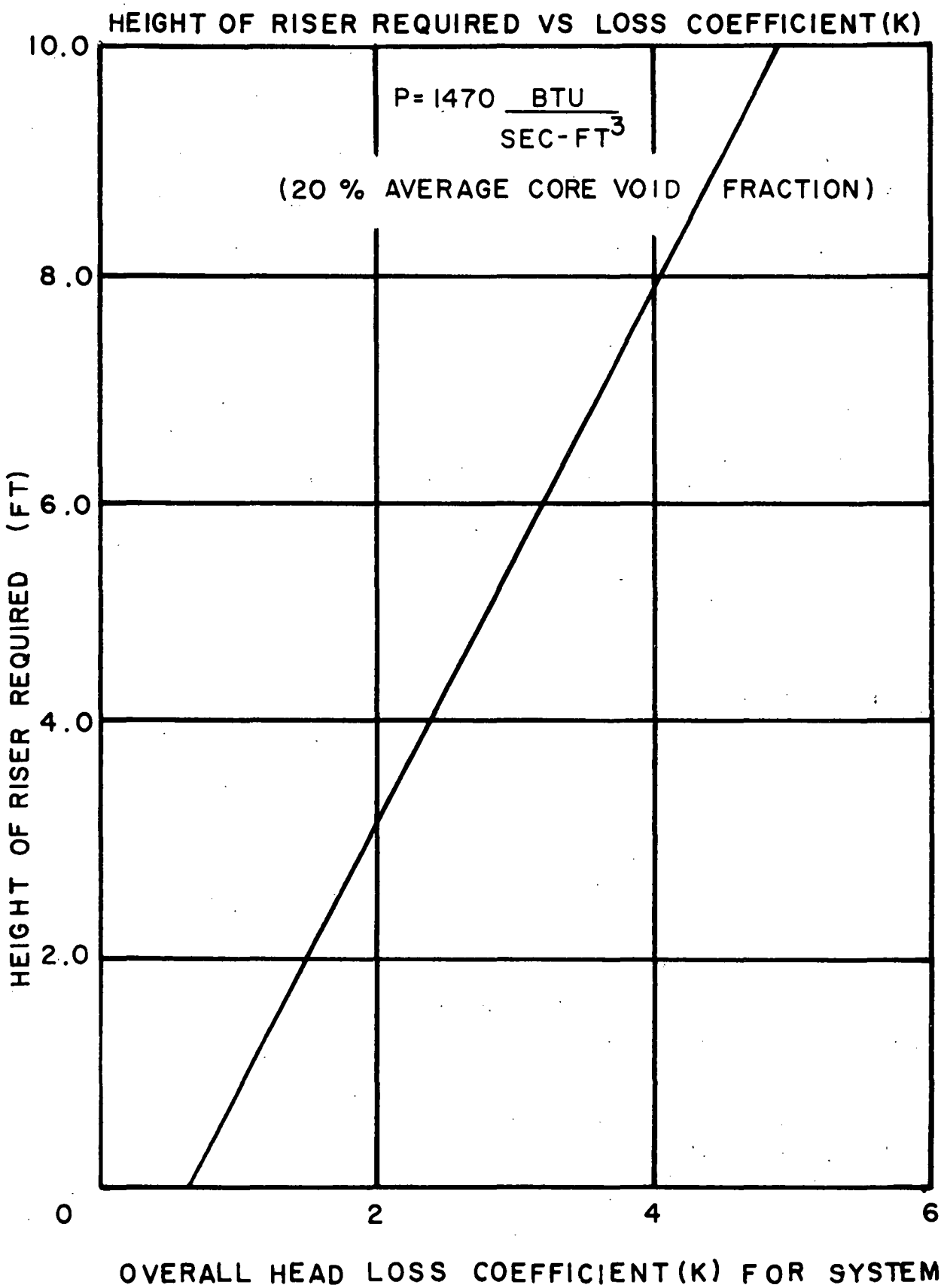

For two-phase flow, this is not strictly true, but is a good approximation over a limited range. The method used to find a good value for K was to solve for the individual pressure drops throughout the system (see Appendix 12.4), sum them up and solve for the K which satisfies the above equation. This method would, of course, be accurate at design conditions; however, for a parameter study over a wide range, the validity of this number is somewhat questionable. It is felt that the value of K found in this manner is sufficiently accurate for variations in density or velocity of the order 50%. For changes greater than this, it is suggested that individual pressure drops again be solved, and a new K calculated. In solving for individual pressure drops, the methods of Martinelli and Nelson* were used for prediction of pressure drop for two phase flow in the core. Other pressure drops were calculated by using standard head loss coefficients multiplied by the kinetic energy. A total head loss of 95.0 lbs/ft^2 was calculated for this system The corresponding head loss coefficient, K, was found to be 2.23 and the height of riser required, 3.7 ft.

4.7 Parametric Study of System

It was felt that an analysis of the system should be made to derive an equation by which a parametric study could be made on the variables of the system. Boiling in only 7/8 of the axial length of the core was postulated, natural circulation was assumed, and certain other

---

* Prediction of Pressure Drop During Forced Circulation Boiling of Water, Transactions of A.S.M.E., Aug. 1948, Paper No. 47-A-113, Martinelli and Nelson.

limiting assumptions were made in order to approximate a reasonable system. The equation below is the dimensionless result, for which the complete derivation is included in Appendix 12.4.

Equation 4.3

$$\left[\frac{Pv_{fg}}{h_{fg}+h_x}\right]\left[\frac{KZ}{2g}\right]^{1/2}=\left[1-\frac{\rho_2}{\rho_f}\right]\left[\frac{\rho_f}{\bar{\rho}}\right]^{1/2}\left[.875\left(1-\sqrt{\frac{\rho_2}{\rho_f}}\right)+\frac{Z_1}{Z}\left(1-\frac{\rho_2}{\rho_f}\right)+\frac{\Delta P_{SEP}}{Z\rho_f}\right]^{1/2}$$

With the geometry of the system known, the effects of power density, pressure, separative work (if separators are used), sub-cooling, etc., can be evaluated.

4.8 Fuel Element Temperatures

Although, as previously mentioned, the heat transfer coefficients are not well known, an attempt was made to set upper and lower limits on expected surface temperatures and the temperature distribution. Using pessimistic ratios of maximum to average and minimum to average heat fluxes, surface temperatures were calculated and plotted, as shown in Fig. 28, by assuming a central 80% cosine distribution on power (Fig. 29) in the axial direction. These curves are useful from a qualitative viewpoint, however, since stainless steel fuel elements were selected, temperature is not a prime consideration. This is because stainless steel fuel elements have a very high operating temperature.

The maximum temperature existing in the fuel element was found to be 522°F, by assuming a maximum to average heat flux ratio of 4/1. Calculations are shown in Appendix 12.4.

ORNL-LR-Dwg. 6084

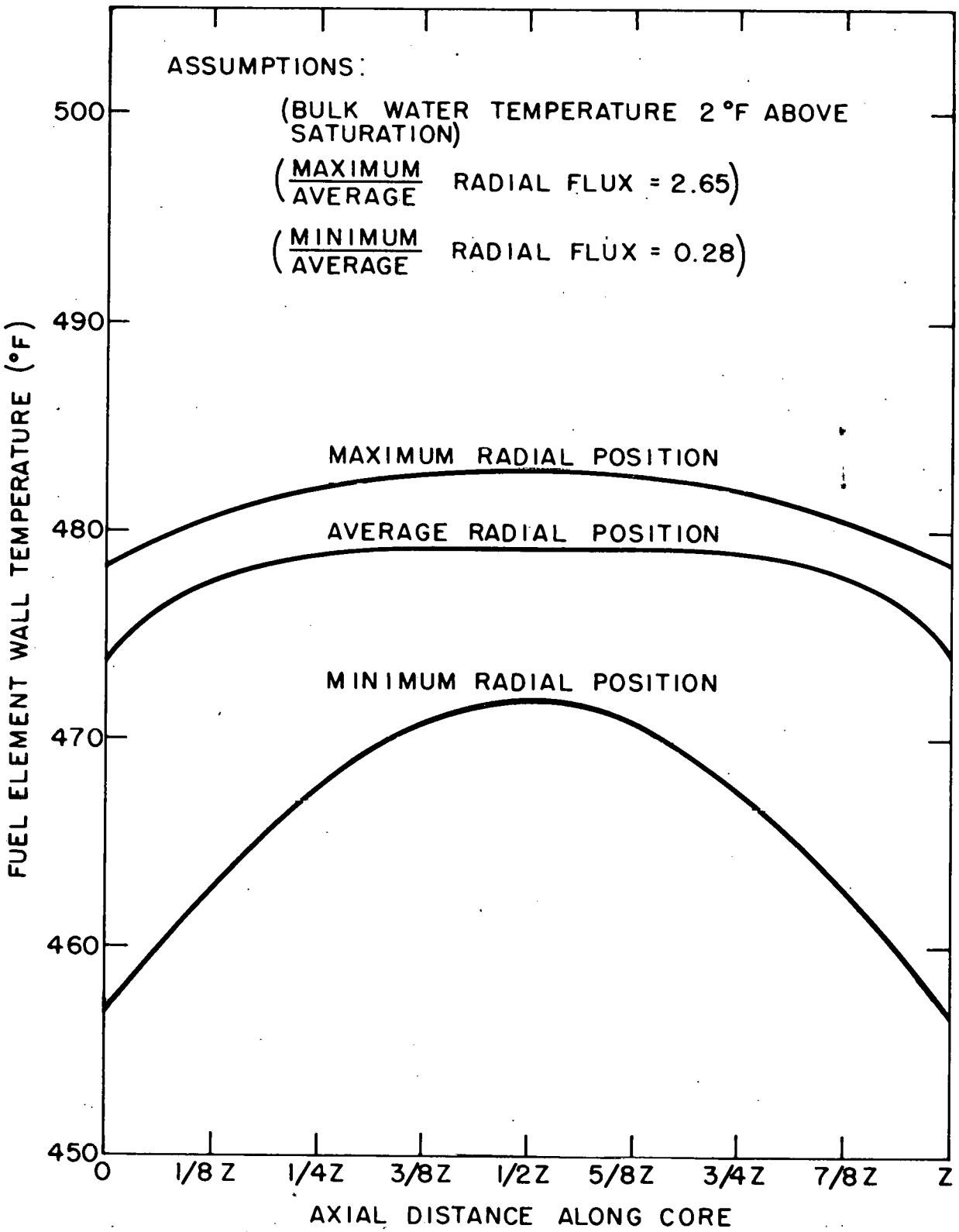

EXPECTED LIMITS ON FUEL ELEMENT WALL TEMP. VS. AXIAL DISTANCE ALONG CORE

Figure 28

ORNL-LR-Dwg. 6085

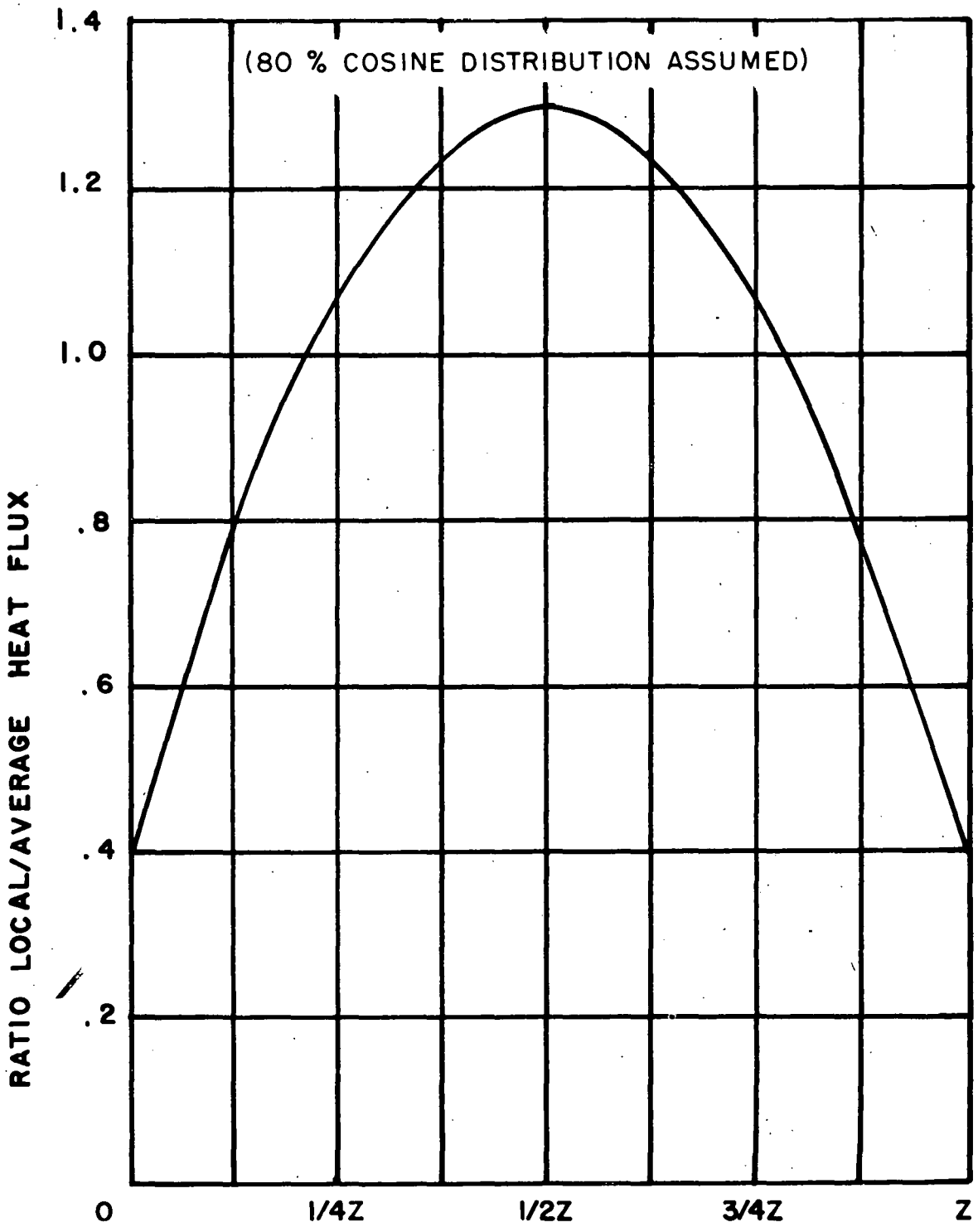

RATIO LOCAL/AVERAGE HEAT FLUX VS AXIAL DISTANCE ALONG CORE

FIGURE 29

4.9 Fuel Element Stresses

The fuel plate maximum stress was found to be about 11,200 psi which represents a satisfactory safety factor compared to the working stress ($\approx$15,000 psi) for stainless steel. Calculations are shown in Appendix 12.4.

4.10 Calculation of Local Coolant Density in Core

Because nuclear properties of a reactor depend on local density, an equation was developed describing density along the vertical axis of the core, assuming 10 Mw power, 20% average void fraction, and boiling in the final 7/8 of the core. The result of these calculations (see Appendix 12.4) is Equation 4.4. A plot of this equation is shown in Fig. 30.

Equation 4.4

$$\frac{\rho}{\rho_2} = \frac{1}{1 - 0.569\left(1 - \frac{\rho_2}{\rho_f}\right)\left(0.951 + \cos \pi Z'\right)}$$

$$Z' = \frac{z + 0.125Z}{1.25Z} \qquad \text{when} \quad .2 \leq Z' \leq .9$$

$$\text{and} \quad \rho = \rho_f \qquad \text{when} \quad .1 \leq Z' \leq .2$$

Z --- Total core length

z --- Fraction of total core length

ρ --- Variable core density

ρ_f --- Saturated fluid density

ρ_2 --- Density at core exit

ORNL-LR-Dwg. 6086

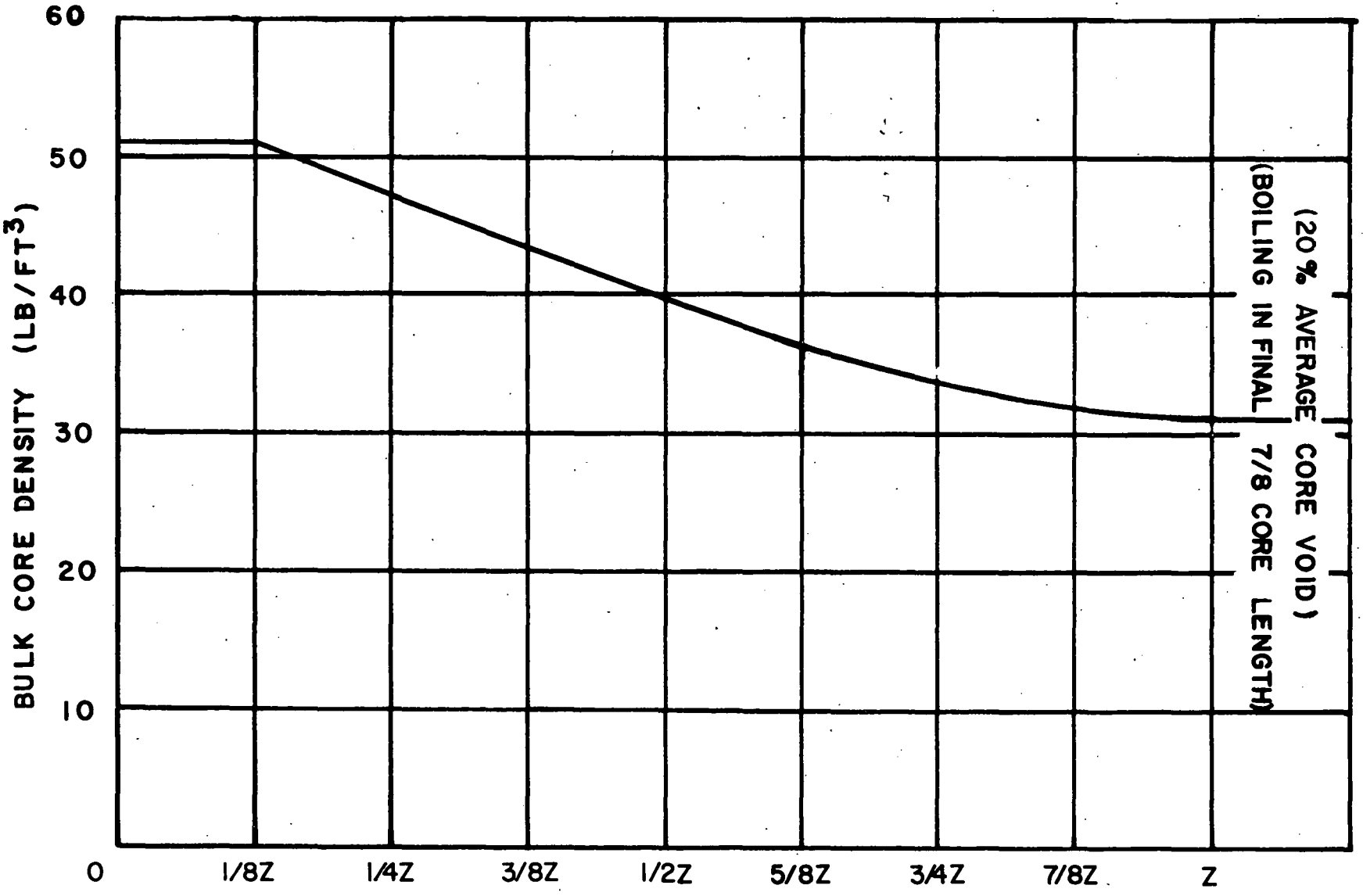

BULK CORE DENSITY VS AXIAL DISTANCE ALONG CORE

FIGURE 30

Since local void fraction and local density are directly related, a plot was made also of void fraction vs axial distance along core (see Fig. 31), both for boiling throughout the entire length of core and for boiling in the final 7/8 of the core. On the basis of these curves, a linear density distribution along the length of the core would be a good approximation. No attempt was made to compare the coolant density and axial neutron flux because it is felt that control rods will distort the neutron flux sufficiently to make detailed calculations worthless.

4.11 Vapor Lock and Restriction of Flow Leading to Unstable Operation

There are two ways to look at this problem. The first is the possibility of a peaking of weight flow as a function of power. In a region of increasing weight flow with increasing power output, the average coolant density is a slowly varying function. However, at the peak there is a region of diminishing return and void fractions climb drastically. A design in this region could readily lead to burnout. The reactor should therefore be designed to operate well below this peak in weight flow. Calculations were made (see Appendix 12.4), with certain limiting assumptions, resulting in Equation 4.5.

Equation 4.5

$$\frac{W^2}{0.928 \times 10^{10}} = \frac{\left[280.62 - \left(\frac{157.5}{.0194 + \frac{\mathcal{H}}{W}}\right)^{\frac{1}{2}} - \left(\frac{3.7}{.0194 + \frac{\mathcal{H}}{W}}\right)\right]}{\left[2.323\ \frac{\mathcal{H}}{W} + .0785\right]}$$

where W is expressed in lbs/hr

and $\mathcal{H} = \frac{PAZv_{fg}}{h_{fg} + h_x}$

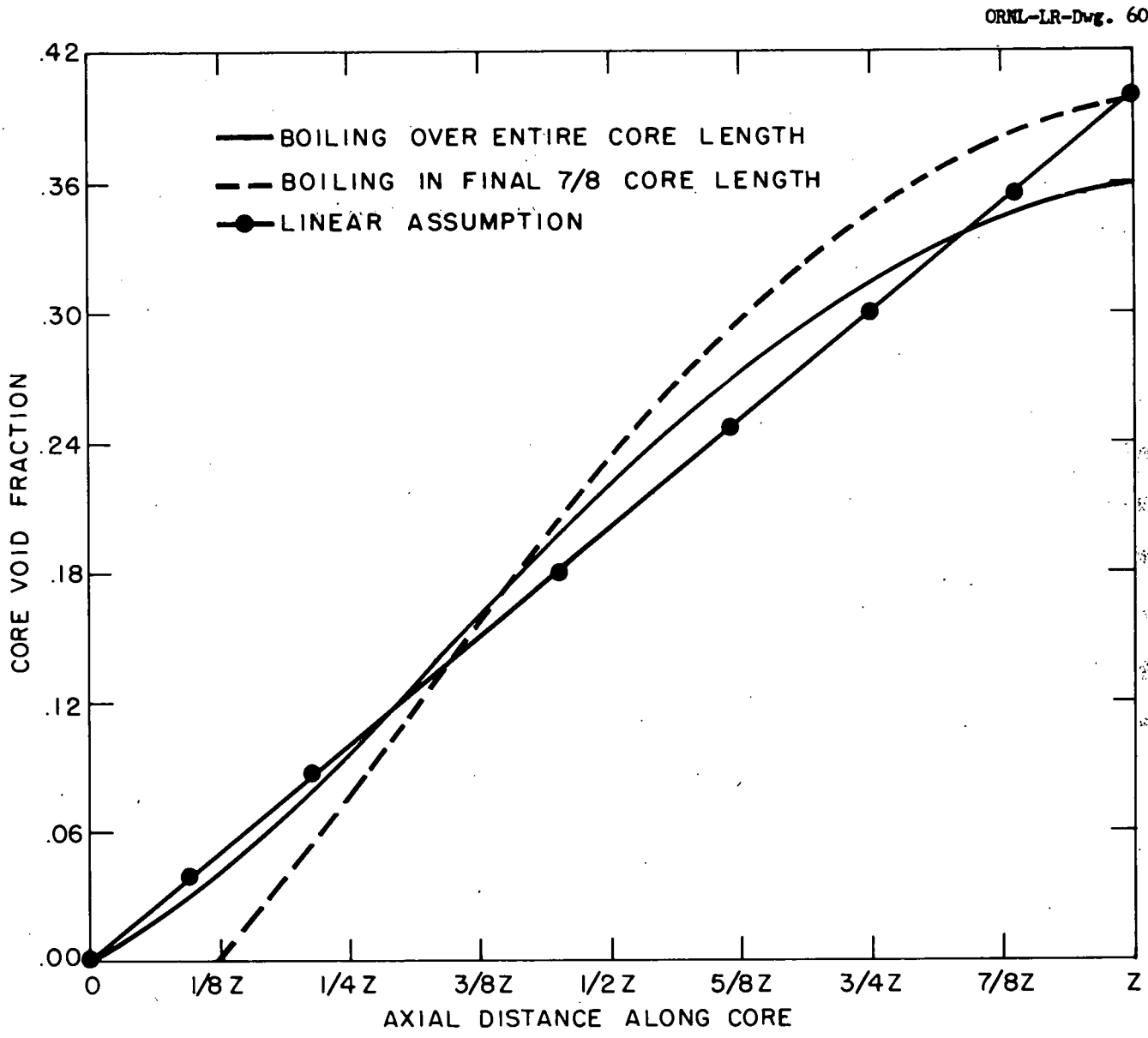

CORE VOID FRACTION VS. AXIAL DISTANCE ALONG CORE
(FOR 20 % AVERAGE CORE VOID)

Figure 31

A plot of this equation is shown as Fig. 32. A second model was postulated for an individual fuel element (see Appendix 12.4). Calculations for this model resulted in Equation 4.6, also shown in graphical form as figure 33.

Equation 4.6

$$\frac{W^2}{3.86 \times 10^6} = \frac{\left[157.1 - \left(\frac{157.5}{0.0194 + \frac{\chi}{W}}\right)^{\frac{1}{2}} - \left(\frac{.50}{0.0194 + \frac{\chi}{W}}\right)\right]}{\left[1.967\,\frac{\chi}{W} + 0.552\right]}$$

On the basis of these two models, the design is apparently not subject to heating tube burnout below 200% full power. However, above 200%, void fractions are expected to increase drastically and burnout will probably occur. A plot of void fraction as a function of per cent power (up to 200%) is shown as Fig. 34.

A second way of looking at this problem is to plot pressure drop from the bottom of the core to the liquid-vapor interface vs weight flow through the core. However, because of mixing in the riser, this was done for an individual fuel tube. For this calculation (see Appendix 12.4), power was assumed constant. For 100% steam flow as one model and 100% liquid flow as a second model, two limiting curves can be drawn (Fig. 35). The pressure drop for two-phase flow must lie somewhere between these two extremes. It has been noted* that occasionally a pressure drop peak occurs in this region. As the weight flow along the liquid line deceases a point is reached where net boiling can occur.

* Volume II (Engineering), Reactor Handbook.

ORNL-LR-Dwg. 6088

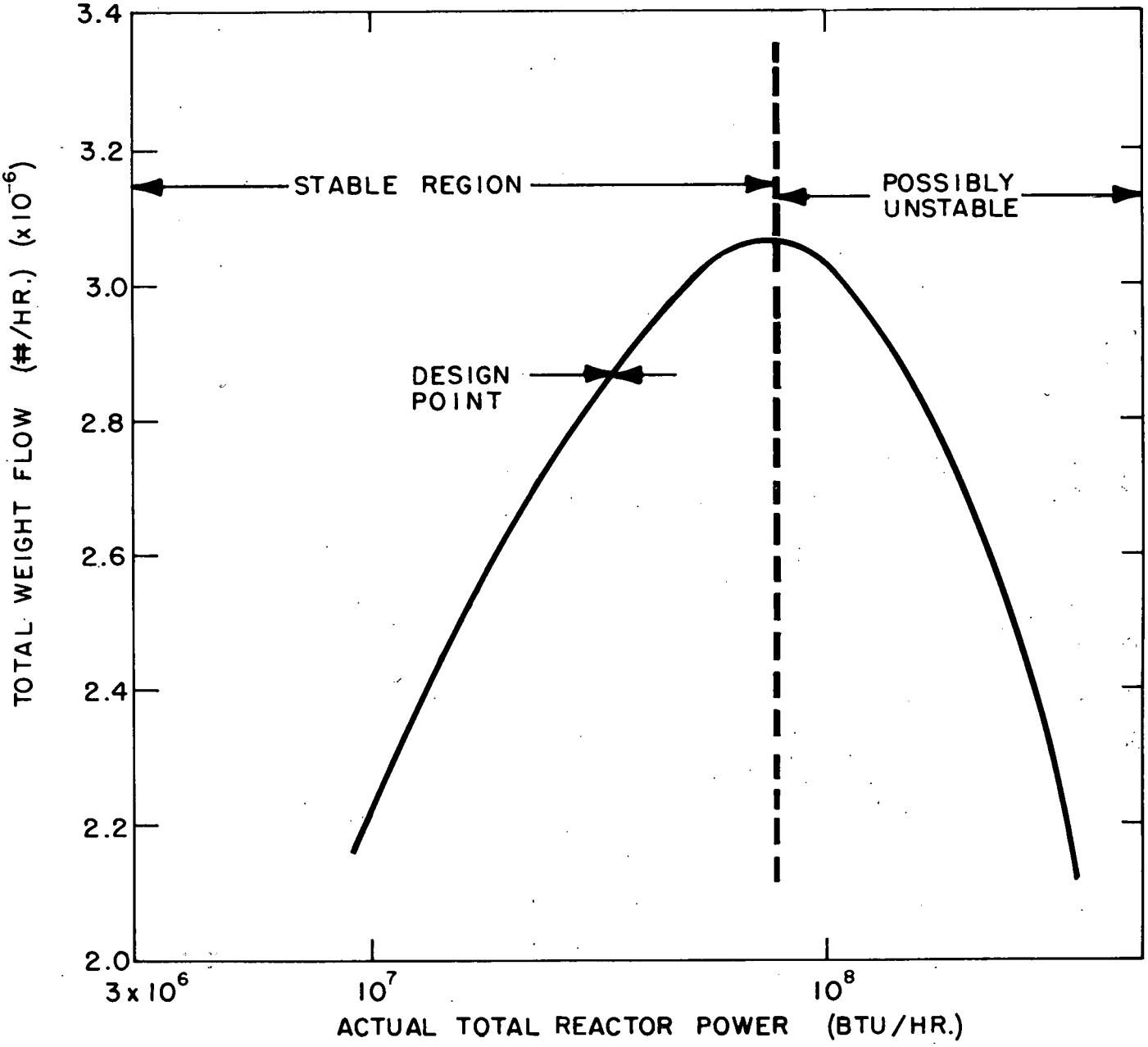

REACTOR POWER VS. WEIGHT FLOW
(ASSUMING CONSTANT POWER DISTRIBUTION)

Figure 32

ORNL-LR-Dwg. 6089

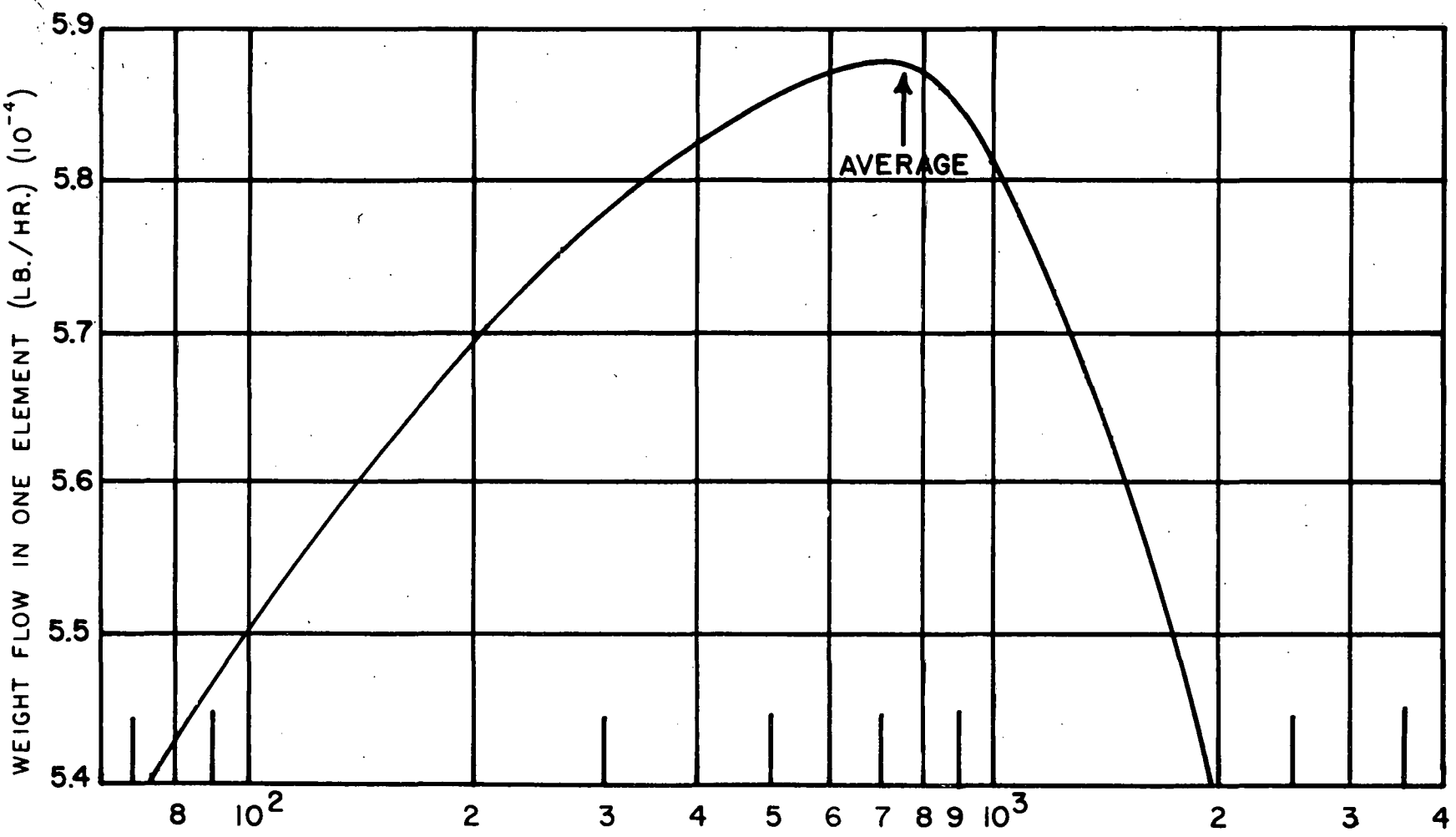

WEIGHT FLOW VS POWER - ONE ELEMENT

FIGURE 33

ORNL-LR-Dwg. 6090

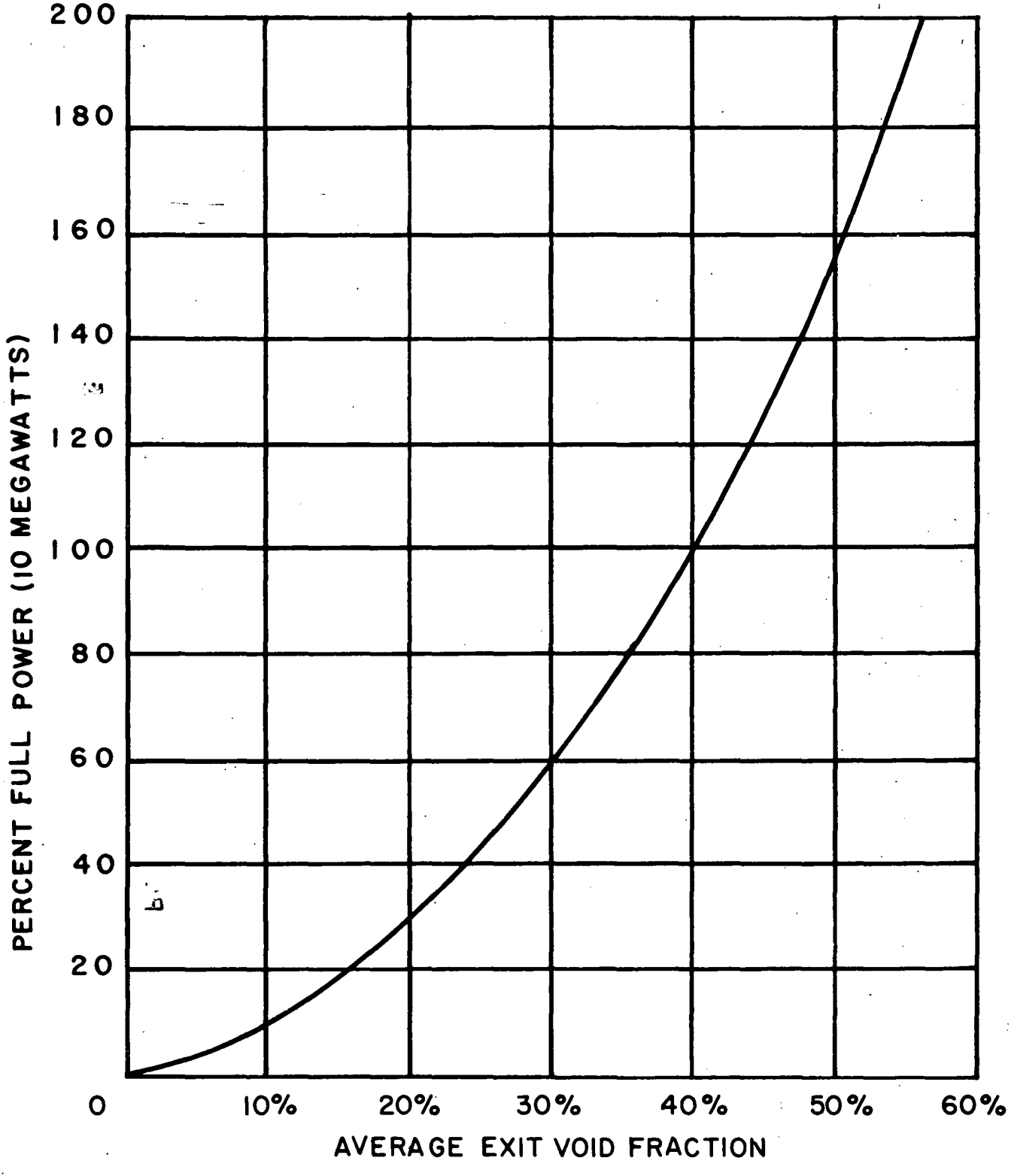

PERCENT FULL POWER VS AVERAGE EXIT VOID FRACTION

FIGURE 34

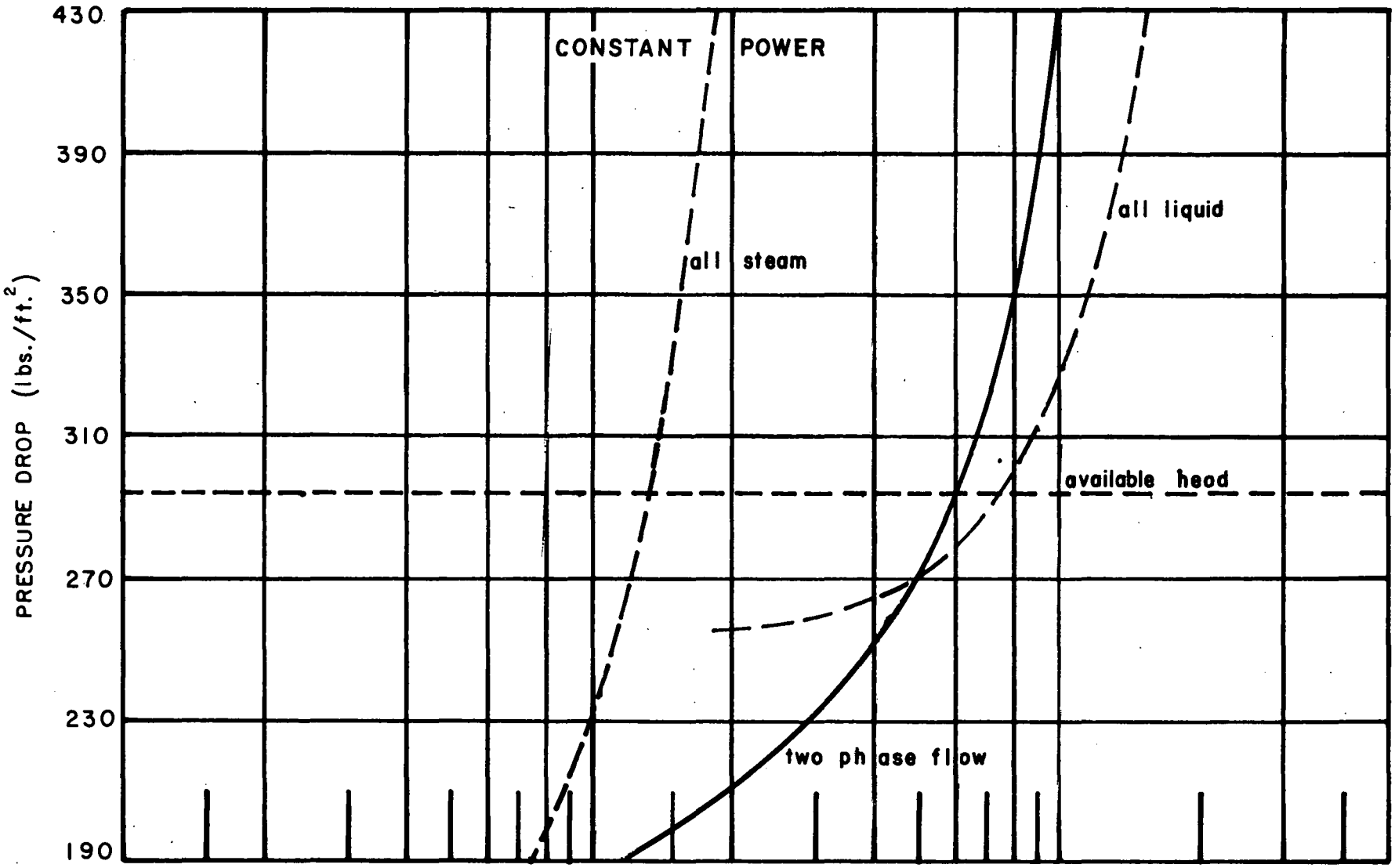

PRESSURE DROP VS TOTAL WEIGHT FLOW (one tube)

FIGURE 35

The resulting increased friction losses and acceleration losses drive the pressure drop up, so that it more than compensates for the drop in weight flow. As the peak is passed, and net boiling is well established, further decrease in weight flow lowers the pressure drop. The method used to handle this situation was to set up pressure drop equations for different power levels, with net boiling at all times. A separate equation was developed giving the critical weight flow (flow at which net boiling initiates) and at this point the calculated two-phase pressure drop was reduced abruptly to that of liquid flow.

According to Martinelli & Nelson* one may postulate either completely separated flow (characterized by low void fraction) or homogeneous fog-type flow (characterized by high void fraction). Equation 4.7 is the result when separated flow is postulated.

Equation 4.7

$$\Delta P = \frac{W^2}{2gA_e^2}\left[\frac{1.967\mathcal{H}}{W} + .0552\right]+\left[\frac{.5}{\rho_f^{\frac{1}{}} + \frac{\mathcal{H}}{W}}\right]+\left[\frac{157.5}{\rho_f^{\frac{1}{}} + \frac{\mathcal{H}}{W}}\right]^{\frac{1}{2}} + 136.44$$

When homogeneous fog type flow is postulated, Equation 4.8 is the result.

Equation 4.8

$$\Delta P = \frac{W^2}{2gA_e^2}\left[\frac{2.968\mathcal{H}}{W} + .0552\right]+\left[\frac{.5}{\frac{1}{\rho_f} + \frac{\mathcal{H}}{W}}\right]+\left[\frac{157.5}{\frac{1}{\rho_f} + \frac{\mathcal{H}}{W}}\right]^{\frac{1}{2}} + 136.44$$

When plotted, these two equations give essentially the same curve, the differences being extremely slight. Consequently, for the remainder of the calculations, separated flow was postulated.

---

* Prediction of Pressure Drop During Forced Circulation Boiling of Water, Transactions of A.S.M.E., Aug. 1948, Paper No. 47-A-113, Martinelli and Nelson.

The equation for prediction of net boiling was developed from simple thermodynamic theory. It postulates that net boiling will occur when sufficient heat is generated to saturate the make up water. The result is equation 4.9

$$W_{critical} = 3.88 \mathcal{H} \left[\left(\frac{1.1}{\rho_2^{\frac{1}{2}} - 0.0194} \right) - 1 \right] \qquad \text{Equation 4.9}$$

where ρ_2 is the core exit density

A plot of these curves for various power levels is shown as Fig. 36. It should be noted that, apparently, this system is quite stable to hydrodynamic fluctuations (chugging). This can be accounted for by any of several explanations. Since the amount of sub-cooling in the system is very slight, the critical weight flow is large. Secondly, since the system head losses are low, the available head can be designed low and out of the peaking region. Low core velocities also tend to keep operation out of the peaking region.

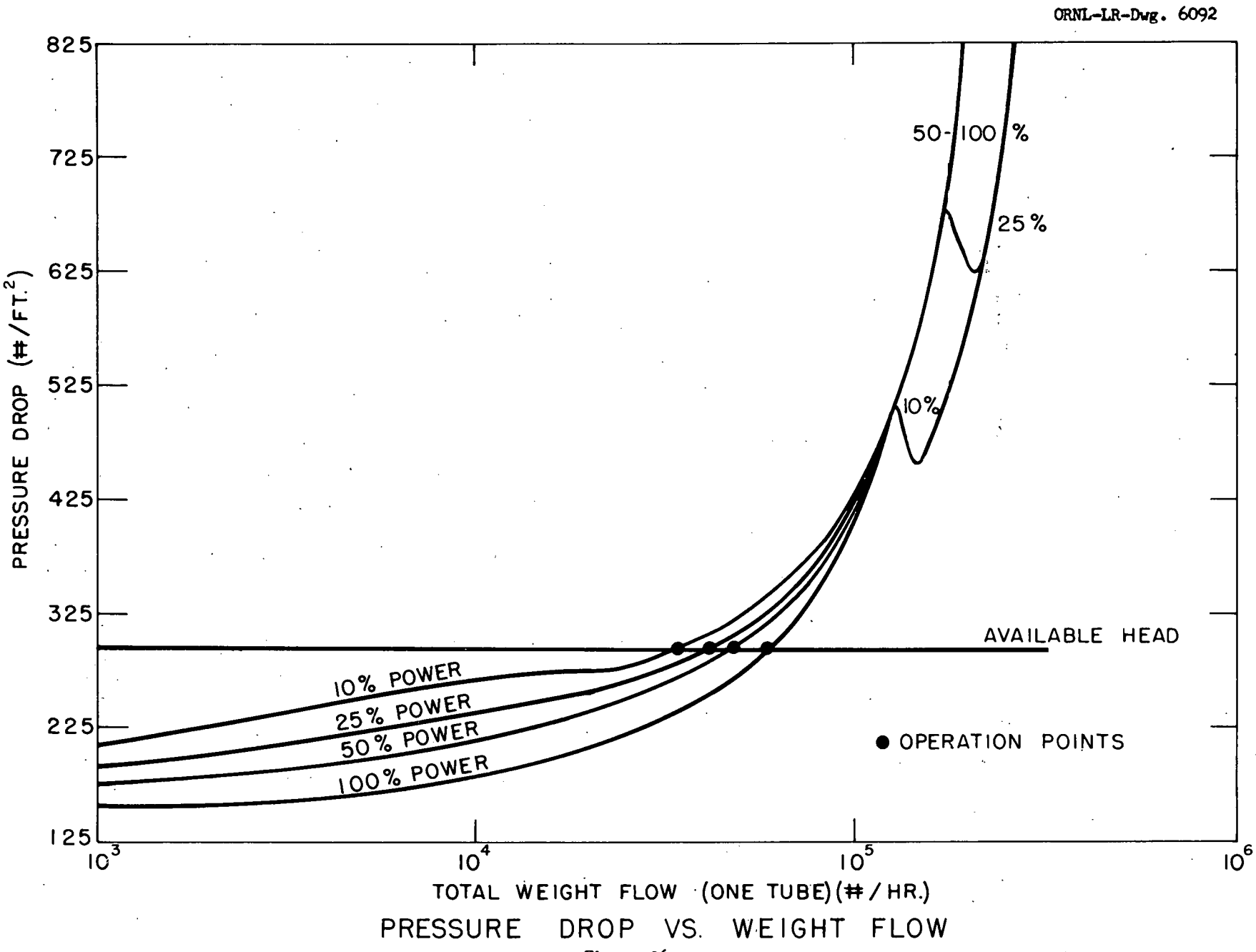

PRESSURE DROP VS. WEIGHT FLOW

Figure 36

5.0. STEAM SYSTEM

5.1 Introduction

The steam system proposed for the boiling package reactor embodies the four basic design premises, namely: simplicity, reliability, low cost, and utilization of standard equipment. With this in mind, the system was designed to utilize 10,000 kw of reactor heat, of which approximately 35% (3535 kw or 12 x 10^6 Btu/hr) is used in the barracks heating system and the remainder is used in the generation of electrical energy. The resultant gross electrical generation is 1300 kw with an auxiliary power requirement of 250 kw for the plant leaving a net electrical generation of 1050 kw under full load conditions.

Steam is generated in a natural circulation reactor core at 415 psia and 448.2° F under all load conditions. Separation of the steam vapor and the entrained moisture is accomplished by several baffles and a toroidal dry pipe located in the upper part of the reactor vessel. It is estimated that the quality of the steam leaving the separator will be 99.8%.

The reactor pressure is maintained constant at all loads by a pressure regulating valve in the discharge line of the reactor vessel. The reactor feedwater level is maintained at a predetermined level by a three-element control system.

5.2 Components

5.2.1 Turbine Generator. A small condensing turbine operating at 3600 rpm utilizes steam at reactor conditions to drive a direct-connected

generator. The turbine has one non-automatic extraction point at 40 psia which is used to heat and deaerate condensate and drains. The turbine speed is controlled by a standard centrifugal fly-ball type governor which regulates the flow of steam to the turbine and is protected by an overspeed governor which acts independently of the speed governor.

Sealing of the turbine glands is accomplished by steam seals. The high pressure leakage is piped to the exhaust gland where the steam is used to seal against incoming air leakage. The outboard leakoff point is maintained at a few inches of water, negative pressure. This results in steam from the glands and air from the room being withdrawn from the leakoff point and prevents any steam from leaking out into the turbine room. The slight negative pressure is maintained by a gland steam air ejector which uses reactor steam. The gland steam and motive steam is condensed in a small integral condenser by condensate from the hotwell. The condensed steam is drained to the hotwell through a loop seal and the air is vented to the vent stack.

The generator is of the open type, connected directly to the 3600 rpm turbine. The generator output at full load conditions is 1300 kw at 0.8 power factor with electrical characteristics of 4160 volts, 3 phases and 60 cycles.

5.2.2. Turbine Condenser. The condenser is of the horizontal, two pass, shell-and-tube type and is mounted directly under the turbine generator and is connected to it by a rubber expansion joint. Heat is removed from the condenser by either water or ethylene glycol solution,

depending upon the outside air temperature, and dissipated to the outside air by two air-cooled heat exchangers. Two large propeller-type fans circulate air through the heat exchanger surfaces. The outlet coolant temperature at the heat exchanger is controlled by a by-pass valve with a temperature sensing device to prevent freezing of the condensate in the condenser due to below freezing coolant temperatures.

A steam jet air ejector is operated in conjunction with the condenser to remove non-condensible gases which would inhibit heat transfer. A small amount of reactor steam is used for motivation and is condensed in the inter and after condensers by condensate from the hotwell. The condensed steam is drained to the hotwell by a loop seal while the gases are vented to the stack.

5.2.3 Deaerating Feedwater Heater. The deaerator in the steam cycle heats the incoming condensate from the hotwell and the drains from the barracks heat exchanger to a saturation temperature of 222° F by using extraction steam from the turbine. All incoming feedwater is deaerated so the oxygen content does not exceed 0.005 cc perlitre. The deaerator is maintained at 18 psia at all loads by a reducing valve located in the turbine extraction line. Non-condensible gases are removed through a vent in the deaerator section and discharged to the vent stack.

After the feedwater is deaerated and heated it flows into a storage tank having a capacity of 500 gal which serves as a surge tank for the reactor feed pumps. The storage tank level is maintained by an

external float control valve arrangement. The storage tank contains seven minutes supply of feedwater under full load conditions.

5.2.4. Pumps. The pumping system for the steam cycle provides one pump that will handle the full normal load requrements and a spare pump of the same capacity to serve as standby. This has been done for the hotwell, reactor feedwater, condenser coolant and condensate return pumps. Only in the case of the startup circulatiing pump is there no spare.

Pumps handling radioactive condensate or feedwater are provided with mechanical seals to prevent activity from leaking from the system. The condenser coolant and condensate return pumps are equipped with standard packing glands since leakage in these cases is not objectionable from an activity standpoint. The following table describes the pumps in the steam cycle.

Pumps	Number	Capacity, gpm	Head, ft	Horsepower
Hotwell	2	45	100	3
Reactor feedwater	2	75	1100	60
Condenser coolant	2	2100	30	25
Condensate return	2	75	75	2
Startup circulating	1	20	40	1/2

5.2.5 Condensate Return Unit. A standard condensate return unit is provided to collect the returns from the barracks heating system. The unit contains a 100-gal receiver and two 75-gpm pumps with an alternator which distributes pump wear evenly between the two pumps.

5.2.6 Startup Unit. The startup unit consists of a heat exchanger which uses site steam to heat up the reactor feedwater to operating temperature and pressure and a pump to circulate the feedwater from the reactor, through the heat exchanger, and back to the reactor vessel. This unit may also be used at shutdown to cool the water in the reactor by circulating it through the heat exchanger. Under these conditions condenser cooling water may be used to remove the heat from the heat exchanger.

5.3 Controls and Instrumentation

5.3.1 Reactor Level Control. The most important variable to be controlled in the steam system is the liquid level in the reactor. It is essential that this liquid level be maintained within fairly close limits for stability of operation. If the liquid level were too low, this could result in burnout of the fuel elements due to either exposed surface or insufficient circulation of coolant. On the other hand too high a liquid level could result in flooding the steam separators and the carryover of water to the steam turbine.

The control system proposed for this application monitors feedwater flow to the reactor, steam from the reactor, and liquid level in the reactor. Control is accomplished by making two comparisons; the steam flow with the feedwater flow, and the actual liquid level with a set liquid level. An output air signal from either of these two comparisons actuates an air-operated control valve in the reactor feedwater line. A large error in flow would cause the flow signal to predominate while a small error in flow would cause the level signal to predominate.

As an example of how the control system would respond to change in operating conditions, assume that the reactor is operating at half power at steady load conditions when the turbine control valve is suddenly opened, allowing the reactor steam flow to increase. Since a large difference exists between the steam and feedwater flows, the flow signal predominates and actuates the control valve to allow the reactor feedwater flow to increase. When the flow difference is small, the level signal predominates and adjusts the control valve to restore the liquid level to the set position.

5.3.2 Hotwell Level Control. For this particular application, a simple differential pressure relay, used in conjunction with two air-operated control valves, maintains the hotwell level constant. Control is accomplished by comparing the actual level with the set level. If the actual level is greater than the set level, an air signal opens an air-operated control valve allowing condensate to be pumped to the storage tank. However, if the actual liquid in the hotwell is less than the set level, an air signal opens the control valve allowing condensate to flow from the storage tank to the hotwell. See Flow diagram Fig. 5.

5.3.3. Pressure Controls. There are several locations in the steam system where it is desirable to maintain constant pressures. This can be readily accomplished by a pressure control which consists of a pressure transmitter acting through a controller to actuate an air-operated pressure control valve. Applications of this system are used in maintaining both the reactor and deaerator pressures and the steam pressure to the barracks heating system.

5.3.4 Temperature Control. The condenser inlet coolant temperature is the only parameter in the steam system regulated by a temperature control system. It consists of a temperature transmitter monitoring the outlet coolant temperature from the air-cooled heat exchanger, a controller through which the transmitter acts, and an air-operated control valve in a by-pass line. The control system begins to function when the outlet coolant temperature from the air-cooled heat exchangers becomes low enough to freeze the condensate in the condenser. Below this temperature the control valve in the by-pass line opens allowing the warmer coolant to by-pass the heat exchanger and this maintain the desired coolant temperature.

5.3.5 Instrumentation. Instrumentation to monitor the following system parameters are installed in the central control room. Some of these parameters are both indicated and recorded while others are only indicated or recorded. The following table lists the parameters and methods of monitoring.

Parameter	Indicating or Recording or Both
Reactor:	
1. Reactor liquid level	I and R
2. Reactor pressure	I and R
3. Steam flow	R
4. Feedwater flow	R
5. Feedwater temperature	I and MPR
Turbine Generator:	
1. Turbine load	I and R
2. Inlet pressure	R
3. Exhaust pressure	R
4. Rpm	I
5. Bearing temperature	MPR

Condenser:

1. Coolant inlet temperature	MPR
2. Coolant outlet temperature	MPR
3. Hotwell temperature	MPR

Barracks Heat Exchanger:

1. Steam flow	R
2. Drain temperature leaving preheater	MPR
3. Barracks steam pressure	I

Demineralizer:

1. Water flow	R also Integration
2. Water temperature leaving the reactor	MPR
3. Water temperature entering the demineralizer	MPR

Miscellaneous:

1. Reactor compartment temperature	MPR
2. Outside temperature	MPR
3. Storage tank liquid level	I

where: I - indicated on a gage
R - recorded on a strip chart
MPR - recorded on a multipoint recorder

Along with the previously tabulated instrumentation are the usual annunciator alarms and signals for extreme liquid levels and flow conditions.

5.4 Design Considerations

5.4.1 Introduction. The main advantage offered by a boiling reactor system over the pressurized water system is the elimination of the costly primary coolant system. This introduces, however, the problem of providing a leak-tight steam system without excessive costs. In order to realize this economic gain, one must abandon the idea of using stainless steel as a standard material of construction, as well as using costly canned-rotor pumps.

5.4.2 Steam and Water Leakage. There are several sources of steam and water leaks in the present day operating steam power plants namely, turbine seals, valve stem packing, and pump packing glands. The leakage of steam from the turbine into the operating room can be eliminated by the use of steam seals. This method of sealing sucks a small amount of air from the operating room along the turbine shaft in the opposite direction of steam leakage. A leakoff point is provided to remove this air along with some steam that leaks from the turbine. This system is further described under Section 5.2.1.

Standard centrifugal pumps are being used in the steam system with one modification, mechanical shaft seals replace the standard stuffing box. This modification results in the elimination of pump shaft leakage.

Another source of leakage is the valves in the high pressure part of the system. One possible solution would be to install bellows-type valves; these are rather costly but would eliminate the leakage problem. The problem has not been completely resolved at this writing.

5.4.3 Components. It is proposed to use Schedule 40 seamless steel piping of ASTM specification A53 throughout the steam system since the maximum operating conditions are 400 psi and 448° F. Piping was sized by using the following conservative flow velocities: steam 7000 fpm, condensate or feedwater 6 fps and drains 3 fps.

In general the design of the components of the boiling reactor are very similar to those of the present package reactor as described

on pages 177-182 of ORNL-1613. There are several slight variations which will be mentioned briefly.

Since the available heating steam from the reactor is radioactive, a barracks heat exchanger is provided to evaporate condensate from the barracks heating system. In order to improve the overall thermal efficiency of the cycle at relatively low cost, a preheater was installed in series with the barracks heat exchanger. As a result, the flow of reactor steam through the barracks heat exchanger is reduced, since more heat is removed per lb of steam, and the flow to the turbine is increased. This results in a greater generation of electrical energy and hence a greater thermal efficiency, since the heat input remains the same.

Another slight variation in component design is the selection of a condenser with 10-ft tube length. Two condenser sizes were considered, 10 and 14-ft tube lengths. The prices of both condensers were very similar as were the pump costs, pumping power, and piping costs. The 10-ft tube length condenser was chosen since it would appreciably reduce the area occupied by the steam system components, and at the same time give the same operating performance as the condenser with 14-ft tubes.

5.5 Performance

A full load heat balance showing steam and condensate conditions at all points in the steam cycle is shown in Fig 37. Several of the parameters such as reactor heat, barracks heat, barracks heating steam and condensate conditions, and condenser pressure were maintained the same as in the present package reactor system in order to compare the two systems.

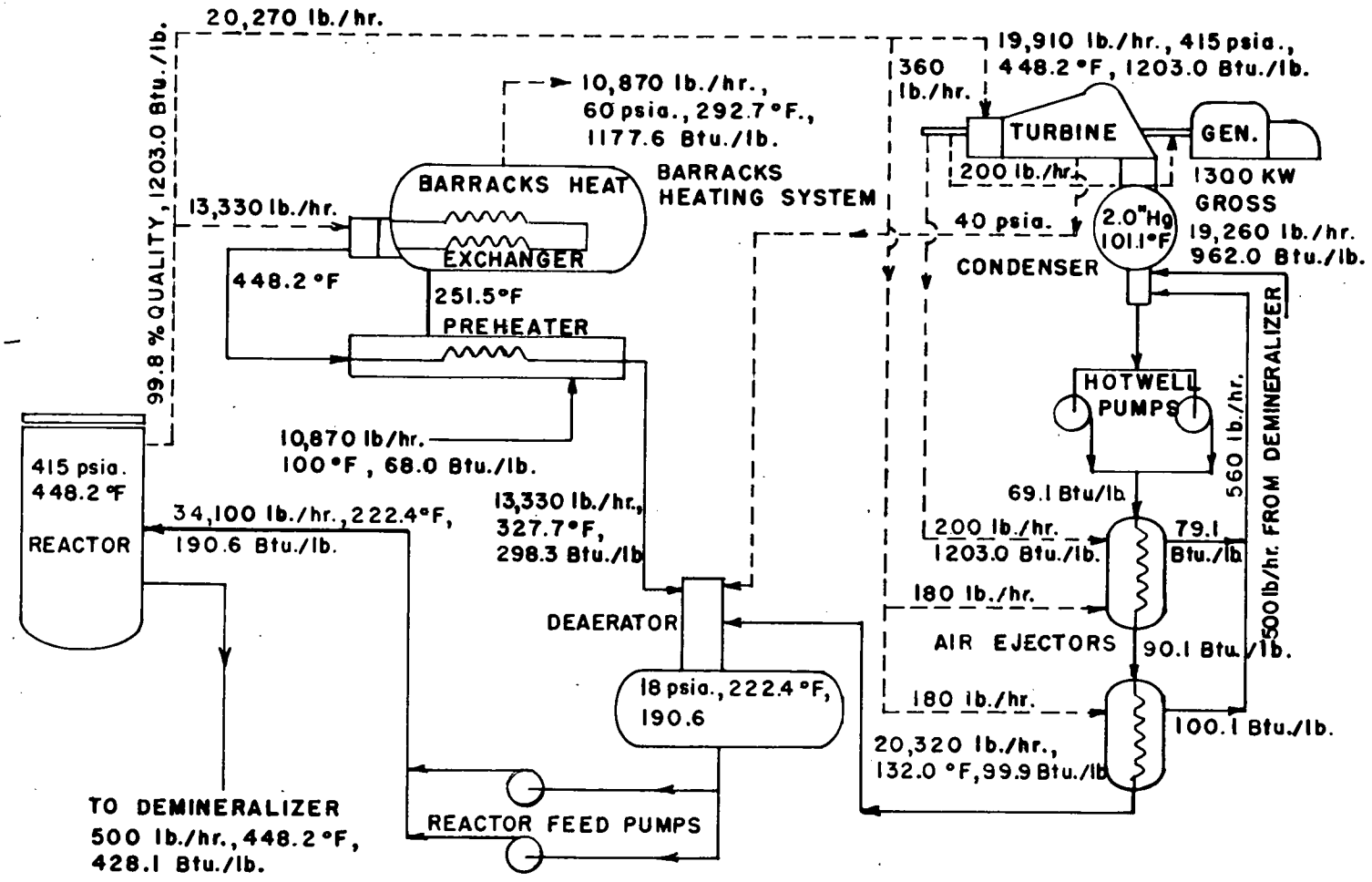

FULL LOAD HEAT BALANCE: REACTOR POWER - 10,000 KW., BARRACKS HEAT - 3535 KW., GROSS ELECTRIC GENERATION - 1300 KW., AUXILIARY POWER - 250 KW., NET ELECTRIC GENERATION - 1050 KW., THERMAL ELECTRIC GENERATION - 16.2 %, OVERALL THERMAL EFFICENCY - 45.9 %, CORE LIFE BEFORE REFUELING - 15 Mw./yr.

SYSTEM HEAT BALANCE

Figure 37

With the reactor operating at full power of 10,000 kw, the barracks heating load is 3535 kw, while the gross electrical generation is 1300 kw. Auxiliary power in the boiling reactor is 250 kw, 50 kw less than the present package reactor which is due primarily to the elimination of the primary coolant pumps and the pressurizer.

One other point of interest is the moisture in the steam leaving the turbine; it is 14% at full load. This value is slightly higher than that recommended for turbines with unstellited last stage buckets. It is felt that since the amount of time at which the turbine is operating at full load is quite small, the resultant erosion will be unimportant.

5.6 Water Purity

When water is used in a reactor as a coolant and as a moderator that will be intimately associated with the core structure, it is necessary to give careful consideration to the purity desired and the method of obtaining this pure water. Several outstanding advantages to be gained by keeping the reactor water as pure as possible are as follows:

1. Reduce the amount of foreign material in the core to give a minimum of excess neutron poisoning.
2. Corrosion rates have been shown to be lower when high water purity is maintained.
3. Decomposition of the water due to gamma ray and neutron irradiation can be assumed negligible when high water purity is maintained and when the temperature of operation is as high as it is in this reactor.
4. By keeping impurities in the water to a minimum, high, long-lived activity can be reduced and water storage tanks and pipe lines will require less shielding.
5. When high purity water is available the heat transfer characteristics will remain better and more constant because problems due to transport corrosion products will be minimized.

Much consideration was given to the type of water purification that would be used. It was decided that a mixed or Mono-bed demineralizer has several distinct advantages over multiple bed mineralizers and evaporators. The principle deciding factor was the high effluent purity obtainable (greater than 10^6 ohm/cm^3), regardless of the nature of the influent, and the minimum amount of make-up water required. Since the quality of the water obtainable will vary greatly depending upon the location of this reactor, this method held most promise. Also, since regeneration is accomplished simply and rapidly, this method is even more desirable.

In operation, a by-pass stream from the reactor is first cooled, sent through a reducing valve, and then passed through the demineralizer. The effluent is then passed through a ten-micron pore-size Micro-metallic filter. This removes all the flake corrosion products and resin "fines" from the demineralizer that are not retained on the resin bed. The demineralizer water then goes to the hot-well of the condenser.

The makeup water to the system is also passed through this demineralizer with the bypass stream. This has the advantage of requiring only one pair of demineralizers and allowing the radioactivity on the bed to be diluted. This serves to distribute the sources and reduces the tendency for resin decomposition. Preliminary calculations and the references* show that there need be no concern in this regard.

---

* ORNL-990
TID-5122
WAPD-MR-35

Physically there are two Mono-bed demineralizer tanks and two Micro-metallic filters that can be used in parallel, or separately, with either demineralizer that is in operation. Two units provide reliability against plugging and exhaustion.

Operation of the Mono-bed unit is very simple. During operation, the anion and cation resins are intimately mixed and produce the same effect as many multiple bed units in series. Upon exhaustion, which is generally determined by lowered resistivity of the effluent or, as in this case, by an alarm that indicates when a predetermined amount of water has passed through the unit, the demineralizer is taken off the line and regenerated, while the spare is put into service. To regenerate, the unit is backwashed by reversing the flow. This allows classification of the resins into two separate layers and the washing of accumulated solids into the waste water holdup tank. Flow is then stopped and the regenerants are put into the demineralizers. Sulphuric acid is brought in through the bottom distributor and taken out of the distributor at the interface of the anion and cation resins. Simultaneously, sodium hydroxide solution is brought in through the top distributor and removed at tbe interface distributor. After regeneration, air is bubbled through the bed and water so as to re-disperse the resins. The excess regenerant is then rinsed from the bed, and the unit is again ready for service.

Operation will be slightly more difficult in that some of the solids removed from the water will be radioactive, which will necessitate some shielding around the vessels. Automatic operation gives no problems but even the cheaper, more trouble-free, manual operation can be

accomplished easily by using extended valve handles projected through the shielding. Since the regenerant charging tanks will never be radioactive they can be placed outside the shield in some convenient location.

Specifications for the demineralizers are given in Section 1.6.4. Rohm and Hass data for Amerlite IR120 and IRA400 were used in the design of the demineralizers. A strongly basic anion resin, IRA400 was used because it has the best temperature characteristics and best silica removal properties. Amberlite IR120 is the most rugged, strongly acid cation resin manufactured. Two conditions were chosen for the designing of the demineralizer. The first makeup of 1 gpm using tap water, of the analysis given in Table 1, blended with the reactor by-pass stream of 1.3 gpm and 2 ppm solids content considered as ferrous hydroxide. The second condition was that of pure water makeup at 1 gpm (as might be obtained from melted snow) and the same reactor by-pass stream flow.

The allowable concentration of solids in the reactor water was calculated as follows:

1. It was determined that the maximum allowable fuel element temperature was 600° C.* Above this, or operating in this range, there was danger of sensitizing the stainless steel by carbide precipitation at the grain boundaries. This condition is very undesirable because of the decreased corrosion resistance of the metal.
2. Next, using the best data available on density and thermal conductivity,** an amount of scale to give the maximum temperature allowable at the location of highest heat flux, was calculated.

---

* Private communication with J. E. Cunningham (ORNL).

** ANL-5195
McAdams, Heat Transmission, 3rd ed.

3. Assuming that the solids contained in all of the evaporated water were deposited uniformly on the heat transfer surface, it was possible to determine the maximum allowable solids concentration in the water. Modifying the number slightly, to be more realistic, an allowable solids concentration was set at 2 ppm.
4. To estimate the solids buildup in the water, the total metal area, both carbon steel and stainless steel, continually in contact with water, was determined. A corrosion rate of 0.05 mg/cm^2-mo seemed reasonable and was used to obtain the continual buildup of solids.
5. The demineralizer size was calculated, assuming all the solids in the reactor water to be ferrous hydroxide and using the makeup water in the correct proportion.

The demineralizer also has another important function which was not investigated thoroughly. In the event of a fuel element rupture, the water would become highly contaminated with fission products and other elements that were corroded in the water. It is visualized that the reactor would be shut down when this happened, and the water circulated through the demineralizer until the long-lived activity was reduced to a tolerable value. The pressure vessel could then be opened and the ruptured element removed. If this were not done there would be carry-over into the steam which would increase the activity about the exposed pipes and equipment.

TABLE I: TYPICAL TAP WATER ANALYSIS OF ORNL WATER

ph		7.9
Phenolphthalein Alkalinity	ml	0
Methyl Orange Alkalinity	ml	9.2
Specific resistance	ohm-cm	5.57×10^3
Soap hardness (as $CaCO_3$)	ppm	95
Ca, Mg hardness (Calculated as $CaCO_3$)	ppm	85
CO_2	ppm	1
Dissolved solids	ppm	140.3
Non volatile solids	ppm	72.5
Fe	ppm	0.040
Al	ppm	0.039
Cu	ppm	0.02
Ni	ppm	0.02
Cr	ppm	0.02
Ca	ppm	23.8
Mg	ppm	6.6
Na	ppm	1.1
$SO_4^=$	ppm	23.8
Cl^-	ppm	7.4
$CO_3^=$	ppm	55.2
HCO_3^-	ppm	12.2
NO_3^-	ppm	1.2
$PO_4^{\equiv}$	ppm	4.6
F^-	ppm	1
SiO_2	ppm	2.5

6.0 SHIELDING

6.1 General Considerations

The biological shielding proposed for this reactor was designed assuming that excavation or rock shielding are impractical due to the uncertain site conditions and special problems connected with a remotely located reactor power plant. Ordinary concrete, with an assumed density of 2.33, is the shielding material considered. Its use is justified by the requirements for transportability. Assuming that aggregate is locally available, only the cement and reinforcement steel need be shipped. If ground excavation is practical, or advantage can be taken of the terrain, e.g. construction against a cliff, savings in shielding material will be possible.

Time limitations on this study precluded detailed preparation of shield configuration, and therefore the investigation was restricted to the thicknesses of concrete required to meet design tolerances opposite the centerlines of the reactor. However, the following general features can be outlined: The reactor should be separated from the other components of the system to allow maintenance accessibility to as much of the system as possible. All pipes connecting through the shield to the reactor should pass through the wall off-center relative to the reactor to prevent streaming of radiation.

A metal lining should be provided in the reactor compartment, sealed to the pressure vessel near the top. This makes it possible to flood the well over the reactor when loading and unloading the core.

Openings in the shield wall should be provided where necessary for maintenance accessibility, the openings being filled with removable shielding blocks during operation.

The pit in which the reactor vessel is located should be a minimum of 6 feet in diameter to allow for installation, but enlarged to approximately 8 foot diameter, located eccentrically above the top of the reactor, to provide space for coffins and handling tools during unloading operations. A water-filled well alongside the reactor vessel should be provided for storage of spent fuel elements and also to act as a sump into which leakage from seals and other places can be drained.

Since experimental facilities are not required, the shield configuration should be designed with economy of materials and ease of construction as the primary considerations.

All shielding calculations are based on a continuous reactor power of 10 Mw. The design is based on the shield proposed for the ORNL package reactor.* Tolerance is arbitrarily defined as 300 mrep per week over a 56-hour work period, or 5.36 mrep/hr. Estimated dosage rates are plotted for various locations to obtain one-tenth, one, and ten times tolerance. Conservatism has governed all estimates in the calculations. Dose rates after shutdown were not investigated, but should be directly comparable with data reported on ORNL 1613; a detailed analysis of the biological shielding requirements is included in Appendix 12.5.

---

* W. R. Pearce, Analysis of Biological Shielding and Thermal Shielding Requirements for the ORNL Package Reactor, CF-53-10-81, Oct. 13, 1953.

6.2 Primary Shield Calculations

The similarity of this reactor to the Bulk Shielding Reactor permits extensive use of modified BSR data. The penetration of gamma rays is energy-dependent. Due to the mechanisms involved, the harder end of the spectrum governs the shielding requirements. The fluxes obtained from the BSR were therefore divided into four energy groups and each group attenuated separately. The 7-Mev gamma group, assumed as containing those gamma rays whose energy exceeds 5.5 Mev, was found to predominate the shield design.

The magnitude of total gamma radiation and fast and thermal neutron flux as a function of distance from the BSR was obtained from ORNL-CF-51-10-70.* These data, adjusted for lower water density, geometry, and power level, were used to determine the flux at the edge of the reflector and at points of interest above the reactor.

The gamma spectrum from the BSR at the distances under investigation was interpolated from the known spectrum vs distance data reported in Nucleonics.** Corrections were applied to the flux for each selected energy group in consideration of the greater amount of self-absorption in the iron bearing core and the difference in capture gamma production.

From the composition, size, and temperature of each reactor, the relative leakage of fast and thermal neutrons was obtained and corrections were made to the values of neutron flux obtained from the

---

* Blizard, E. P., Introduction to Shield Design, CF-51-10-70, Jan. 30, 1952.

** Maienschein, and Love, "Gamma-Ray Spectrum of the Bulk Shielding Reactor", Nucleonics, Vol. 12, No. 5, May, 1954.

work sheet. Capture gammas in the shell, lid, etc., were computed by assuming slab geometry and uniform thermal neutron flux through the thickness of each component. The thermal neutron flux used in each case was the average of the exponential flux obtained for slab geometry from diffusion theory. Each neutron capture in the steel was assumed to result in 1-7 Mev gamma.

With these methods and an attenuation through the wall of the pressure vessel, the fluxes were obtained for each radiation at the top and sides of the vessel.

6.2.1 Radial Shielding. A spherical source was assumed with surface source strength equal to the fluxes obtained at the inner surface of concrete and with radius equal to the radial distance from the core axis to the shield. The dosage rates determined at a point opposite the reactor centerline are plotted as a function of concrete thickness in Fig 38. Tolerance is obtained with a thickness of 10.2 ft. The specified centerline thicknesses are:

For ten times tolerance	9.0 ft
For tolerance	10.2 ft
For one-tenth tolerance	11.4 ft

6.2.2 Axial Shielding. A point source was assumed of such a magnitude that the flux of 7-Mev gammas at the water surface, 6 feet from the center of the core, equaled the flux predicted on the basis of adjusted BSR data. In these calculations, capture gammas from the upper support plate and control mechanisms were neglected. Further analysis may show that this radiation might increase the shielding requirements by several inches of concrete.

Tolerance resulted in 7.9 feet of concrete, see Fig. 39.

ORNL-LR-Dwg. 6094

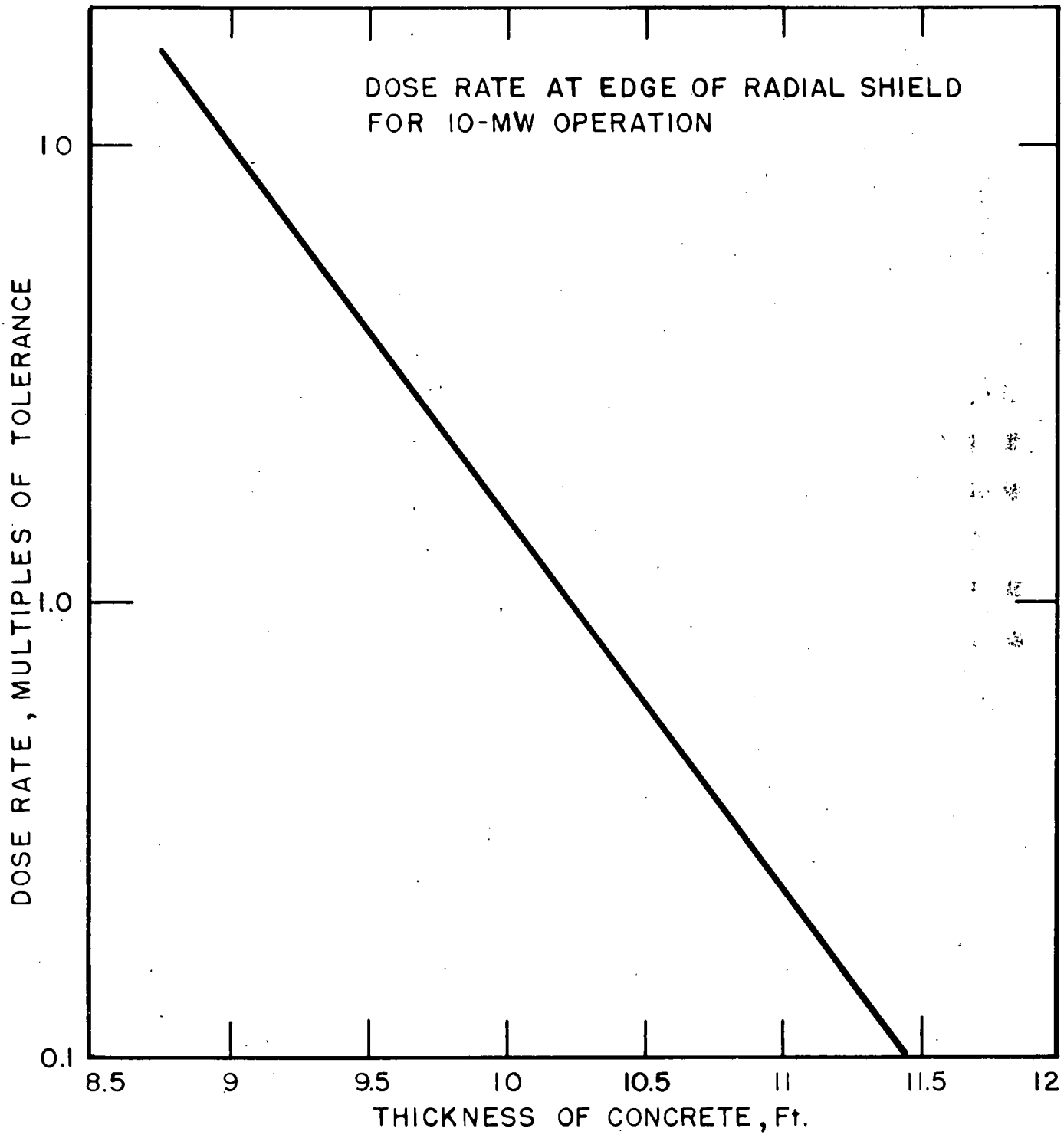

Figure 38

ORNL-LR-Dwg. 6095

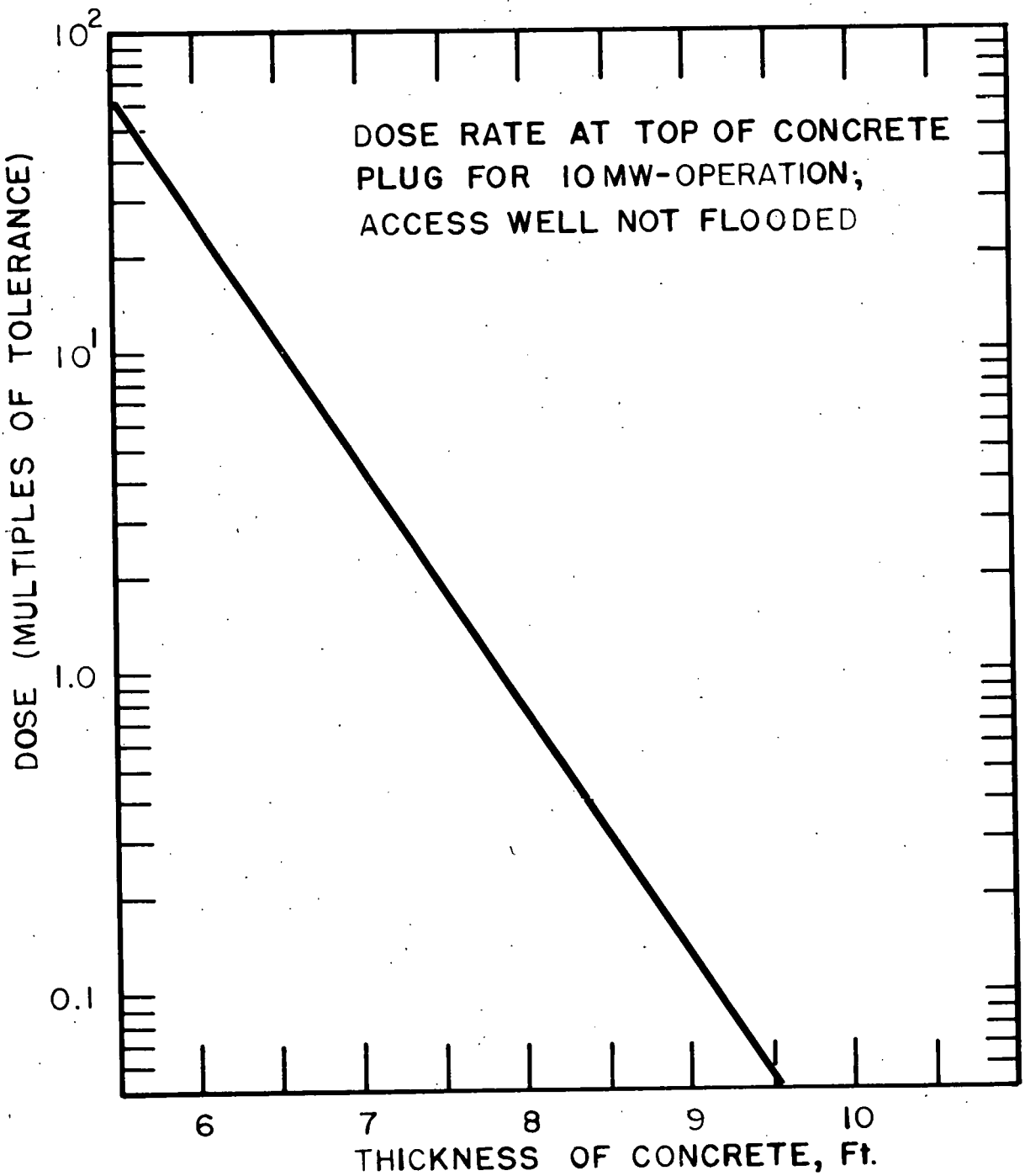

Figure 39

6.3 Secondary Shielding

6.3.1 Water Activation. The maximum, saturated activity of the coolant in the pressure vessel was calculated from the following equation:*

$$A_i = \frac{N_i \sigma_i \phi_o \quad (1 - e^{-tr\lambda_i})}{\lambda_i \quad (1 - e^{-t_c\lambda_i})}$$

where

A_i = the number of i atoms activated in one cc

N_i = the number of i atoms in one cc

σ_i = the activation cross section for i atoms

λ_i = the decay constant for activated i atoms

ϕ_o = the activation flux

t_c = the total cycle time for an i atom

t_r = the fraction of t_c for which i atoms are exposed to the activation flux

The saturated activity was calculated for each gamma-emitting activated atom. The predominant activity was found to be due to the decay of N^{16} formed by the O^{16} (n,p) N^{16} reaction. The activation of corrosion products and recoil atoms was calculated from the same equation, with appropriate changes in the value of N_i. The results, shown in the following table, indicate that there will be appreciable gamma activity from the decay of Mn^{56}. This activity is confined to the core since there is a decontamination factor of 10^{-5} for entrainment of solids

---

* Reactor Handbook, Vol II.

in the steam. Activation of other corrosion and recoil atoms is negligible compared to that of Mn^{56} because of lower reaction cross sections and lower energy, decay gammas.

The Maximum Activity of Steam Leaving Core

Activity	A_i active atoms per cc	γ energy	Active atoms per pound steam
N^{16}	2.22×10^4	6 to 7 Mev (80%)	1.22×10^7
Mn^{56}	1×10^5 (in water)	2 Mev (40%)	550
	1 (in steam)		

6.3.2 Solids Carryover. The reactor cooling water has an allowable dissolved solids concentration of 2 ppm; since these atoms become activated, it is necessary to consider carryover with the steam. Ordinarily carryover is accomplished in any, or all of several ways, including entrainment, splashing, and foaming, and is a function of boil-up rate, free-board on the vessel, and the amount and type of dissolved solids. After reviewing the available literature,* it was determined that a decontamination factor of 10^4 to 10^5 could be used in this case. This is based on a very low dissolved solids content, adequate splashing protection, and an almost neutral pH condition tending to reduce foaming to a minimum.

* B. Manowitz, R. Bretton, R. V. Horrigan, The Occurence and Control of Radioactive Entrainment in Evaporative Systems, BNL-1639, October 1953.

Chemical Technology Division Progress Report, August 1, 1951 to February 10, 1952. ORNL-1311.

A. E. Wibble, Purex Evaporator De-Entrainment Studies. ORNL-CF-51-11-103, November 1951.

W. B. Watkins, Evaluation of Full-Scale Savannah River Project Evaportor, ORNL-CF-51-11-113, November 1951.

Richards, R.B., Progress Report-Chemical Development Section, HW-20248 January 1951.

6.3.3 Component Shielding. The shielding requirement of the turbine was investigated by assuming all the Mn^{56} was plated out in the turbine. It was found that this activity was equal to 8.18×10^{-5} millicuries of 2-Mev gammas. In this case, the shell of the turbine is sufficient for shielding.

In like manner, the turbine, condenser hotwell, barracks heat exchanger, and preheater were investigated for possible shielding requirements due to the N^{16} activity. These calculations were made with the following assumptions:

a. The decay rate of the N^{16} was determined by the time since irradiation of an average pound of coolant in the core.

b. The hold-up time in the pressure vessel was 5 seconds.

c. Each component was approximated by a spherical source of the same volume with the activity at the center.

In each case it was found that the thickness of the component shell and $1/r^2$ attenuation were sufficient to reduce the activity in the component to below tolerance at the outside of the component.

6.4 Biological Shield Ventilation

Shielding requirements are such that a shell of concrete about the pressure vessel approximately 11 feet thick is necessary. The radiation is assumed to be essentially gammas and is expected to produce a good deal of heat in the concrete; cooling is necessary to avoid excessive temperatures. Shielding calculations (see Appendix 12.6) result in Equation 6.4.1 for gamma heating at any radius.

Equation 6.4.1

$$H_{(r_o)} = .78 \times 10^{-8} \frac{r}{r_o} \mu I_o E_\gamma e^{-\mu(r_o - r)}$$

where

r is the inner radius of the shield

I_o is the radiation on the inner surface

E_γ is the energy of the gamma ray

μ is the absorption coefficient (energy dependent)

r_o is the radius of the point under consideration

The radiation intensity was assumed such that:

I_o	E_γ	μ
8.0×11^{11} γ/cm^2-sec	7 Mev/γ	.059 cm^{-1}
2.2×10^{12}	4	.073
3.3×10^{12}	2	.105
1.0×10^{12}	1	.146

The heating from each of these sources of radiation was plotted as a function of r_o and the sum was taken to the total heat generation within the shield. As a close approximation, Equation 6.4.2 gives the heat generation as a function of radius in BTU/hr-ft^3.

Equation 6.4.2

$$H_{(r_o)} = 2.12 \times 10^{6} \quad e^{-.068 r_o}$$

For calculation purposes, a cylinderical shield was assumed and arbitrarily broken up into 6-inch annular rings. The total heat production in each ring was calculated and from this the number of holes required to cool that ring was found. As the diameter of the shield increased, the number of holes decreased but it was decided to set 3 feet of arc length

as the maximum distance between holes in any ring. The maximum heat production occurs in the first ring and was found to be of the order 9,200 BTU/hr-ft^3. Entering air was assumed to be 50°F and allowed to rise to 150°F in the shield. The diameter of the holes was assumed to be 1 inch. Calculations show that 145 holes will be required in the first 6 inch ring, 36 holes in the second ring, 22 holes in the third ring, etc.

The head loss coefficient (K) was assumed to be 2 and a fan was selected to provide 3 in. H_2O pressure rise. Calculations then showed the allowable velocity to be 83.5 feet/second. It was further found that with the pressure head selected, about 26.2 cubic feet of air per minute would be circulated through one hole. Totaling the holes in all rings in the 11 feet of shield thickness gave 415 holes and a total flow of about 11,000 CFM.

A heat transfer coefficient at the tube wall surface was calculated to be 18 BTU/hr-ft^2-°F. For the hottest ring (inner ring) the wall temperature would run about 100 °F above the circulating air temperature. This is not considered to be excessive. Activation of the air was not calculated, but is thought to be very slight.

7.0 ELECTRICAL SYSTEM

The load distribution for this design is shown by Fig. 40. For a description of these systems see Chapter 8.0 in ORNL-1613.

8.0 BUILDING AND AUXILIARY EQUIPMENT

With the limited time available, it was not possible to evaluate accurately the entire package unit and, since it was felt that the building would change least from the one described in ORNL-1613, very little consideration was given to this part of the project.

A possible plant layout and elevation are shown in Figs. 41 and 42. It will be noted that there is one foot of concrete shown around all equipment. Although calculations indicated that this shielding was not required, it was included not only to be on the conservative side, but to provide an exclusion area around the equipment. It also allows for better circulation of air over the equipment to flush any radioactive gases and vapors from the equipment and out the stack. Part of the end of the equipment compartment is made of stacked and mortared block so that it is easily accessible in the event that one or more pieces of the heat transfer equipment need retubing. An access door could also be provided to the equipment area, for inspection purposes.

Items such as the control room, service area, shop, waste storage, and raw water storage are not shown but no difficulties are anticipated in their location.

ORNL-LR-Dwg. 6096

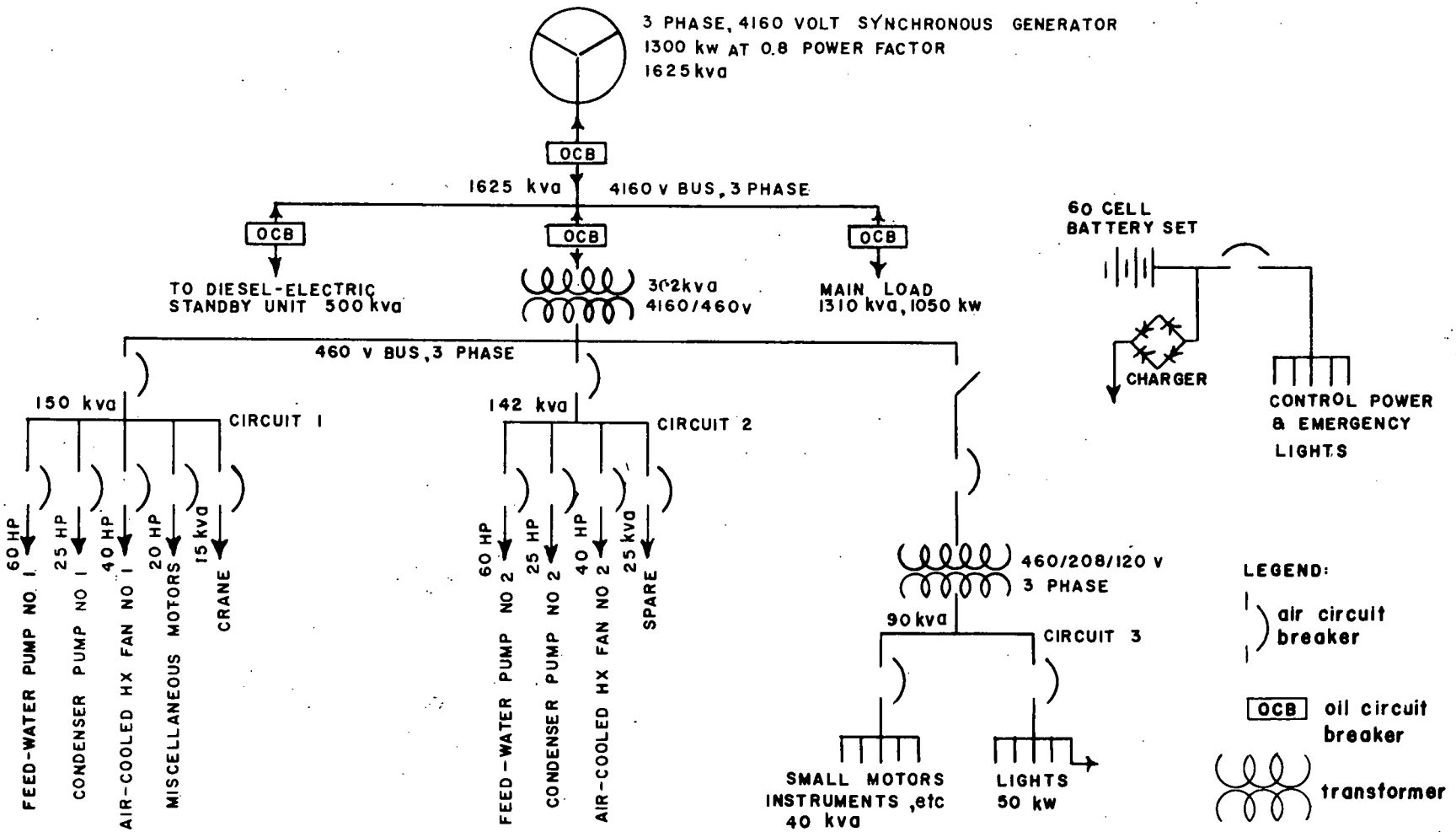

LOAD SUMMARY:
MAIN LOAD = 1310 kva AT 0.8 POWER FACTOR
MAXIMUM AUXILIARY LOAD = 302 kva AT 0.8 POWER FACTOR

FIG 40 ELECTRICAL LOAD DISTRIBUTION

ORNL-LR-Dwg. 6097

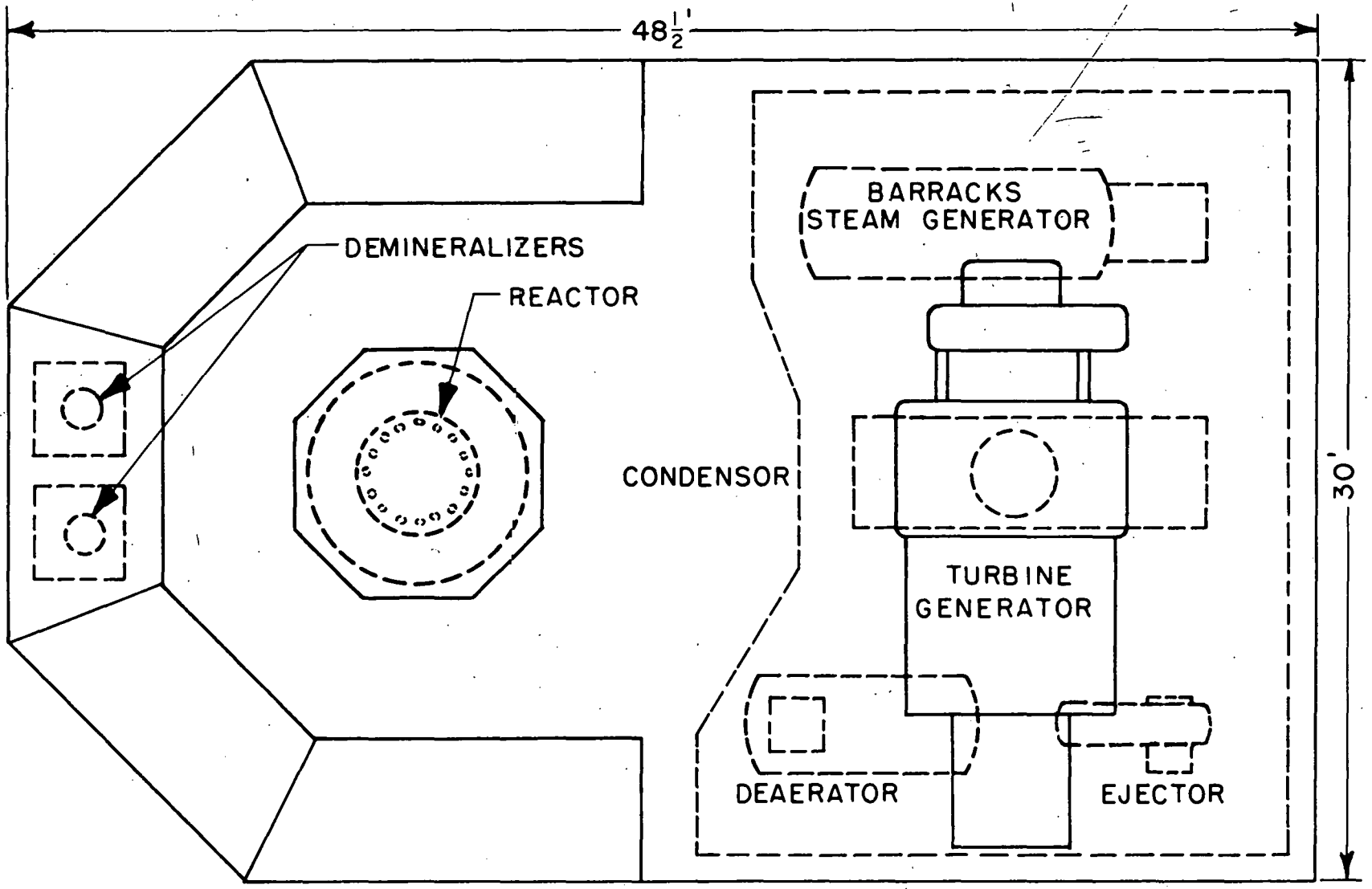

PLANT LAYOUT

Figure 41

ORNL-LR-Dwg. 6098

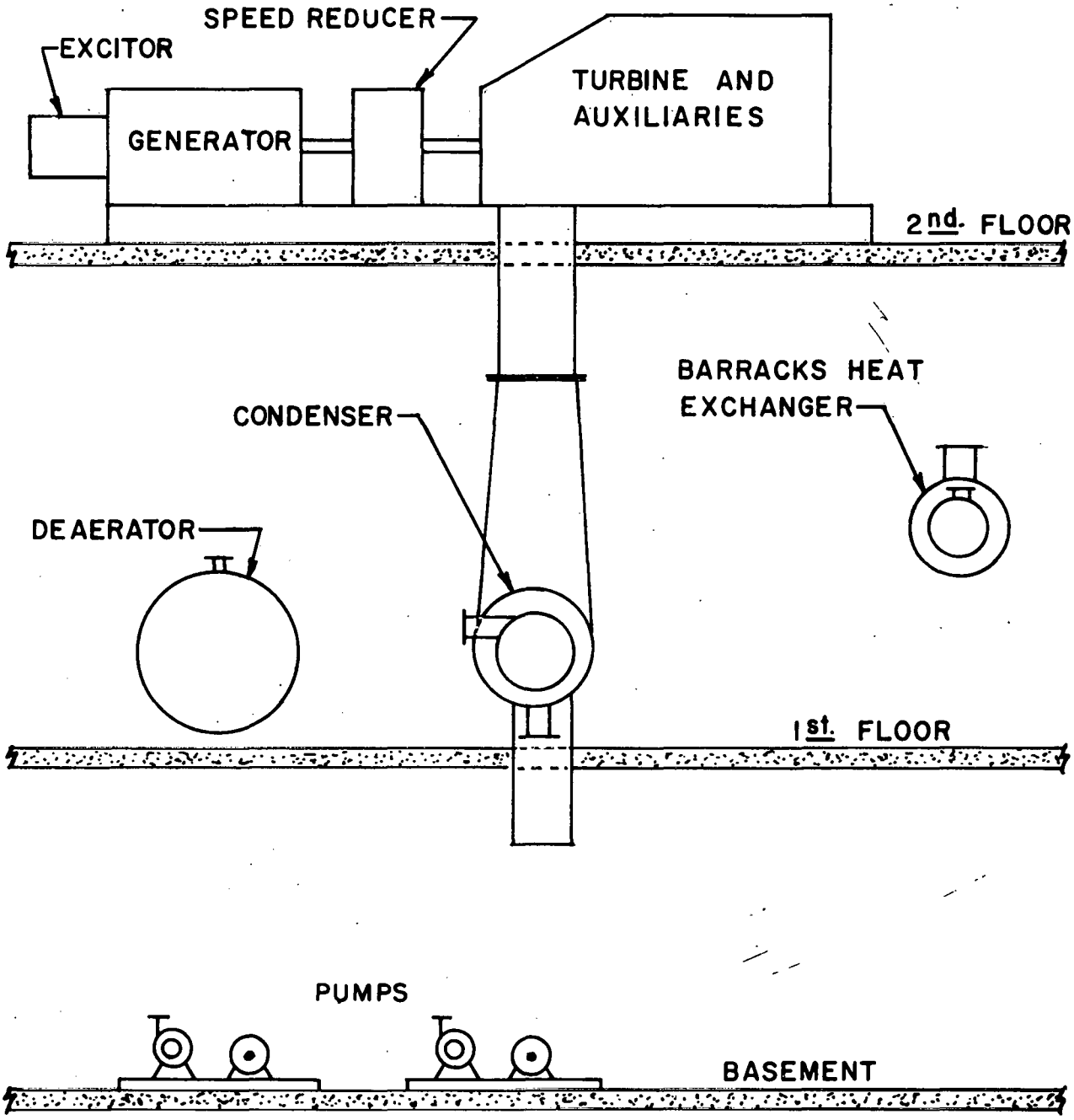

PLANT ELEVATION

Figure 42

9.0 OPERATION

9.1 Startup

9.1.1 Discussion. Two main problems are encountered in the startup of this reactor. First, the reactor power must be increased approximately nine decades to 3% of full power on a safe period. This will be done by the operator who will be backed up by the usual safety devices incorporated in reactor control systems, i.e., period scram, cut back. Second, the time rate of temperature rise from ambient to operating condition must be limited to a specified amount, determined by thermal stress considerations.

The first problem, that of nuclear safety, is not unique in itself and therefore does not warrant much discussion. In addition, the negative void coefficient of reactivity acts as a stabilizer, as was demonstrated in the Borax Experiment.

It is felt that the safest way of bringing the system to operating temperature would be by an external heater, rather than the reactor. It is estimated that the temperature of the system cannot be raised faster than 100° F per hour, which means roughly four hours in total time. While this could be done with the reactor the small cost of an external heater is more than compensated for in increased safety. For a description of the heater, see section 5.2.6.

9.1.2 Procedure. The steam line from the reactor is equipped with a pressure control valve which operates to maintain the reactor pressure at 415 psia. Therefore, this valve will remain closed until the reactor

pressure reaches the design point.

The startup procedure is as follows:

1. The reactor level control system is left inoperative. With one or two control rods partially out, the pressure vessel is filled. Since the water will expand when heated, the reactor should be filled to a level approximately 1.5 ft below the design level (this is still 6 in. above the top of the riser). The control rods are reinserted when filling is completed.

2. With all control rods fully inserted and the turbine throttle open, the external heater is turned on.

3. Since the pressure control valve is closed, the reactor will pressurize itself as the coolant temperature is increased. The rate of coolant temperature rise will be controlled by the external heater to limit thermal stresses in the piping and pressure vessel to a safe value.

4. When the system reaches design conditions (448° F and 415 psia), the pressure control valve operates to maintain the system at 415 psia. Any net steam generated will pass through the turbine and condenser. The system is now at design temperature. The reactor level control system should be placed in operation at this time.

5. With the heaters still on, the control rods are withdrawn intermittantly until the reactor is critical. The reactor power is then increased until the power is high enough so that the external heater can be shut off. Provided the pressure control valve functions properly, the reactor will now be self-regulating.

6. Before raising the reactor to a very high power, the turbine should be warmed up by passing a small amount of steam through it for as long as necessary.

9.2 Part Load Operation

Since the reactor is expected to run most of the time at loads below full design power, the operating characteristics at part loads must be considered.

From a natural circulation point of view, the flow from zero power to 200% power is a steadily increasing function, indicating not too drastic changes in core-void fraction, as shown in Fig. 34. There are no abrupt void changes in the part-load region. Thus, part-load operation from this standpoint is expected to be stable.

From a hydrodynamic standpoint, vapor lock is also impossible as shown in Fig. 36, for the region of interest, and there is only one point of operation, indicating stability. It should be noted, however, that the tendancy is to become less and less hydrodynamically stable as power is decreased. This is shown by the flatening of the two phase flow curves of Fig. 36.

Predicting the nuclear stability, as effected by void fractions and pressures, is equally as difficult to predict at part loads as it is at full load. This type of analysis is best done with a reactor simulator. Two trends should be noted, however, see Fig. 34. At low powers, any perturbation of power will result in large incremental changes of void changes. At higher powers, this effect is not as noticeable. Secondly, at high powers a perturbation of pressure is expected to change void fraction, which considerably changes the reactor power. At small loads, this effect is not as great. While the ultimate result of these features cannot be predicted, they should be looked at rather closely for future study.

It should also be noted that the change in reactivity from zero to full power is only about 3%, resulting from changes in steam voids. This would indicate that the reactor can be controlled over

its entire range by less than the total effect of one control rod. For a further discussion of response at part loads, reference is made to paragraph 2.4.3.

10.0 COST ANALYSES

10.1 Basis of Cost Estimates

In all of the following estimates the best information available from various sources was used. All major plant components were engineered sufficiently to enable several reliable manufacturers to quote realistic construction costs. In the absence of direct courtesy quotations from manufacturers, costs were estimated by comparing the component to similar existing items.

The costs shown are believed to be realistic for construction at a developed site similar to Oak Ridge, Tenn. No attempt was made to estimate the costs for construction of the plant at an arctic base where labor costs could be expected to run approximately three times that for eastern United States. The estimated costs for the plant, $1,258,400, includes a 10% engineering charge, and 10% for contingencies. Additional costs would be required to cover any development deemed necessary.

10.2 Reactor Plant Cost Estimate

Reactor		$139,000
Reactor vessel (including structural supports and thermal shield)	$44,000	
Core fuel assemblies (49)	29,000	
Control rods and guides (5)	25,000	
Control-rod drive, release, and indicating mechanisms (5)	25,000	
Reactor vessel insulation	6,000	
Leakage collection system (1)	10,000	
Steam System		186,000

Turbo-generator set (1500 kw) (1)	$100,000	
Main condenser (1)	20,000	
Barracks steam generator (1)	6,000	
Hot-well pumps (2)	2,000	
Feed-water pumps (2)	8,500	
Piping, valves, insulation	43,500	
Condensate return unit (1)	1,500	
Deaerator feed-water heater and storage tank (1)	4,500	
Main condenser cooling system		$61,500
Pumps (2)	4,000	
Piping and valves	25,000	
Air coolers and fans	30,000	
Storage tank (1)	2,500	
Water purification system		31,000
Filters (2)	1,500	
Purification tanks (2)	9,000	
Pump (1)	2,500	
Storage tank (1)	3,000	
Piping and valves	13,000	
Cooler (1)	2,000	
Instrumentation and controls, Reactor		90,000
Safety and control circuits, instruments and indicator	78,000	
Control panels	8,000	
Fission-chamber drive	4,000	
Instrumentation and Control, Process		38,500
Steam system	32,500	
Miscellaneous systems	6,000	
Electrical Systems		82,000
Generator switch gear and distribution equipment	44,000	
Electrical distribution and lighting in plant	30,000	
Metering and controls	8,000	

Building (including crane, platforms, and ventilating equipment)	$260,000
Off-gas stack	10,000
Reactor shielding (~700 cu yds)	100,000
Lubrication system	4,000
Core handling and replacement equipment	20,000
Compressed air system	6,000
CO_2 fire protection system	12,000
Contingencies (10%)	104,000
Engineering (10%)	114,400
TOTAL PLANT COSTS	$1,258,400

10.3 Installed plant Costs per Kilowatt

The reactor will produce 1050 kw net electrical power and 12.065 x 10^6 Btu/hr (3535 kw) in the form of steam for heating purposes. An analysis of the plant costs indicates that 45% can be charged to steam and 55% to electric power.

55% of $1,259,000 = $692,450 (electric power)

45% of $1,259,000 = $566,550 (steam heat)

The costs per installed kilowatt are, therefore:

$\frac{\$692,450}{1050}$ = $659/kw net electric power

$\frac{\$566,550}{3535}$ = $160/kw steam heat

10.4 Kilowatt-hour costs

In calculating the costs per kilowatt hour for net steam and electricity delivered, the following assumptions were used:

The plant amortization rate would be 13.5%.

The fuel inventory rate would be 10%.

$20 per gram of U 235 would be charged for burnup.

$3.00 per gram would be charged for chemical reprocessing of the fuel (including U238 and U236).

The initial fuel loading would be 18.1 kg of U 235.

The operating costs would be based on a 15-Mw-yr core life, before refueling.

1.4 grams of U 235 would be used per megawatt-day of reactor operation.

$150,000 per year would be allowed for operations and routine maintenance of the reactor plant.

		Mills/kw-hr			
		60% Av Load		100% Av Load	
Capital Costs	Rate	Electric	Steam	Electric	Steam
Complete plant	13.5%	16.94	4.12	10.16	2.47
Fuel inventory	10.0%	3.61	0.88	2.16	0.53
Sub Total		20.55	5.00	12.32	3.00
Operating Costs					
Fuel burn-up		6.11	1.49	6.11	1.49
Fuel fabrication		1.20	0.29	1.20	0.29
Chemical Reprocessing		1.51	0.37	1.51	0.37
Labor and maintenance		14.95	3.63	8.97	2.18
Sub Total		23.77	5.78	17.79	4.33
Total Costs		44.32	10.78	30.11	7.33

10.5 Summary of Costs

A summary of the cost estimates is as follows:

Plant construction costs	$1,258,400
Installed plant costs per kilowatt	
Electric	$659
Steam	$160
Cost per kilowatt-hour (60% average load)	
Electric	4.43 cents
Steam	1.08 cents
Cost per kilowatt-hour (100% average load)	
Electric	3.01 cents
Steam	0.73 cents

11.0 FUTURE PROGRAM

11.1 Introduction

Obviously, in the short time available for this design, it was not possible to optimize the entire system. This chapter will discuss those areas where further investigation or development might lead to an optimized system and/or lower costs. There will also be discussed changes in the design for lower power levels.

11.2 Fuel Element Design

The fuel element design chosen for this system is very conservative. Later information from the ORNL Metallurgy Division indicates that the side plate thickness chosen (80 mils) is excessive. This thickness could easily be lowered to 50 mils without serious loss in strength. Investigations are now being carried out for the design of a fuel element which has no side plates at all.* This element is held together by the end boxes and strengthened in the center by bolts and spacers. These improvements lead to a lower stainless steel content in the core and a resulting lower critical mass.

11.3 Reactor Physics

The results of the nuclear calculations are conservative since they are vased on a simple, two-group model. It is felt that a more sophisticated model using machine calculation methods should yield a critical mass lower by 5 to 10% than that reported here. No invest-

---

*Private communication, J. E. Cunningham, ORNL

igation was made of possible uneven burn-up and the efrects at the corners of the reactor. This information would be helpful in determining a schedule for the control rods, ana in deciding whether fuel assemblies should be moved from time to time to different places in the lattice. Investigation of the corners might indicate that the worth of the four corner assemblies is not sufficient to keep them in the lattice.

11.4 Heat Transfer

Perhaps the most important unknown about this system is the boiling heat-transfer curve. An experiment should be run, under operating conditions, to determine exactly the point of incipient boiling and the burnout point. Since it is felt that a pessimistic value for burnout was selected, no difficulty is expected in this respect.

Equally important would be a core mock-up experiment to determine the fraction of core undergoing net steam generation, since this has a rather large effect on the average core void. A very desirable set of experimental curves would be axial distance of sub-cooled heating vs inlet enthalpy (up to saturation) for various power levels, and approximate design velocity over flat plates.

Still another important design point to be checked is the core and circulating pressure drop. This could be accomplished by means of a cold mock-up. Once single-phase pressure drop is established

by the method of Martinelli & Nelson *, it is relatively easy to extrapolate this to two-phase flow with fair accuracy. Accurate establishment of the pressure drop may neccesitate a change in the height of riser and, as a consequence, possible change the height of core.

Establishing heat transfer area, flow area, height of core, effects of average core density for a given power level could be done best by use of Equation 4.3 (paragraph 4.7) or a similar one, depending on the density distribution to be assumed. When designing for lower power levels, one should be expecially careful with the pressure drop vs weight flow curve, such as Fig. 36, since as previously noted, the tendancy is for multiple points of operation to approach the operating range as power is decreased.

11.5 Control and Stability

It is strongly recommended that the kinetics of this reactor be investigated further. Much of the work involved in solving the kinetic equations by electronic analog methods is included in this report. Such an investigation is necessary to complete a control system design. If future study shows that the time response of the reactor, to changes in load, is comparatively fact, then the design point should be changed. As pointed out in section 2.4.3, operation at either higher pressure or lower void fraction would improve the system stability. It is also possible to improve system stability

---

*Martinelli & Nelson, Prediction of Pressure Drop During Forced Circulation Boiling of Water, Trans. of A.S.M.E., Aug. 1948, Paper No. 47-A-113

by including a larger steam chest external to the reactor to provide inertia to the system, which, in effect, increases the time lag between changes in the throttle setting and the awareness of the reactor to the change. Another possible method of improving system stability would be to provide a dumping transition from the turbine throttle to the condenser, bypassing the turbine. Thus, changes in the turbine load could be compensated for by the dumping transition, leaving the reactor load unchanged. In any case, these changes should not cause any drastic design changes in any of the system components.

11.6 Steam System

One item of major importance in the development of the boiling package reactor which deserves further consideration is leakage in the steam system. This may be the leakage of active steam or condensate from valve stem packings into the equipment space or possibly the leakage of condenser coolant into the steam system through the tube joints at the condenser tube sheets. It is desirable, if not necessary, to either eliminate or prevent any such leakage.

It is hoped that the answer to these problems may be obtained from further developments in the PWR design since similar leakage problems are being encountered with that design.

12.1 APPENDIX A: ALUMINUM CORROSION

12.1.1 Fuel Element Selection

Initially, it was thought desirable to use aluminum as the principal material for fuel element construction. The fuel element under consideration was an assembly of sandwich plates similar to the MTR type or APPR type element. The cladding would have been 2S aluminum or some corrosion resistant aluminum alloy and the "fuel meat" a uranium-aluminum solid-solution alloy.

Aluminum is a very desirable material of construction because: 1) it is cheap, 2) it has a low thermal-neutron absorption cross section, giving greater neutron economy, 3) its activity due to neutron capture is very short-lived and thus its contribution to the total activity of the fission products is small, 4) it is relatively easy to work and fabricate; and finally, 5) the chemistry and chemical processing is simple and cheap compared to other metals.

An extensive literature survey and general investigation was made.

12.1.2 Discussion

Of the aluminum alloys, 2S (commercially pure) seems to have the smallest corrosion rate in distilled water, although the corrosion rates of all the alloys are similar.[1] The variation of corrosion rate with temperature is regular on an Arrhenuis

plot (log corrosion rate vs reciprocal of absolute temperature) (Fig. 43) and reasonable corrosion rates are expected in the range of operation. Corrosion is uniform over the surface [1, 12].

Corrosion tests with a couple of aluminum and brazing materials apparently have not been run. The long term effect is thus not known. Although, in that sodium chromate is added to untreated water and operation is at low temperature and low power, an indication of possible trouble presents itself on inspecting elements that have been in the reactor. Elements show pitting attack on the surface adjacent to brazing. This could possible be due to the brazing flux or more seriously, due to the brazing alloy [18].

At temperatures of 200° C and above (another installation reports it at 150° C) a different type of attack occurs in addition to the uniform surface attack. In this case, attack is intergranular in nature and complete disintegration of the specimen occurs within a matter of hours [1,4,15,19]. Only two installations mention this type of behavior. The results are not reproducible to any degree of reliability as far as temperature or attack is concerned. However, the attack has been observed, and the results are conclusive enough to cause concern as to the use of aluminum in high temperature distilled water.

An effort has been made to find some protective treatment to inhibit this intergranular attack but, although several devices show future promise, none are sufficiently perfected to warrant

ORNL-LR-Dwg. 6099

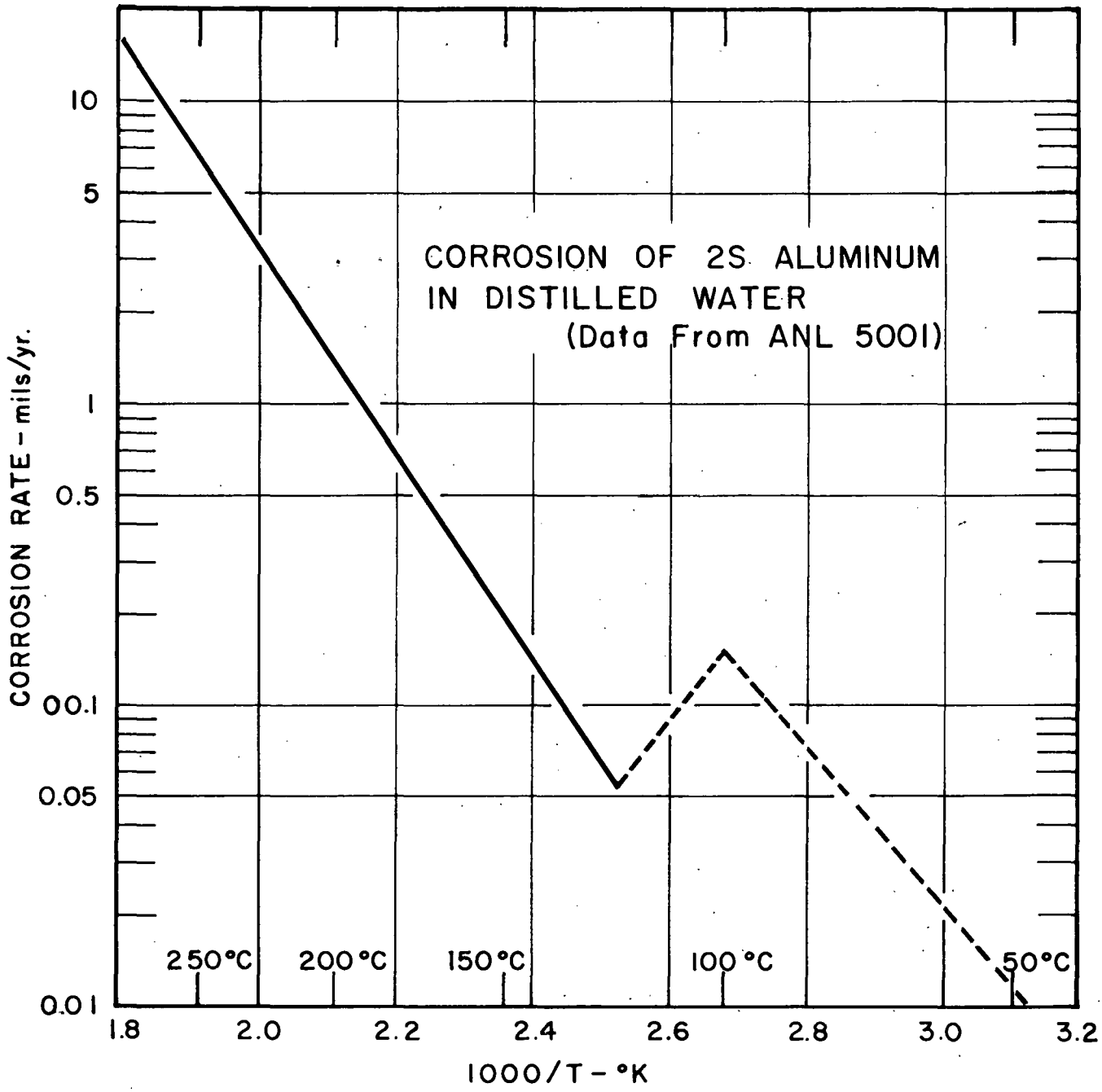

Figure 43

present use. J. E. Draley of Argonne National Laboratory is doing extensive work on aqueous corrosion of aluminum and he believes that the intergranular attack is caused by penetration of atomic hydrogen (produced as the cathodic product in the corrosion reaction) into the metal and the build-up of local gas pressure pockets. Work has shown that any method which causes hydrogen to be released at sites other than the aluminum metal surface is successful in preventing attack. Two methods appear feasible and both involve the use of nickel deposits on the aluminum surface as the preferred sites for hydrogen liberation. Nickel sulfate solution would be simple and permanent protection but suffers from the disadvantage that a complex nickel sulfate deposits on surfaces at high temperatures, and reduces heat transfer coefficients. Dissolved salts in general are not desirable from the steam carry-over and entrainment standpoint. A porous nickel coating on the surface offers excellent protection but tests have not been extensive enough to indicate how long the nickel plate will remain on the surface and whether or not it will protect after it is in contact with only oxide beneath it rather than with metal [1,12].

Coupling aluminum with a metal cathodic to it such as nickel, cobalt, cadmium, or stainless steel or using an anodic current are feasible methods of preventing hydrogen liberation on the aluminum but have the tendency to increase the overall rate of reaction between aluminum and water [1]. With this type of protection it is necessary that the aluminum be in reasonable proximity to the

cathodic metal which seriously limits the application of this method as this is not always convenient in reactor design. In the case of the reactor under consideration, say with a plate-type element, it might be possible to make the side plates of stainless steel or one of the other metals and still have the fuel plate clad with aluminum. Even this would not be too desirable, where the amount of poison in the core is to be held to a minimum, but present a possible compromise.

Other methods of protection considered include inhibitors (such as dichromate ion), pH control, alloying with silicon, anodizing, or saturating the solution with a gas; however, none of these seem to solve the problem (1,13,14). Dichromate solutions are not effective at elevated temperatures but even more important, the chromium ion is reduced in the radiation field of a reactor (1,2,3).

Control of the pH has been shown to be effective in retarding or even preventing intergranular corrosion but at temperatures of 225° C and above, the optimum pH is in the region of 3.5. Sulphuric and nitric acids at high temperatures are not thermally stable and the low pH also simultaneously destroys the corrosion resistance of stainless steel. Thus aluminum and stainless steel systems, of the type under consideration, are incompatable unless some sort of inhibition is possible (1,16).

Chalk River has attempted alloying pure aluminum with 0.1% silicon and this device gave initial indications of promise. Further work has given inconsistant results [19,20].

Surface treatment, such as anodizing, has been found unsuccessful by several installations. It provides a hard, tough initial coating for handling and other mechanical treatment but does not decrease the rate of corrosion; rather, it seems to promote a more uniform attack [1,6]. Protection by this mechanism cannot be relied on for more than about three or four weeks.

Saturation of the solution with helium and oxygen was tried. At 250° C in helium-saturated water an accelerated form of blister corrosion, suspected of being intergranular in nature, was noted after about ten days of exposure. This destructive type of corrosion was not found after 20 days of exposure in oxygen-saturated water. Apparently, the effect of the oxygen was to keep the over-all oxide film in better repair, for longer periods of time [14].

The effects of various other factors have been studied briefly and are summarized. Increasing the fluid velocity increases the corrosion rate but the effect is negligible in comparison to the overall corrosion rate. The same is true with a boiling solution [1,2]. There is no effect on corrosion rate in varying the total static pressure of the system[14]. Chloride ion has been shown to be the most harmful impurity in

the water even when present in quantities of about 5 ppm. Reduction of chloride ion content to 0.1 ppm or lower should be helpful [13]. At these elevated temperatures the oxide film is quite thick, but this is not expected to lower the heat transfer coefficient [10,11].

12.1.3 Conclusions

The specifications of a package reactor indicate the desirability of small components, a minimum core life of two and one-half years, and a high degree of reliability during the operating life. To reduce equipment size to a reasonable value, especially for transportation to arctic locations, steam pressures of 200 psia and above are indicated. The saturation temperature corresponding to 200 psia is about 195° C, which means that the metal surface temperature in the core will be well over 200° C. Unfortunately this is the region in which the intergranular attack of aluminum is known to occur. Fuel element treatment would be acceptable but no dependable method has yet been found. Additives to the boiling water are unsatisfactory from the steam entrainment and carry-over considerations and have not been proven reliable. Certainly, there is no known method of protection that would insure a reliable aluminum-clad fuel element for use at temperatures above 200° C for a period of two and one-half years.

In view of the above arguments, it was decided to abandon the use of aluminum as the principal material of construction for the fuel elements. However, in the future, if an acceptable device can

be found for inhibiting the intergranular attack of aluminum, the reconsideration of aluminum for this application seems definitely worthwhile.

12.1.4 Bibliography (for section 12.1 only)

1. Private communication; Draley, J. E. (ANL) to Livingston, R.S. (ORNL), June 11, 1954.

2. Wilson, C. D., The Effect of Water Velocity on 2S Aluminum Slug Jacket Corrosion, Hw-26033, Oct. 23, 1952.

3. Eschback, E. A. and Snow, W. R., Status of Fuel Element Development at Hanford for January and February, HW-28100, Apr. 1, 1953

4. Draley, J. E. and Ruther, W. E., Aqueous Corrosion of 2S Aluminum at Elevated Temperatures, AECU-2301, Oct. 1952.

5. Link, L. E., Corrosion Rates of 2S Aluminum, Preliminary Literature Survey, ANL-JRH-41, Oct. 17, 1950.

6. Asai, R. I., Flow Laboratory Corrosion Test of Anodized Slugs, HW-27128, Feb. 12, 1953.

7. Goldsmith, S., Laboratory Studies of 2S Aluminum Corrosion at Elevated Temperatures, HW-24584, May 27, 1952.

8. Atwood, John M., Process Water pH Effects, HW-24007, May 15, 1952.

9. MacCormack, R. S., Dayan, S. S., Parge, H., Weinshelboum, H., Bibliography on the Corrosion of Aluminum in Water, CU-1-53-At-dP-ChE, July 1953.

10. Strom, P. O., Boyer, M. H., Static Corrosion of Aluminum Alloys at 350° F and 480° F in Distilled Water, IRL-64, Oct. 1953.

11. Strom, P. O., Litz, L. M., Boyer, M. H., Reproducibility of 480° F Static Aqueous Corrosion of Pure Aluminum, IRL-112, Mar. 1954.

12. Loftness, R. L., Feldman, M. H., Corrosion Problems in the NPR, NAA-SR-94, Dec. 1950.

13. Metallurgy Division Quarterly Report for July, August, and September 1953, ANL-5153, Sept. 1953

14. Metallurgy Division Quarterly Report for April, May and June, ANL-5097, June 1953.

15. Draley, J. E. and Ruther, W. E., Aqueous Corrosion of 2S Aluminum at Elevated Temperatures, ANL-5001, Feb. 1, 1953.

16. Reactor Handbook, Vol. 2, Engineering, RH-2, First Ed, Sept. 1953.

17. Reactor Handbook, Vol. 3, Materials, RH-3, First Ed., Spr. 1953.

18. Private communication, English, J. (ORNL), Compere, E. (ORNL), and Klotz, C. E. (ORNL).

19. Laurence, G. C. et al, Chalk River Progress Report, PR-CE-18, Apr-June 1953.

20. Laurance, G. C. et al, Chalk River Progress Report, PR-CE-20, Oct. to Dec. 1953.

21. Private communication, Bowen, F. J. (Kaiser Aluminum & Chemical Company) to Klotz (ORNL), July 8, 1954.

22. Private communication, Sansonetti, S. J., (Reynolds Metal Company) to Klotz (ORNL), July 16, 1954

23. Private communication, Goers, H. J., (Aluminum Company of America) to Klotz (ORNL), July 20, 1954

12.2 APPENDIX B: THE KINETIC EQUATIONS OF A BOILING REACTOR

12.2.1 Nomenclature

A_F	heat transfer area in core
A	average flow area in core
A_1	flow area at core inlet
A_2	flow area at core exit
A_{pv}	effective heat transfer area of pressure vessel
A_{SM}	effective heat transfer area of steam dome metal
A_x	flow area at distance X in circulating loop
B	fraction of neutrons which are delayed
B_i	fraction of neutrons which are delayed by i-th group
C_i	concentration of i-th group of delayed neutron precursors
C_f	specific heat of liquid
C_F	specific heat of fuel elements
C_{pv}	specific heat of pressure vessel metal
C_{SM}	specific heat at steam dome metal
D_1	constant relating neutrons per second and Btu per second
D_2	$A(\rho_g h_{fg}) / \Delta T_s$, constant
D_3	constant, $\Delta\rho_g / \Delta T_s$
D_4	constant relating wt, ρ_g, and $\overline{X}$
D_5	constant relating P_o, ρ_g and $\overline{X}$
D_6, D_7, D_8	constants relating pressure drops to geometry of system

$\bar{f}_v$ average vapor fraction in core

f_{v2} vapor fraction at core exit

F() function of ()

g 32.2 ft/sec^2

G mass flow per unit area

h_f average enthalpy of liquid in core

h_{f1} enthalpy of liquid at core entrance

h_{f2} enthalpy of liquid at core exit

h_{ff} enthalpy of feedwater

h_{fg} latent heat of vaporization

h_g enthalpy of steam in steam dome

h_{g2} enthalpy of vapor at core exit

h_{g3} enthalpy of vapor at throttle

H head

h heat transfer coefficient between fuel and fluid

h_{pv} heat transfer coefficient between pressure vessel and fluid

K_{eff} effective multiplication constant

h_{SM} effective heat transfer coefficient between steam and metal in steam dome

ℓ^* mean neutron lifetime

M_d mass of liquid in downcomer

M_{pv} mass of pressure vessel (adjacent to downcomer)

M_{SM} mass of metal in steam dome

M_U total momentum of mass in circulating loop.

P_1, P_2, etc. Pressure drop

P reactor power

P_o power demanded by load

Q heat transfer rate

r empirical function described by equation (38)

S_1 transport delay in downcomer

S_2 transport delay in riser

T_f average liquid temperature in core

T_{f1} liquid temperature at core entrance

T_{f2} liquid temperature at core exit

T_{f3} liquid temperature at top of riser

T_{fd} liquid temperature in downcomer (average)

T_F temperature at wall of fuel element

T_{pv} temperature of pressure vessel

T_S saturation temperature

T_{SM} temperature of metal in steam dome

$U_{(x)}$ velocity of fluid at point X

U_1 fluid velocity at reactor inlet

U_2 fluid velocity at reactor outlet

V_d volume of liquid in downcomer

V_f volume of fuel elements

V_{SC} volume of steam dome

W mass flow rate around recirculating loop

W_T mass flow rate of feedwater, and steam (at throttle)

x distance along recirculating loop

$\bar{X}$ throttle setting

Z core height

Z_1 riser height

λ_i delay constand of i-th group of delayed neutron precursors

$\overline{\rho}$ average density of fluid in the core

ρ_2 average fluid density at core exit

ρ_f average liquid density in core

ρ_{f1} average liquid density at core entrance

ρ_{f2} average liquid density at core exit

ρ_{fd} average liquid density in downcomer

ρ_F average density of fuel elements

ρ_g vapor density

$\rho_{(x)}$ fluid density at distance x along circulating loop

12.2.2 System Model

As the first step in writing the kinetic equations which describe the behavior of a boiling reactor it is necessary to define the model. For a drawing of the system, refer to Fig. 50. It consists of a large pressure vessel, which contains a heterogeneous reactor core, coolant (water), and a steam dome. The riser shown above the core is provided to insure sufficient head for natural circulation.

The following assumptions complete the model:

(a) The mass-flow rate of feed water into the vessel equals the mass-flow rate of steam out of the steam dome at all times (as a result the water level may fluctuate). (b) The velocity of any steam bubbles leaving the core is the same as the water leaving the core, i.e., no slip. (c) The density of vapor is a function of saturation temperature only. (d) The density of the liquid is a function of liquid temperature only. (e) The rated steam pressure is 415 psia for all loads. (f) There is no entrainment of vapor in the downcomer. (g) Surface vaporization can be neglected. (h) The bubble density within the core is

increasing linearly and in the riser is constant.

12.2.3 Reactor Power as a Function of Density

Equations (1) and (2) describe the time behavior of the reactor.

$$\frac{d\,P(t)}{d\,t} = \left[\frac{(1-B)\,K_{eff} - 1}{\ell^*}\right] P(t) + D_1 \sum_{i=1}^{5} \lambda_i C_i(t) \qquad (1)$$

$$D_1 \frac{d\,C_i(t)}{d\,t} = -D_1 \lambda_i C_i(t) + B_i K_{eff} P(t) \qquad (2)$$

K_{eff} is some function of the fluid density in the core. This relationship is expressed by equation (3).

$$K_{eff}(t) = K_o \; K(\bar{\rho}) \qquad (3)$$

K_o accounts for control rod position and the reactor's past history while $K(\bar{\rho})$ accounts for effect of average fluid density, $\bar{\rho}$, on the multiplication constant.

12.2.4 Fuel Temperature as a Function of Reactor Power and Heat Transfer Rate

This function is described by equation (4) which is an energy balance on the fuel elements.

$$C_F \rho_F V_F \frac{d\,T_F}{d\,t} = P(t) - Q(t) \qquad (4)$$

The first term of this equation represents the time rate of change of the fuel elements heat content. The second term has already been defined in equation (1) while the third term represents the heat transfer rate between the fuel elements and the water.

12.2.5 Heat Transfer Rate as a Function of System Temperatures

In a boiling system part of the total heat transferred to the fluid is required to heat the liquid entering the system to a temperature slightly above saturation. The remainder of the heat transferred vaporizes the liquid, i.e., generates steam.

As compared to other everyday phenomona, the information on boiling heat transfer is very meager. A survey of the literature reveals that the total heat transfer rate, Q, is a function similar to that shown in the figure below.

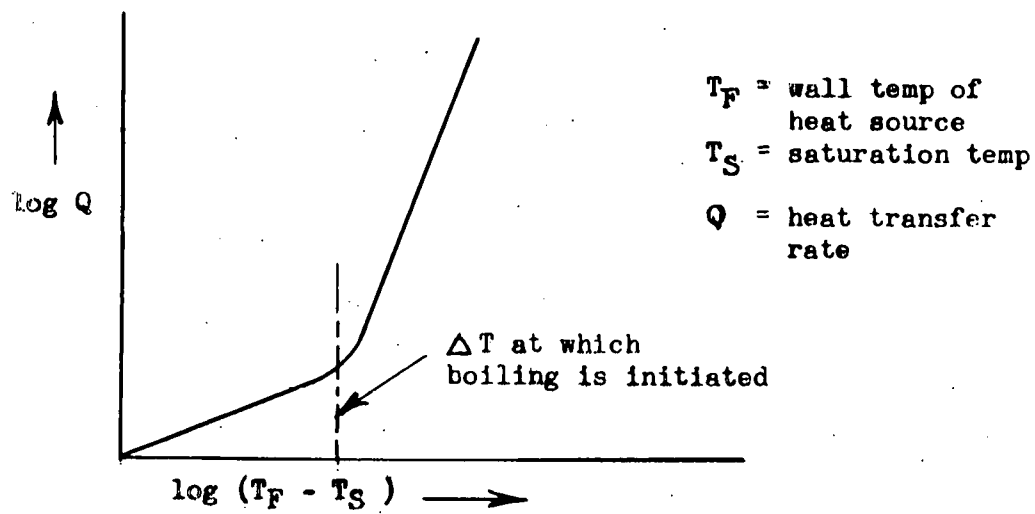

Steam generation does not take place until the wall temperature of the heat source is a few degrees above saturation. The nature of the boiling (i.e., subcooled or ordinary) is determined by the liquid temperature. If the liquid temperature is below saturation, subcooled boiling will take place. For ordinary boiling to occur, the liquid must be slightly superheated.

These facts lead to the postulation that the heat transfer rate consists of two functions, one describing the heat transfer rate required to heat the liquid, and a second describing the heat transfer rate which results in net steam generation. Another way of saying this is that the first function describes that portion of the heat transferred which is manifested as sensible heat while the second describes that portion which is manifested as latent heat. Equations (5), (6), (7), and (8) result.

$$Q = Q_1 + Q_2 \qquad (5)$$

$$Q_1 = WC_f (T_S - T_{f1}) \qquad (6)$$

= heat transfer rate required to heat liquid to saturation.

$$Q = A_f h \left[T_F - T_f\right] \qquad (7)$$

= total heat transfer rate

$$h = F (T_F - T_S) \qquad (8)$$

= total heat transfer coefficient.

In equations (6) and (8) the fact that the liquid must be heated a few degrees above saturation, has been neglected.

12.2.6 Liquid Temperature in Reactor as a Function of System Parameters

This function can be obtained by writing a balance of the sensible heat (i.e., heat which is manifested by change in temperature) over the core. This is done in equation (9).

$$\frac{d (\bar{\rho} AZh_f)}{d t} = Q_1 - (h_{f2} U_2 A_2 \rho_2 - h_{f1} U_1 A_1 \rho_{f1}) \qquad (9)$$

The first term in equation (9) equals the time rate of change of the heat content of the fluid (less latent heat) in the core. The second term has already been defined, while the third term

represents that portion of energy which is removed from the core as sensible heat. The various parameters are defined by the following equations.

$$h_f = C_f T_f \tag{10}$$

$$U_2 A_2 \rho_2 = U_1 A_1 \rho_{f1} = W \tag{11}$$

$$\bar{\rho} = \rho_g \bar{f}v + (1 - \bar{f}v)\rho_f \tag{12}$$

$$\frac{d(\bar{\rho} AZh_f)}{dt} = (\rho_g - \rho_f) AZh_f \frac{d\bar{f}v}{dt} + \bar{f}v\, AZh_f \frac{\partial \rho_s}{\partial T_s} \frac{dT_s}{dt} + (1-\bar{f}v)\, AZh_f \frac{\partial \rho_f}{\partial T_f} \frac{dT_f}{dt} + \bar{\rho}\, AZc_f \frac{dT_f}{dt}$$

$$\simeq -\rho_f AZ\, c_f T_f \frac{d\bar{f}v}{dt} + \bar{\rho}\, AZ\, c_f \frac{dT_f}{dt} \tag{13}$$

The neglect of the term in equation (13) which contains the derivative of T_s postulates that the change in the mass of the fluid in the core, due to vapor density changes is negligible. Substitute equations (10), (11), and (13) in equation (9). Thus:

$$\bar{\rho}\, AZ\, c_f \frac{dT_f}{dt} - \rho_f AZ\, c_f T_f \frac{d\bar{f}v}{dt} = Q_1 - WC_f (T_{f2} - T_{f1}) \tag{14}$$

If the recirculation ratio is high and feedwater heating is employed, the liquid entering the core is very quickly heated to saturation. Therefore a reasonable approximation is to let $T_f = T_{f2}$ and $\rho_f = \rho_{f2}$. The final result is equation (15).

$$\bar{\rho}\, AZ\, c_f \frac{dT_{f2}}{dt} - \rho_{f2} AZ\, c_f T_{f2} \frac{d\bar{f}v}{dt} = Q_1 - WC_f (T_{f2} - T_{f1}) \tag{15}$$

At this point it would be well to define the dependence of T_{f1}. The feedwater, as shown in figure 50 is injected at the top of the downcomer. This is mixed with the water flowing over the riser into the downcomer. As a result the bulk temperature of the

water at the top at the downcomer, T_{fd}, is higher than the temperature of the feedwater, T_{ff}, but lower than that flowing over the riser, T_{f3}. From this follows equations (16) and (17).

$$T_{f1}(t) = T_{fd}\ (t - S_1) \tag{16}$$

where S_1 = delay time from top of downcomer to core entrance

$$T_{f3}(t) = T_{f2}\ (t - S_2) \tag{17}$$

where S_2 = delay time from core exit to top of riser

12.2.7 Vapor Fraction as a Function of System Parameters

The average vapor fraction in the core can be obtained by writing a "latent heat" balance on the vapor in the core. This could be called an energy balance on the vapor in the core except that the sensible heat of the vapor is included in equation (15). Equation (18) is a balance of the latent heat.

$$\frac{d(\bar{f}v\ AZ\rho_g h_{fg})}{d\ t} = Q_2 - U_2\ A_2\ f_{v2}\ \rho_g\ h_{fg} \tag{18}$$

The first term in equation (18) represents the time rate of change of latent heat content; the second, the rate heat is added; and the last term, the rate heat is removed.

As a consequence of the assumption of linear bubble density, equation (19) can be written.

$$f_{v2} = 2\bar{f}v \tag{19}$$

The first term in equation (18) is expanded in (20).

$$\frac{d\ (fv\ AZ\ \rho_g\ h_{fg})}{d\ t} = \rho_g h_{fg}\ AZ\ \frac{d\ \bar{f}v}{d\ t} + \bar{f}v\ AZ \frac{\partial(\rho_g h_{fg})}{\partial\ T_S}\ \frac{d\ T_S}{d\ t} \tag{20}$$

$$\text{let}\quad \frac{\partial(\rho_g\ h_{fg})}{\partial\ T_S} \approx \frac{\Delta(\rho_g h_{fg})}{\Delta\ T_S} = D_2' \tag{21}$$

Substitute (19), (20), and (21) in (18):

$$\rho_g h_{fg} AZ \frac{d\bar{f}v}{dt} + \bar{f}v D_2 AZ \frac{d T_S}{dt} = Q_2 - 2U_2 A\bar{f}v \rho_g h_{fg} \qquad (22)$$

12.2.8 Saturation Temperature as a Function of Average Vapor Fraction and Throttle Setting

The saturation temperature can be obtained by writing an energy balance on the steam dome. This is done in equation (23).

$$\frac{d(V_{SC}\rho_g h_g)}{dt} = U_2 A_2 fv_2 \rho_g h_{g2} - W_T h_{g3} - A_{SM} h_{SM} (T_S - T_{SM}) \qquad (23)$$

Equation (23) can be simplified if the following approximations can be made: The change in heat content of the vapor is manifested largely be a change in vapor density, ρ_g.

This approximation postulates constant volume, and that $\left|\frac{\partial \rho_g}{\partial T_S}\right| \gg \left|\frac{\partial h_g}{\partial T_S}\right|$. The change in ρ_g compared to the change in h_g is in fact large. The validity of neglecting the volume change will depend on the geometry of the system.

Using these approximations and equation (19) equation (23) can be written as:

$$V_{SC} h_g \frac{\partial \rho_g}{\partial T_S} T_S = 2U_2 A_2 \bar{f}v \rho_g h_{g2} - W_T h_{g3} - A_{SM} h_{SM} (T_S - T_{SM}) \qquad (24)$$

Let $\frac{\partial \rho_g}{\partial T_S} \approx \frac{\Delta \rho_g}{\Delta T_S} = D_3$ and (25)

Let $h_g = h_{g2} = h_{g3} =$ constant (26)

The mass flow rate at the throttle, W_T, will depend on throttle setting, $\bar{X}$, and the steam density, ρ_g. This dependence is expressed by equation (27).

$$W_T = D_4 \rho_g \bar{X} \qquad (27)$$

where $\bar{X} = 1$ at rated load

Substituting (25), (26) and (27) in (24) results in (28).

$$V_{SC} D_3 \frac{d T_S}{d t} = 2 U_2 A_2 \bar{f}v \rho_g - D_4 \rho_g \bar{X} - A_{SM} h_{SM} (T_S - T_{SM})/h_g \qquad (28)$$

The last term in equation (28) represents the heat transferred from the steam to the metal in the steam dome.

12.2.9 Temperature of Steam Chest Metal as a Function of Saturation Temperature

This function is expressed by equation (28a).

$$M_{SM} C_{SM} \frac{d T_{SM}}{d t} = A_{SM} h_{SM} (T_S - T_{SM}) \qquad (28a)$$

12.2.10 Power Demand as a Function of Throttle Setting and Vapor Density

Since the turbine operates at fairly constant exhaust pressure, the power demand is directly proportional to throttle setting and steam density. This relationship is expressed by equation (29).

$$P_o = D_S \rho_g \bar{X} \qquad (29)$$

12.2.11 Temperature of Liquid in Downcomer as a Function of Mass Flow in Core, etc.

The temperature of the liquid in the downcomer, T_{fd}, is obtained by writing an energy balance on the mass of fluid in the downcomer.

This is done in equation (30).

$$\frac{d\,(V_d\,C_f\,\rho_{fd}\,T_{fd})}{d\,t} = \left[Q - 2A_2\,U_2\,\bar{f}v\,\rho_g\,h_g\right] + W_T\,h_{ff} - h_{pv}\,A_{pv}\,(T_{fd} - T_{pv}) \qquad (30)$$

In (30) the first term accounts for the time rate of change of heat content, and the last term accounts for the rate heat is lost to the pressure vessel by conduction (the actual method is by convection).

The first in (30) is expanded in (31).

$$\frac{d\,(V_d\,C_f\,\rho_{fd}\,T_{fd})}{d\,t} = C_f\,M_d\,\frac{d\,T_{fd}}{d\,t} + C_f\,T_{fd}\,\frac{d\,M_d}{d\,t} \qquad (31)$$

Substitute (31) in (30):

$$C_f\,M_d\,\frac{d\,T_{fd}}{d\,t} + C_f\,T_{fd}\,\frac{d\,M_d}{d\,t} = \left[Q - 2A_2\,U_2\,\bar{f}v\,\rho_g\,h_g\right] + W_T\,C_f\,T_{ff} - h_{pv}\,A_{pv}\,(T_{fd} - T_{pv})$$

12.2.12 Mass of Fluid in Downcomer as a Function of Mass Flows

Neglecting changes due to changes in average core density, equation (32) can be written.

$$\frac{d\,M_d}{d\,t} = W_T - 2A_2\,U_2\,\bar{f}v\,\rho_g \qquad (32)$$

12.2.13 Temperature of Pressure Vessel as a Function of Temperature in Downcomer

This function is given by equation (33).

$$M_{pv}\,C_{pv}\,\frac{d\,T_{pv}}{d\,t} = K_{pv}\,A_{pv}\,(T_{fd} - T_{pv}) \qquad (33)$$

12.2.14 Mass Flow in the Core as a Function of System Densities and Vapor Fraction

In deriving this function two assumptions are made, (a) mass flow, W, is not a function of distance along the circulating loop, and (b), the

model consists of a constant mass of fluid circulating in a loop of varying cross section. Equation (34) is a force balance on the entire mass.

$$\frac{d\,(MU/A)}{d\,t} = H - \sum_i pi \qquad (34)$$

In equation (34) the first term represents the time rate of change of the total momentum per unit area. The second term equals the total head per unit area (i.e., driving force) and the third term equals the total pressure drop around the loop due to friction (i.e., resistance). These terms are defined and expanded in the following equations.

$$\frac{d\,(MU/A)}{d\,t} = \frac{d}{d\,t}\oint \frac{\rho_{(x)}\,A(x)\,U(x)}{g\,A(x)}\,d_x \qquad (35)$$

Substitute (11) in (35)

$$\frac{d\,(MU/A)}{d\,t} = \frac{d}{d\,t}\oint \frac{W\,d_x}{g\,A_{(x)}} = \frac{d\,W}{d\,t}\left(\oint \frac{d_x}{g\,A(x)}\right) \qquad (36)$$

Equation (37) defines the dependence of H. It is assumed that the liquid density is constant around the loop. This is sufficiently accurate for high recirculation ratios.

$$\begin{aligned} H &= Z\,(\rho_{fd} - \bar{\rho}) + Z_1\,(\rho_{fd} - \rho_2) \\ &= Z\,(\rho_{f2} - \bar{\rho}) + Z_1\left[\rho_{f2} - (2\bar{\rho} - \rho_{f2})\right] \\ &= (Z + 2Z_1)\,(\rho_{f2} - \bar{\rho}) \end{aligned} \qquad (37)$$

The total pressure drop around the loop is equal to the sum of the following pressure drops.*

p_1 = pressure drop due to acceleration

$$p_1 = r\,\frac{G^2}{g} = \frac{W^2}{2\,A_2^2 g}\,2r \qquad (38)$$

where

$$r = F_1(\bar{f}v)\;F_2(T_S) \qquad (39)$$

$$p_2 = D_6\,\frac{W^2}{2\,A_2^2\,g\,\rho_{f_2}}\;F_3(\bar{f}v)\;F_4(T_S) \qquad (40)$$

= pressure drop due to friction losses in core during two phase flow.

D_6 depends on the geometry of the system.

p_3 = pressure drop due to friction losses in section from top of downcomer to core entrance (constant density region)

$$p_3 = D_7\,\frac{W^2}{2A_2^2\,g\,\rho_f} \qquad (41)$$

p_4 = pressure drop due to friction losses in core and riser

$$p_4 = D_8\,\frac{W^2}{2A_2^2\,g\,\rho_2} \qquad (42)$$

In the above equations the constants D_7 and D_8 will depend on geometry. The functions $F_1(\bar{f}v)$, $F_2(T_S)$, $F_3(\bar{f}v)$, and $F_4(T_S)$ can be calculated from curves included in a paper by Martinelli & Nelson.*

Equation (42) completes the analytical model. These equations pose a formidable problem. The most attractive method for solving the problem appears to be with an analogue computer. A layout of the com-

---

* Martinelli & Nelson, Prediction of Pressure Drop During Forced Circulation Boiling of Water, Trans ASME, Aug, 1948.

puter components required shows that eighteen multipliers, eleven function generators, and twenty seven operational amplifiers would be required.

The only other alternative approach to this problem is to build a scale model. While this method would be more accurate it would be much less flexible in studying parametric changes.

12.3 APPENDIX C: BOILING REACTOR SIMULATOR

It was not possible to simulate the system because sufficient equipment was not available at this laboratory. However, most of the work involved (outside of setting up the actual electronic equipment) was accomplished. If, in the future there is enough interest in the problem to warrant its simulation, this study should be of assistance.

This appendix is concerned with the electronic equipment required to simulate the model described in Appendix 12.2, and the tabulation of the necessary constants and variables of the system. The symbols and notations used here are the same as those in Appendix 12.2. The equation numbers referred to are those equations in 12.2.

Figure 44 is a diagram of a computer proposed to simulate the system. By comparison with a pressurized-water reactor, the simulator required for a boiling reactor is rather elaborate.

The block in Figure 44 marked "reactor simulator" represents equations (1), (2), and (3). The circuitry involved is for the most part conventional and descriptions of it can be found elsewhere.* The simulation of equation (3) will require a function generator relating K_{eff} to $\bar{\rho}$. The curve for this function generator can be obtained by replotting Figure 21 in terms of fluid density rather than vapor fraction. The effect of neutron temperature on K_{eff} as far as cross section change is concerned has been neglected since it is quite small compared to the density effect.

---

* J. J. Stone, E. R. Mann, ORNL Reactor Controls Computer, ORNL-1632.

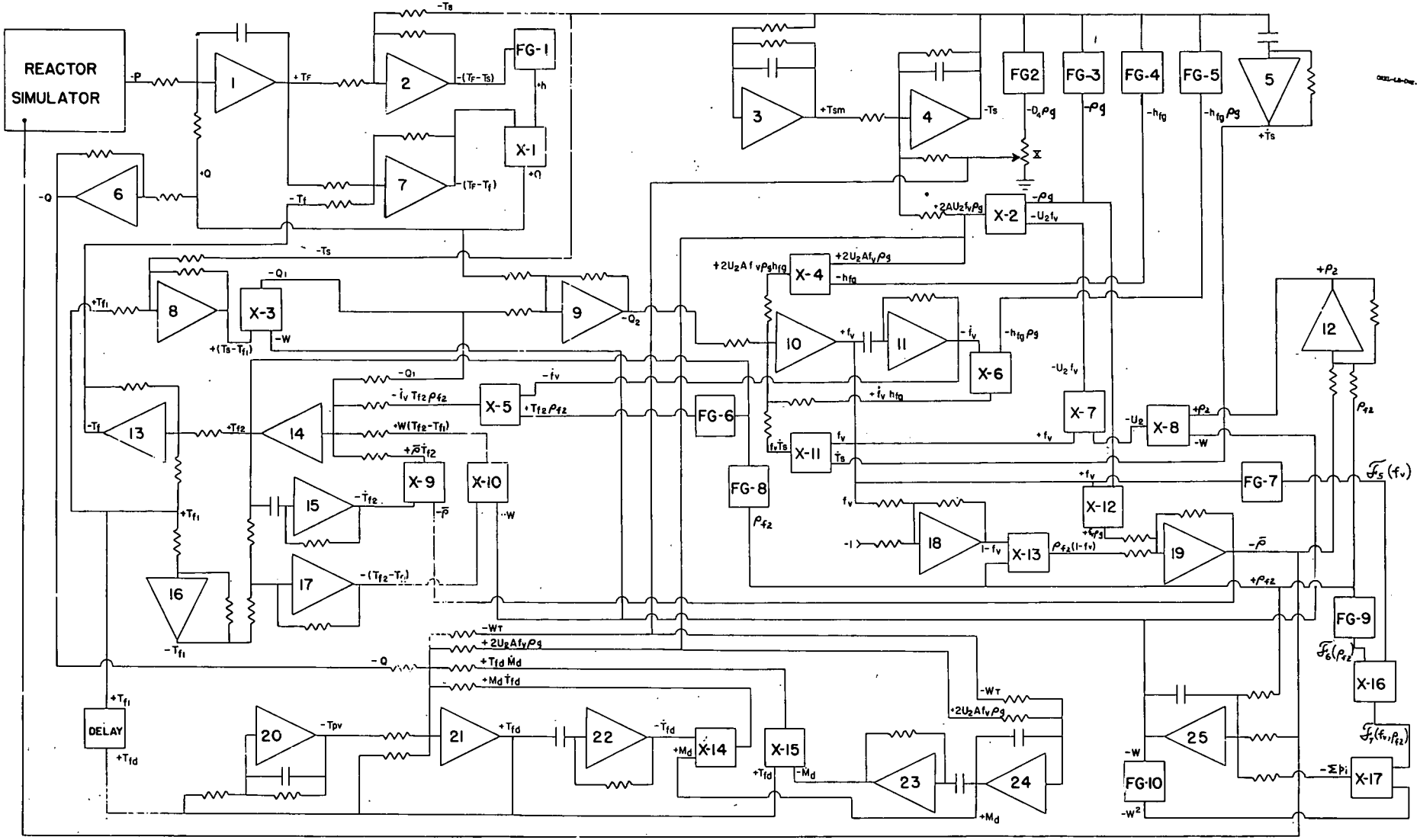

FIGURE 44 SIMULATOR DIAGRAM

Equation (4) is simulated by operational amplifier 1 (which is shown in Figure 44 as a triangle) and its associated circuits. The capacitor in the feedback network represents the product of C_F, ρF, and V_F.

The heat transfer equations, (5), (6), (7), and (8) are simulated by operational amplifiers 2, 7, 8 and 9; multipliers X-1 and X-3; and function generator FG-1. The selection of the curve for function generator, Figure 45, presented a problem. The data on boiling heat transfer is such, that evaluation of the heat transfer coefficient is difficult. Therefore, Figure 45 is more qualitative than quantitative. The error introduced by the uncertainty of $\underline{h}$ is not important since only the fuel temperature, T_F, will be affected. The design value of T_F is far below the maximum for stainless steel; its actual value is of little interest.

The dependence of the liquid temperature T_{f2}, as described by Equation (15) is simulated by operational amplifiers 14, 15, 16, and 17; multipliers X-5, X-9 and X-10; and function generator FG-6. It is recognized that differentiation with an operational amplifier, as with amplifier 15, should be avoided but here there was no alternative. The constants in Equation (15) not shown in Figure 44 are represented by the particular input impedances; this also applies to the rest of Figure 44. For example, the resistor between X-5 and operational amplifier 14 represents the reciprocal of $A.Z.C_f$. In some instances, parameters are represented by multiplier constants (i.e., +2A in X-2). The curve for FG-6 is shown in Figure 46. The block marked "delay" corresponds to Equation (16).

ORNL-LR-Dwg. 6101

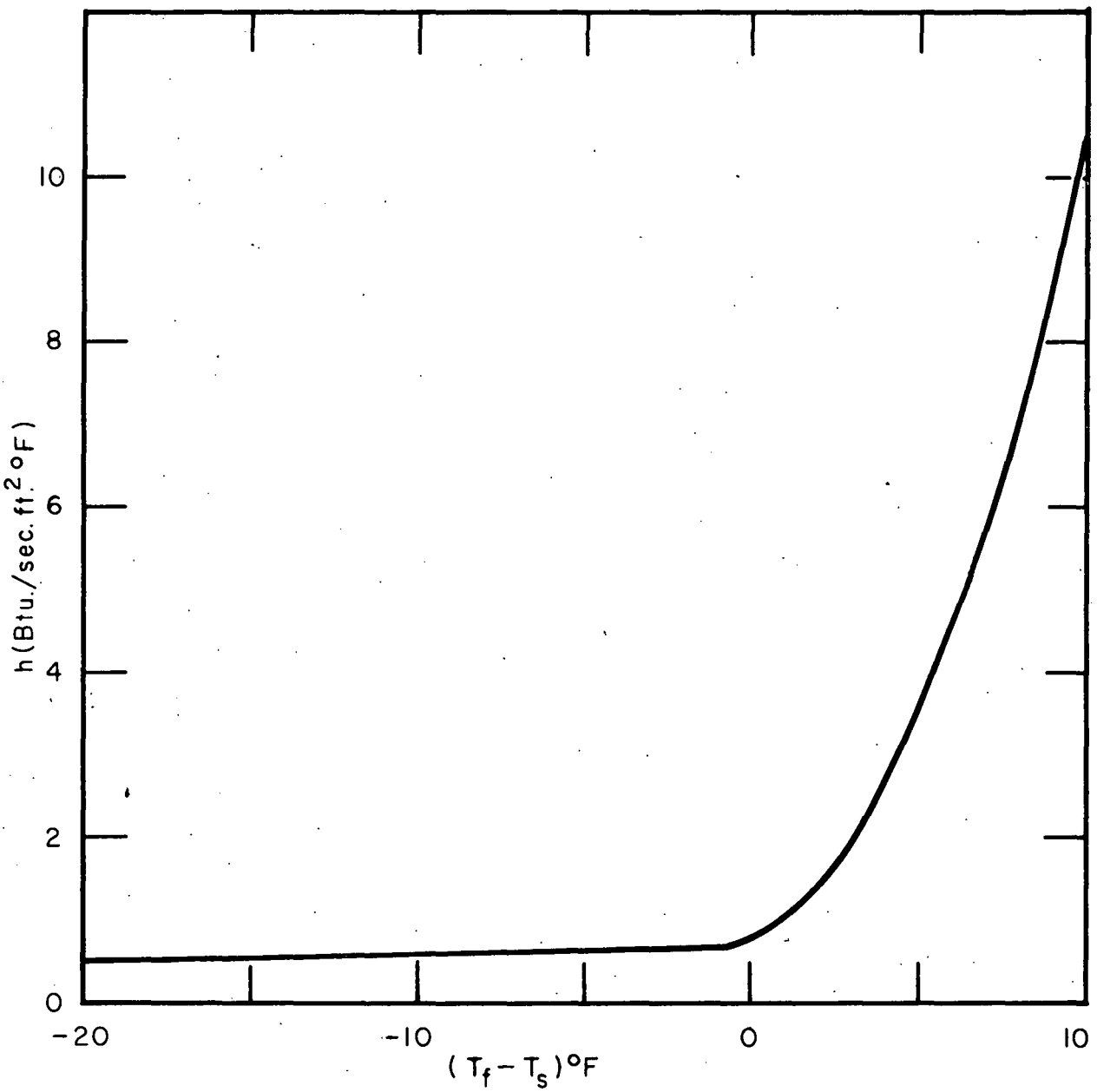

FIGURE. 45 CURVE FOR FG-1

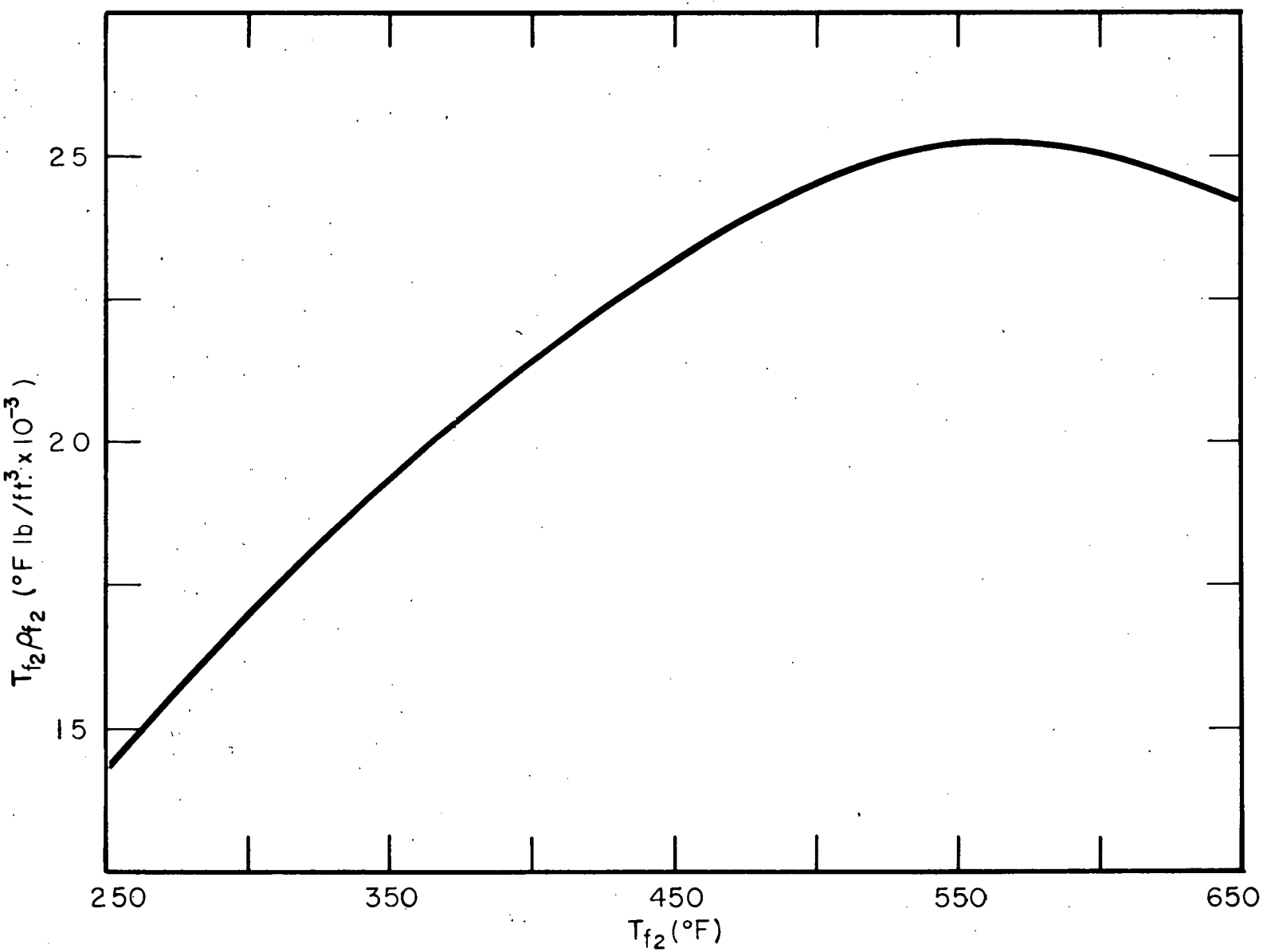

FIGURE. 46 CURVE FOR FG-6

Operational amplifiers 5, 10 and 11; and multipliers X-2, X-4, X-6, X-7 and X-11 are required to describe Equation (22). Here again it was necessary to resort to differentiation with operational amplifiers.

Equation (28) is simulated with operational amplifier 4, multiplier X-2, and FG-2, and FG-3. The setting of the potentiometer at the output of FG-2 represents throttle setting $\bar{X}$. The curve for function generator FG-2 is shown in Figure 47. The curve for FG-3 can be obtained from steam tables, as can the curves for FG-4 and FG-5.

Operational amplifier 3 simulates equation (28a) in which perfect insulation of the steam chest was assumed. The two input resistors represent the reciprocal of $A_{pv}\ h_{pv}$. This assumes that the heat transfer coefficient between the steam and surrounding metal in the steam chest (h_{pv}) is constant. Actually, h_{pv} varies tremendously depending on whether the steam dome metal is superheating or condensing the steam. Since response for conditions of rising steam temperature is of greater interest, the larger value of h_{pv} was chosen.

The simulator shown in Figure 44 does not compute power demand, which is described by equation (29). However, this could be done very easily by adding another ganged potentiometer to the output of FG-2.

The average fluid density, $\bar{\rho}$, is computed by operational amplifiers 18 and 19 together with multipliers X-12 and X-13, and FG-8. The curve for FG-8 is given in Figure 48. This is according to Equation (12).

The average fluid density at the core exit, ρ_2 is computed by operational amplifier 12 where: $\rho_2 = 2\bar{\rho} - \rho_{f2}$.

ORNL-LR-Dwg. 6103

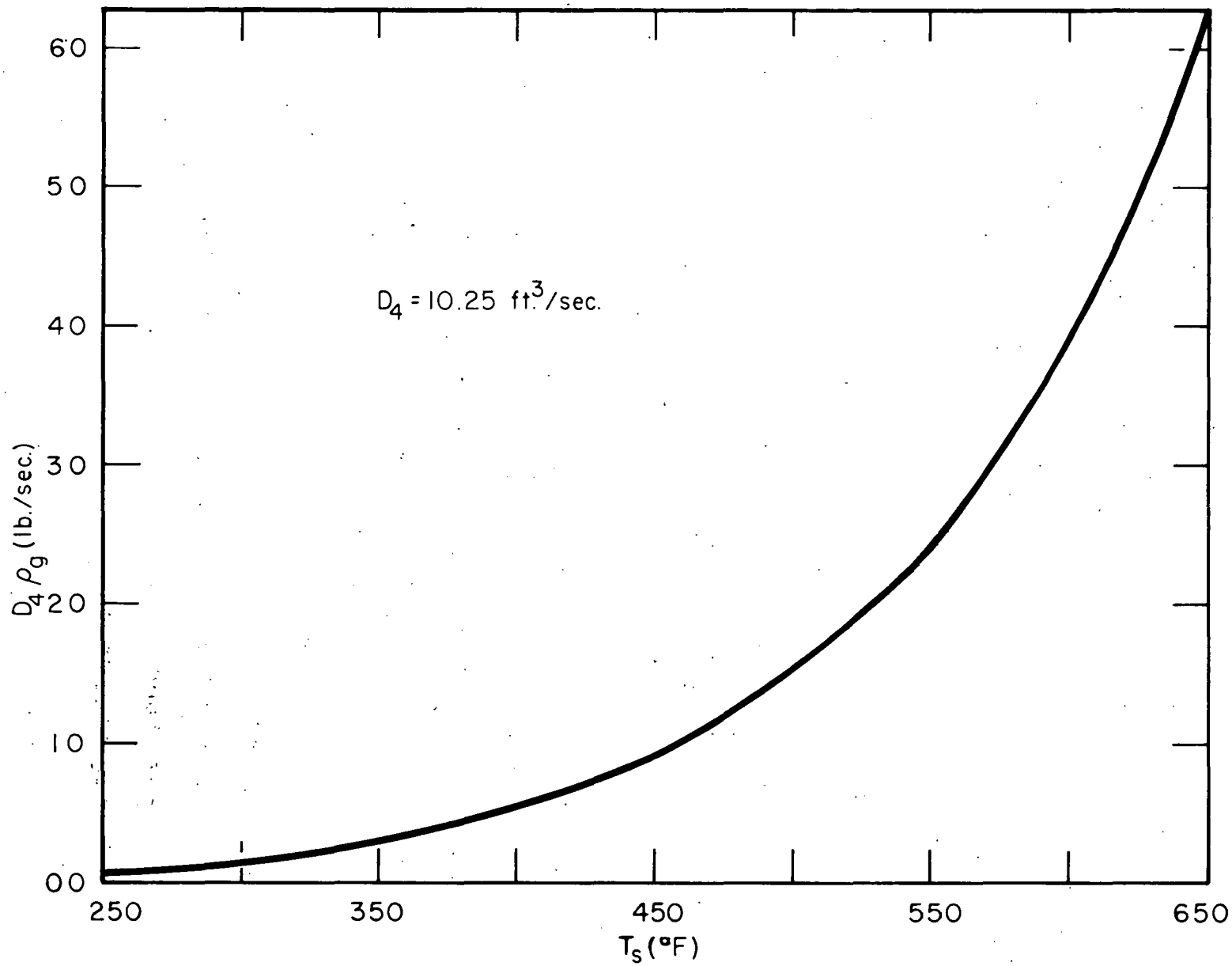

FIGURE. 47 CURVE FOR FG-2

ORNL-LR-Dwg. 6104

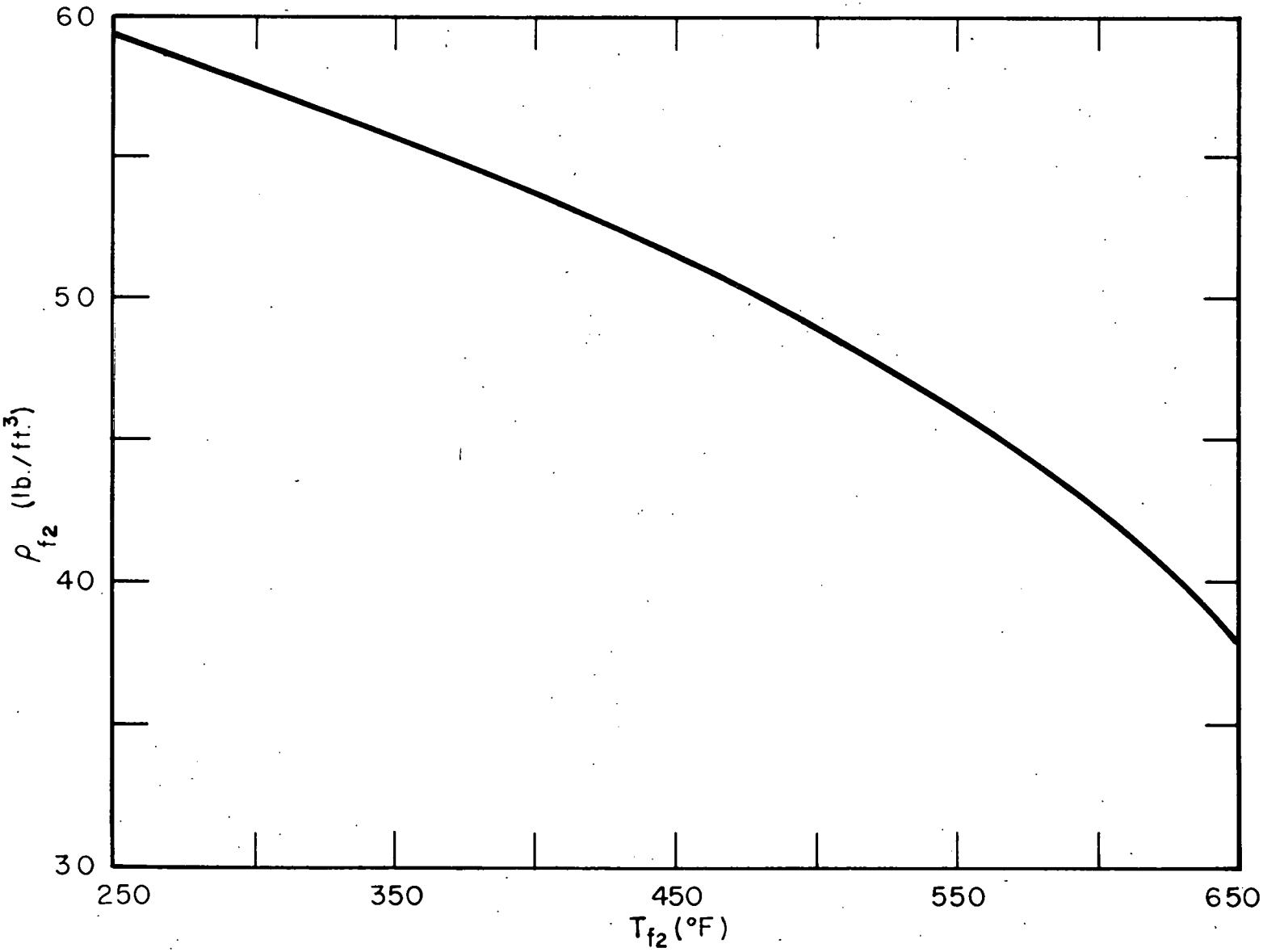

FIGURE. 48 CURVE FOR FG-8

The simulation of equations (31), (32), and (33) involves the use of operational amplifiers 20, 21, 22, 23, and 24 together with multipliers X-14 and X-15.

The simulation of the transient behavior of mass flow rate in the reactor, W, would be very difficult using equations (38) through (42) to compute pressure drops. Instead, this term is supplied by three function generators FG-7, FG-9 and FG-10 and multipliers X-15 and X-17. The curves for FG-7 and FG-9 can be obtained from Figure 49 which is a plot of pressure drop divided by mass flow rate, squared. Operational amplifier 25 together with its associated circuits completes the components required to represent equation (34). The value of the feedback capacitor represents $\oint \frac{dx}{gA(x)}$.

Time did not permit tabulation of all the components' values in Figure 44 nor the scale factors for the variables. The system constants and variables are listed in Tables 12.3.1 and 12.3.2, respectively.

ORNL-LR-Dwg. 6105

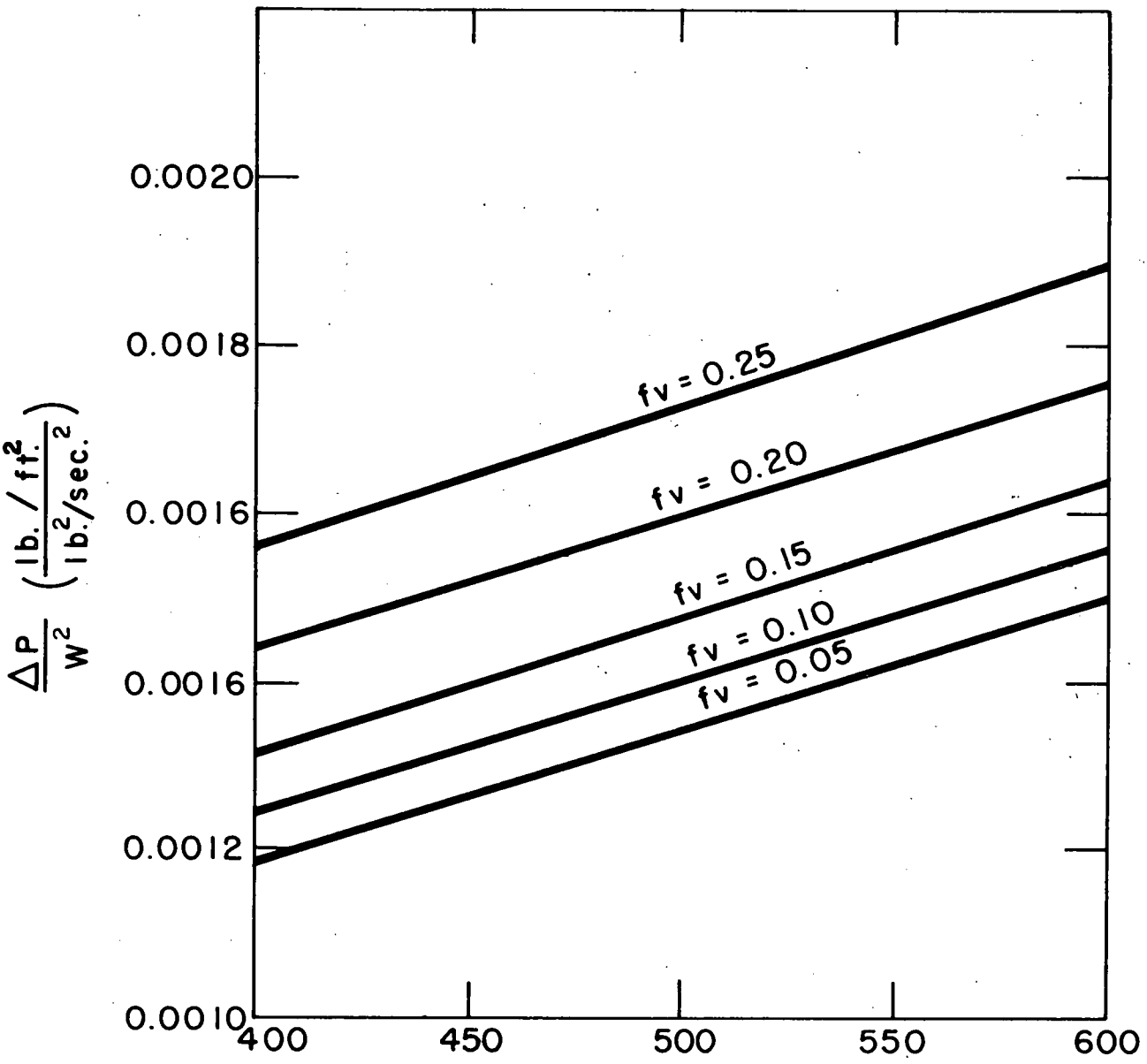

CURVE FOR FUNCTION GENERATORS NO. 7 AND 9

Figure 49

TABLE 12.3.1: SYSTEM CONSTANTS

Constant	Value
A_F	324 ft^2
A	3.34 ft^2
A_1	3.34 ft^2
A_2	3.34 ft^2
A_{pv}	80 ft^2
A_{SM}	40 ft^2
C_f	1 Btu/lb-°F
C_F	0.10 Btu/lb-°F
C_{pv}	0.12 Btu/lb-°F
C_{SM}	0.12 Btu/lb-°F
D_2	7 Btu/°F-ft^3
D_3	0.0077 lb/ft^3-°F
D_4	10.25 ft^3/sec
D_5	1041 Btu ft^3/sec-lb
h_{pv}	0.22 Btu/°F-ft^2-sec
h_{SM}	0.55 Btu/°F-ft^2-sec
M_{pv}	10,000 lb
M_{SM}	1600 lb
V_F	0.8529 ft^2
V_{SC}	48.5 ft^3
Z	23.25 in.
Z_1	3.7 ft
ρ_F	505 lbs/ft^3
$\oint \frac{dx}{gA(x)}$	0.078 sec^2/ft^2

TABLE 12.3.2: SYSTEM VARIABLES

Variable	Value at Design Condition
$\bar{f}_v$	0.20
f_{v2}	0.40
h_b	4.17 Btu/°F-ft^2-sec (1.5×10^4 Btu/°F-ft^2-hr)
M_d	5875 lbs
P	9480 Btu/sec
P_o	9480 Btu/sec
Q	9480 Btu/sec
T_f	446.5°F
T_{f1}	445°F
T_{f2}	448°F
T_{fd}	445°F
T_F	453.5°F
T_{pv}	445°F
T_S	448°F
T_{SM}	448°F
U_2	7.75 Ft/sec
W	793 lbs/sec
W_T	9.33 lbs/sec
$\bar{X}$	1.0
$\bar{\rho}$	41.4 lbs/ft^3
ρ_2	31.3 lbs/ft^3
ρ_f	51.5 lbs/ft^3
ρ_{f1}	51.5 lbs/ft^3
ρ_{f2}	51.5 lbs/ft^3
ρ_{fd}	51.5 lbs/ft^3
ρ_g	0.91 lbs/ft^3

12.4 APPENDIX D: CORE HEAT TRANSFER AND HYDRODYNAMIC CALCULATIONS

12.4.1 Nomenclature

A_1 - downcomer cross-sectional area at top

A_2 - core cross-sectional area at top

h_{fg} - latent heat of vaporization

h_x - enthalpy required to raise make-up to saturation

K - flow loss coefficient

P - average power density

$P_{(Z)}$ - axial power distribution

a - half width of core in x direction

b - half width of core in y direction

z - height in axial direction

Z - height of reactor core

Z_1 - height of riser above core

U_1 - velocity at A_1

U_2 - velocity at A_2

U_{fg} - specific volume change in evaporation

ρ_1 - density at top of downcomer

ρ_2 - density at top of core

ρ_i - average density of core

ρ_o - average density of downcomer

$\bar{\rho}$ - average density of system

ρ - variable core density

ΔP_{SEP} - flow losses in steam separator

X - steam fraction by weight

$\bar{v}$ - average specific volume

v_f - specific volume of liquid

v_{fg} - specific volume change from liquid to vapor

v_g - specific volume of vapor

VF - volumetric foid fraction in core

Z_1' - height of exit neck on fuel element

RCR - recirculation ratio

W - weight flow

W_T - total weight flow through core

F_D - drag force

F_A - accelerating force

C - drag coefficient for spheres

g - acceleration of gravity

d - estimated bubble diameter

V - velocity of coolant

V_1 - velocity at core entrance

V_2 - velocity at core exit

t - time variable

RR - steam release rate

r_1 - acceleration loss coefficient (fog-type flow)

r_2 - acceleration loss coefficient (separated flow)

k - variable core friction coefficient in two phase flow

$\mathcal{dl}$ - function of reactor power

A_c - Core flow area

A_e - Single fuel element flow area

Power distribution assumed such that

$$P(Z) = C \sin \pi Z'$$

$$Z' = \frac{z + 0.125Z}{1.25Z} \qquad 0 < z < Z$$

(This assumes flux as central 80% of cosine distribution.. see derivation for natural circulation)

12.4.2 Boiling Hetrogeneous Natural Circulation System

Postulates

1. Reactor core is rectangular. In the core the fluid flows down through an annular downcomer region to the bottom of the reactor core, reverses, and flows through the central riser region to the top of the reactor core.

2. At the center of the downcomer the average fluid velocity normal to the annular cross sectional area A_1 is U_1. At the top of the core the average fluid velocity normal to the central cross sectional area A_2 is U_2. All the circulating fluid passes through A_1 and A_2 respectively.

3. As the fluid flows from A_2 to A_1, a complete vapor separation is effected and an equal mass rate of unsaturated $(h_{sat} - h_x)$ liquid is added so that the average density of the fluid increases from ρ_2 to ρ_1.

4. In the core this unsaturated liquid becomes saturated at a rate proportional to the power density.

5. The circulation velocities are sufficiently greater than the vapor velocities relative to the liquid that the fluid may be considered homogeneous.

6. The core and downcomer have uniform cross sectional areas.

7. Steam separation is complete and there is no vapor entrainment in the downcomer.

Sketch of System:

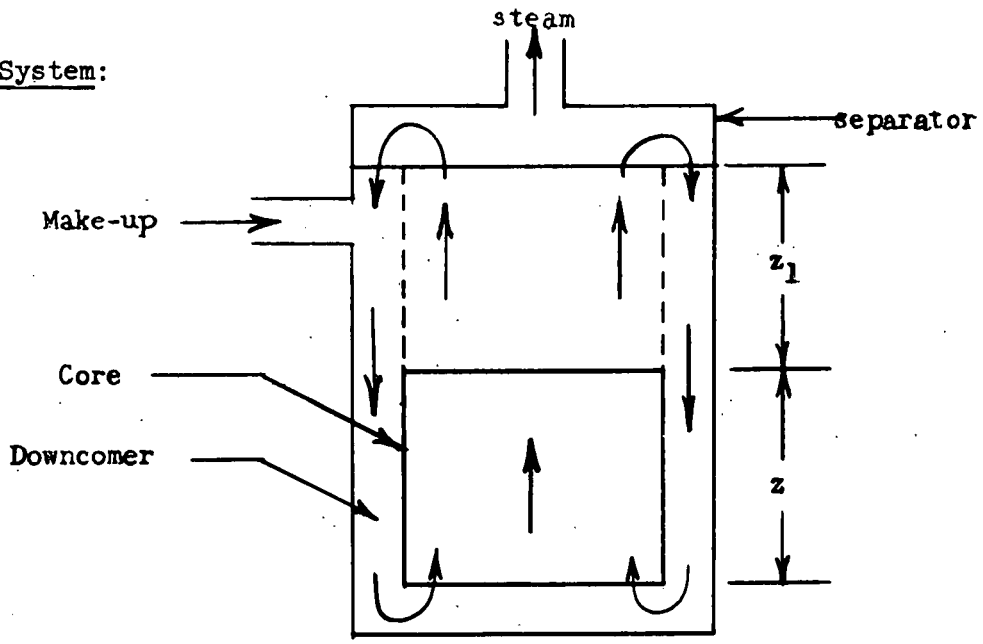

Conservation of mass requires that:

$$U_1 A_1 \rho_1 = U_2 A_2 \rho_2$$

Volumetric balance requires that:

$$U_1 A_1 - U_2 A_2 + \frac{P A_2 Z}{h_{fg} + h_x} \frac{U_{fg}}{} = 0$$

Combining to eliminate A_1 and solving for P:

$$P = \frac{U_2 (h_{fg} + h_x)}{Z\, U_{fg}} \left\{ 1 - \frac{\rho_2}{\rho_1} \right\}$$

The natural circulation can be coupled to the density by equating the difference between the buoyant forces of the downcomer and the riser to the flow losses:

$$Z\,(\rho_o - \rho_i) + Z_1\,(\rho_1 - \rho_2) = \bar{\rho} K \frac{U_2^2}{2g} + \Delta P_{SEP}$$

$$U_2 = \left[\frac{2g}{\bar{\rho} K} \left\{ Z\,(\rho_o - \rho_i) + Z_1\,(\rho_1 - \rho_2) - \Delta P_{SEP} \right\} \right]^{1/2}$$

For a given system the turning, friction, and acceleration losses all depend, in first approximation, on the product of the density and square of the velocity. A more elaborate evaluation of the kind given by Martinelli is used to help establish a reasonable value for K. See page 699, $K = \frac{r_2}{vI} + K_{friction}$.

Postulate

8. The mass rate of vapor formation at any point is directly proportional to the neutron flux. A cosine distribution is assumed such that

$$P_{(Z)} = C \sin \pi Z^1$$

where

$$Z^1 = \frac{z + 0.125Z}{1.25Z} \qquad 0 < z < Z$$

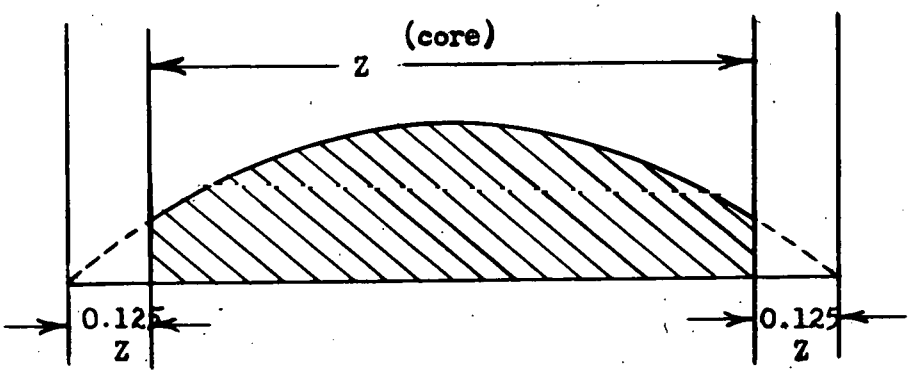

Limits of Integration:

$$Z^1_1 = \frac{0 + 0.125Z}{1.25Z} = 0.1$$

$$Z^1_2 = \frac{1.125Z}{1.25Z} = 0.9$$

$$dz = (1.25Z)\, dZ^1$$

For a differential height of core and writing a volumetric balance for this element:

$$\frac{d(A_2U)}{dz} = \frac{P(Z)A_2U_{fg}}{h_{fg} + h_x}$$

Conservation of mass requires that:

$$UA_2\rho - U_2A_2\rho_2 = 0$$

$$d(UA_2) = -\frac{U_2A_2\rho_2}{\rho_2} \, d\rho$$

$$U_2A_2\rho_2 \int_{\rho_2}^{\rho} \frac{d\rho}{\rho^2} = -C\ 1.25\ Z\ U_{fg}A_2 \int_{0.9}^{Z^1} \sin \pi Z^1 \, dZ^1$$

where $C = \dfrac{\text{average radial heat flux at maximum axial position}}{(h_{fg} + h_x)}$

$$U_2A_2\rho_2\left(\frac{1}{\rho_2} - \frac{1}{\rho}\right) = + \frac{C\ 1.25Z\ U_{fg}A_2}{\pi} \ (0.951 + \cos \pi Z^1)$$

$$P = \frac{C(h_{fg} + h_x)}{Z} \int_{0.9}^{0.1} \sin \pi Z^1 \ dZ^1 \ (1.25Z)$$

$$P = \frac{C(h_{fg} + h_x) \ (1.25) \ (1.902)}{\pi} = C(h_{fg} + h_x) \ (0.757)$$

$$C = \frac{P}{(h_{fg} + h_x)\ 0.757}$$

$$U_2A_2\rho_2\left(\frac{1}{\rho_2} - \frac{1}{\rho}\right) = \frac{P(1.25Z)\ U_{fg}\ A_2 \ (0.951 + \cos \pi Z^1)}{(h_{fg} + h_x) \ (0.757) \ (\pi)}$$

and from previous:

$$\frac{P\ Z\ U_{fg}}{h_{fg} + h_x} = U_2 \left\{ 1 - \frac{\rho_2}{\rho_1} \right\}$$

$$U_2 A_2 \rho_2 \left(\frac{1}{\rho_2} - \frac{1}{\rho}\right) = 0.526\ A_2 U_2 \left(1 - \frac{\rho_2}{\rho_1}\right) (0.951 + \cos \pi Z^1)$$

$$\left(\frac{1}{\rho_2} - \frac{1}{\rho}\right) = \frac{0.526}{\rho_2} \left(1 - \frac{\rho_2}{\rho_1}\right) (0.951 + \cos \pi Z^1)$$

$$\frac{\rho}{\rho_2} = \frac{1}{1 - 0.526 \left(1 - \frac{\rho_2}{\rho_1}\right) (0.951 + \cos \pi Z^1)}$$

$$\rho_i = \frac{1.25Z}{Z} \int_{0.1}^{0.9} \frac{\rho_2}{1 - 0.526 \left[1 - \frac{\rho_2}{\rho_1}\right] (0.951 + \cos \pi Z^1)}\ dZ$$

$$\simeq \frac{1.25\ \rho_2\ (0.800)^*}{\left[1 - (1.902)\ (0.526)\ \left(1 - \frac{\rho_2}{\rho_1}\right) - 0.0956 \left\{0.519 \left(1 - \frac{\rho_2}{\rho_1}\right)\right\}^2\right]^{1/2}}$$

$$\rho_i \simeq \frac{1.00\ \rho_2}{\left[1 - 0.987 \left(1 - \frac{\rho_2}{\rho_1}\right)\right]^{1/2}}$$

$$\rho_o = \rho_i = \text{Constant}$$

This assumes no heat transfer in down comer

$$\bar{\rho} = \frac{1}{2} \left(\rho_1 + \frac{1.00\ \rho_2}{\left[1 - 0.987 \left(1 - \frac{\rho_2}{\rho_1}\right)\right]^{1/2}} \right)$$

---

* In order to reduce this integral to a usuable form, it was necessary to assume in the first approximation that $\frac{\rho_2}{\rho_1} = 0.65$. This is the equivalent of about 0.945 wt. % steam at the core exit(35.5% by volume).

Combining previous equations:

$$P = \left(\frac{2gZ}{K\rho Z^2}\right)^{1/2} \left[(\rho_o - \rho_i) + \frac{Z}{Z}_1 (\rho_1 - \rho_2) - \frac{\Delta P_{SEP}}{Z}\right]^{1/2} \frac{(h_{fg} + h_x)}{U_{fg}} \left\{1 - \frac{\rho_2}{\rho_1}\right\}$$

$$\frac{PU_{fg}}{h_{fg} + h_x}\left(\frac{KZ}{2g}\right)^{1/2} = \left\{1 - \frac{\rho_2}{\rho_1}\right\} \left(\frac{\rho_1}{\rho}\right)^{1/2} \left[\left\{1 - \frac{1.00\ \rho_2/\rho_1}{\left[1\text{-}0987\ (1-\frac{\rho_2}{\rho_1}\right]^{1/2}}\right\} + \frac{Z_1}{Z}\left(1 - \frac{\rho_2}{\rho_1}\right) - \frac{\Delta P_{SEP}}{Z\rho_1}\right]^{1/2}$$

Rewriting:

$$\left(\frac{PU_{fg}}{h_{fg} + h_x}\right)\left(\frac{KZ}{2g}\right)^{1/2} = \left(1 - \frac{\rho_2}{\rho_1}\right)\left(\frac{\rho_1}{\rho}\right)^{1/2} \left[\left\{1 - \frac{1.00\ \rho_2/\rho_1}{\left[1\text{-}0.987\ (1-\frac{\rho_2}{\rho_1})\right]^{1/2}}\right\} + \frac{Z_1}{Z}\left(1 - \frac{\rho_2}{\rho_1}\right) - \frac{\Delta P_{SEP}}{Z\rho_1}\right]^{1/2}$$

12.4.3 Calculation of Bubble Slip Velocities

In order to justify the assumption of homogeneous flow a simple calculation was made to determine the magnitude of slip velocities we might expect.

Drag force = $F_D = \frac{C\pi}{g}\ \frac{d^2}{\delta}\ \rho_f\ (V_g - V_f)^2$

where C = drag coefficient for spheres - see Chemical Engineers Handbook by Perry (1941)

Accelerating force (net bouyancy) = $F_A = \frac{\pi}{6}\ d^3\ (\rho_f - \rho_g)$

where the subscripts refer to: g = vapor bubble; f = fluid medium

$$\frac{\pi d^3}{6}(\rho_f - \rho_g) - \frac{C\pi d^2 \rho_f}{8}(V_g - V_f)^2 = \frac{W_b}{g}\frac{dV_g}{dt}$$

W_b = 1/2 mass of displaced liquid*

$$= \frac{\pi d^3}{12}\rho_f$$

$$\left[\frac{2g}{\rho_f}(\rho_f - \rho_g) - \frac{3}{2}\frac{C}{d}\frac{\rho_g}{\rho_f}V_f^2\right] - \left[\frac{3}{2}\frac{C}{d}\frac{\rho_g}{\rho_f}\right]V_g^2 + \left[\frac{3}{2}\frac{C}{d}\frac{\rho_g}{\rho_f}\right](2V_gV_f)$$

$$= \frac{dV_g}{dt}$$

$$b - aV_g^2 + 2aV_fV_g = \frac{dV_g}{dt}$$

$$\frac{dV_g}{dt} = -aV_g^2 + kV_g + b$$

$$a = 3/2\ \frac{C}{d}$$

$$b = 2g\left(1 - \frac{\rho_g}{\rho_f}\right) - 3/2\ \frac{C}{d}V_f^2$$

$$k = 3\frac{C}{d}V_f$$

This can be written as

$$t = \int \frac{dV_g}{-aV_g^2 + kV_g + b} + C$$

Using the boundary condition that when t = o $V_g = V_f$

and integrating we get:

$$t = \frac{1}{\sqrt{4ab + k^2}}\left[\ln\frac{(k - 2aV_g - \sqrt{4ab + k^2})(k - 2aV_f + \sqrt{4ab + k^2})}{(k - 2aV_g + \sqrt{4ab + k^2})(k - 2aV_f - \sqrt{4ab + k^2})}\right]$$

* According to Lamb (Hydrodynamics) the inertia mass of a bubble moving through a fluid is 1/2 mass of displaced fluid in the range 20-30% steam void.

This can be reduced and rearranged to the form:

$$(V_g - V_f) = \frac{\left[\frac{b}{a} + V_f^2\right]^{1/2} \left[e^2 \left(\frac{b}{a} + V_f^2\right)^{1/2} at - 1\right]}{e^2 \left(\frac{b}{a} + V_f^2\right)^{1/2} at + 1}$$

where $(V_g - V_f)$ = slip velocity

or substituting for a and b

$$(V_g - V_f) = \frac{\left[\frac{4dg(\rho_f - \rho_g)}{3C\rho_f}\right]^{1/2} \left[e^{\left\{\frac{12\,Cg}{d}\left(1 - \frac{\rho_g}{\rho_f}\right)\right\}^{1/2} t} - 1\right]}{e^{\left\{\frac{12\,Cg}{d}\left(1 - \frac{\rho_g}{\rho_f}\right)\right\}^{1/2} t} + 1}$$

Using C = 0.44 $(N_R > 500)$

$d \leq 0.44" = 0.0367$ ft

$\rho_f = 51.6$ #/ft^3

$\rho_g = 0.893$ #/ft^3

(See Perry, Chemical Engineers Handbook, 1941)

$$(V_g - V_f) = \frac{1.88\,(e^{4560t} - 1)}{e^{4560t} + 1}$$ which indicates an instantaneous velocity increase of about 1.4 ft/sec over the fluid velocity.

It has been assumed in this calculation that the effect of wall friction on the bubbles is negligible. In order to calculate for the worst condition, a maximum permissable (by plate spacing) bubble diameter was assumed. By comparison with the calculated fluid velocities through the core, the assumption of homogeneous flow is not too bad, (i.e., for a fluid velocity of 6 ft/sec, the maximum slip velocity will be only 31%).

12.4.4 Recirculation Ratio as Function of Voids

$$\frac{1}{RCR} = \frac{\#steam/hr}{\#water/hr}$$

$$= \frac{\dfrac{PA_2Z}{h_{fg} + h_x}}{\rho_2 A_2 U_2 - \dfrac{PA_2Z}{h_{fg} + h_x}}$$

$$\frac{1}{RCR} = \frac{1}{\dfrac{\rho_2 U_2 (h_{fg} + h_x)}{PZ} - 1}$$

and

$$P = \frac{U_2(h_{fg} + h_x)}{Z\, V_{fg}} \left\{ 1 - \frac{\rho_2}{\rho_1} \right\}$$

$$\frac{U_2(h_{fg} + h_x)}{PZ} = \frac{V_{fg}}{\left\{ 1 - \dfrac{\rho_2}{\rho_1} \right\}}$$

$$\frac{1}{RCR} = \frac{1}{\dfrac{\alpha V_{fg}}{(1 - \rho_2)\,\rho_1}} - 1$$

$$RCR = \frac{V_{fg}}{\left(\dfrac{1}{\rho_2} - \dfrac{1}{\rho_1}\right)} - 1$$

and

$$\rho_i = \frac{0.075\ \rho_2}{\left[1 - 1.000\ \left(1 - \dfrac{\rho_2}{\rho_1}\right)\right]^{1/2} + 0.125\ \rho_1}$$

This however is $0.875\sqrt{\rho_2\ \rho_1} + 0.125\ \rho_1$.

$$\text{then } \rho_2 = \frac{1}{\rho_1}\left[\frac{\rho_i - 0.125\ \rho_1}{0.875}\right]^2$$

$$\text{RCR} \cong \frac{V_{fg}}{\left[\left\{\frac{\rho_i - 0.125\ \rho_1}{0.875}\right\}^2 - \frac{1}{\rho_1}\right]} - 1$$

where ρ_i can be calculated from the percent steam void.

$$\frac{1}{\rho_i} = V_f + \frac{(VF)\ V_{fg}}{VF + (1 - VF)\ \frac{V_g}{V_f}}$$

12.4.5 Calculation of Variable Core Void Fraction

$$\frac{dX}{dz} = \frac{P(Z)\ A_2}{W_T\ (h_{fg} + h_x)}$$

$$\frac{dX}{dz} = \frac{C \sin \pi Z'\ A_2}{W_T\ (h_{fg} + h_x)}$$

$$dz = 1.25\ Z\ dZ'$$

when $z = 0$, $Z = 0.1$

$$X(Z) = \frac{CA_2\ (1.25Z)}{W_T\ (h_{fg} + h_x)} \int_{0.1}^{Z} \sin \pi Z'\ dZ'$$

$$X(Z) = \frac{CA_2\ (1.25Z)}{\pi W_T\ (h_{fg} + h_x)} \left[0.951 - \cos \pi Z\right] + C_1$$

when $z = 0.1$ $\quad X(z) = 0$

then $C_1 = 0$

$$X(Z) = \frac{0.398\ CA_2\ Z}{W_T\ (h_{fg} + h_x)} \left[0.951 - \cos \pi \frac{Z}{} \right] \qquad (I)$$

$$\bar{v} = v_f + X\ v_{fg} = v_f + \frac{(VF)\ v_{fg}}{VF + (1 - VF)\ \frac{v_g}{v_f}}$$

$$X = \frac{1}{1 + \left(\frac{1-VF}{VF}\right)\ \frac{v_g}{v_f}} \qquad (II)$$

By combination of Equations (I) and (II) we get the following result:

$$VF = \frac{v_g}{v_{fg} + \frac{W_T\ (h_{fg} + h_x)\ v_f}{0.398\ CA_2\ Z\ (0.951 - \cos \pi\ Z)}}$$

or

$$(VF)_Z = \frac{v_g}{v_{fg} + \frac{K_1\ v_f}{(0.951 - \cos \pi\ Z)}}$$

Assuming that the constants of the system (K_1) can be adjusted to fit any desired void fraction, we can sole directly for this unkown.

From previous work:

ρ_i = average core density $\simeq \sqrt{\rho_o\ \rho_{(Z)}}$

Assume average core void of 20%

$$\frac{1}{\rho(p)} = v_f + \frac{v_{fg}}{1 + \frac{(1-VF)}{VF}\left(\frac{v_g}{v_f}\right)}$$

$$\rho_i = 41.4 \quad \rho_o = \frac{1}{v_f} = 51.5$$

$$\rho_{(Z)} = 33.3$$

$(VF)_{Exit.} = 36\%$

at core exit Z = 0.9

Evaluating for K_1 gives 193

$$(VF)_Z = \frac{v_g}{v_{fg} + \frac{193\ v_f}{(0.951 - \cos \pi Z)}}$$

at pressure = 415 psi

$$(VF)_Z = \frac{1.1194}{1.100 + \frac{3.76}{(0.951 - \cos \pi Z)}}$$

$$(VF)_Z = \frac{1}{0.984 + \frac{3.36}{(0.951 - \cos \pi Z)}}$$

See curve of void fraction vs core distance Fig. 31.

Based on about a 4 ° temperature through the external loop it is estimated that no boiling will occur in the lower 1/8 of the core, hence:

$$X(Z) = \frac{CA_2\ (1.25Z)}{W_T\ (h_{fg})} \int_{0.2}^{Z} \sin \pi Z'\ dZ'$$

$$X(Z) = \frac{CA_2\ (1.25Z)}{\pi\ W_T\ (h_{fg})} \left[0.809 - \cos \pi Z\right] + C_1$$

$$C_1 = 0$$

$$(VF)_Z = \frac{v_g}{\frac{K_1}{v_{fg}} + \frac{v_f}{(0.809 - \cos \pi Z)}}$$

$$P = \frac{C\ h_{fg}}{Z} \int_{0.9}^{0.2} \sin \pi Z'\ dZ'\ (1.25Z)$$

$$C = \frac{P}{0.70\ h_{fg}}$$

$$U_2 A_2 \rho_2 \left(\frac{1}{\rho_2} - \frac{1}{\rho}\right) = 0.569\, A_2 U_2^2 \left(1 - \frac{\rho_2}{\rho_1}\right)(0.951 + \cos \pi Z)$$

$$\frac{\rho}{\rho_2} = \frac{1}{1 - 0.569\left(1 - \frac{\rho_2}{\rho_1}\right)(0.951 + \cos \pi Z')}$$

$$\rho_i = \frac{1.25Z \int_{0.2}^{0.9} \frac{\rho_2 \, dZ'}{1 - 0.569\left(1 - \frac{\rho_2}{\rho_1}\right)(0.951 + \cos \pi Z')} + \rho_1 \int_0^{0.125Z} dz}{Z}$$

$$\rho_i \simeq \frac{\frac{0.875\, \rho_{2z}}{\left[1 - 1.00\left(1 - \frac{\rho_2}{\rho_1}\right)\right]^{1/2}} + 0.125\, \rho_1}{Z}$$

$$\rho_i \simeq 0.875 \sqrt{\rho_2 \rho_1} + 0.125\, \rho_1$$

Again assume average VF = 20%

$$\rho_i = 41.4 \quad \rho_1 = \frac{1}{v_f} = 51.5$$

$$\rho_2 = 31.1$$

$$(VF)_{Exit} = 40.1\ \%$$

Recalculation of K_1 gives 153

$$(VF)_Z = \frac{1}{0.984 + \frac{2.66}{(0.809 - \cos \pi Z')}}$$

$$(0.2 < Z < 0.9)$$

$$VF = 0 \quad (0.1 < Z < 0.2)$$

See dotted curve in Fig. 31.

12.4.6 Calculation of Height of Riser Required for Natural Circulation

Assuming that only 7/8 of the core is boiling we can rewrite the original natural circulation calculation s where:

$$\rho_o = \rho_1$$

$$\rho_i = 0.875\sqrt{\rho_2 \rho_1} + 0.125\,\rho_1 \text{ (see previous work)}$$

$$\bar{\rho} = 1/2\left[1.125\,\rho_1 + 0.875\sqrt{\rho_2 \rho_1}\right]$$

Then combining with original equations and setting $\Delta P_{SEP} = 0$

$$\left(\frac{P\ v_{fg}}{h_{fg} + h_x}\right)\left(\frac{KZ}{2g}\right)^{1/2} = \left(1 - \frac{\rho_2}{\rho_1}\right)\left(\frac{\rho_1}{\bar{\rho}}\right)^{1/2}\left[0.875\left(1 - \sqrt{\frac{\rho_2}{\rho_1}}\right) + \frac{Z_1}{Z}\left(1 - \frac{\rho_2}{\rho_1}\right)\right]^{1/2}$$

$P = 1420 \frac{\text{Btu}}{\text{sec-ft}^3}$ $\qquad$ $v_{fg} = 1.100$

$2g = 64.4$ $\qquad$ $\rho_2 = 31.1$ (average 20% steam void)

$Z = 1.94$ ft $\qquad$ $\bar{\rho} = 46.50$

$h_{fg} + h_x = 1014$ $\qquad$ $\rho_1 = 51.5$

By substituting in the above conditions:

$$K = 0.470 + 0.475\ Z_1$$

$$Z_1 = \frac{K - 0.470}{0.475}$$

Since we expect to have a 1/2 ft extension on the fuel element, the actual height of riser $Z_A = Z_1 - 1/2$. This indicated riser height was plotted.

For $\Delta P = 95.0$ #/ft^2 (see pressure drop calculations)

$$\Delta P = \frac{K \bar{\rho} U_2^2}{2g}$$

$$K = \frac{(95.0)\ (64.4)}{(7.69)^2 (46.5)} = 2.23$$

This is an apparent height of riser about 3.7 ft

12.4.7 Pressure Drop Calculations (see Fig. 50)

Position	Area (Ft^2)	Velocity(Ft/sec)	Friction Factor	K(entering)
Riser	4.0	5.50 (mixture)	------	0.180
Pressure Vessel	12.0	$\approx$ 0	------	1.25
Downcomer	8.6	1.81	0.0125	0.08
180° Turn	7.5	2.06	------	1.50
Entrance	4.0	3.90	------	0.05
Entrance Neck	2.51	6.2	------	0.142
Core	3.3355	4.65(Entrance) 5.78(Average) 7.69 (Exit)	$\left\{\begin{array}{l}(K=0.7)\ (f=0.013)\\ \frac{\Delta P_{TPF}}{\Delta P_o} = 2.0\end{array}\right.$	0.06
Exit Neck	2.51	9.8(Mixture)	------	0.08

Core Pressure Losses:

$$\Delta P \text{ (acceleration)} = \frac{r_2 G^2}{g} = \frac{(.016)\ (0.859 \times 10^6)^2}{(4.17 \times 10^8)} = 28.3 lb/ft^2$$

$$\Delta P \text{ (Friction)} = \frac{\Delta P_{TPF}}{\Delta P_o} \frac{K \rho_f v_f^2}{2g} = \frac{(2.0)\ (0.7)\ (51.5)\ (4.65)^2}{64.4} = 23.1$$

$$\Delta P \text{ (Core-exit neck)} = \frac{K \rho_m v_m^2}{2g} = \frac{(0.08)\ (31.1)\ (9.8)^2}{64.4} = 3.7$$

ORNL-LR-Dwg. 6106

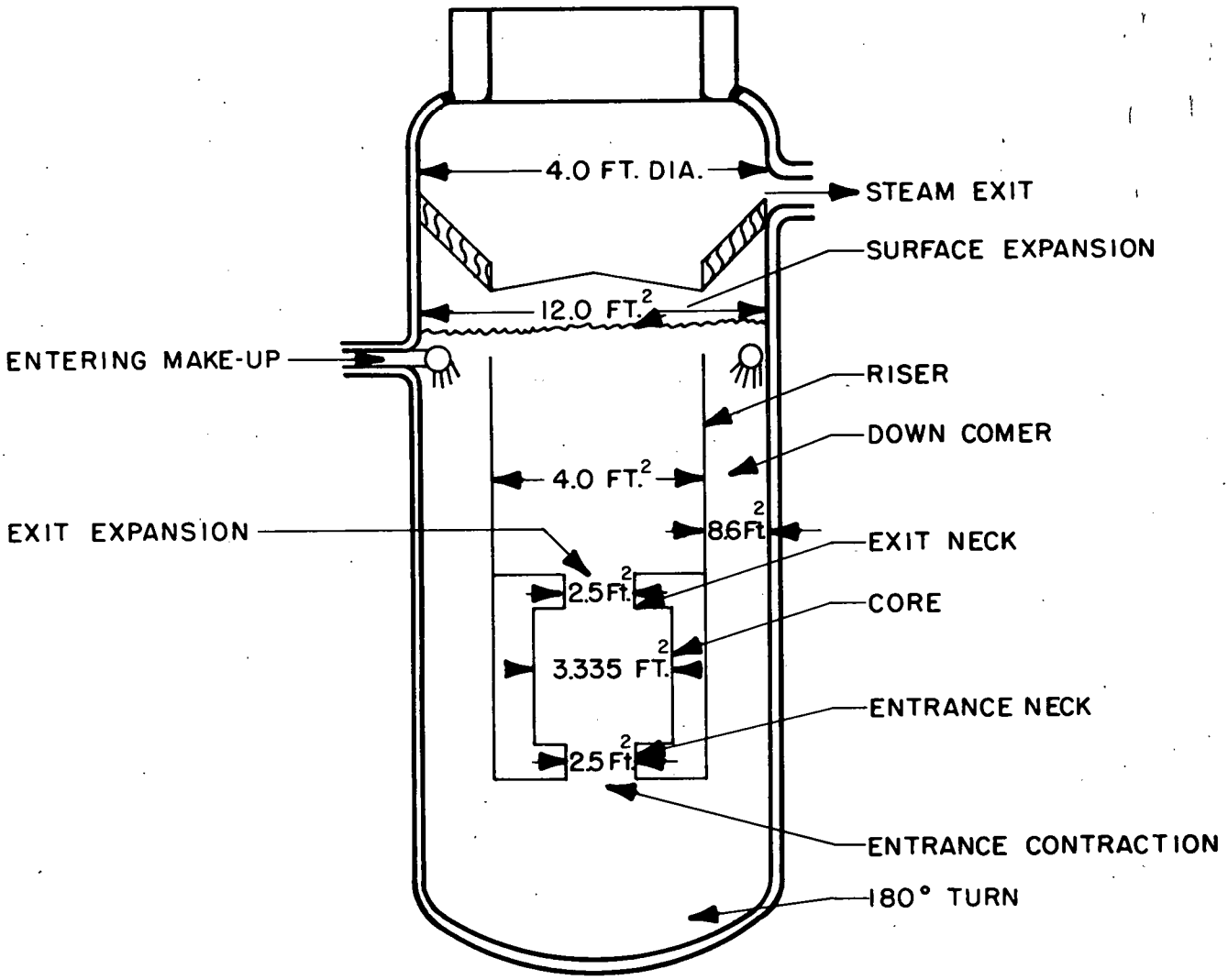

PRESSURE DROP CALCULATIONS INSIDE PRESSURE VESSEL

Figure 50

$$\Delta P \text{ (exit neck-riser)} = \frac{K\rho_m V_m^2}{2g} = \frac{(0.180)\ (31.1)\ (5.50)^2}{64.4} = 8.4$$

$$\Delta P \text{ (riser-pressure vessel)} = \frac{K\rho_m V_m^2}{2g} = \frac{(1.25)\ (31.1)\ (5.50)^2}{64.4} = 18.2$$

$$\Delta P \text{ (pressure vessel-downcomer)} = \frac{K\rho_f V_f^2}{2g} = \frac{(0.08)(51.5)(1.81)^2}{64.4} = 0.22$$

$$\Delta P \text{ (friction in downcomer)} = \frac{f\rho_f V_f^2}{2g} = \frac{(0.0125)(51.5)(1.81)^2}{64.4} = 0.03$$

$$\Delta P \text{ (180° turn)} = \frac{K\rho_f V_f^2}{2g} = \frac{(1.50)(51.5)(3.9)^2}{64.4} = 5.0$$

$$\Delta P \text{ (entrance)} = \frac{K\rho_f V_f^2}{2g} = \frac{(0.05)(51.5)(3.9)^2}{64.4} = 0.61 \text{ lb/ft}^2$$

$$\Delta P \text{ (entrance-entrance neck)} = \frac{K\rho_f V_f^2}{2g} = \frac{(0.142)(51.5)(6.2)^2}{64.4} = 4.4$$

$$\Delta P \text{ (entrance neck-core)} = \frac{K\rho_f V_f^2}{2g} = \frac{(0.06)(51.5)(6.2)^2}{64.4} = 2.1$$

TOTAL HEAD LOSS 95.0 lb/ft^2

12.4.8 Evaluation of Liquid-Steam Separation at Liquid Interface

Maximum permissable steam release rate is given as function of saturation pressure by reference 14; it is included in this report in graphical form. For the design pressure of 415 psi, this maximum release rate $\sim$ 2200 lb/ft^2-hr.

$$R\ R = \frac{\text{lb steam/hr}}{\text{Liquid surface area}} = \frac{33{,}710}{12.2}$$

$$= 2750 \text{ lb/hr-ft}^2$$

Obviously this is well above the maximum permissable release rate; however, with a low velocity in the downcomer, countercurrent vapor flow is expected to eliminate the vapor entrainment problem.

12.4.9 Calculation of Conditions Necessary for Vapor Lock and Restriction of Flow Leading to Unstable Operation

Analysis for a system that has many parellel channels is complicated by the fact that mixing can occur in the vertical riser and by the two types of flow possible. At low steam voids, the flow is essentially a two-phase separated condition. As higher steam voids are reached one approaches the condition of homogeneous-fog flow. As a result of these conditions, calculations were limited to certain simplifying postulates.

Model 1. (1) The entire system is considered, and all calculations are based on average values. (2) Power is assumed to be constant throughout the reactor core. (3) Coolant flow is postulated to be homogeneous and a two-phase separated condition. As such, the acceleration pressure drop term is that function defined by r_2 in the pressure drop notes by Martinelli & Nelson. (see Ref. 2) (4.) No vapor entrainment in the downcomer.

Friction outside the core can be separated into two parts:

$$\Delta p_1 = \frac{K_1 \rho_f V_f^2}{2g} \quad ; \quad \Delta P_2 = \frac{K_2 \rho_2 V_2^2}{2g}$$

One is a function only of liquid properties, the other a function of mixture properties, each applying in a specific region. The loss coefficients for the two functions were determined from individual pressure drop calculations.

Pressure balance:

$$0 = \Delta P + \frac{\rho V^2}{2g} + \rho Z + \text{Friction}$$

$$\Delta P = \text{Constant} = \text{Available head} = \rho_f (Z_1 + Z)$$

$$\frac{\rho V^2}{2g} = \text{Acceleration losses (Core only)} = \frac{r_2 W^2}{g A_c^2}$$ (See Martinelli & Nelson's Method for Two-Phase Flow)

$$\rho Z = \text{Variable density head in core, neck, and riser} = \rho_i Z + \rho_2 Z_1$$

Friction losses , Core Friction . $\Delta P_1 + \Delta P_2$

$$= \frac{k_2 \rho_f V_f^2}{2g} + \frac{K_1 \rho_f V_f^2}{2g} + \frac{K_2 \rho_2 V_2^2}{2g}$$

where k_2 can be predicted from method introduced by Martinelli & Nelson

$$V_f^2 = \frac{W^2}{\rho_f^2 A_c^2} \qquad V_2^2 = \frac{W^2}{\rho_2^2 A_c^2}$$

and from previous work:

$$\rho_i = .975 \sqrt{\rho_2 \rho_f} + .125 \rho_f$$

(This is based on a cosine power distribution and boiling only in 7/8 of the axial core length.)

$$\rho_f (Z_1 + Z) = .875 \sqrt{\rho_2 \rho_f}\, Z + .125 \rho_f Z + \rho_2 Z_1 + \frac{W^2}{2gA_c^2}\left[\frac{k+K_1}{\rho_f} + \frac{K_2}{\rho_2} + 2r_2\right]$$

$$\frac{W^2}{2gA_c^2} = \frac{\left[\rho_f(Z_1 + Z) - Z\left\{.875\,(\rho_2 \rho_f)^{1/2} + .125\,\rho_f\right\} - Z\rho_2\right]}{\left[\frac{K + K_1}{\rho_f} + \frac{K_2}{\rho_2} + \frac{2r_2}{}\right]}$$

k and r_2 can be found from curves by Martinelli and Nelson as functions of the exit quality (and density):

$$r_2 \simeq \frac{.50}{\rho_2} \qquad k \simeq \frac{28.0}{\rho_2} + .50$$

substituting these and $\rho_f = 51.5$ lb/ft^3 gives:

$$\frac{W^2}{2gA_c^2} = \frac{\left[\rho_f(Z_1 + Z) - Z\left\{.875\,(\rho_2 \rho_f)^{1/2} + 6.44\right\} - Z_1\rho_2\right]}{\left[\frac{1.543 + K_2}{\rho_2} + \frac{K_1}{\rho_f} + .0097\right]}$$

Taking a volumetric balance over the core:

$$V_2A_2 - V_1A_1 = \frac{PAZ_{vfg}}{H_{fg} + H_x} \qquad \text{and} \quad \rho_2A_2V_2 = \rho_1A_1V_1$$

then $$\rho_2 = \frac{1}{\frac{1}{\rho_f} + \frac{PAZ_{fg}}{W(h_{fg} + h_x)}} = \frac{1}{\frac{1}{\rho_f} + \frac{\mathcal{H}}{W}}$$

For this particular system:

$K_1 = 1.22$ $\qquad$ $K_2 = .78$

$Z = 2$ feet $\qquad$ $Z_1 = 3.7$ feet

$A_c^2 = 11.12$ ft^4 $\qquad$ $2g = 8.34 \times 10^8$

W (Design average) $= 2.865 \times 10^6$ lb/hr

$\mathcal{H}$ (Design average) $= 3.7 \times 10^4$

Substitution of these values reduces the equation to:

$$\frac{W^2}{.928 \times 10^{10}} = \frac{\left[280.62 - \left(\frac{157.5}{.0194 + \frac{\mathcal{H}}{W}}\right)^{1/2} - \left(\frac{3.7}{.0194 + \frac{\mathcal{H}}{W}}\right)\right]}{\left[\frac{\mathcal{H}}{W}(2.323) + .0785\right]}$$

A plot of this equation is included as Fig. 32.

Since the first model merely gives an indication of the average response of the reactor, a second model was postulated so that, over a limited power range, we can obtain some idea of the response of a single fuel tube.

Model 2. (1) It is assumed that only one tube is varying in power and that the average outlet density is not effected by the change in power of this one tube. (2) Due to mixing in the riser, the pressure drop across the core will be assumed constant. (3) Changes in tube power output will be reflected in coolant density of the tube and the 1/2-foot exit neck of that tube. (4) Since there are 49 fuel tubes, a change in weight flow through only one or two tubes will have little effect on downcomer weight flow and flow losses in this region. Consequently, only the weight flow through the element under consideration will be considered as variable. The flow in the remainder of the system is taken as 2.865×10^6 lb/hr (average design).

As previously:

$$\Delta P = \rho_f (Z_1 + Z)$$

$$\text{Acceleration Losses} = \frac{r_2 \; W^2}{g A_e^2}$$

$$\rho_Z = \rho_i Z + \rho_2 Z_1' + 99.5 \text{ (constant riser head)}$$

Friction Losses = Core Friction + Constant Circulating Losses + Entering Losses + Exit Losses

$$= \frac{k \rho_f V_f^2}{2g} + 24.06 + \frac{K_1 \rho_f V_f^2}{2g} + \frac{K_2 \rho_2 V_2^2}{2g}$$

Again assume $\rho_i = .875 \sqrt{\rho_2 \rho_f} + .125 \rho_f$

Summing Up:

$$\rho_f (Z_1 + Z) = \frac{W^2}{2 g A_e^2} \left[\frac{K + K_1}{\rho_f} + \frac{K_2}{\rho_2} + 2 r_2 \right] + 24.06 + \rho_2 Z_1'$$

$$+ (.875 \sqrt{\rho_2 \rho_f} + .125 \rho_f) Z + 99.5$$

As before:

$$\rho_2 = \frac{1}{\frac{1}{\rho_f} + \frac{\alpha}{W}}$$

from pressure drop calculations: $K_1 = 0.376$

$K_2 = 0.424$

$\rho_f = 51.5$

$Z = 2$ feet

$Z_1 = 3.7$ feet

$Z_1' = 0.5$ feet

$2gA_e^2 = 3.86 \times 10^6$

$$\frac{W^2}{3.86 \times 10^6} = \frac{\left[157.1 - \left(\frac{157.5}{\frac{1}{\rho_f} + \frac{\mathcal{H}}{W}}\right)^{1/2} - \left(\frac{.50}{\frac{1}{\rho_f} + \frac{\mathcal{L}}{W}}\right)\right]}{\left[\frac{1.967\,\mathcal{H}}{W} + .0552\right]}$$

W (Design average) $= 5.85 \times 10^4$ lb/hr

$\mathcal{H}$ (Design average) $= 7.55 \times 10^2$

A plot of this equation is included as Fig. 33.

This, however, is a somewhat simplified picture of the pressure drop phenomena. Actually, as the weight flow is increased, with power and coolant inlet temperature held constant, a point is reached where no net steam generation occurs, and the pressure drop reduces drastically to that calculated by 100% liquid flow.

Hydrodynamic instability is a result of there being two or more operating conditions for a given head. This dual condition would lie between the 100% steam curve and the 100% liquid curve. Its occurance would be noted by a peaking of the pressure drop curve, brought about by the phenomena described above.

Probably the best method of predicting where the point of no net steam generation will lie is to make a thermodynamic heat balance on the flow. This postulates that when less than the amount of heat needed to saturate the coolant is given off by a heating tube, no net steam generation is possible. Although the method is crude, there appears to be little choice in its use, since experimental data is lacking.

The amount of sub-cooling of the coolant is simply the average of the circulating saturated water and the sub-cooled make-up water. The make-up enters the core about 238 btu/lb subcooled and should be weighted by the recirculation ratio in order to average it with the saturated water.

$$W_{critical} = \frac{Q}{\Delta h}$$

But $$Q = PAZ = \frac{\mathcal{H}(h_{fg} + h_x)}{v_{fg}} = \frac{\mathcal{H}1014}{1.10}$$

and $$\Delta h = \frac{238}{RCR}$$

$$RCR = \frac{v_{fg}}{\left(\frac{1}{\rho_2} \quad \frac{1}{\rho_f}\right)} - 1$$

combining:

$$W_{critical} = (3.88)(\mathcal{H}) \left[\frac{1.1}{\left(\frac{1}{\rho_2} - (.0194)\right)} - 1\right]$$

We can now plot curves of pressure drop vs weight flow for all powers and superpose the peaking at the critical weight flow as calculated above.

EQUATIONS FOR 100% POWER (10 megawatts)

Steam Flow: $\Delta P = \frac{3.194W^2}{2gA_e^2} + 125.8$ (Based on Martinelli & Nelson's method for two-phase flow)

Liquid Flow: $\Delta P = \frac{0.0291W^2}{2gA_e^2} + 252.3$ (Based on pressure drop loss coefficients)

Two-Phase Flow (separated: where $\mathcal{H} = 755$

$$\Delta P = \frac{W^2}{2gA_e^2}\left[\frac{1.967\mathcal{H}}{W} + .0552\right] + \left[\frac{.5}{\frac{1}{\rho_f} + \frac{\mathcal{H}}{W}}\right]\left[\frac{157.5}{\frac{1}{\rho_f} \quad \frac{\mathcal{H}}{W}}\right]^{1/2} + 136.44$$

Two-Phase Flow (homogeneous-fog type):

$$\Delta P = \frac{W^2}{2gA_e^2}\left[\frac{2.968\mathcal{H}}{W} + .0285\right] + \left[\frac{.5}{\frac{1}{\rho_f} + \frac{\mathcal{H}}{W}}\right] + \left[\frac{157.5}{\frac{1}{\rho_f} + \frac{\mathcal{H}}{W}}\right]^{1/2} + 136.44$$

A plot of the separated and homogeneous-fog type flow shows that there is very little difference between these two theories, consequently, separated two-phase flow was postulated for the remainder of the calculations.

$W_{critical} = 2.49 \times 10^5$ lb/hr

EQUATIONS FOR 50% POWER

Steam Flow: $\Delta P = \frac{3.194W^2}{2gA_e^2} + 141.3$

Liquid Flow: $\Delta P = \frac{0.0291W^2}{2gA_e^2} + 267.8$

Two-Phase Flow:

$$\Delta P = \frac{W^2}{2\,gA_e^2}\left[\frac{1.967\,\mathcal{L}}{W} + .0552\right] + \left[\frac{.5}{\frac{1}{\rho_f} + \frac{\mathcal{L}}{W}}\right]\left[\frac{157.5}{\frac{1}{\rho_f} + \frac{\mathcal{L}}{W}}\right]^{1/2} + 151.9$$

where $\mathcal{L} = 377.5$

$W_{critical} = 2.2 \times 10^5$ lb/hr

EQUATIONS FOR 25% POWER

Steam Flow: $\Delta P = \frac{3.194W^2}{2gA_e^2} + 149.6$

Liquid Flow: $\Delta P = \frac{0.0291W^2}{2gA_e^2} + 276.2$

Two Phase Flow:

$$\Delta P = \frac{W^2}{2gA_e^2} + \left[\frac{1.967\,\mathcal{L}}{W} + .0552\right] + \left[\frac{.5}{\frac{1}{\rho_f} + \frac{\mathcal{L}}{W}}\right] + \left[\frac{157.5}{\frac{1}{\rho_f} + \frac{\mathcal{L}}{W}}\right]^{1/2} + 160.3$$

where $\mathcal{L} = 189$

$W_{critical} = 1.825 \times 10^5$ lb/hr

EQUATIONS FOR 10% POWER

Steam Flow: $\Delta P = \frac{3.194W^2}{2gA_e^2} + 156.7$

Liquid Flow: $\Delta P = \frac{0.0291W^2}{2gA_e^2} + 283.3$

$$\Delta P = \frac{W^2 \mathcal{L}}{2gA_e^2}\left[\frac{1.967}{W} + .0552\right] + \left[\frac{.5}{\frac{1}{\rho_f} + \frac{\mathcal{L}}{W}}\right] + \left[\frac{157.5}{\frac{1}{\rho_f} + \frac{\mathcal{L}}{W}}\right]^{1/2} + 167.4$$

where $\mathcal{L} = 75.5$

$W_{critical} = 1.35 \times 10^5$ lb/hr

See Fig. 36 for a plot of these equations.

12.4.10 Calculation of Fuel Element Temperature Distribution

Nomenclature:

G - heat generation per unit volume

k - thermal conductivity

T - fuel plate temperature and clad temperature

x - thickness measured from midplane of fuel element

y - thickness of clad measured from edge of fuel plate

a - fuel plate half thickness

T_{max} - fuel plate center temperature

From a homogeneous flat plate with uniform heat generation, the temperature distribution is found as follows:

$$\frac{\partial^2 T}{\partial x^2} = -\frac{G}{K}$$

then:

$$\frac{\partial}{\partial x}\left(\frac{\partial T}{\partial x}\right) = -\frac{G}{k}$$

$$\frac{\partial T}{\partial x} = -\frac{G}{k}x + C_1$$

at $x = 0$, $\frac{\partial T}{\partial x} = 0$; so that $C_1 = 0$

$$\frac{\partial T}{\partial x} = - \frac{Gx}{k}$$

$$T = - \frac{Gx^2}{2k} + C_2$$

at $x = 0$, $T = T_{max}$; therefore $C_2 = T_{max}$

then the temperature distribution is:

$$T_{max} - T = \frac{Gx^2}{2k}$$

There is no heat generation in the cladding, thus:

$$Ga = - k \frac{\partial T}{\partial y}$$

thus:

$$\frac{\partial T}{\partial y} = - \frac{Ga}{K}$$

$$T = - \frac{Gay}{k} + C_3$$

at $y = 0$, $T = T_{max} - \frac{Gx^2}{2k}$

thus $C_3 = T_{max} - \frac{Gx^2}{2k}$

The clad temperature distribution is:

$$T = T_{max} - \frac{Gx^2}{2k} - \frac{Gay}{K}$$

Assume a fluid temperature of 450° F and a film drop of 30° F. The clad surface temperature is then 480 ° F.

Assuming a maximum to average ratio of 4/1, the maximum ΔT across the clad is:

$$\frac{Gay}{K} = \frac{(4.0)(1.053 \times 10^5)(.005)}{(9.42)(12)} = 18.6 \ ^\circ F$$

The maximum ΔT across the meat is:

$$\frac{Ga^2}{2k} = \frac{(4.0)(1.053 \times 10^5)(.0125)}{(2.0)(9.42)(12)} = 23.3 \ ^\circ F$$

Therefore the fuel plate center temperature is:

$$T_{max} = 450 + 30 + 18.6 + 23.3 = 521.9 \ ^\circ F$$

or about 522 °F

12.4.11 Fuel Plate Stresses

Fuel plate stresses were calculated by using the formulas developed by Dr. L. G. Alexander, ORSORT, for a homogeneous plate assuming uniform heat generation in the meat and no heat generation in the clad. The expressions are as follows:

$$\sigma_{max(compressive)} = - \frac{E\alpha Q/A\, a}{2k(1-\nu)} \left[\frac{C}{a} + \frac{1}{3} \left(\frac{1}{1 + \frac{C}{a}} \right) \right]$$

$$\sigma_{max(tensile)} = \frac{E\alpha Q/A\, a}{2k(1-\nu)} \left[1 + \frac{C}{a} - \frac{1}{3} \left(\frac{1}{1 + \frac{C}{a}} \right) \right]$$

where: E - modulus of elasticity

α - coefficient of thermal expansion

Q/A - maximum heat flux in reactor

a - meat half thickness

C - clad thickness

k - thermal conductivity

ν - Poisson's ratio

The calculated stresses were:

$$\sigma_{max}(\text{compressive}) = - \frac{(30 \times 10^6)(9.8)(10^{-6})(4.0)(1.053 \times 10^5)(.0125)(.638)}{(2)(9.42)(.7)(12)}$$

$$= - 6500 \text{ psi}$$

$$\sigma_{max}(\text{tensile}) = + \frac{(30 \times 10^6)(9.8 \times 10^{-6})(4)(1.053 \times 10^5)(.0125)(1.162)}{(2)(9.42)(.7)(12)}$$

$$= 11{,}200 \text{ psi}$$

Bibliography (for section 12.4 only)

1. Zmola, P. C., et al, Power Removal from Boiling Homogeneous Reactor, TID-2013, (secret).

2. Martinelli and Nelson, Prediction of Pressure Drop during Forced Circulation Boiling of Water, Transactions of A.S.M.E., Aug. 1948, Paper No. 47-A-113.

3. Keenan and Keyes, Thermodynamic Properties of Steam

4. Brown and Marco, Introduction to Heat Transfer

5. Eshbach, Handbook of Engineering Fundamentals

6. McAdams, Heat Transmission

7. Perry, Chemical Engineers Handbook, (1941)

8. Lamb, Hydrodynamics

9. Studies in Boiling Heat Transfer, University of California, COO-24.

10. Argonne National Laboratory, Borax Reports, ANL-(Several) (Secret).

11. Hawkins, G. A., A Brief Review of the Literature on Boiling Heat Transfer

12. McAdams, W. H., Some Recent Developments in Heat Transfer

13. Heat Transfer, TID-278

14. Modern Power and Engineering, Vol. 35, April 1941.

15. Volume II (Engineering), Reactor Handbook (Secret)

12.5 APPENDIX E: BIOLOGICAL SHIELDING

This section details the methods used in designing the biological shield. It is based on the shield proposed for the ORNL Package Reactor (APPR) by Pearce [1]

12.5.1 Radial Shielding

A spherical source was assumed with surface strength equal to the fluxes obtained at the inner surface of the concrete and with radius equal to the radial distance, r, from the core axis to the concrete as shown by the figure below.

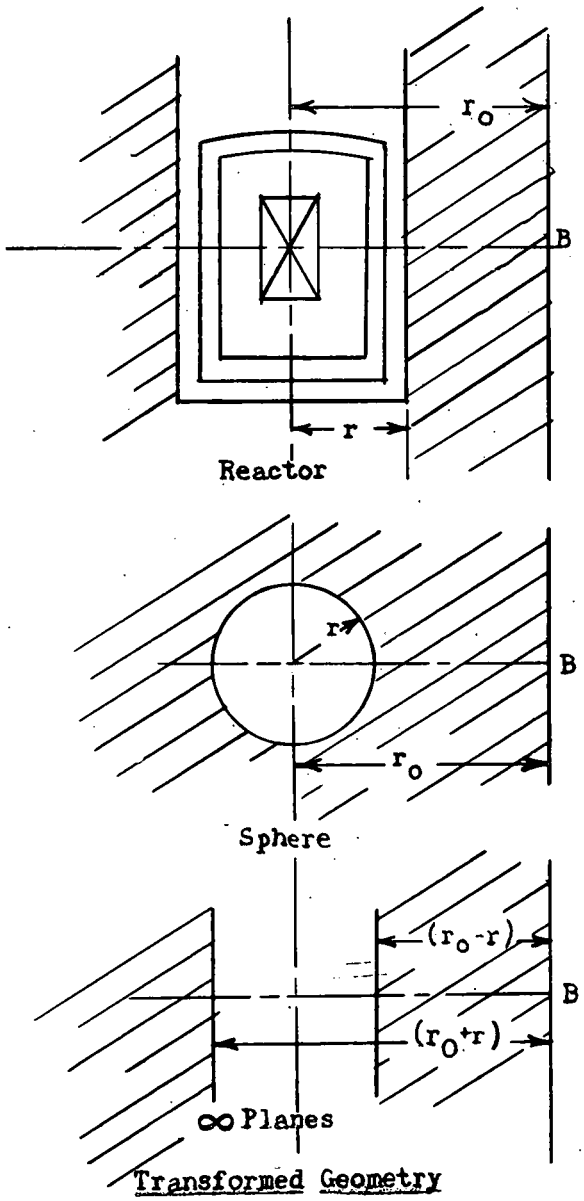

Blizard's [2] transformation from spherical to plane geometry is:

$$D_S(r_o, r) = \frac{r}{r_o} D_{PL}(r_o - r, \infty) - D_{PL}(r_o + r, \infty)$$

This assumes that the shielding properties of the core and shield are identical. (The composite linear absorption of the core is slightly greater than that of concrete.) For $\frac{r}{r_o} \ll 1$, the second term is negligible with respect to the first term.

The response of a "milligoat" detector at point B is now determined by using the infinite plane source.

For gammas, using a buildup factor equal to the number of relaxation lengths, Blizard [2] obtains:

$$D_{PL}(r_o - r, \infty) = \frac{\sigma}{2} e^{-\mu (r_o - r)}$$

where σ = the surface strength of the infinite plane
μ = linear absorption coefficient

For pure exponential attenuation, as for the fast neutrons, he obtains the same result, if many relaxation lengths are traversed.

Therefore the response of a milligoat detector, in units of gamma and fast neutron flux, is:

$$\phi = \frac{\phi_o}{2} \frac{r}{r_o} e^{-\mu (r_o - r)}$$

where we let $\sigma = \phi_o$, the flux values at the inner edge of concrete.

The use of a buildup factor equal to the number of relaxation lengths is conservative by at least a factor of two in dosage from high energy gammas, if the buildup in concrete behaves as the buildup in water and in aluminum.

12.5.2 Axial Shielding

Because the fluxes could be based on calculations at a greater distance from the core (6 ft from centerline), it was felt that a point source and spherical geometry assumption would yield the best results.

Assume $M = \frac{SB\ e^{-\sum_i \mu_i t_i}}{4\pi R^2 T}$

where M = dose in multiples of tolerance
B = buildup factor equal to $\sum \mu_i t_i$
R = radial distance from center of reactor core to point under consideration
S = point source evaluated from $\phi(6\text{ ft}) = \frac{SB\ e^{-\mu t}}{4\pi R^2}$
T = tolerance flux for energy group
t_i = thickness of i^{th} component

12.5.3 Design Criteria

Linear absorption coefficients used [2] are:

Mev	Concrete* [2,3,4]	Iron	Water Standard
1	0.145 cm^{-1}	0.46 cm^{-1}	0.079 cm^{-1}
2	0.105	0.32	0.049
4	0.073	0.26	0.034
7	0.059	0.24	0.025

Fast neutrons.

Relaxation length in concrete[3] = 11.1 cm
Relaxation length in iron[3] = 5.95 cm

Dosage. Tolerance is arbitrarily defined as 300 mrep/week over a 56-hour work period, or 5.36 mrep/hr. From Blizard[2], the gamma flux for each energy group is obtained which yields 1 R/hr. Multiplying each value by 3.56×10^{-3}, we find the flux for each energy which alone would produce the tolerance dosage rate.

Radiation	Tolerance Flux
1-Mev gamma	2800 γ's/cm^2/sec
2-Mev gamma	1700 γ's/cm^2/sec
4-Mev gamma	1000 γ's/cm^2/sec
7-Mev gamma	650 γ's/cm^2/sec
Fast Neutrons	47 neutrons/cm^2/sec

* Upon oral confirmation from E. P. Blizard, the linear absorption coefficient for concrete was found by using the value listed for aluminum and correcting for the difference in density. This agrees with values for concrete listed in RH-1 and by Foster, B. E., "Absorption by Concrete of X-rays and Gamma-rays", J. of A.C.I, Vol. 25, No. 1, Sept 1953, Proceedings Vol. 50.

The response of the milligoat detector is determined in multiples of tolerance dose rate for each radiation and these are totaled to determine the total dose as a function of concrete thickness.

12.5.4 Application of BSR Data

Flux per kw is obtained directly from the BSR work sheet as a function of distance from the BSR in standard temperature water. The effective radius of the BSR if regarded as a cylinder, is 8.9 in., and for the BPR (Boiling Package Reactor) the effective radius is 11.7 in. The flux at the distance R inches from the BPR core in water of density 52 lb/ft^3 is assumed to be:

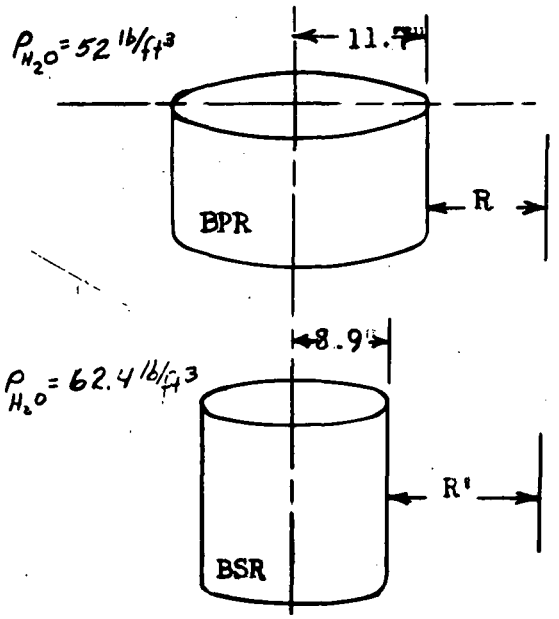

$$\phi_{BPR}(R) = \phi_{BSR}(R') \times \frac{8.9 + R}{11.7 + R}$$

$$\text{where } R' = R \times \frac{52}{62.4}$$

The total gamma flux thus obtained was apportioned according to the estimated spectrum at point R. Neutron fluxes from the BSR were corrected by the ratio of the leakage probabilities calculated for each reactor.

Determination of gamma spectrum. The gamma spectrum of the BSR in photons/cm^2-sec-Mev-steradian measured at various distances from the BSR was obtained from reference (5). These data were replotted with distance as the abscissa and the energy of the radiation as a parameter. It was then possible to estimate the spectrum at any desired distance from the BSR. These data were replotted linearly (e.g., Fig. 51) as photons/cm^2-sec. Energy groups were arbitrarily selected as follows (to agree with APPR):

Group	Energy Range
1-Mev	0.5 to 1.5-Mev gammas
2-Mev	1.5 to 3.0-Mev gammas
4-Mev	3.0 and 5.5-Mev gammas
7-Mev	5.5-Mev and above

The total flux was graphically apportioned to each group in percent of total flux.

Correction to BSR Spectrum. Because of the difference in composition of the BPR core, the gamma spectrum will differ from that of the BSR. Since high energy capture gammas are of greatest importance, and since the capture gamma spectra from aluminum and iron are nearly identical[6,7], correction to the BSR data may be made simply. Pearce[1] calculated that the APPR produces 1.375 times as many captures per kw as does the BSR. The 1, 2, and 4-Mev gamma-production rates are assumed equal. Because of the similarity of our reactor to the APPR, this value was used. Because of the lower water-to-metal ratio in the BPR as compared to the APPR, this value is undoubtedly conservative.

ORNL-LR-Dwg. 6107

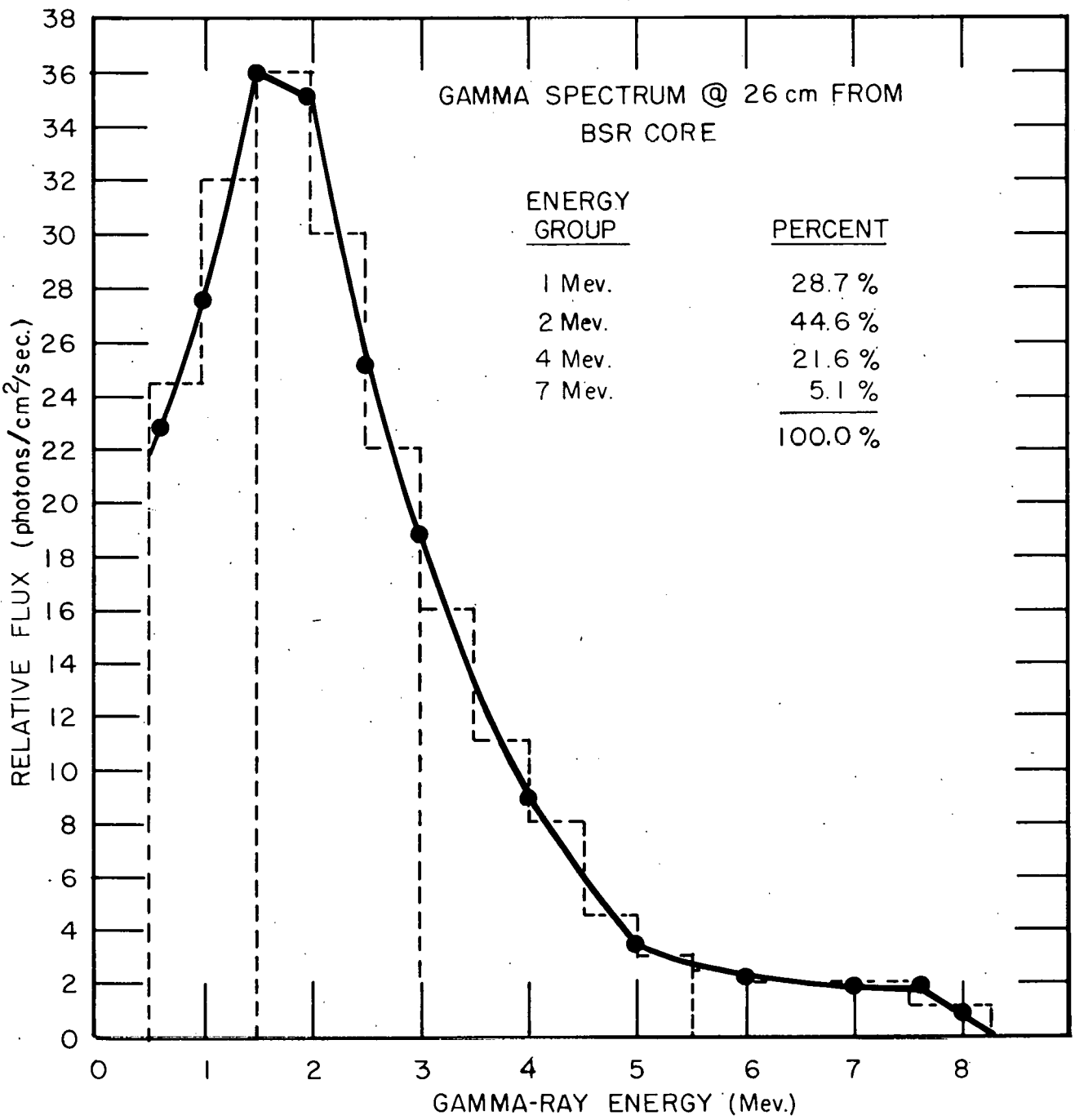

Figure 51

Self Shielding Capacities. The fraction, "f", of each energy group escaping the core is obtained for each reactor from Figure 14 of KAPL-783 [8]. The fraction of radiation escaping a finite cylinder with uniform production is plotted as a function of a parameter ξ where

$$\xi = 2 \times \frac{\text{Reactor volume}}{\text{Reactor surface}} \times \sigma$$

σ = linear absorption coefficient of reactor

We, therefore, define a composite σ as follows:

$$\sigma = \sum_i \left(\frac{\text{gm}}{\text{cc}} \text{ of the } i^{th} \text{ component} \times \frac{\mu i}{\rho i}\right)$$

μ_i/ρ_i = mass absorption coefficient of the i^{th} component

Component	gm/cc BPR	gm/cc BSR[1]	μ_i/ρ_i[2] 7 Mev	4 Mev	2 Mev	1 Mev
H_2O	0.589	0.585	0.025	0.034	0.049	0.070
U	0.145	0.0358	0.048	0.044	0.047	0.082
Al	---	1.12	0.025	0.031	0.043	0.061
Fe	0.78	---	0.030	0.033	0.041	0.059

$$\frac{2 \text{ vol}}{SA} = 16.1 \text{ cm BSR} = 19.7 \text{ cm BPR}$$

	7 Mev	4 mev	2 Mev	1 Mev
$\frac{f_{BPR}}{f_{BSR}}$	0.88	0.93	0.94	0.89

to be conservative, assume:

Relative production rate times relative escape rate

= 1 for 1,2, and 4-Mev gammas

= 1.30 for 7-Mev gammas

12.5.5 Neutron Data

The relative leakage per fission for fast neutrons, $(1 - e^{B^2 t})$, was computed for each reactor by using the following data:

	BSR	BPR
$B^2 (cm^{-2})$	0.00792	0.00444
$t\ (cm^2)$	64	67.2

The ratio of the leakage probabilities is 0.65. Again to be conservative 0.8 was used.

12.5.6 Capture Gammas

A. Concrete. The methods used for the MTR shield were followed[9]. Assume all fast neutrons are captured at a distance equal to an age displacement (31.8 cm = 12.5 in. for concrete), that 1 gamma-ray is produced by each capture and that all γ's continue in a forward direction. This is a conservative estimate.

Whether or not these capture gamma rays are important in the design of the shield depends upon the energy assumed for each gamma ray. A common assumption has been that each gamma ray has an energy between 7 and 8 Mev. If this were true, capture gammas would govern shield thickness.

Very few data are available concerning the energy of capture gammas from concrete; however, a report on the reactor recently built at Livermore, California with an ordinary concrete shield would seem to indicate that the predominant capture gamma from hydrogen is 2.2 Mev[10]. See Fig. 52. The slight capture gamma peak at $\sim$ 7.6 Mev was postulated as due to the capture of neutrons by the reinforcing steel. On the basis of this report, it has been assumed that the contribution of capture gammas to biological dose rates is negligible.

ORNL-LR-Dwg. 6108

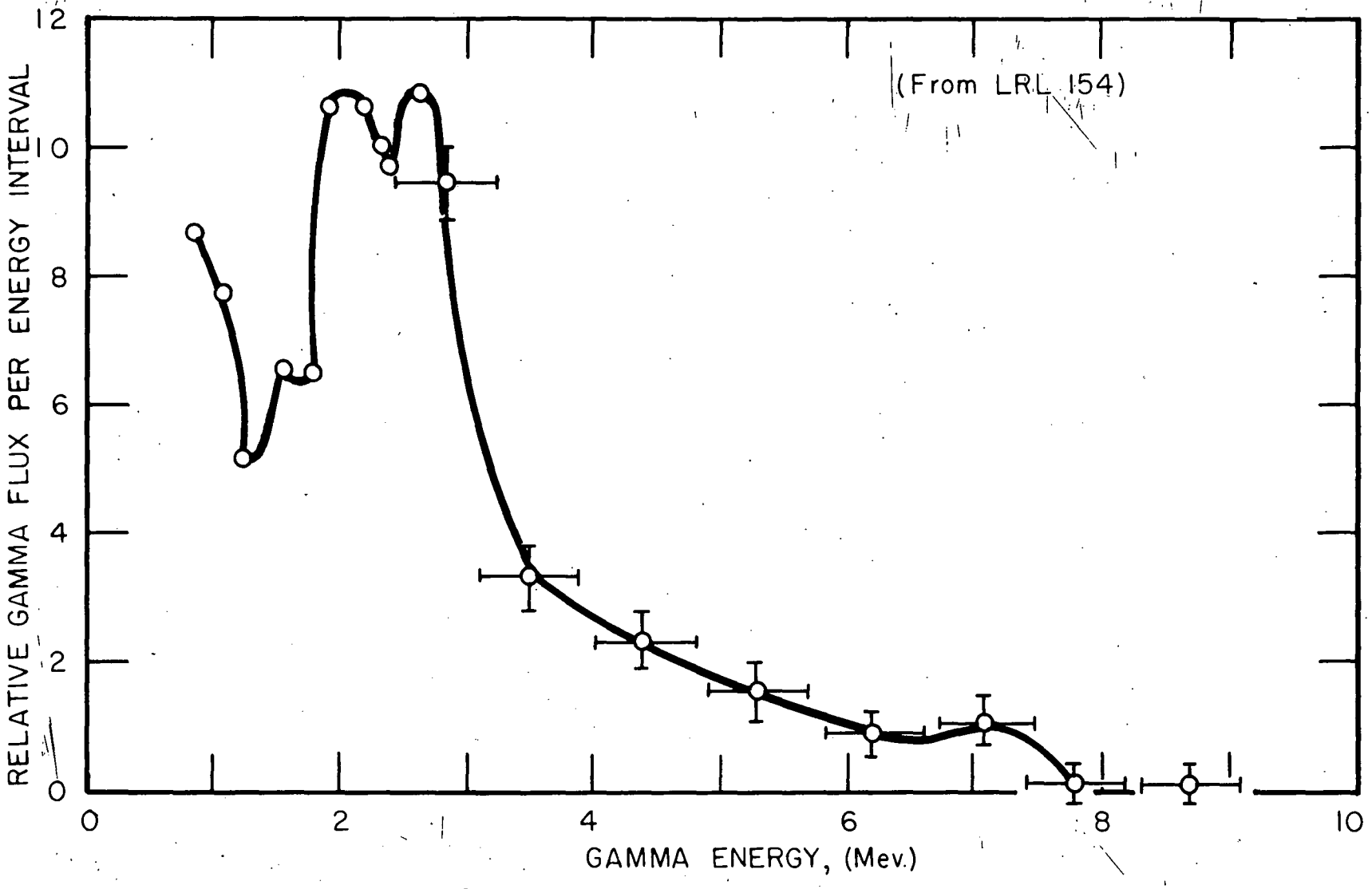

GAMMA SPECTRUM FROM CONCRETE

Figure 52

B. Iron. Each neutron capture in steel is assumed to produce one 7-Mev gamma. In Fig. 53 is reproduced the fraction of emitted radiation that escapes from one surface of a finite slab with constant source strength per unit volume[8]. The neutron flux in a slab adjacent to an infinite plane source is, according to diffusion theory, of the form:

$$\phi = \phi_o e^{-\mathcal{H}x}$$

where ϕ_o = source or incident flux

$\mathcal{H}$ = reciprocal of diffusion length

= 0.766 cm^{-1} for thermal neutrons in iron

A uniform flux $\bar{\phi}$, is assumed through the slab.

$$\bar{\phi} = \frac{\int_o^t \phi \, dx}{t} = \frac{\phi_o}{\mathcal{H} t} \quad 1 - e^{-\mathcal{H} t}$$

where t is the thickness of the slab in cm.

The number of 7-Mev gammas escaping from one surface per cm^2 per sec is:

$$\phi_{c.g.}(7 \text{ Mev}) = f.t. \sum_a \bar{\phi}$$

where f = fraction of emitted radiation, from Fig. 53

$\sum_a$ = 0.21 cm^{-1} for thermal neutrons in iron.

This value was assumed as the flux of capture gammas from the thermal shield, pressure vessel, and lid.

ORNL-LR-Dwg. 6109

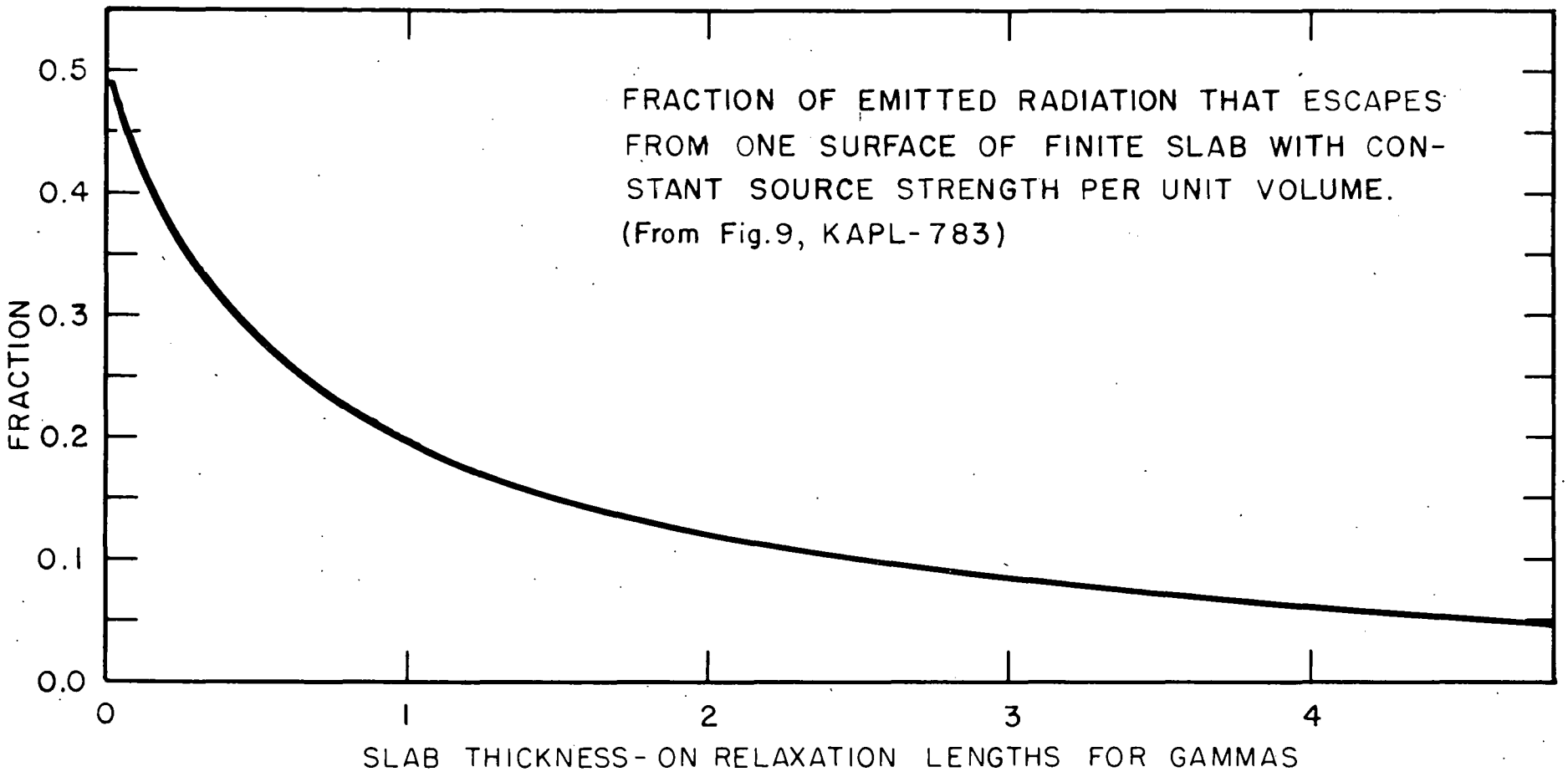

Figure 53

12.5.7 Determination of Fluxes

The following steps were taken to determine fluxes at the inner surface of concrete.

a. The flux distribution at the thermal shield and at the pressure vessel without the thermal shield, were determined from BSR data as outlined before.

b. The fluxes at the thermal shield were attenuated through 1 in. of steel according to $\phi_2 = \phi_1 \frac{r_1}{r_2} e^{-\mu t}$

where ϕ_1 = flux at inner surface of thermal shield
r_1/r_2 = radial correction factor

r_1 = inner radius thermal shield
r_2 = outer radius thermal shield

c. The flux at the pressure vessel with the thermal shield was found by assuming:

$$\phi(1_3) = \phi'(r_2) \times \frac{r_3}{(r_3 - 1)} \times f_1$$

where $\phi'(r_3)$ = flux at pressure vessel, no thermal shield

$\frac{r_3}{(r_3 - 1)}$ = factor to account for 1 in. less of water to transverse due to presence of thermal shield

f_1 = factor for reduction of intensity by thermal shield

$f_1 = \frac{r_1}{r_2} e^{-\mu t}$

r_3 = internal radius of pressure vessel

d. The flux at the outer surface of the vessel was found from

$$\phi(r_4) = \phi(r_3) \frac{r_3}{r_4} e^{-\mu x}$$

e. The flux at the inner surface of the concrete was now found from:

$$\phi(r) = \phi(r_4) \frac{r_4}{r}$$

by assuming only a radial correction across the insulation.

12.5.8 Results

Radiation	Flux at Pressure Vessel: No Shield	Flux at Pressure Vessel: With Thermal Shield	Flux at Shield 8" from core	Flux at Inner Surface of Core with Thermal Shield
1 Mev γ	10×10^{12}	3.1×10^{12}	2×10^{13}	7.9×10^{11}
2 Mev γ	15.6×10^{12}	6.9×10^{12}	3×10^{13}	2.6×10^{12}
4 Mev γ	7.6×10^{12}	3.9×10^{12}	1.4×10^{13}	1.7×10^{12}
7 Mev γ	2.3×10^{12}	$1.4 \times 10^{12*}$	4.4×10^{12}	$6.3 \times 10^{11*}$
Fast Neutron	1.1×10^{11}	7.2×10^{10}	4.7×10^{11}	4.6×10^{10}
Thermal "	9.6×10^{11}	1.6×10^{11}	4.7×10^{12}	3.9×10^{10}

* includes 7-Mev capture γ's from steel.

The only gammas found important in shield design are the 7-Mev group. The other groups were calculated for use in thermal stress analysis. Fast neutrons were also insignificant with respect to biological dose rates. The biological dose rate for various concrete thicknesses are reported in Section 6.

12.5.9 Shield Ventilation Calculations

From shielding calculations

$$I_{(r_o)} = \frac{r}{r_o} \frac{I_o}{2} e^{-\mu(r_o - r)}$$

then

$$H_{(r_o)} = C \mu I_{(r_o)} E\gamma \quad \text{Btu/hr-ft}^3$$

where C is a constant conversion factor = 1.56×10^{-8}

$$H_{(r_o)} = .78 \times 10^{-8} \frac{r}{r_o} \mu I \; E\gamma \; e^{-\mu (r_o - r)}$$

and $r = 29$ inches $= 73.6$ cm

The gamma radiation was broken down into four categories as described in section 6.4 and the following four equations for shield heating resulted.

$$H_{7\ Mev} = \frac{190,000}{r_o} e^{-.059(r_o - 73.6)}$$

$$H_{4\ Mev} = \frac{368,000}{r_o} e^{-.073(r_o - 73.6)}$$

$$H_{2\ Mev} = \frac{398,000}{r_o} e^{-.105(r_o - 73.6)}$$

$$H_{1\ Mev} = \frac{83,900}{r_o} e^{-.146(r_o - 73.6)}$$

where r_o is in cm and H is in Btu/hr-ft^3

The total heating effect is the sum of these four equations.

A cyclindrical shield was assumed with the heated portion about 5 ft high. Assume also that the entering air temperature is 50°F and the allowable temperature rise of the air is 100°F. The shield was arbitrarily broken up into 6-inch annular rings.

$$\text{Volume of 1st ring} = \pi (r_{o1}^2 - r^2)\ 5 = 41.5\ \text{ft}^3$$

$$\bar{H}_{1st\ ring} = 9,200\ \text{Btu/hr-ft}^3$$

$$Q_{1st\ ring} = \bar{H}\ V = (9,200)(41.5) = 382,000\ \text{Btu/hr}$$

$$\Delta h_{air} = C_p \Delta T = (.24)(150-50) = 24\ \text{Btu/hr/lb}$$

$$W_{air}\ (1st\ ring) = \frac{382,000}{24} = 15,900\ \text{lb air/hr}$$

Assume a flow loss coefficient of 2 and set the pressure rise of the fan at 3 in. H_2O = 15.15 lb/ft^2

$$\Delta P = \frac{K \rho V^2}{2g}$$

where ρ is about 0.07 lb/ft^3

$$V = \sqrt{\frac{2g\Delta P}{K}} = \sqrt{\frac{(2)(32.2)(15.15)}{(2)(.07)}}$$

V = 83.5 ft/sec or 288,000 ft/hr

Assume ventilation holes to be 1 in. in diameter, Area = .00545 ft^2 each.

$$W = N \rho A V$$

where N is the number of holes required

$$N = \frac{W}{\rho A V} = \frac{15,900}{(0.07)(0.00545)(288,000)} = 145 \text{ holes for 1st ring}$$

Similarly, the outer rings were calculated. It was not considered advisable, however, to use less than one hole per 3 feet of circumference, in order to keep the temperature between holes down.

Fan Rating. As previously chosen: ΔP = 3 in. H_2O

$$Q = NAV = N\ (0.00545)(83.5)(60) = 26.2 \text{ cfm}$$

where N is the number of holes in shield

when N = 415 holes

Q = 11,000 cfm

Maximum Concrete Wall Temperature.

From Reference No. 4 (Heat Transfer, Brown and Marco)

$$h = \frac{0.0037\ G^{.8}}{D^{.2}} = 0.006\ G^{0.8}$$

$$G^{.8} = \left(\frac{W}{A}\right)^{0.8} = (\rho V)^{0.8} = (0.07)(288{,}800)^{0.8} = 300$$

$$h = 18 \text{ Btu/hr-ft}^2\text{-°F}$$

$$Q = hA\Delta T$$

where A is the surface area of 1 foot of tube (0.262 feet)

and the heat load (1st ring) = 528 Btu/hr-ft of tube = Q

$$(T_{wall} - T_{air})_{max} = \frac{528}{(18)(.262)} = 101\ °F$$

Then the temperature difference between the wall and the circulating air is not expected to exceed about 100 °F.

The number of holes required in each annular ring is tabulated below, where the thickness of the annualar ring is given as the distance from the inner surface of the cylindrical shield.

Ring (ft)	Holes	Ring (ft)	Holes
0 - $\frac{1}{2}$	145	$5\frac{1}{2}$ - 6	12
$\frac{1}{2}$ - 1	36	6 - $6\frac{1}{2}$	13
1 - $1\frac{1}{2}$	22	$6\frac{1}{2}$ - 7	13
$1\frac{1}{2}$ - 2	11	7 - $7\frac{1}{2}$	14
2 - $2\frac{1}{2}$	10	$7\frac{1}{2}$ - 8	14
$2\frac{1}{2}$ - 3	10	8 - $8\frac{1}{2}$	15
3 - $3\frac{1}{2}$	10	$8\frac{1}{2}$ - 9	15
$3\frac{1}{2}$ - 4	10	9 - $9\frac{1}{2}$	16
4 - $4\frac{1}{2}$	10	$9\frac{1}{2}$ - 10	16
$4\frac{1}{2}$ - 5	11	10 - $10\frac{1}{2}$	17
5 - $5\frac{1}{2}$	12	$10\frac{1}{2}$ - 11	17
		11 - $11\frac{1}{2}$	18

12.5.10 Bibliography (appendix 12.5 only)

1. Pearce, W. R., Analysis of Biological Shielding and Thermal Shielding Requirements for the ORNL Package Reactor, CF 53-10-81, Oct. 25, 1954.

2. Blizard, E. P., Introduction to Shield Design, CF 51-10-70 (two parts), (1952).

3. Reactor Handbook, Volume No. 1 (Physics)

4. Foster, B. E., "Absorption by Concrete of X-rays and Gamma-rays," J. of A.C.I., Vol. 25, No. 1, Sept. 53, Proceedings V. 50.

5. Maienschein, Fred and Love, Temple, "Gamma-ray Spectrum of the Bulk Shielding Reactor," Nucleonics, Vol. 12, No. 5, May 1954.

6. Kinsey and Bartholemew, "Neutron Capture γ's from Fe....", Phys. Rev., Vol. 89, No. 2, p. 381 (1953).

7. Kinsey and Bartholemew, "Neutron Capture γ's from Al....", Phys. Rev., Vol. 83, No. 3, p. 527 (1951).

8. Storm, Hurwitz and Roe, Gamma Ray Absorption Distributions for Plane, Spherical, and Cylindrical Geometries, KAPL-783, July 24, 1952.

9. Buck, J. H. and Leyse, C. F., Materials Testing Reactor Handbook, ORNL-963 (1951).

10. Shortall, J. W., et al, Biological Shield Evaluation of the Water Boiler, LRL-154, June 1954.